Low and non-PGM materials for use in three-way catalytic converters in the treatment of gasoline exhaust

A Thesis Submitted to Cardiff University

in Fulfilment of the Requirements for the

Degree of Doctor of Philosophy

by David Robert Watson

PhD Thesis October 2015

Cardiff University

DECLARATION

This work has not been submitted in substance for any other degree or award at this or any other university or place of learning, nor is being submitted concurrently in candidature for any degree or other award.

Signed: David Robert Watson Date: 18/02/2016

STATEMENT 1

This thesis is being submitted in partial fulfillment of the requirements for:
the Degree of Doctor of Philosophy

Signed: David Robert Watson Date: 18/02/2016

STATEMENT 2

This thesis is the result of my own independent work/investigation, except where otherwise stated.

Other sources are acknowledged by explicit references. The views expressed are my own.

Signed: David Robert Watson Date: 18/02/2016

STATEMENT 3

I hereby give consent for my thesis, if accepted, to be available for photocopying and for inter-library loan, and for the title and summary to be made available to outside organisations.

Signed: David Robert Watson Date: 18/02/2016

CANDIDATES LAST NAME		Watson	
CANDIDATES FIRST NAME(S)		David Robert	
CANDIDATES ID NUMBER		0706141	
SCHOOL		CHEMISTRY	
TITLE OF DEGREE		PhD	
FULL TITLE OF THESIS		Low and non-PGM materials for use in three-way catalytic converters in the treatment of gasoline exhaust	
IS THIS A RESUBMISSION?		NO	
THESIS SUBMITTED FOR EXAMINATION IN		Permanent binding [] Temporary binding [x]	
CANDIDATES SIGNATURE	David Watson	DATE	2/18/2016

Acknowledgments

I have had the privilege of working with a group of fantastic individuals and working for fantastic supervisors. My experience has taught me more about myself than I thought I knew and has developed me in a way I am truly grateful for. My first dedication is to my project supervisors Prof Stanislaw Golunski and Prof Stuart Taylor, without whom I would never have reached this stage and have supported my growth as a researcher with patience and dedication and good humour. I would also like to thank my post-doc Dr David Sellick, whose guidance early on in my PhD was invaluable and whose knowledgeable grasp of the field helped me get to where I am now.

The CCI has been like a family to me over the course of my studies. Thank you to Prof Graham Hutchings for heading the group and providing the staff and students with such opportunities. I'd like to thank Dr Rob Jenkins whose advice on analytical techniques was invaluable, Dr David Morgan who provided the XPS data for my thesis and all the post –docs for their help along the way. I would like to thank all the students I helped supervise, in particular Jordan Marianccio who assisted in developing the Chapter 5 with me. To everyone at Jaguar Land Rover, thank you for the support you have provided both financially and academically.

I would like to thank everyone in the CCI, the names of whom are too numerous to list here, as colleagues your advice and assistance has been beyond helpful, and as friends you have carried me through the highs and the lows, thank you.

I couldn't possibly have done this without the support of my family. My mother and father who have always given me a hot meal and a place to sleep when I've needed it and whose support and patience has ultimately brought me to where I am now, I couldn't have done it without you. To my brothers, who kept me fighting to achieve what I thought was beyond me, thank you as well, and to all my relatives, thank you for everything you have done for me.

Last but not least, to Anna, you have supported me and been there for me throughout my university life, through the good times and the bad, I couldn't have done it without you.

Dedicated to my Family, Friends and Anna

List of Abbreviations

°C	Degree Celsius
Å	Angstrøm
acac	Acetylacetonate
A/F	Air to Fuel Ratio
BET	Brunauer–Emmett–Teller
DOE	Design Of Experiments
EDX	Energy-Dispersive X-ray Spectroscopy
EtOH	Ethanol
FT-IR	Fourier Transform Infrared Spectroscopy
g	Grams
h	Hour/hours
L	Litres
m	Minutes
mg	Milligrams
mL	Millilitres
NEDC	New European Driving Cycle
nm	Nanometer
OSC	Oxygen Storage Capacity
ppm	Parts per million
ppb	Parts per billion
rt	Room temperature

SEM	Scanning Electron Microscopy
TEM	Transmission Electron Microscopy
TEAM	Transmission Electron Aberration-Corrected Microscopy
TGA	Thermogravimetric Analysis
TPR	Temperature Programed Reduction
TWC	Three Way Catalyst
WGS	Water Gas Shift
XPS	X-ray Photoelectron Spectroscopy
XRD	X-ray Diffraction

Abstract

The aftertreatment of vehicular exhaust has been a silent revolution in public health, however catalysts continue to be dependent on resources that are expensive, difficult to extract from the crust and are extremely expensive. This thesis sets out to address the problem of tightening legislation and the increasing scarcity of precious resources by taking steps away from the dependence on platinum group metals, either by reduction of their use or elimination. In Chapter 3 of this thesis, mechanochemical synthesis of perovskites was carried out with Ag doped $LaMnO_3$ as well as a novel reactive grind process whereby nitrates were mixed in pestle and mortar and reacted with NaOH before being calcined. A reduced 3FI statistical design was carried out to determine the important variables in high energy ball mill synthesis and the interaction between these variables. In Chapter 4, Pt and Pd catalysts were synthesised via novel physical grind with acetylacetonate salt precursors along with base metal dopants (Co, Fe) and a combustion stage to produce highly dispersed and highly active catalysts with high activity in lean exhaust mixtures. The effects of weight loading of the base metals were investigated, focusing on the influence on particle size and activity. These catalysts showed moderate activity for exhaust aftertreatment reactions. Additionally Pt catalysts were synthesised in a variety of ways from a modified impregnation procedure utilising toluene to produce better dispersed metallic nanoparticles on the surface of a hydrophobic material such as SiC, SnO_2, Si_3N_4 and BN, the SiC catalysts showed good activity towards both CO oxidation and propane oxidation as well as displaying the features of a WGS reaction and CO_2 activation.

Table of contents

Chapter 1: Introduction

1.1 Preface

According to the Offshore Industry Advisory Commute, the production of motor vehicles manufactured in 2014 was over 180 million, approximately 68 million of which were cars. To fit a converter on every car, assuming a 2 litre engine is fitted to each requiring 2g of palladium and 0.2g of rhodium per vehicle then the total value of precious metals in each catalytic converter reaches to over 4 billion US dollars. This disregards the R&D, manufacture and other materials present. Catalytic converters can cost up to $1000 per vehicle, often exceeding the cost of all other components. This puts huge economic pressure on the company implementing them and in some markets makes TWCs non-viable. Platinum group metal catalysts are victims of their own success, being rare and valuable metals which are unrivalled in their performance and durability with alternatives often trading one of these qualities for the other.

The principal aim of this project is to provide alternative catalyst systems for three way catalytic converters, which either reduce or remove the requirement for platinum group metals. This thesis will detail 3 main areas of research, mechanochemical routes for the production of silver doped perovskites, the use of a thermal decomposition method for the dispersion of platinum metals on a catalyst, and finally the use of a modified impregnation procedure for hydrophobic supports to alter the interaction of the catalyst with gas phase water. The objective is not necessarily to replace platinum group metals entirely, but to thrift them with alternative materials, and reduce the overall cost to the manufacturer, to the customer and ultimately, the planet.

1.2 Catalysis

The first usage of the term catalysis in reference to this chemical process was by Jöns Jacob Berzelius[1]. He referred to it as the 'catalytic force' to explain his observations of materials that were involved in, but not consumed by certain chemical processes. Since then, catalysis has become an important part of modern industrial chemistry as it enables vast energy savings over the course of a reaction and in some cases allows an uneconomical process to become viable. The Haber-Bosch process[2] is the classic example of how catalysis has benefited and shaped the modern world. This process stands out as the major contributing factor to the increase in population over the last century supporting the lives of 4 billion people since 1908[3] and consumes approximately 1% of the global energy supply[3].

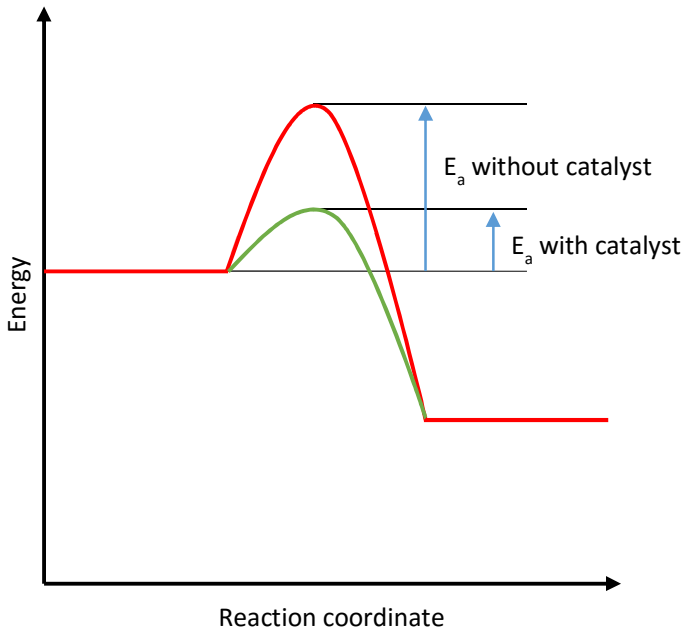

Figure 1. A simplified representation of a catalysed and non-catalysed process showing the difference in activation energy required to initiate the reaction

A catalyst is a substance that increases the rate of the reaction without itself being altered in the process. This is achieved by providing an alternative reaction

pathway that requires a lower activation energy for the reaction to proceed (Figure 1). To do this a catalyst must facilitate an alternative transition state or states for the reaction pathway, allowing it to overcome kinetic limitation inherent in the non-catalysed pathway. A catalyst by definition has no effect on the thermodynamics of a reaction and has no effect on the equilibrium of the reaction.

Although in principal a catalyst remains unchanged over the course of a reaction, in reality external factors contribute to the deactivation of catalyst over time. This can be due to poisoning either by secondary reactants or products[4-7], sintering of metal particles[8, 9] or processes such as coking[10-12]. This is an important consideration in automotive catalysis where complicated gas streams are treated by increasingly complex multi-component catalysts under aggressive conditions.

Catalysis can be divided into three major categories; heterogeneous, enzymatic and homogeneous catalysis. A homogeneous catalysis is a material that catalyses a reaction while in the same phase as the reactants, typically the liquid phase. Homogeneous catalysts commonly consist of a metal ion with ligands specifically chosen to enhance the selectivity and activity of the catalyst. Enzymatic catalysts are biologically derived process whereby proteins are used to enhance the rate of chemical reactions. These proteins are derived from the natural world and commonly carry out organic chemistry in the liquid phase, and like homogeneous catalysts, operate in the same phase as their reactants. A heterogeneous catalyst is a substance that exists in a separate phase to the reactants it catalyses, this is typically a solid phase catalyst with liquid or gaseous phase reactants. Heterogeneous catalysts commonly consist of an active phase such as platinum deposited onto a support material which typically consists of an inert oxide, for instance alumina.

1.3 Catalysis with platinum group metals

One of the earliest examples of platinum catalysis being put into practical use was in 19th century miner's lamps. Davy lamps as they were known, were the result of a discovery by Sir Humphry Davy that when a heated platinum gauze was exposed to coal gas, the metal continued to glow red hot as it catalysed the gas without producing a

flame and catalysed other combustible compounds also[13]. This allowed the lamp to be operated without igniting the flammable gases that may be present in a mine and it is the first discovery of heterogeneous oxidation catalysis.

Since these early applications, platinum group metals (ruthenium, rhodium, palladium, osmium, iridium and platinum) have seen wide spread industrial use. They possess desirable properties such as stability, durability and exceptional activity for a multitude of oxidation and reduction reactions. The vast majority of rhodium mined globally is used in catalytic converters as it is an excellent reduction catalyst for NO to N_2 and O_2. Palladium is another metal that sees the majority of its industrial use in catalytic converters. Palladium carries out reduction of NO and oxidation of CO and hydrocarbons in a three way catalytic converter. Although it is not as active as platinum in this role it does exhibit higher stability, maintaining its particle size over time due to its less volatile oxide. For this reason it has been the metal of choice. Platinum is an exceptionally active metal for oxidation and has been a major component of catalytic converters since their invention and continues to be so today. Rhenium, iridium, and osmium have found no practical use in automotive catalysis due to their poor stability[14], a result of their highly volatile oxide phases and osmium specifically is highly toxic. One quality all of these metals share however is their extremely high price due to their relative scarcity.

1.4 Internal combustion and exhaust aftertreatment

The introduction of the automobile in the early 20th century was a cultural revolution and played a crucial role in the growth of almost all modern societies. The rapid rise to ubiquity brought some unexpected consequences however and issues soon became apparent with exhaust emissions. While some pollutants such as lead and sulphur were a matter for supply companies to handle there was a considerable contribution from the processes of internal combustion itself. There are many pollutants in exhaust fumes but the three major components dealt with by catalytic converters are CO, NO/NO_2 (NO_x) and hydrocarbons. Carbon monoxide is generated from the incomplete combustion of fuel and is an unavoidable component of exhaust

fumes due to rapid combustion in the cylinder. CO is extremely toxic as it bonds irreversibly to haemoglobin and in high enough concentrations can starve the body of oxygen. NO_x emissions are formed from molecular oxygen and nitrogen under the very high temperatures and pressures found in car engines, the NO_x component is toxic as well as notorious for generating photochemical smog, a hazardous haze of chemicals caused by the photo-reduction of NO_x with various volatile organic compounds (which may also be found in exhaust gas). Photochemical smog blights cities where automobile populations are most dense and has often been the driving force for the kind of environmental legislation that brings about the mandatory use of catalytic converters in many western economies.

1.4.1 Catalytic converters.

Thanks to the elimination of lead from fuel, the first catalytic converters used on internal combustion engines were introduced to American cars in the mid 1970s. At first these were exclusively oxidation catalysts used for the conversion of hydrocarbons and CO under excess oxygen. At the time, NO_x emissions were controlled directly by changing the conditions in the engine and so early catalysts were passive additions to the exhaust. However, this early method of emission control could not keep up with the increasingly strict legislation placed on NO_x emissions but advances in electronics and oxygen sensors allowed a movement towards active reduction/oxidation catalysts and paved the way for the modern three-way catalytic converter.

A typical modern catalytic converter consists of a monolithic support, typically cordierite or $(Fe,Mg)_2Al_3(Si_5AlO_{18})$. This plays no role other than to support the active catalyst under the extremely harsh conditions found in a TWC as cordierite has low thermal expansion, making it resilient to thermal shock. The washcoat on top of this contains the catalyst, which is typically a high surface area alumina supporting a mixture of platinum, palladium, and/or rhodium metallic nanoparticles depending upon the application and requirements. In addition to the PGMs, a quantity of ceria/zirconia is added as an oxygen storage material for oxidation reactions under rich conditions,

and BaO, which acts predominantly as a buffer for NO_x. These components are discussed in more detail later on in this chapter.

1.4.2 Exhaust gas components

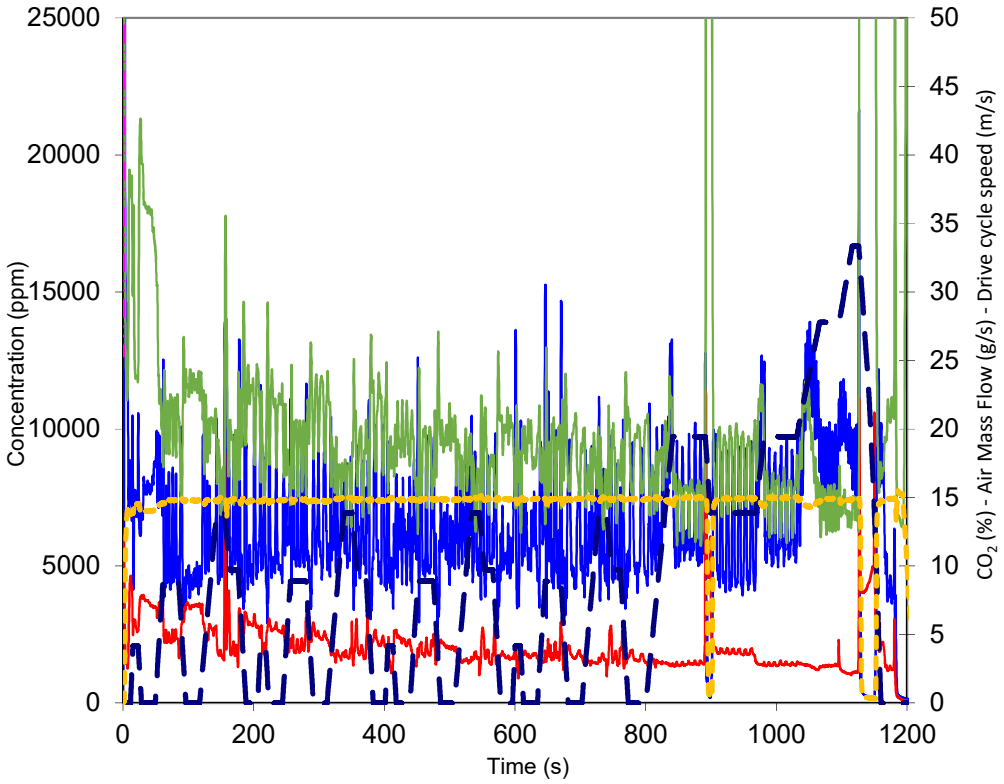

Figure 2. Exhaust emissions pre catalytic converter in an unspecified engine during an NEDC cycle. Carbon Monoxide (blue), Total Hydrocarbon Content (Red), Oxygen (green), CO_2 (yellow).

Automotive exhaust is complex and constantly changing depending on a host of independent factors such as the driver, engine type, fuel quality, and road type. Even during a controlled test on a rolling road the results are highly variable (Figure 2). As a result, all mixtures of exhaust gas that attempt to emulate conditions in an exhaust by necessity must be simplified for an analysis to be carried out. Spark-ignited gasoline engines often have an air to fuel ratio (A/F) (equation 1) that oscillates above and below the stoichiometric point of 14.7:1 by weight for pure octane, this allows the catalyst to carry out reduction and oxidation simultaneously. Lambda is the A/F

equivalence ratio as a fraction of the actual A/F ratio over the stoichiometric ratio (equation 2), i.e. an engine running exactly at the stoichiometric point has a λ value of 1 with lean conditions being higher than 1 and rich lower than 1.

$$A/F = \frac{mass\ of\ air\ consumed\ by\ engine}{mass\ of\ fuel\ consumed\ by\ engine} \qquad (1)$$

$$\lambda = \frac{Actual\ engine\ A/F}{stoichiometr\quad engine\ A/F} \qquad (2)$$

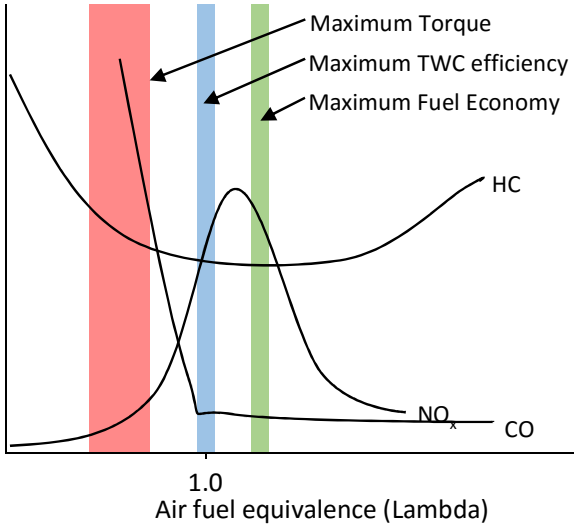

Figure 3. Simplified graph of major regulated exhaust components over the A/F ratio.

The composition of the exhaust gas is dependent on the air/fuel ratio (Figure 3). While running under rich conditions the exhaust gas contains uncombusted hydrocarbons and carbon monoxide, however as the engine runs cooler there is less NO_x generated as nitrogen is oxidised only at very high temperatures. Under lean conditions there is a reduction in CO emissions and, to a lesser extent, hydrocarbons. At the point of maximum engine efficiency, NO is generated in larger quantities while the exhaust gas is oxidising in character, making the NO difficult to reduce. The stoichiometric point is the ideal position for TWC catalysis to take place, but due to the varying demands placed on the engine, it is rarely achieved in practice. Under steady load the lambda value oscillates around 1 but under acceleration or deceleration the A/F tends to rich or lean conditions respectively.

A gas mixture was prepared that changed the bare minimum between compositions to allow a valid comparison. The only varied parameter between a lean and stoichiometric test therefore was the oxygen content and the N_2 balance to compensate (Table 1. Exhaust gas composition selected for testing).

Table 1. Exhaust gas composition selected for testing

Gas	Lean Burn Conditions	Stoichiometric Conditions
Nitrogen	Balance	Balance
Carbon Monoxide	1%	1%
Nitric Oxide	300 ppm	300 ppm
Propane	1000 ppm	1000 ppm
Oxygen	8%	1%
Water	8%	8%
Carbon Dioxide	6%	6%

1.3.4 Carbon monoxide

Carbon monoxide is a kinetically stable diatomic molecule of triple bonded oxygen and carbon. It is an unavoidable by-product of internal combustion due to the rapid oxidation of fuel in a cylinder and rich fuel/air mixes that favour partial oxidation. As an extremely toxic molecule the removal of this gas from exhausts is of utmost priority. CO is kinetically a very stable molecule and has an extremely strong triple bond of 1076.63 ± 0.06 $kJmol^{-1}$ under standard conditions[15], stronger even than nitrogen. However, the formation of CO_2 from CO and O_2 is a very thermodynamically favourable reaction and has a very large exotherm. It was a major component of coal gas and was used to light and heat homes in the early part of the 20^{th} century.

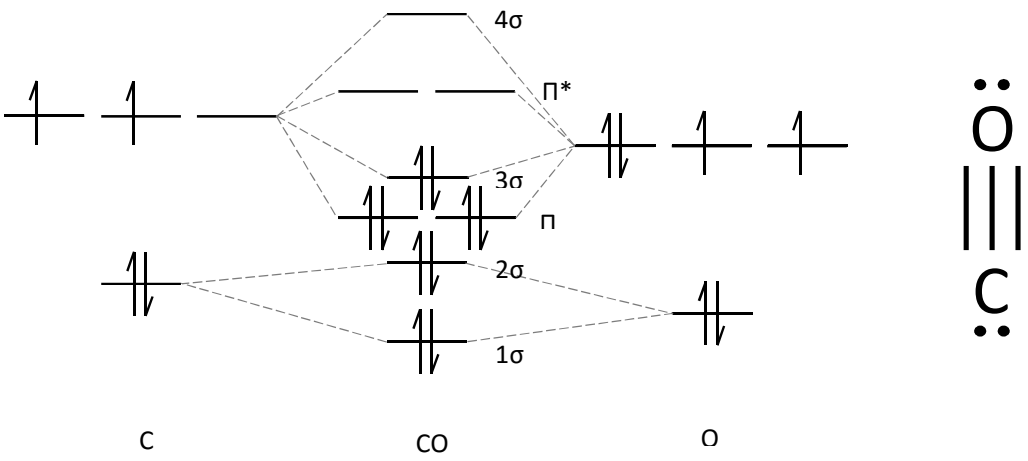

Figure 4. Molecular Orbital diagram of Carbon Monoxide (left), Lewis dot structure of carbon monoxide (right).

The lewis structure of carbon monoxide in Figure 4 (right) shows a single lone pair of electrons on the carbon and oxygen and the molecular orbital diagram (left) shows how the electrons distribute themselves to form a stable molecule. The lone pair on the carbon (3σ) is the highest occupied molecular orbital (HOMO) and is the most reactive. When the HOMO coordinates to the lowest unoccupied molecular orbital (LUMO) of another atom, such as when adsorbed to a metal atom, as the donor 3σ coordinates to a d_{Z^2} orbital this pushes electrons into the lowest unoccupied molecular orbital (LUMO), which in the case of carbon monoxide is an antibonding pi orbital. This weakens the CO bond and produces a more reactive molecule, lowering the activation energy for CO oxidation. The interaction between antibonding pi orbitals and metal d orbitals is referred to as pi backbonding.[16]

1.4.4 NO_x

Nitrogen itself is an extremely unreactive molecule and is usually considered a cheap alternative to noble gases in laboratory situations, however in the heat and pressure found in an internal combustion engine the endothermic recombination of N_2

and O_2 into the various oxides of nitrogen takes place. Natural sources of NO include lightning strikes, which generate the temperatures required to oxidise nitrogen.

The vast majority of NO_x produced is nitric oxide (NO) with a smaller but still significant quantity of NO_2. NO_x is regulated because of its ability to form photochemical smog; NO_x and volatile organic compounds (VOCs) react in the atmosphere under sunlight to produce a characteristic orange haze, especially evident in highly populated cities with lax emissions regulations (Figure 5). Photochemical smog contains highly reactive and oxidising compounds such as ozone and peroxyacyl nitrates and they have extremely serious implications for respiratory health.

Figure 5. Photochemical smog in São Paulo Brazil

Nitrous oxide (N_2O), while not as dangerous as the mono-nitrogen oxides, is still an extremely potent greenhouse gas with almost 300 times the global warming potential of CO_2 over the course of 100 years. However, N_2O emissions are considerably less toxic than other NO_x emissions and so do not constitute as serious a risk.

NO is removed from exhaust gas by a reduction catalyst such as rhodium. In a TWC the NO is either directly reduced to N_2 and O_2 on platinum or can be reduced with CO over rhodium[17]. The adsorption of NO on a metal is a similar mechanism to CO with pi backbonding weakening the NO bond (Figure 6).

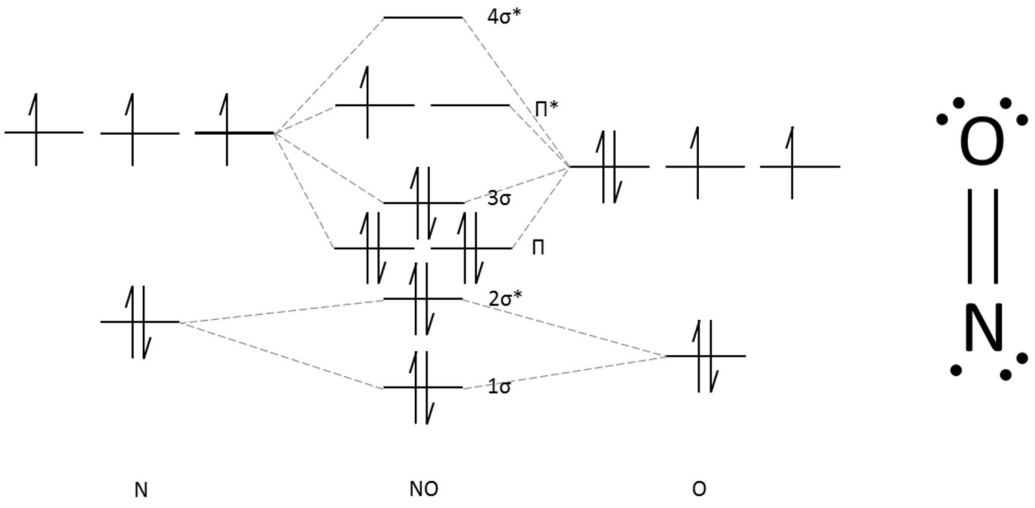

Figure 6. Molecular orbital diagram for NO

1.4.4.1 Lean NOx control

Lean NO_x control is particularly challenging because of the affinity of metal surfaces active for NO reduction for oxygen. This oxygen poisoning makes NO reduction extremely challenging under oxidising conditions. Traditionally, this had greater implications for diesel heavy duty vehicles, where engines produce a great deal of NO under very lean exhaust gas mixtures, however the increasing severity of passenger diesel vehicle exhaust regulation makes this an issue of significance. For gasoline, there is also a push towards lean burn gasoline engines which also presents a challenge (As lean burn delivers great efficiency gains). Practical solutions to this problem are difficult to implement, with urea injection as a reducing agent and NO_x storage traps being the principal methods used. NO_x storage issimilar to the method used for NO control during rich exhaust events in TWCs (Figure 7). BaO present on the catalyst acts as a buffer for NO when the catalyst is operating under lean conditions. Pt oxidises the NO to NO_2 and stores it as barium nitrate in close proximity to the Pt. During a change to rich conditions, the NO_2 is used by the Pt to oxidise CO and NO and reduce the NO_2 to N_2. Lean NO_x traps however, use a high surface area material such as a zeolite to store NO_x during lean phases and releases this during rich phases when it can be oxidised.

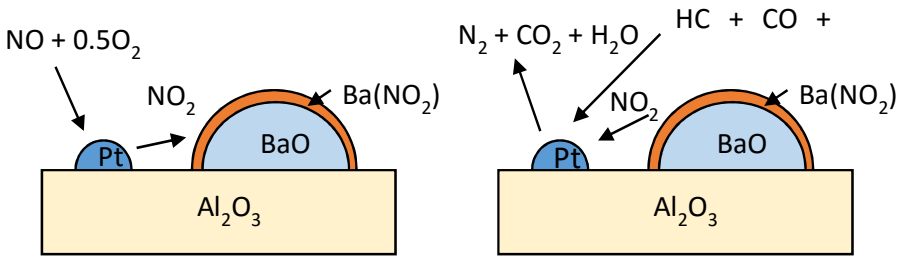

Figure 7. Behaviour of BaO in TWCs under lean (left) and rich (right) exhaust conditions.

1.4.5 Hydrocarbons

Complete oxidation of fuel to CO_2 and H_2O often doesn't take place in the engine during a combustion cycle so there is an appreciable concentration of partially oxidised and unburnt fuel in the exhuast. The composition of this gas varies depending upon a great number of factors, including but not limited to the engine design, fuel type and air/fuel ratio. Hydrocarbon (HC) content is regulated in terms of total carbon content, which is the number carbon atoms from any hydrocarbon material in the exhaust expressed as total hydrocarbon content or THC as a value in ppm. An analysis of exhaust gas found in gasoline vehicles in Australia produced from 1972 to 1982 demonstrates the variety of compounds released, in excess of 50 major components were described, with the most significant being ethylene, toluene, xylenes and benzene [18]. In a laboratory environment the replication of exhaust gas HC is impractical. In order to simplify the testing procedure a representative molecule must be used. There are two possible directions to take with an HC model, either a molecule representative of a typical activation energy can be used such as a higher alkane or an alkene (ie octane or propylene), or a typically difficult to oxidise alkane can be used as a worst case scenario. Generally if a catalyst will totally oxidise C1-C3 alkanes then it will be capable of oxidising the higher alkanes, alkenes and other functionalised materials.

The mechanism for the combustion of alkanes over platinum is thought to first involve interaction between the C2 hydrogen atom and a platinum atom. The hydrogen reacts with adsorbed oxygen to form water and the remaining hydrocarbon then readily reacts with dissociated oxygen on the platinum surface.

1.4.6 Other components

Although the above are the major components legislated for, they are not the only emissions found in exhausts. SO_2 is an unavoidable consequence of sulphur in fuels. Implementation of TWCs was limited until sulphur concentrations in fuel could be brought down by treatment technologies as SO_2 is a potent poison for many catalysts. In modern fuels in developed countries, the concentration of sulphur in fuels has been brought down to extremely low levels. SO_2 is still an important consideration for very basic materials, perovskites for instance, typically have a basic metal cation that is susceptible to the formation of sulphates. In traditional catalytic converters SO_2 can poison both the precious metal surfaces and the ceria. As a result a sacrificial agent barium oxide is used to reduce long term deactivation

Additionally there are other minor considerations with fuel additives. In Canada, methylcyclopentadienyl manganese tricarbonyl is added as an anti-knocking agent. The manganese will be partially combusted and much of the manganese will be deposited on the catalyst in the form of ash. This is not considered a problem for current catalytic converters on the market, but for any significant changes in material the effects of fuel additives may have on their activity must be considered.

1.5 PGM free catalysts

It has long been the goal of emissions control to eliminate the requirement for platinum group metals from catalytic converters. A three way catalytic converter can represent a very significant portion of the expense of manufacturing and so drives up the cost of the vehicle significantly. It is also a serious barrier to implementation in poorer countries where the option to have a PGM catalyst on board isn't economically feasible. However, PGMs are extremely effective materials and alternatives are confronted with several issues related to durability and cold-start efficacy. One material that has received a lot of attention is the perovskite group of metal oxides.

1.5.1 Perovskites[19]

Perovskites are materials which share the structure of $CaTiO_3$, a mineral of the same name and it refers to the structure shown in Figure 8, which is an example of an ideal Perovskite. Ideal perovskites have a cubic structure where the larger cation A^{2+} has a twelve-fold coordination to oxygen anions and B^{4+} which is coordinated to six oxygen atoms.

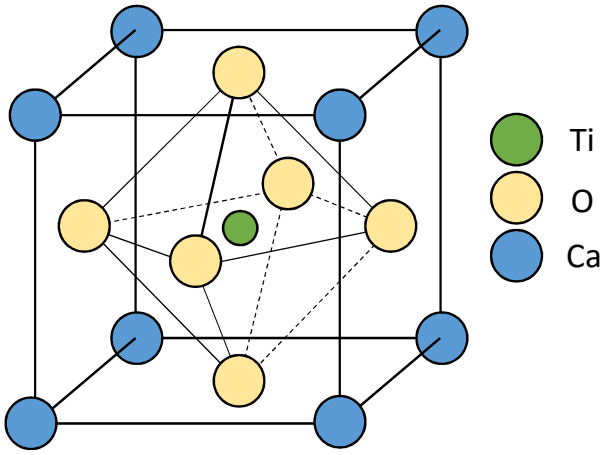

Figure 8. Example of the Perovskite structure using $CaTiO_3$ as a model.

Perovskite-phase mixed oxides are promising candidates for the treatment of exhaust gases and they have the potential to be very cheap in comparison to current catalysts based on noble metals and rare earth oxides such as ceria. Perovskites potential arises from a highly customisable atomic configuration $A^{2+}B^{4+}O_3$ or $A^{3+}B^{3+}O_3$ and about 90% of the metallic elements are suitable for incorporation into these structures. Catalytic activity arises from the non-stoichiometric arrangement of atoms in the lattice and oxygen vacancies introduced by variation of oxidation state. This can be used to control the number of oxygen vacancies and hence the catalytic activity of the samples. Ions suitable for incorporation in this framework are described in Equation 3, where r_A is > 0.09 nm, r_B is > 0.051 nm and r_O is the radius of O_2. Typically,

the A ion is a group 1 or 2 metal or a lanthanide, while the B site is occupied by a suitable transition metal.

$$t = \frac{(r_A + r_O)}{\sqrt{2}\,(r_B + r_O)} \quad (3)$$

Deviation from the ideal cubic Perovskite structure occurs when the t values from equation 1 are less than or greater than 1. Above and below this value, this idealised structure is distorted to accommodate the ions into the lattice. Any change in charge, or size or variations in structure by the partial substitution of A or B lattice ions will result in a distortion of the positions of the oxygen atoms in the lattice. Varying the charge on either cation will also result in either a deficiency or overabundance of charge, this is accounted for by the introduction of anionic or cationic vacancies (typically anionic in Perovskites) in the lattice in order to preserve the neutrality of the compound. Such changes can give rise to vacant oxygen sites which are responsible for catalytic activity.

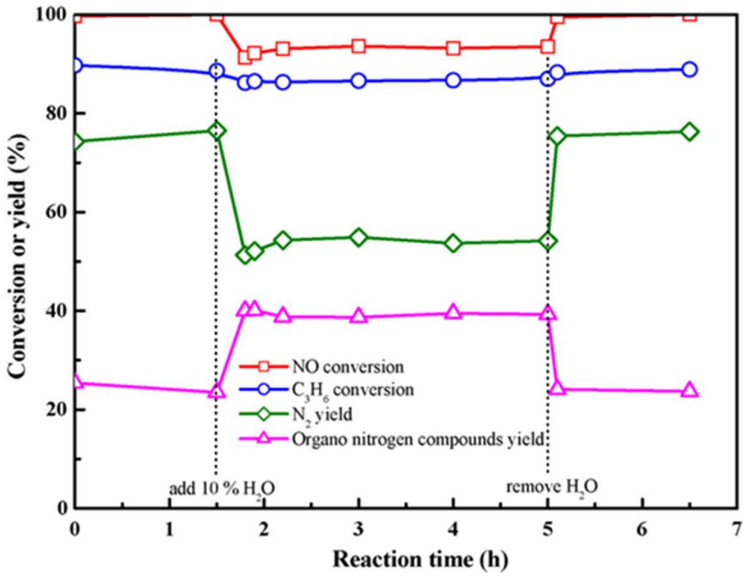

Figure 9[4] Reversibility of vapour deactivation for $LaFe_{0.8}Cu_{0.2}O_3$ during NO reduction by propene in the presence of oxygen. Conditions: 3000 ppm NO, 3000 ppm C_3H_6, 1% O_2, 0 or 10% H_2O, 600 °C, 50,000 h^{-1}

Base metal perovskites as catalysts for exhaust gas treatment have several problems to overcome in order to pass the requirements of automotive emissions legislation and economic reality. Firstly, with the rising cost of fuel, increasing numbers of manufacturers are looking towards lean burn engines to ensure complete combustion, as a result future catalysts would ideally be capable of operating in oxygen rich environments. Perovskites have particular issues eliminating NO_x emissions under these conditions. The problem has thus far been tackled by using a small quantity of perovskite in tandem with PGMs; however other routes could exist to address this problem such as the improvement of existing perovskites through dopants, ie adding reduction catalysts such as Rh. Secondly, steam deactivation is an issue; approximately 8% of exhaust gas is H_2O and it has a significant impact on N_2 yields when reduced by hydrocarbons (Figure 9). While this is entirely reversed on the elimination of H_2O from the feed this is not a feasible solution for applications on automobiles. Steam itself is likely to be a competitive inhibitor as it absorbs to the sites responsible for the catalytic decomposition of NO, this is currently addressed by introducing as many oxygen vacancies as possible. Finally, sulphur poisoning is a major problem. SO_2 can be responsible for competitive adsorption with reactants, or it can react with and decompose the perovskite structure, for example $La(SO_4)_3$ can be formed from $LaFe_{0.8}Cu_{0.2}O_3$ perovskite lattices irreversibly poisoning the catalyst. Some Perovskites have demonstrated a resistance to SO_2 such as $BaFeO_3$ but this often at the expense of catalytic activity.

Initial methods for the production of perovskites were based on the ceramic method[20-22]. This involved heating mixed oxide powders to a high temperature until they come together into the perovskite phase. The ceramic method, while effective for producing the perovskite phase, also produced a catalyst of a very low surface area of approximately 1-2 m^2g^{-1} which is of limited utility for catalysis. Much of the research has been carried out into techniques for synthesising high surface area materials. Coprecipitation[23-27] is a highly tunable and reproducable method for the synthesis of perovskites, catalysts are precipitated in solution from their nitrates, typically with sodium carbonate, surface areas are dependant on the ions used as calcination temperature can be highly variable depending on affinity for the perovskite phase. Sol-

gel procedures[28-32] achieve a high surface area by combusting a a gel of an organic complex of desired metal ions, the combustion stage during heat treatment produces a rapid expansion resulting in a voluminous and high surface area catalyst on the order of 10-20 m^2g^{-1}. Freeze dry and spraying methods have also yeilded good results with high surface area's of up to 30 m^2g^{-1} [33-35]. Such methods take advantage of the intimate mixtures present in the liquid phase that are lost upon even rapid percipitation, this significantly lowers the required temperature for the formation of the perovskite[36].

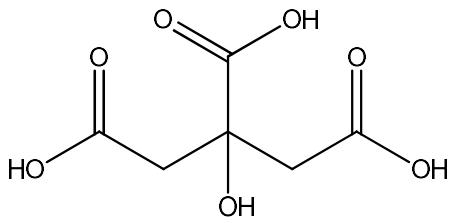

Figure 10. Citric acid structure

The sol-gel method of catalyst synthesis uses a complexing agent to form a gel. Typically, citric acid[30, 37, 38] or oxalic acid[39-41] is used to coordinate to the ions in solution, often with multiple metal ions coordinated to the same organic molecule. Citric acid can chelate at 3 COO^- sites when in solution, allowing the formation of bridging ligands which facilitates an intimate mixture of metal ions. Upon the formation of the gel during synthesis the mixture is dried to remove all water and then the solid is thermally decomposed. At this stage, the sample undergoes a rapid expansion as the ligands combust. This expanded precursor sinters back on conversion to the perovskite phase but still retains much of its high surface area characteristics. Surface areas of up to 30 m^2g^{-1} can be achieved but typically surface areas are around the 20 m^2g^{-1} mark

Supercritical preparations of perovskites have been reported in the literature. Zhang *et al*.[42] produced a highly active $LaCoO_3$ catalyst by simultaneous coprecipitation in supercritical water. These catalysts were reported to have surface areas of between 3-5 m^2g^{-1}. The catalyst shows good activity for toluene and methane oxidation when compared to a citrate method catalyst. However supercritical preparations require complex equipment meaning it can be difficult to scale up to an industrial setting.

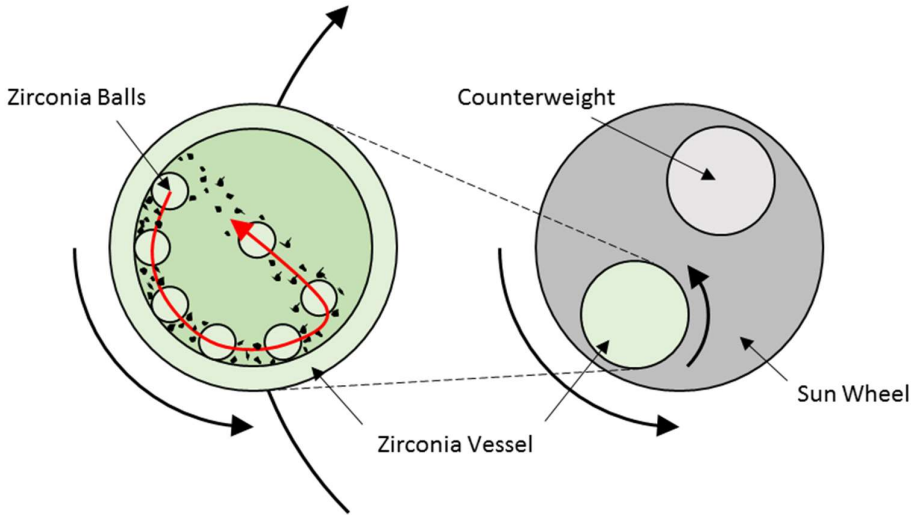

Figure 11. Diagram of a planetary ball mill showing the motion of the cell and balls.

High energy planetary ball milling (Figure 11) has been known as an effective tool for materials synthesis for decades. This technique can drastically reduce the requirement for heat treatments and decomposition steps providing a great deal of localised energy in impacts between the sample and the balls. For the direct synthesis of perovskites from their oxidic precursors, ball milling is an ideal alternative to the ceramic method as it eliminates the requirement for prolonged and aggressive heat treatments that reduce the surface area so dramatically. Such mechanochemical procedures can even replace entirely the requirement for a heat treatment step and consequently reduce the sintering that occurs during heat treatment, providing a route for relatively high surface area perovskites.

Mechanochemical sythesis often results in structural defects and vacancies that are thought to be the active sites of perovskites in catalysis, and because the grain size is kept to a minimum, there will be an increased number of grain boundaries known to be important for oxygen transport. An isotopic analysis[43] demonstrates the extent of oxygen mobility in and between perovskite crystals (Figure 12). Logically, if there are more grain boundaries then oxygen transport will be enhanced throughout the perovskite, increasing its ability to regenerate after carrying out a Mars-Van Krevelan oxidation with oxygen from the bulk. Such grain boundaries are also porous, increasing the effective surface area of the catalyst. With greater surface area, more active sites

are avaiable allowing the catalyst is will be able to turnover more molecules in a given time and reduce the risk of mass transfer limitations.

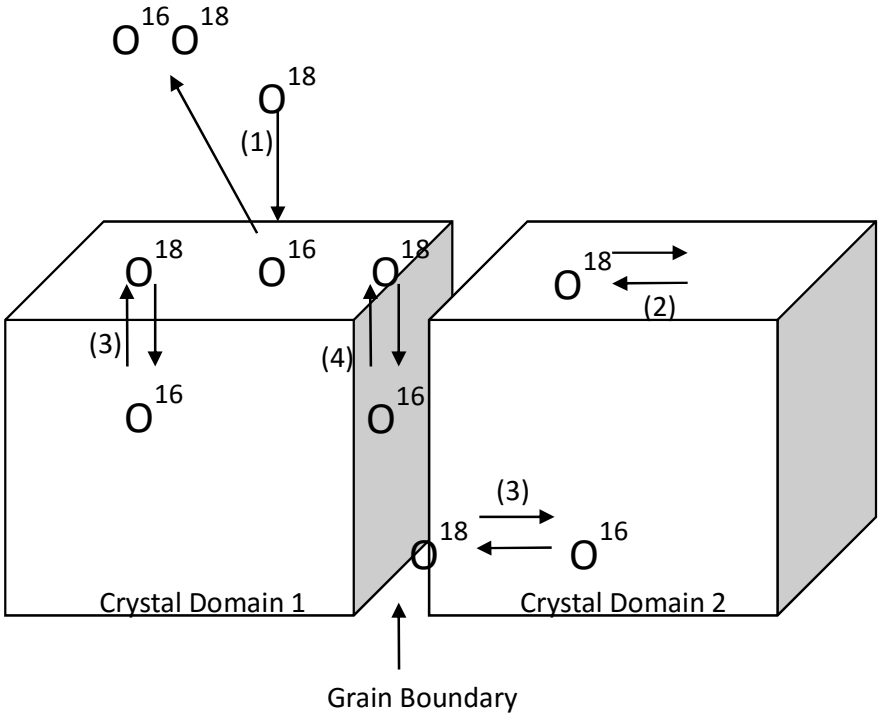

Figure 12. Oxygen diffusion and transport on perovskite surfaces (2), into the bulk (3) and along grain boundaries (4) by isotopic analysis.[43]

The important paramters in ball milling are the ball mass to sample mass ratio and the speed of the mill. These two variables ultimately define the energy input into the system. Greater ball mass means that for a given acceleration there is more energy input into the system. The speed of the mill is also important, as the kinetic energy of a system is half the mass multiplied by the square of the velocity (equation 4) and that due to material/space constrictions in the mill. It is often easier and more effective to vary the speed of the mill. Due to differences in the contruction of mills between manufacturers, the speeds between models of mill often does not translate directly as a consequence of sunwheel diameter and cell diameter.

$$KE = \frac{1}{2}mv^2 \quad (4)$$

$LaMnO_3$ perovskites synthesised by this method[44] have achieved no more than 10 m^2g^{-1} which is not an exceptional surface area for this class of catalyst. The use of additives and different atmospheres had provided some progress however[45] with water soluble salts used to increase the surface area of the catalyst. The salts occupy space in the perovskite lattice after formation and are removed by leaching in water NaCl was used as an additive in the formation of modified Lanthanum manganite catalysts which achieved surface areas of 28-45 m^2g^{-1}. ZnO can also be used as a grinding agent which is then removed with ammonium chloride and achieved surface areas as high as 83 m^2g^{-1}. However while this technique is effective for improving surface area it detracts from the main advantage of ball milling which is the reduction of solvent waste streams which adds to the cost of production.

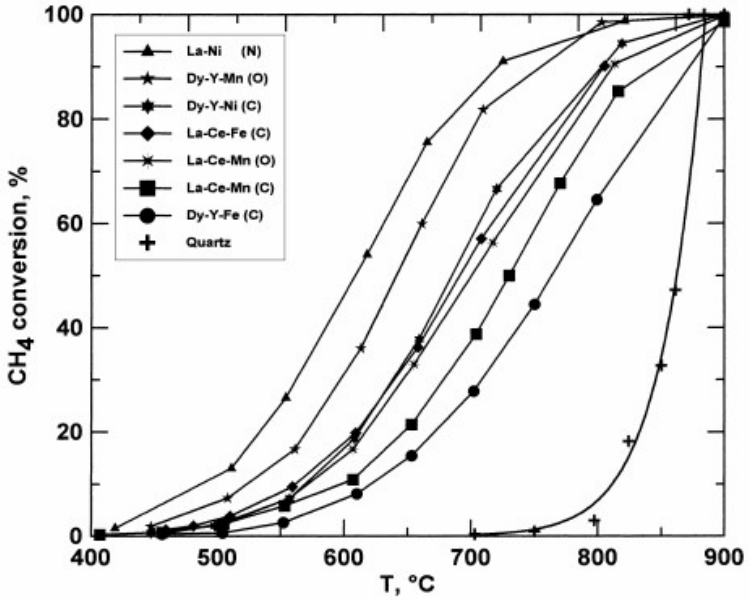

Figure 13.[46] The effect of temperature on methane conversion for powder catalysts (0.4% CH_4, 2% O_2 in He, GHSV 60,000 h^{-1}): C = Carbonate precursor; N = Nitrate precursor; O = Oxide precursor.

Mechanochemically synthesised perovskites have also been demonstrated as methane combustion catalysts by Ciambelli *et al.*[46], an increasingly important area of

exhaust emissions control. Methane is considered one of the hardest hydrocarbons to combust hydrocarbons and is very stable, C1 emissions account for the vast majority of hydrocarbon slip from the tail pipe. The researchers demonstrate that catalysts prepared by mechanochemical grinding from a variety of different precursors perform effectively and with great variation over different configurations (Figure 13). S. Petrović *et al.*[47] have also demonstrated the efficacy of various mechanically prepared perovskites based on the formula $LaMO_3$ where M = Mg, Ti, Fe (Figure 14). The authors also note that the stability of the catalyst was significantly influenced by the abundance of one particular ion, Fe, and that the active component of the catalyst was likely an Fe(II) Fe (III) redox couple.

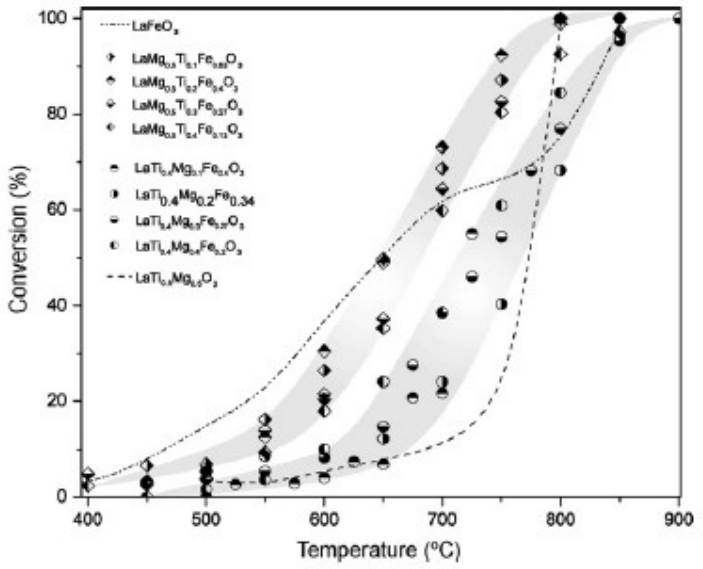

Figure 14.[47] Methane conversion over various $LaMO_3$ catalysts, GHSV = 100,000 h^{-1}, 1%CH_4, 15%O_2 and N_2 balance.

Much of the research around perovskites for exhaust gas catalysis has focused on perovskites with lanthanum in the A site such as lanthanum manganite, lanthanum cobalt oxide, and lanthanum ferrite and derivatives thereof. Lanthanum ferrite doped with palladium and other PGM metals is often discussed in the literature for exhaust specific applications[48-51].

1.5.2 Intelligent catalysts

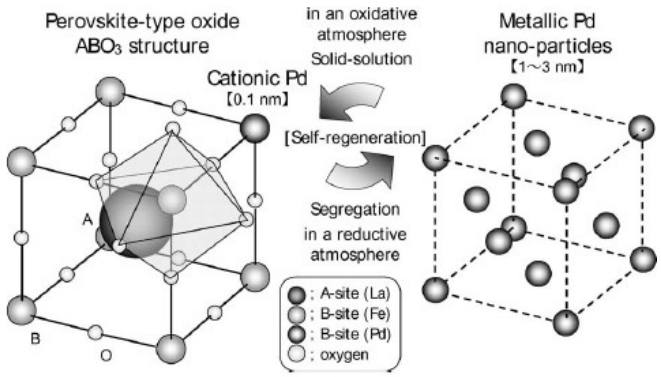

Figure 15.[49] Demonstrating the self-regeneration aspect of the 'intelligent catalyst'.

The 'intelligent catalyst' is a concept described by Tanaka *et al*.[48] It is a Lanthanum ferrite perovskite with a B-site substitution of palladium. The 'intelligence' part of this catalyst is the way in which it exploits the rapid oxidation and reduction of small palladium nanoparticles to regenerate the palladium (Figure 15). Under reducing conditions the palladium forms small metallic nanoparticles of approximately 1-3nm[52] in size, while oxidising conditions cause the Pd to distribute into the perovskite lattice. When exposed to the oscillating conditions encountered in an engine's exhaust the result is a self-regenerating catalyst with extraordinary long term stability even under harsh conditions (Figure 16). Techniques such as this one can be used to great effect to increase the efficacy and life time of an already effective precious metal catalyst.

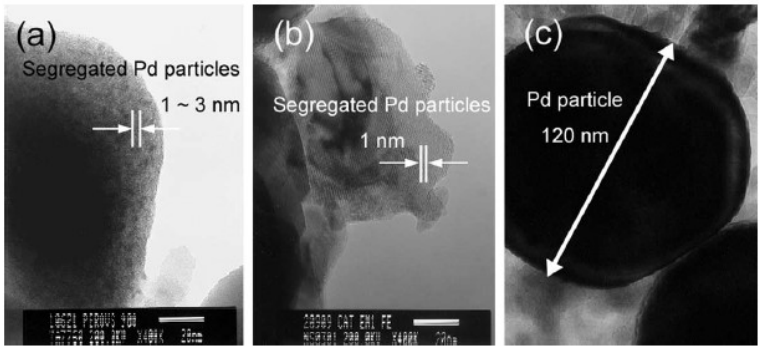

Figure 16.[53] TEM photographs for (a) $LaFe_{0.57}Co_{0.38}Pd_{0.05}O_3$, (b) $LaFe_{0.95}Pd_{0.05}O_3$ and (c) Pd/alumina, after engine ageing at 900 °C for 100 h.

These catalysts are prepared by a sol-gel reaction and show an excellent low temperature activity for CO oxidation[54] in comparison to a basic $LaFeO_3$ catalyst. Figure 16 shows the activity of Pd supported on $LaFeO_3$ and it can be seen to be as effective as the intelligent catalyst in its reduced state (Figure 17). While the activity isn't as great, the long term stability is greatly enhanced.

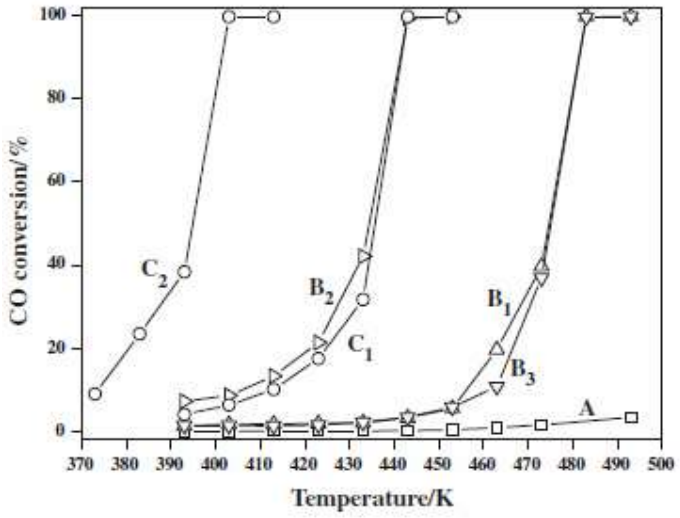

Figure 17.[54] Oxidation of CO on $LaFeO_3$ (a), and $LaFe_{0.95}Pd_{0.05}O_3$ (b) :B1 as-prepared, B2 pre-reduced, B3 consecutive reduction–oxidation; and $Pd/LaFeO_3$(c): C1 as-prepared and C2 pre-reduced. 1% CO, 20% O_2, He, 18,000 mL/(g h)

1.5.3 Silver doped perovskites

Silver has been used as an oxidation catalyst for the combustion of CO and hydrocarbons[55, 56] and has often been supported on a high surface area support such as alumina or silica. Silver also has exceptional activity for the decomposition of NO[57-59]. However silver has several problems that impede its implementation, first is that silver oxide is highly volatile and readily formed in harsh oxidising conditions and secondly silver has a very low melting point relative to commercial catalysts, and will sinter very readily[8] under exhaust conditions. If the silver could be stabilised in the catalyst,

perhaps in a method similar to the 'intelligent catalyst' mentioned earlier, then it may be of more utility.

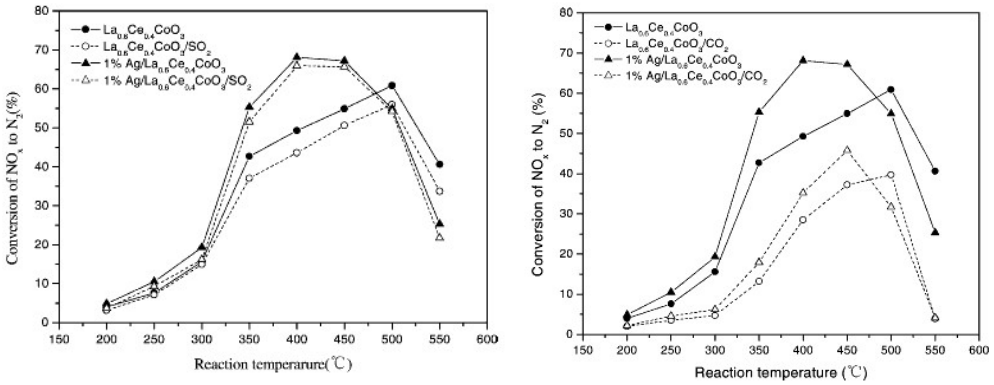

Figure 18. Effects of 1 wt% silver doping on the reduction of NO to NO_2 in $La_xCe_xCoO_3$. NO = 1000 ppm, O_2 = 8%, GHSV = 30,000 h^{-1}.

Silver doped perovskites have been utilised for NO reduction in exhaust applications before[60-62] and have shown good activity. Figure 18 shows the effects of 1 wt% silver supported on a cerium doped lanthanum cobaltite (Figure 18)[63]. Liu et al. also found that these catalysts were more resilient to SO_2 and H_2O poisoning and less to CO_2. Interestingly, they also find that the presence of oxygen, usually a potent inhibitor of NO reduction was actually critical for the performance of the catalyst. Kumar *et al.* showed a lanthanum manganite catalyst doped with barium to be active for the decomposition of N_2O, a potent greenhouse gas, they demonstrate that the incorporation of silver and barium altered the ratio of Mn^{3+} to Mn^{4+}, the redox couple attributed to the activity[62].

1.6 Low-PGM catalysts

The platinum group metals are extremely effective and resilient catalysts with outstanding activity for oxidation and reduction reactions in exhausts. Replacing them entirely while retaining their excellent catalytic ability is an extremely difficult task, and

PGM catalysts have subsequently remained the status quo since their inception in the 1970's. For this reason, promoting the activity of these catalysts, rather than simply increasing metal loading, is a viable alternative to simply increasing the metal loading as legislation increases in severity which suffers from diminishing returns at a substantial cost.

1.6.1 Platinum group metals

The platinum group metals utilised in exhaust catalysis are typically a mixture of platinum, palladium and rhodium, platinum for oxidation, palladium for oxidation and reduction and rhodium as a reduction catalyst. Platinum is the most unreactive of the three metals, however its oxide, which forms under prolonged hot and oxidising conditions, is more prone to sintering than palladium. Palladium despite its lower melting point than platinum, has more durable nanoparticles on account of its more stable oxide. Rhodium very readily forms an oxide when heated and reacts with supports such as alumina as detailed in equations 5-7.[14] As it is the metallic phase that is active for NO reduction and, oscillation between rich and lean conditions is required. As rhodium is quick to oxidise and slow to reduce, maintaining the metallic phase is critical for NO emissions regulations to be met.

$$2Rh + 1.5O \rightarrow Rh_2O_3 \quad (5)$$

$$Rh_2O_3 + Al_2O_3 \rightarrow Rh_2O_3.Al_2O_3 \quad (6)$$

$$Rh_2O_3.Al_2O_3 + 3H_2 \rightarrow Rh + Al_2O_3 + 3H_2O \quad (7)$$

The other PGM metals are not suited for TWC conditions, iridium has an oxide form that is too volatile under the extreme conditions in exhaust, as do ruthenium and osmium (which is both volatile and extremely toxic). This for all practical purposes limits the PG metals to platinum, palladium and rhodium.

1.6.1 Ceria

One such method to boost activity is to provide an oxygen storage and transport component to a catalyst such as ceria. Ceria is very readily reduced from the +4 to the +3 oxidation state by losing an oxygen atom which provides a source of oxygen during fuel rich, oxygen poor excursions[64], additionally it provides readily available oxygen to the metal particles to carry out oxidation of CO and hydrocarbons. Ceria was found to be extremely effective and found its way into the earliest catalyst washcoats, %wt loadings of 3% saw a marked improvement in efficiency for the CO-NO crossover as well as improved hydrocarbon conversion under lean conditions.[65] Ceria suffers from some of the same problems as precious metals due to its low concentration ores and occurrence with the other chemically similar lanthanides, making its extraction difficult and costly[66, 67]. Despite this the efficacy of ceria is such that it has become the industrial standard for OSC and oxidation catalysis in car exhausts[68].

Improvements to catalysts since the introduction of ceria have largely been centred on the introduction of further ceria and the modification of preparative procedures to improve contact of the ceria with the precious metals. This increase in ceria had some consequences however as cerium, being a basic metal, has a strong affinity for SO_2. This SO_2 stored on the ceria under lean conditions was then converted to small quantities of H_2S under rich exhaust gas producing a foul odour from the tailpipe. This problem was largely tackled with the use of H_2S scavengers and improvements in fuel quality. The problem however also revealed issues with catalyst lifetime, as fresh catalysts produced larger quantities of H_2S and then gradually stopped converting. It was revealed that the cause of this was the sintering of the cerium oxide to form large, low surface area particles. This was during a time where legislation was demanding increases in longevity of catalysts and as at that time the only solution to tightening regulation was to add more ceria, a solution was required to improve OSC over the catalyst's lifetime.

Ceria is a material prone to sintering and 100% pure, crystalline ceria is not as effective an OSC material as impurities and defects distort the structure enhancing the mobility of lattice oxygen. Therefore, to stabilise ceria a material was needed that could block the sintering of the ceria and introduce defects into the lattice. One of the ways in which high surface area ceria can be stabilised is through the introduction of another metal oxide via coprecipitation or simple mixing, the most well-known and successful of these is zirconia[69]. The addition of zirconia introduces defects within the ceria lattice and greatly enhances the oxygen transport taking place, the degree of OSC can be altered by changing the ratio of ceria to zirconia[9]. In addition to this doping with zirconia has also been shown to improve the stability of ceria by acting as a sintering barrier[70] thus prolonging the high activity of the ceria over the catalyst's lifetime. M. Ozawa *et al.* noted that under hydrothermal aging conditions the average particle size of ceria supported on alumina increased to 27nm while ceria zirconia was found to be 20nm and in general the size reduced with increased zirconia loading up to 50mol%.

Aside from the oxygen mobility, ceria is a particularly effective system because it forms a $Ce^{3+/4+}$ redox couple[71] and so a system that provides an alternative oxygen storage/transport material should potentially contain a similar redox pair to make this oxygen accessible to the catalyst system.

1.6.2 Physical mixing and thermal decomposition of organic salts

One way of modifying the activity of a catalyst is to improve the dispersion of the metal on the support, as often in catalysis an increase in activity is associated with a decrease in particle size. In a standard impregnation procedure, a precious metal catalyst will have a wide range of particle sizes, but for the reactions being catalysed the majority of the work may only be carried out by particles in a small range, therefore the particles that exist outside of this range represent underutilised material, which is increasingly becoming difficult to justify. While there are many methods to control particle size distribution, relatively few are cost effective enough for an industrial setting. In order to come up with a practical solution that can find usage industrially, simplicity and cost must always be at the forefront of priorities.

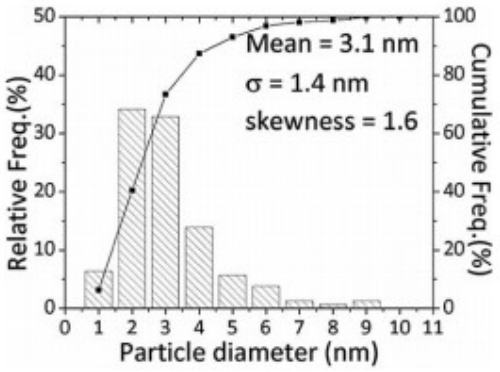

Figure 19. Size distribution of sub-10 nm AuPd alloy particles in the 2.5 wt % Au + 2.5 wt% Pd/C catalyst produced by physical grinding

Physical mixing can be done in a variety of ways, from a simple pestle and mortar procedure[72] lasting a few minutes to long duration using high energy ball milling[73-75]. Low energy, short procedures are ideal for mixing of sensitive systems and avoid the more significant thermal effects of high energy procedures, while high energy milling is suited for carrying out chemistry or significantly altering the particle size of the support. Kondrat *et al.*[72] determined that the physical grinding of gold acetate and palladium acetate produced highly dispersed and active catalysts for alcohol oxidation and direct hydrogen peroxide synthesis, they theorised that the high dispersion achieved was a result of the thermal decomposition of the acetates. The metal acetates used sublimed during the heat treatment and auto-reduced as they decomposed, the result is high dispersion, reduced metal nanoparticles that are highly active for this chemistry (Figure 19). This preparative procedure could potentially be adapted to produce highly dispersed catalysts for other purposes, such as exhaust catalysis, potentially producing results that are extremely difficult to achieve through other more conventional methods with relative ease.

1.6.3 Hydrophobic supports

Hydrophobic materials are a potentially interesting class of catalyst supports that do not strongly interact with water, such materials typically lack the OH terminator group on the surface which is largely responsible for interaction with water by hydrogen bonding, and this strong adsorption can have an inhibitory effect on the catalyst. There are many hydrophobic materials available and with increasing utilisation across a variety of different industries more are becoming commercially available with passing time. Several candidate materials stand out as promising catalytic supports due to their properties and availability; SiC, Si_3N_4, BN, and SnO_2.

1.6.3.1 Silicon carbide

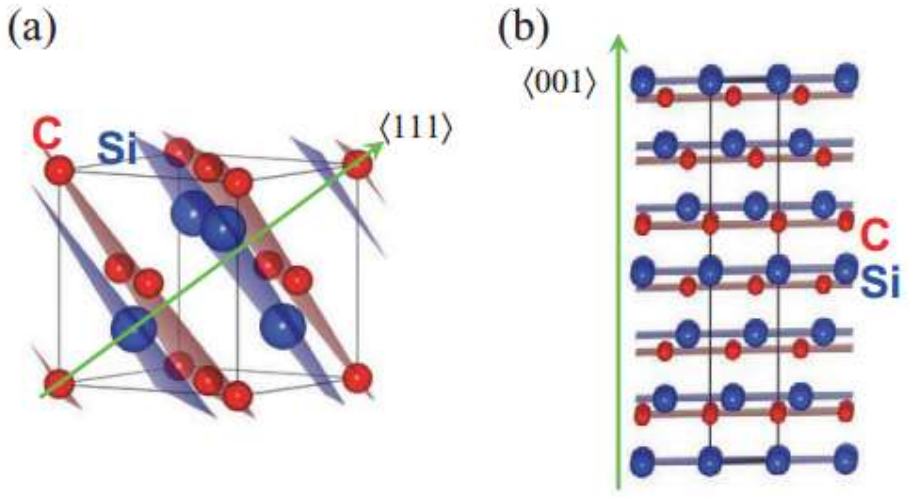

Figure 20. 2 Common polymorphs of SiC, 3C-SiC (cubic zinc-blende structure) and 6H-SiC (Hexagonal wurzite structure)[76]

SiC is a material that has seen a great deal of use in high performance applications because of its extraordinary hardness and inertness and its use has mainly been for engineering applications requiring exotic material properties. Its most common polymorph is α-SiC (Figure 21) and has a hexagonal unit cell, this material is of

limited use in catalysis because of its low surface area, despite this M.Boutonnet Kizling *et al.*[77] discussed the use of α-SiC in catalysis and foiund that it was unable to compete with current industrial standards. β-SiC however is a cubic zinc-blende structure and has a considerably higher surface area which has generated interest in this material as a catalyst support[78].

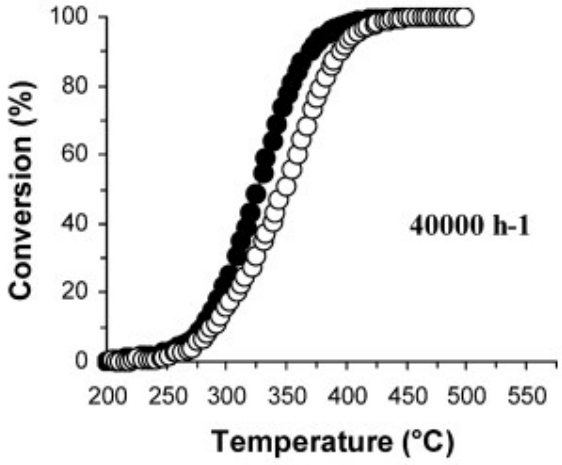

Figure 21. Methane oxidation activity for Pd/SiC prepared by biphasic method

SiC has been a material of significant interest in the exhaust aftertreatment industry for some time, it is currently used as a filter system in diesel vehicles to remove particulates and it has been looked at as a potential catalyst support in three way systems. Initial investigations studied an established system of Pt-Rh on SiC[79]. They found that although performance was lacking, the addition of ceria brought the system in line with current catalyst performance. A further study has looked at a Pd/SiC as a system for emissions control in heavy duty vehicles, a biphasic impregnation was used in which the $Pd(NO_3)_2$ was dissolved in water and impregnated onto beta-SiC and $Pd(acac)_2$ dissolved in toluene was subsequently impregnated[80]. This biphasic method was to take advantage of the dual hydrophobic/hydrophilic nature of the system whereby the pores were postulated to have a more hydrophilic character due to an elevated presence of SiO_2[81]. The authors noted that the performance for CH_4 oxidation was greatly increased over the catalyst (Figure 21) that was formed by a traditional water base impregnation where the catalyst would deposit inside the pore structure.

1.6.3.2 Boron nitride

Boron nitride is another support with potential. BN has 3 major polymorphs, (h-BN which has a graphitic lattice, β-BN which displays a diamond like structure and w-BN which has a structure similar to wurzite. Of particular interest in catalysis is h-BN, which has a non-oxidic hexagonal graphite like structure and is the more stable of the BN isomers, one of which being it's high thermal conductivity[82]. Often in catalyst applications an exotherm is generated during reaction. In a difficult to control environment such as that found in a catalytic converter a large uncontrolled exotherm can lead to catastrophic failure by destroying the catalyst through thermal shock, more routinely however localised heating can lead to the sintering of metal and deactivation over the long term.

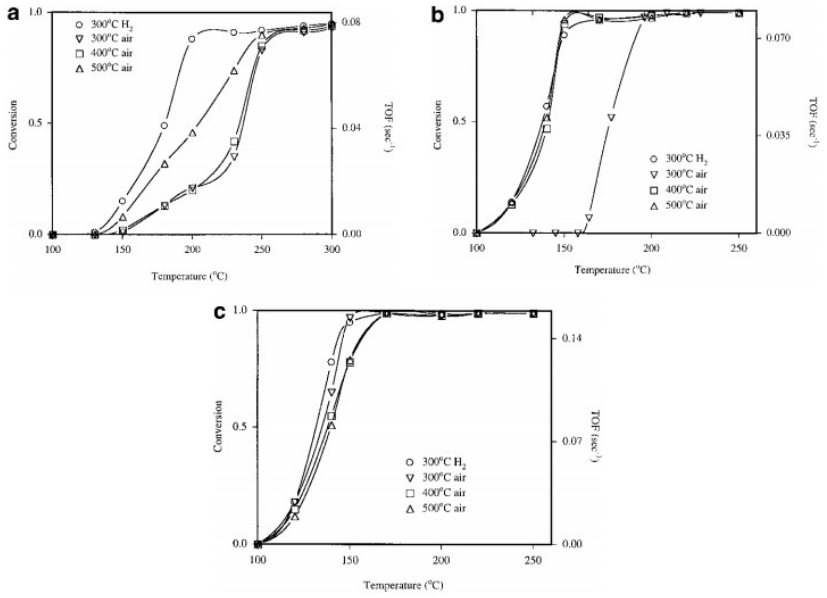

Figure 22[83]. Conversion of 640 ppm of benzene on catalysts under various pre-treatments. 0.37 wt% Pt/Al_2O_3 (a), 0.3 wt% Pt/h-BN (b), and 0.37 wt% Pt/a-BN (c)

h-BN's high thermal conductivity can remove this heat more efficiently than a typical oxidic support such as alumina. Boron nitride also lacks the surface acid and

base sites that strongly interact with water and also present potential structural vulnerabilities to acid or base attack. These properties could potentially control degrading performance and improve catalyst lifetime. BN's hydrophobic character also makes BN resistant to hydrothermal aging and its resistance to oxidation can help it survive soot combustion events. The h-BN structure also contains B-O terminating groups[84] which the diamond structure a-BN lacks. These are thought to be important for the binding of platinum to the catalyst support and has implications for the metal support interaction effect and sintering.

BN has been demonstrated as a hydrocarbon oxidation catalyst[83, 84], with regards to oxidation of hydrocarbons over Pt (Figure 22). It is hypothesised that the Pt is maintained in a reduced state due to the poor metal-support interaction between the BN and the Pt, thus favouring highly mobile surface oxygen species which will carry out oxidation more readily.

1.6.3.3 Silicon nitride

Si_3N_4 is another hydrophobic support material with promise. Si_3N_4 has been studied as a catalyst support previously due to the interest in its relatively high metal support interaction and extremely high thermal conductivity and stability[85-88]. This could favour the formation of small particles and produce a resilient metal phase.

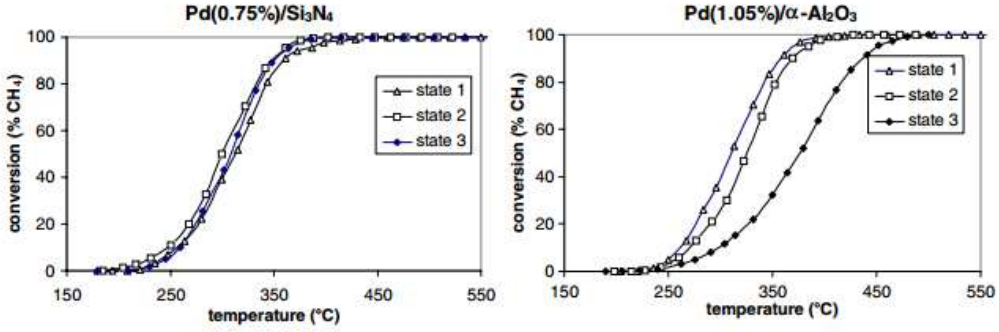

Figure 23. Methane conversion for a 0.75 wt% catalyst (left) and a 1.05 wt% catalyst right) showing fresh (state 1), after 3 h at 600 °C under testing conditions (state 2), and after 3 h at 800 °C. All tests carried out in 4% oxygen, 1% methane, N_2 balance 6.5 L/h^{-1}

In a similar manner to SiC and BN, it has a high thermal conductivity that allows the efficient removal of heat from metal nanoparticles[89]. Palladium supported on Si_3N_4 in particular shows good activity for methane conversion[89], which is widely considered the more difficult hydrocarbon to combust. The compound also shows good stability over time at lower loadings and analysis also reveals a support that is more resistant to oxidation than the Si in SiC. Leclercq *et al.* demonstrated Si_3N_4 to be the optimum support for platinum catalysts in the catalytic reduction of NO with CO, with the caveat that for optimum catalytic activity in a comparison with alumina and chromium carbide, a preparative procedure must be developed to produce a higher dispersion of the catalyst.

1.6.3.4 Tin oxide

Tin oxide has been shown to be an effective hydrocarbon oxidation catalyst support for platinum and palladium, Roth *et al.*[90] have demonstrated the activity of platinum and palladium supported on tin oxide for the combustion of methane (Figure 24). The authors showed that while the use of tin oxide didn't improve Pd catalysts, it enhanced that activity of the Pt catalysts in comparison to Pt/Al_2O_3, however activity was not maintained when using tin oxide as a dopant on an alumina support as the SnO_2 was theorised to sinter.

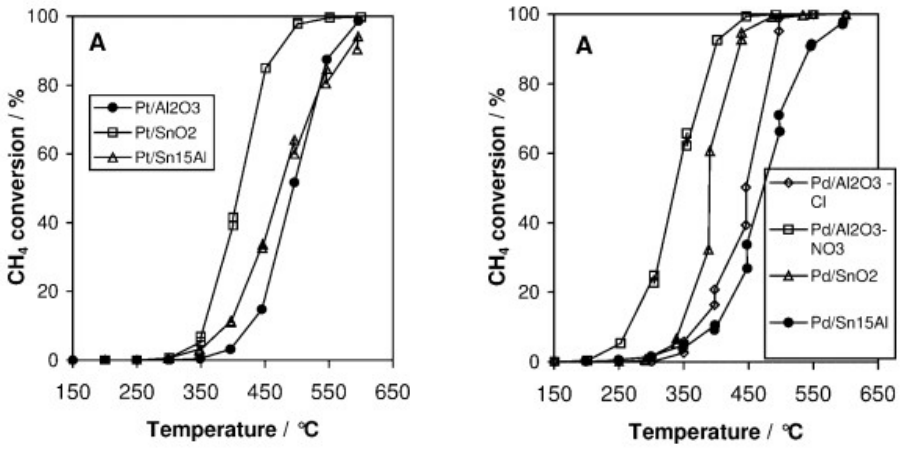

Figure 24.[90] Tin oxide supported on Al_2O_3, SnO_2 and 15 wt% Sn on Al_2O_3.

1.7 Future challenges

As Regulations tighten around vehicle exhausts and carbon emissions become a serious concern for the manufacturers there are a few considerations for the future of gasoline emissions control. There is an increasing pressure to shift towards lean burn gasoline engines. Such engines are highly efficient compared to those with a rich burn cycle and as a result drive down the emissions of carbon dioxide and fuel costs for the consumer. With lean burn technologies however there are a few challenges facing aftertreatment systems. Firstly, without a reducing atmosphere in the exhaust from a rich engine cycle, it will become increasingly difficult to treat NO emissions in gasoline vehicles. Diesel engines already operate in a lean burn cycle and these vehicles have benefited from lax emissions control on NO compared to gasoline, however regulations are tightening and manufacturers are turning towards ammonia SCR technologies to manage NO emissions. Gasoline already has extremely strict emissions control for NO and so lean burn engines will have to meet these requirements. However due to the more oxidising nature in the engine, hydrocarbon and CO emissions are reduced somewhat, this will mean a reduced requirement for an oxidation catalyst and less need for oxygen storage during rich excursions. Additionally, the challenge of increasingly strict legislation has been dealt with, commercially, by increasing the metal loading on the catalyst. Increasing loading, while sufficient for historical purposes, suffers from diminishing returns and results in an extremely expensive catalyst. Reducing the requirement of PGMs not only serves to reduce financial cost, but also environmental, the mining of PGMs is notoriously energy intensive and as rich deposits are depleted the situation doesn't stand to improve.

1.8 Project outline.

The first part of this project will be to find an alternative synthetic procedure to produce supported metal oxide catalysts. This will utilise the organic salt combustion method outlined earlier to produce highly dispersed Pt catalysts that will then be doped with base metal oxides in order to enhance activity.

The second chapter will approach the PGM free aspect of this project, specifically looking at the perovskite family of materials. These provide a vast range of potential combinations and when combined with the large array of methods for their production, the result is a highly customisable series of catalysts. The project will focus on trying to incorporate aspects of the intelligent catalyst discussed previously with a lanthanum manganite catalyst. The goal is to produce a catalyst that will exhibit the endurance of the intelligent catalyst and exceed the activity of supported silver.

The third chapter will look at various hydrophobic supports for aftertreatment. The aim here is to enhance the activity of the precious metals used and thus reduce future requirements for them to mitigate the effects of diminishing returns of simply increasing metal loading on existing materials.

1.9 References

1. M.W. Roberts, *Catalysis Letters*, 2000, **67**, 1.
2. F. Haber, *USA Pat.,* US1202995 A, 1916.
3. J. W. Erisman, M. A. Sutton, J. Galloway, Z. Klimont and W. Winiwarter, *Nature Geoscience*, 2008, **1**, 636.
4. R. Zhang, H. Alamdari and S. Kaliaguine, *Applied Catalysis B-Environmental*, 2007, **72**, 331.
5. S. Xie, J. Wang and H. He, *Journal of Molecular Catalysis A-Chemical*, 2007, **266**, 166.
6. M. Alifanti, R. Auer, J. Kirchnerova, F. Thyrion, P. Grange and B. Delmon, *Applied Catalysis B-Environmental*, 2003, **41**, 71.
7. D. M. Fernandes, A. Alcover, M. J. B. Cardoso and F. M. Z. Zotin, *Catalysis Today*, 2008, **133**, 574.
8. A. E. B. Presland, G.L. Price, D.L. Trimm, *Journal of Catalysis*, 1972, **26**, 313
9. P. Fornasiero, G. Balducci, R. DiMonte, J. Kaspar, V. Sergo, G. Gubitosa, A. Ferrero and M. Graziani, *Journal of Catalysis*, 1996, **164**, 173.
10. M. Guisnet and P. Magnoux, *Catalysis Today*, 1997, **36**, 477.
11. M. Guisnet, L. Costa and F. R. Ribeiro, *Journal of Molecular Catalysis A-Chemical*, 2009, **305**, 69.
12. X. Meng, C. Xu and J. Gao, *Fuel*, 2007, **86**, 1720.
13. H. Davy, *Philosophical Transactions of the Royal Society of London*, 1817, **107**, 45.
14. M. V. Twigg, *Philosophical Transactions of the Royal Society A-Mathematical Physical and Engineering Sciences*, 2005, **363**, 1013.
15. D. Feller, K. A. Peterson and B. Ruscic, *Theoretical Chemistry Accounts*, 2013, **133**.
16. R. Hoffmann, *Reviews of Modern Physics*, 1988, **60**, 601.

17. D. Chatterjee, O. Deutschmann and J. Warnatz, *Faraday Discussions*, 2001, **119**, 371.
18. P. F. Nelson and S. M. Quigley, *Atmospheric Environment*, 1984, **18**, 79.
19. M. B. Gunther, R. Zhang and S. Kaliaguine, *Heterogeneous Catalysis Research Progress*, Nova Science Publishers, New York, 2008.
20. T. Hernandez, F. Plazaola, T. Rojo and J. M. Barandiaran, *Journal of Alloys and Compounds*, 2001, **323**, 440.
21. M. Sanchez-Andujar, S. Yanez-Vilar, S. Castro-Garcia and M. A. Senaris-Rodriguez, *Journal of Solid State Chemistry*, 2008, **181**, 1354.
22. A. A. Leontiou, A. K. Ladavos, T. V. Bakas, T. C. Vaimakis and P. J. Pomonis, *Applied Catalysis A-General*, 2003, **241**, 143.
23. S. B. Ha, P. S. Cho, Y. H. Cho, D. Lee and J. H. Lee, *Journal of Power Sources*, 2010, **195**, 124.
24. M. Mori, N. M. Sammes and G. A. Tompsett, *Journal of Power Sources*, 2000, **86**, 395.
25. J. Tang, M. Zhu, T. Zhong, Y. Hou, H. Wang and H. Yan, *Materials Chemistry and Physics*, 2007, **101**, 475.
26. M. D. Wu, L. H. Xu and D. Weng, *Catalysis Today*, 2004, **90**, 199.
27. F. Zhang, T. Karaki and M. Adachi, *Powder Technology*, 2005, **159**, 13.
28. A. A. Alemi, E. Karimpour and H. Shokri, *Radiation Effects and Defects in Solids*, 2008, **163**, 893.
29. J. Schafer, W. Sigmund, S. Roy and F. Aldinger, *Journal of Materials Research*, 1997, **12**, 2518.
30. Z. J. Sui, L. Vradman, I. Reizner, M. V. Landau and M. Herskowitz, *Catalysis Communications*, 2011, **12**, 1437.
31. H. Xian, X. W. Zhang, X. A. Li, L. Y. Li, H. H. Zou, M. Meng, Q. A. Li, Y. S. Tan and N. Tsubaki, *Journal of Physical Chemistry C*, 2010, **114**, 11844.
32. Z. Y. Zhong, K. D. Chen, Y. Ji and Q. J. Yan, *Applied Catalysis A-General*, 1997, **156**, 29.
33. M. Bremer and H. Langbein, *European Journal of Solid State and Inorganic Chemistry*, 1996, **33**, 1173.
34. J. Kirchnerova and D. Klvana, *Solid State Ionics*, 1999, **123**, 307.
35. S. H. Lee, J. Y. Lee, Y. M. Park, J.-H. Wee and K.-Y. Lee, *Catalysis Today*, 2006, **117**, 376.
36. H. M. Zhang, Y. Shimizu, Y. Teraoka, N. Miura and N. Yamazoe, *Journal of Catalysis*, 1990, **121**, 432.
37. H. Taguchi, S. Matsuura, M. Nagao, T. Choso and K. Tabata, *Journal of Solid State Chemistry*, 1997, **129**, 60.
38. M. S. G. Baythoun and F. R. Sale, *Journal of Materials Science*, 1982, **17**, 2757.
39. D.-Q. Zhang, Z.-C. Qin, X.-Y. Yang, H.-B. Zhu and M.-S. Cao, *Journal of Sol-Gel Science and Technology*, 2011, **57**, 31.
40. A. Naveenkumar, P. Kuruva, C. Shivakumara and C. Srilakshmi, *Inorganic Chemistry*, 2014, **53**, 12178.
41. L. M. Salah, M. M. Rashad, M. Haroun, M. Rasly and M. A. Soliman, *Journal of Materials Science-Materials in Electronics*, 2015, **26**, 1045.
42. J. Zhang, X. Weng, Z. Wu, Y. Liu and H. Wang, *Applied Catalysis B-Environmental*, 2012, **126**, 231.
43. M. V. Landau, R. Vidruk, D. Vingurt, D. Fuks and M. Herskowitz, *Reviews in Chemical Engineering*, 2014, **30**, 379.

44. Q. W. Zhang and F. Saito, *Journal of Alloys and Compounds*, 2000, **297**, 99.
45. S. Kaliaguine, USA Pat., US6770256, 2004.
46. P. Ciambelli, V. Palma, S. F. Tikhov, V. A. Sadykov, L. A. Isupova and L. Lisi, *Catalysis Today*, 1999, **47**, 199.
47. S. Petrovic, A. Terlecki-Barievic, L. Karanovic, P. Kirilov-Stefanov, M. Zdujic, V. Dondur, D. Paneva, I. Mitov and V. Rakic, *Applied Catalysis B-Environmental*, 2008, **79**, 186.
48. H. Tanaka, I. Tan, M. Uenishi, M. Kimura and K. Dohmae, *Topics in Catalysis*, 2001, **16**, 63.
49. H. Tanaka, M. Uenishi, M. Taniguchi, I. Tan, K. Narita, M. Kimura, K. Kaneko, Y. Nishihata and J. i. Mizuki, *Catalysis Today*, 2006, **117**, 321.
50. H. Tanaka, I. Tan, M. Uenishi, M. Taniguchi, M. Kimura, Y. Nishihata and J. Mizuki, *Journal of Alloys and Compounds*, 2006, **408**, 1071.
51. M. Uenishi, H. Tanaka, M. Taniguchi, I. Tan, Y. Sakamoto, S. Matsunaga, K. Yokota and T. Kobayashi, *Applied Catalysis A-General*, 2005, **296**, 114.
52. Y. Nishihata, J. Mizuki, T. Akao, H. Tanaka, M. Uenishi, M. Kimura, T. Okamoto and N. Hamada, *Nature*, 2002, **418**, 164.
53. Y. Nishihata, J. Mizuki, H. Tanaka, M. Uenishi and M. Kimura, *Journal of Physics and Chemistry of Solids*, 2005, **66**, 274.
54. X. Zhang, H. Li, Y. Li and W. Shen, *Catalysis Letters*, 2011,**142**, 1.
55. M. F. Luo, X. X. Yuan and X. M. Zheng, *Applied Catalysis A-General*, 1998, **175**, 121.
56. F. C. Meunier, J. P. Breen, V. Zuzaniuk, M. Olsson and J. R. H. Ross, *Journal of Catalysis*, 1999, **187**, 493.
57. T. Miyadera, *Applied Catalysis B-Environmental*, 1998, **16**, 155.
58. N. Bogdanchikova, F. C. Meunier, M. Avalos-Borja, J. P. Breen and A. Pestryakov, *Applied Catalysis B-Environmental*, 2002, **36**, 287.
59. Z. P. Liu, S. J. Jenkins and D. A. King, *Journal of the American Chemical Society*, 2004, **126**, 7336.
60. A. Machocki, T. Ioannides, B. Stasinska, W. Gac, G. Avgouropoulos, D. Delimaris, W. Grzegorczyk and S. Pasieczna, *Journal of Catalysis*, 2004, **227**, 282.
61. B. Kucharczyk and W. Tylus, *Applied Catalysis A-General*, 2008, **335**, 28.
62. S. Kumar, Y. Teraoka, Amish G. Joshi, S. Rayalu and N. Labhsetwar, *Journal of Molecular Catalysis A: Chemical*, 2011, **348**, 42.
63. Z. M. Liu, J. M. Hao, L. X. Fu and T. L. Zhu, *Applied Catalysis B-Environmental*, 2003, **44**, 355.
64. H. C. Yao and Y. F. Y. Yao, *Journal of Catalysis*, 1984, **86**, 254.
65. G. Kim, *Industrial & Engineering Chemistry Product Research and Development*, 1982, **21**, 267.
66. M. Kraettli, T. Mueller-Spaeth, N. Ulmer, G. Stroehlein and M. Morbidelli, *Industrial & Engineering Chemistry Research*, 2013, **52**, 8880.
67. L. Ling and N.-H. L. Wang, *Journal of Chromatography A*, 2015, **1389**, 28.
68. J. Kaspar, P. Fornasiero and M. Graziani, *Catalysis Today*, 1999, **50**, 285.
69. N. Kruse, A. Frennet and J. M. Bastin, *Catalysis and Automotive Pollution Control IV*, Elsevier Science, 1998.
70. M. Ozawa, M. Kimura and A. Isogai, *Journal of Alloys and Compounds*, 1993, **193**, 73.
71. C. Bozo, N. Guilhaume and J. M. Herrmann, *Journal of Catalysis*, 2001, **203**, 393.

72. S. A. Kondrat, G. Shaw, S. J. Freakley, Q. He, J. Hampton, J. K. Edwards, P. J. Miedziak, T. E. Davies, A. F. Carley, S. H. Taylor, C. J. Kiely and G. J. Hutchings, *Chemical Science*, 2012, **3**, 2965.
73. B. D. Stojanovic, *Journal of Materials Processing Technology*, 2003, **143**, 78.
74. B. D. Stojanovic, A. Z. Simoes, C. O. Paiva-Santos, C. Jovalekic, V. V. Mitic and J. A. Varela, *Journal of the European Ceramic Society*, 2005, **25**, 1985.
75. Q. W. Zhang, T. Nakagawa and F. Saito, *Journal of Alloys and Compounds*, 2000, **308**, 121.
76. T. Muranaka, Y. Kikuchi, T. Yoshizawa, N. Shirakawa and J. Akimitsu, *Science and Technology of Advanced Materials*, 2008, **9**, 8.
77. M. B. Kizling, P. Stenius, S. Andersson and A. Frestad, *Applied Catalysis B-Environmental*, 1992, **1**, 149.
78. C. Pham-Huu, N. Keller and M. J. Ledoux, *Actualite Chimique*, 2002, 8.
79. P. H. Cuong, S. Marin, M. J. Ledoux, M. Weibel, G. Ehret, M. Benaissa, E. Peschiera and J. Guille, *Applied Catalysis B-Environmental*, 1994, **4**, 45.
80. J. M. Nhut, L. Pesant, N. Keller, C. Pham-Huu and M. J. Ledoux, *Topics in Catalysis*, 2004, **30-1**, 353.
81. N. Keller, C. Pham-Huu, C. Estornes and M. J. Ledoux, *Applied Catalysis A-General*, 2002, **234**, 191.
82. G. Postole, M. Caldararu, N. I. Ionescu, B. Bonnetot, A. Auroux and C. Guimon, *Thermochimica Acta*, 2005, **434**, 150.
83. J. C. S. Wu, Y. C. Fan and C. A. Lin, *Industrial & Engineering Chemistry Research*, 2003, **42**, 3225.
84. C. A. Lin, J. C. S. Wu, J. W. Pan and C. T. Yeh, *Journal of Catalysis*, 2002, **210**, 39.
85. P. Granger, C. Dathy, J. J. Lecomte, L. Leclercq, M. Prigent, G. Mabilon and G. Leclercq, *Journal of Catalysis*, 1998, **173**, 304.
86. I. A. Kurzina, F. J. Cadete Santos Aires, J. C. Bertolini, *Silicon nitride supported platinum catalysts for the total oxidation of methane*, **2004**.
87. F. Monnet, Y. Schuurman, F. C. S. Aires, J. C. Bertolini and C. Mirodatos, *Catalysis Today*, 2001, **64**, 51.
88. R. Shang, W. Sun, Y. Wang, G.-Q. Jin and X.-Y. Guo, *Catalysis Communications*, 2008, **9**, 2103.
89. F. Aires and J. C. Bertolini, *Topics in Catalysis*, 2009, **52**, 1492.
90. D. Roth, P. Gelin, E. Tena and M. Primet, *Topics in Catalysis*, 2001, **16**, 77.

Chapter 2: Experimental

2.1 Catalyst preparation

2.1.1 Wet impregnation

Wet impregnation (WI) is a standard technique for the preparation of catalysts[1]. The metal salts are dissolved in a solvent (typically water) and the support is stirred in. The resulting mixture is heated to draw off the solvent and the salt is deposited on the surface of the catalyst. This supported salt is often decomposed by a thermal treatment in one or more of a variety of atmospheric conditions. This technique has wide use in industry because it is very simple, very scalable and economical, making it very attractive for industrial application. While impregnation is satisfactory in many circumstances the control over how nanoparticles are formed is lesser in extent than other techniques. Uneven size distributions can lead to poorer activity or selectivity which in large applications can mean significant lost profits, or the failing of an emissions test.

2.1.2 Preparation of PGM catalysts on alumina via wet impregnation

The appropriate quantity of potassium tetrachloropalladate (Alfa Aesar, 99.99%) or dihydrogen hexachloroplatinate hexahydrate (Alfa Aesar, 99.99%) was dissolved in 50 mL of deionised water and stirred until dissolved. γ-alumina (Sigma Aldrich, <50 nm particle size) was poured into the mixture and stirred to produce a suspension, this mixture was heated to 80 ° C and the temperature was held under stirring until the liquid had almost entirely evaporated. The resulting powder was dried overnight in an oven at 110 °C, recovered, and ground in a pestle and mortar. The ground precursor was weighed and heat treated for 5 h at 500 °C (10 °C min^{-1}) in static air. The resulting powder was weighed and stored in sealed vials.

2.1.3 Preparation of metals supported on hydrophobic materials by modified impregnation

The following technique was adapted from a previous method[8]. The appropriate quantity of platinum (II) acetylacetonate (Alfa Aesar, Pt 48.0% min) or palladium acetylacetonate (Alfa Aesar, Pd 34.7% min) was dissolved in 50 mL of toluene (anhydrous, 99.8%) and stirred until fully dissolved. β-SiC (nanopowder, <100 nm particle size), Si_3N_4 (nanopowder, <50 nm particle size (spherical), ≥98.5%) or SnO_2 (<100 nm particle size) was added to the solution and the resulting mixture stirred for 24h. The toluene was then removed from the powder by rotary evaporation and the powder was recovered, ground and dried overnight at 110 °C. The dried catalyst was then heat treated at 500 °C (10 °C min^{-1}) for 5h under static air. The resulting powder was weighed and stored in sealed vials.

2.1.4 Incipient wetness impregnation

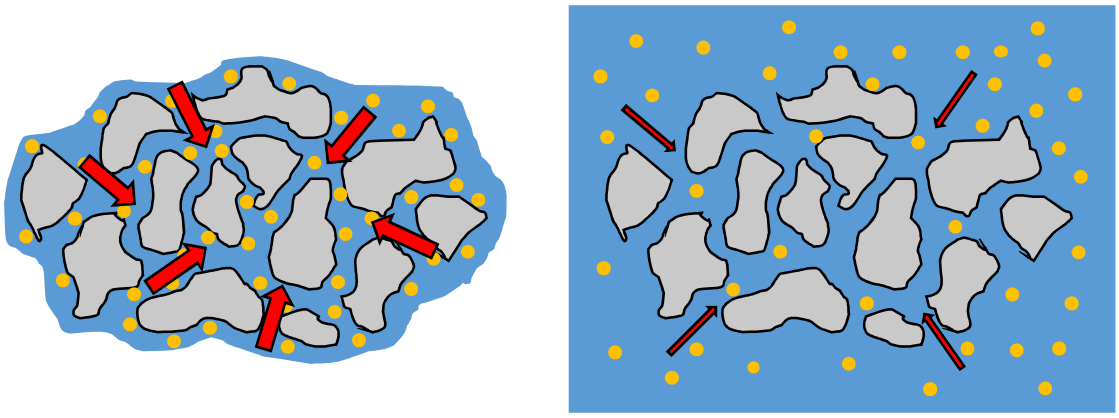

Figure 1: Incipient wetness (left) vs impregnation (right)

Incipient wetness impregnation (IWI)[1] is similar to impregnation in that it loads a dissolved metal salt in a solvent onto a support. The key difference being, that incipient wetness uses a volume of solvent approximately equal to the pore volume. The metal salt is then dispersed through the material via capillary action rather in a diffusional manner (Figure 1). This can lead to a more uniform loading than WI.

2.1.5 Preparation of metals supported on hydrophobic materials by incipient wetness

The appropriate quantity of platinum (II) acetylacetonate (Alfa Aesar, Pt 48.0% min) or palladium acetylacetonate (Alfa Aesar, Pd 34.7% min) was dissolved in a quantity of solvent equal to the pore volume of SiC (nanopowder, <100 nm particle size), Si_3N_4 or SnO_2 (nanopowder, <100 nm particle size) which was determined empirically by weighing a solvent dropped onto a known quantity of support until it attains a paste like consistency. The resulting paste was heat treated in static air at 500 °C (10 °C min^{-1}) for 5h. The resulting powder was weighed and stored in sealed vials.

2.1.6 Physical mixing and thermal decomposition

As outlined by Kondrat *et al.*[7] this test procedure utilised the properties of decomposing organic salts to produce an active and highly dispersed catalyst. The principal behind this preparation is that as the metal acetates decompose they vapourise, resulting in a very high dispersion and tight nanoparticle size distribution. The procedure can be considered green as it produced very little solvent waste and does not require energy intensive steps such as the evaporation of large quantities of water.

2.1.7 Preparation of physically mixed organic PGM salts on alumina by thermal decomposition

The appropriate quantity of platinum or palladium (II) 2,4-pentanedionate, (Alfa Aesar, Pd 34.7%), cobalt, iron or ceria 2,4-pentanedionate (Alfa Aesar) and γ-alumina (Sigma Aldrich, <50 nm particle size) to give the required weight loading were combined in an agate pestle and mortar. The catalyst was ground firmly by hand for 2.5 to 20 minutes to give a uniformly coloured powder, the ground precursor was weighed and heat treated for 2h at 350 °C (5 °C min^{-1}) under an atmosphere of helium. The resulting powder was weighed and stored in sealed vials.

2.1.8 Preparation of coprecipitated perovskites

Metal nitrates (Alfa Aesar, 99%+) were dissolved individually in deionised water in a volumetric flask to give a 0.2M solution. The desired metal nitrates to form the perovskite were mixed in a round bottom flask and heated to 80 °C while stirring. Sodium carbonate (Sigma Aldrich ≥99.5%) in a 0.2M solution was added to the solution drop wise until a pH of 9 was reached, this pH was maintained while stirring for 1h. The resulting suspension was filtered under vacuum and washed 3 times with an equivalent volume of deionised water. The recovered material was dried overnight at 110 °C and heat treated in static air at 600-1000 °C (10 °C min^{-1}) for 2h.

2.1.9 Sol-gel method

The sol-gel method is an organic complexing technique for the production of high surface area materials[2]. When dissolved in water many metal salts will undergo ligand exchange with citric acid as citrate complexes represent a smaller loss of entropy in comparison with an equivalent number of nitrate ligands (with higher degrees of freedom). When the citrate precursor compound undergoes decomposition it evolves a large quantity of CO_2, which causes the material to foam rapidly, this produces a very high surface area oxide. The formation of the perovskite phase involves a high temperature step and perovskites undergo significant sintering, despite this the sol-gel method can produce catalysts with an order of magnitude higher surface area than coprecipitated perovskite.

2.1.10 Preparation of sol-gel perovskites

Metal nitrates (Alfa Aesar, 99%+) in the appropriate quantities were dissolved in water, while stirring, citric acid was added to the solution in a 3:1:1 molar ratio with the metal ions. The solution was heated to 80 °C and stirred until a thick gel was formed, the

gel was dried overnight to form a foam which was then decomposed at 350 °C before being heat treated at an optimal temperature of between 600-1000 °C.

2.1.11 Reactive grinding of perovskites

Perovskites are typically produced from dilute solutions, resulting in a lot of water waste that can be difficult and expensive to treat, the procedure outlined below aims to reduce that waste without sacrificing activity. The nitrates are ground together by hand in a pestle and mortar, a process that is scalable using large industrial ball mills. This method can be seen as similar to a constant pH coprecipitation reaction as the nitrate paste is reacted under extremely alkaline conditions.

2.1.12 Preparation of perovskites by manual grinding

Lanthanum (III) nitrate (Alfa Aesar, 99.9%), manganese (III) nitrate (Alfa Aesar 99.98%) and silver (I) nitrate (Alfa Aesar, 99%) were combined in the desired ratio in a pestle and mortar over 20 minutes to form a paste. To this paste sodium hydroxide was added in a molar ratio of 6:1:1 to the metal ions with a 10% excess. The mixture was ground for 10 minutes until it formed a wet paste. This was then filtered under vacuum and washed with deionised water until the eluting fluid was pH 7. The filtered material was dried overnight at 110 °C and heat treated at an optimised temperature as determined and discussed in chapter 3. The resulting powder was weighed and stored in sealed vials in a desiccator.

2.1.13 High energy planetary ball milling

A high energy planetary ball mill is a physical method for grinding materials. The planetary aspect of the name comes from the mode of motion within the cell (Figure 2). The central ‘sun wheel’ rotates in a specific direction while the sample cell rotates in the

opposite direction, this opposed motion causes the zirconia balls to leave the edge of the cell and traverse a chord across the cell due to centrifugal and Coriolis forces. The energy of the impact of the dense balls against the cell causes localised extreme pressure with enough energy to exact significant chemical changes on a compound such as the combination of oxides into a spinel[3] or perovskite phase[4-6]. They can also be used at low energies to avoid issues with precursor decomposition while still providing a controlled grinding environment.

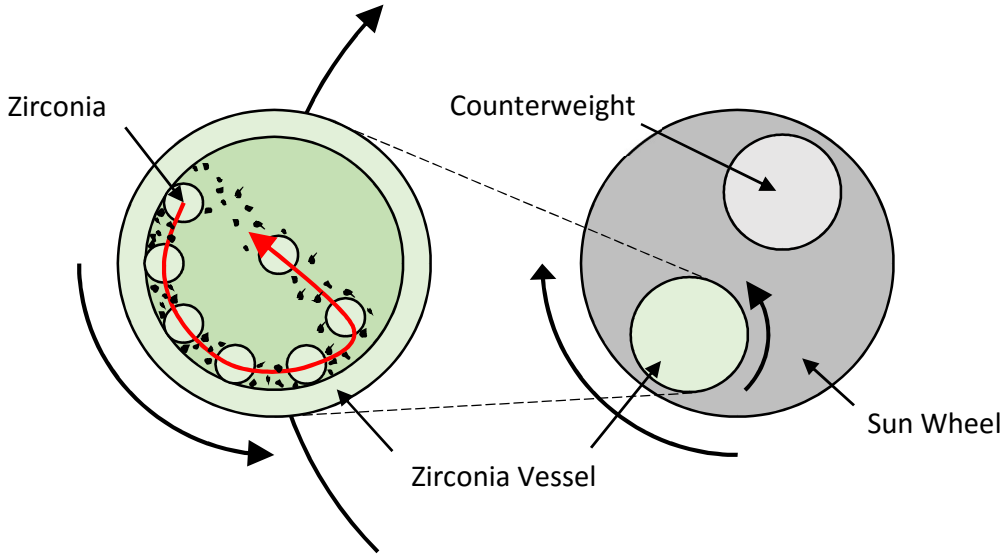

Figure 2. Diagram of a planetary ball mill.

The direct milling of oxide precursors into perovskites is a procedure that takes waste solvent elimination to its extreme limit. In the procedure very minimal or no solvent is used, instead the oxides are placed in a zirconia vessel with zirconia balls and spun at high velocities in a planetary ball mill (Figure 2). Inside the mill the sample will undergo a phase change due to the large input of kinetic energy. It is hoped that such a procedure will produce and preserve a high surface area perovskite as temperatures within the mill are less extreme than those used in conventional methods. The general procedure is outlined below.

While the milling directly from oxides aims to minimise cost and waste output, the grinding of nitrates is an attempt to find a route to a more reproducible method for the formation of $LaMnO_3$ based catalysts. By controlling the speed and duration of the ball mill the energy input can be controlled, also the sealed vessel while grinding offers more control over the atmosphere. For instance, the extremely hydroscopic character of manganese nitrate and sodium hydroxide is limited by the significantly smaller quantity of water vapour present in the dead volume of the mill as compared to the continuously recycling atmosphere present in an open pestle and mortar. Milder grinding conditions were chosen such as to intimately mix the precursors without decomposing them. A general procedure is outlined below.

2.1.14 Preparation of perovskites by high energy ball milling directly from oxides

Lanthanum (III) oxide (Sigma Aldrich, ≥99.9%) and manganese (III) oxide (Sigma Aldrich, ≥99.0%) were mixed together in equimolar ratios, with either the lanthanum or the manganese ion is substituted for an Ag^+ ion in the form of silver (I) oxide (≥99.0%). The combined solids were put into the ball mill with a small quantity of water with the sample volume occupying 1/3 of the cell's capacity with 1/3 volume zirconia balls (7 X 10mm diameter). The precursors were ground at 600 r.p.m. for approximately 6-9h, which was optimised by experimentation and discussed in more detail in Chapter 4. The resulting powder is then either used as is or heat treated at temperature of 600 °C (10 °C min^{-1}) for 5h under static air. The resulting powder was weighed and stored in sealed vials in a desiccator.

2.1.15 Preparation of perovskites by high energy ball milling directly from nitrate precursors

Lanthanum (III) nitrate (Alfa Aesar, 99.9%) and manganese (III) nitrate (Alfa Aesar, 99.98%) were mixed together in equimolar ratios, with either the lanthanum or

the manganese ion substituted for an Ag^+ ion in the form of silver (I) nitrate (Alfa Aesar, 99%). The combined solids were put into the ball mill with a small quantity of water with the sample volume occupying 1/3 of the cell's capacity with 1/3 volume zirconia balls (7 X 10mm diameter). The precursor was ground at 100 r.p.m for approximately 10min. Sodium hydroxide (Sigma Aldrich, ≥98%) was added in a 6:1:1 molar ratio with lanthanum and manganese nitrate at a 10% excess and the milling continued for a duration equal to the initial grind. The resulting paste was then recovered by washing and filtration, dried at 110 °C overnight and heat treated at a temperature of 600 °C (10 °C min^{-1}) for 5h under static air. The resulting powder was weighed and stored in sealed vials in a desiccator.

2.1.16 Preparation of metals supported on supports by physical grinding

The appropriate quantity of precious metal acetylacetonate (typically Pt, Pd, Rh), base metal acetylacetonate (typically Fe, Co) and a support (typically Al_2O_3, SiO_2) to give a specific weight loading were combined in an agate pestle and mortar. The catalyst was ground firmly for 5 minutes to give a uniformly coloured powder. The resulting sample was weighed and heat treated for 2 h at 350 °C (5 °C min^{-1}) under an atmosphere of helium. The resulting powder was weighed and stored in sealed vials.

2.1.17 Statistical design of experiments

Design of experiments (DOE) is a method for maximising the information obtained from the analysis of samples by changing the way in which variables are analysed. In a conventional scientific experiment, variables are selected one at a time and modified to gain an understanding of a system. Sometimes more than 2 variables are modified but the amount of experimentation required increases exponentially. DOE aims to reduce the requirement for a large number of samples by using a 2-factorial design, which is often written as 2^n where n is the number of variables to be studied. Each variable has a binary state which can be a Boolean true or false value, high or low or numeric etc. To test 7 variables, 16 catalysts would be required in a 2 factorial system.

The sacrifice of this system compared to a traditional experimental set up is the resolving power, by reducing the number of experiments, interactions between factors can be lost, depending on the signal to noise ratio of the experiment. The resolution of the information obtained can be improved by adding further samples to these experiments, allowing the interaction of 3, 4 or more variables to be determined.

This technique can be used to optimise a process by generating a response surface. This can indicate the potential positions of peak maxima in optimisation and can determine the factors that interact the most strongly.

All experimental design was carried out on Design Expert 8® developed by Stat-Ease inc. In this thesis a 2 factorial system was utilised exclusively to probe single and 2 factor interaction.

2.2 Reactor and catalyst testing

2.2.1 Reactor setup

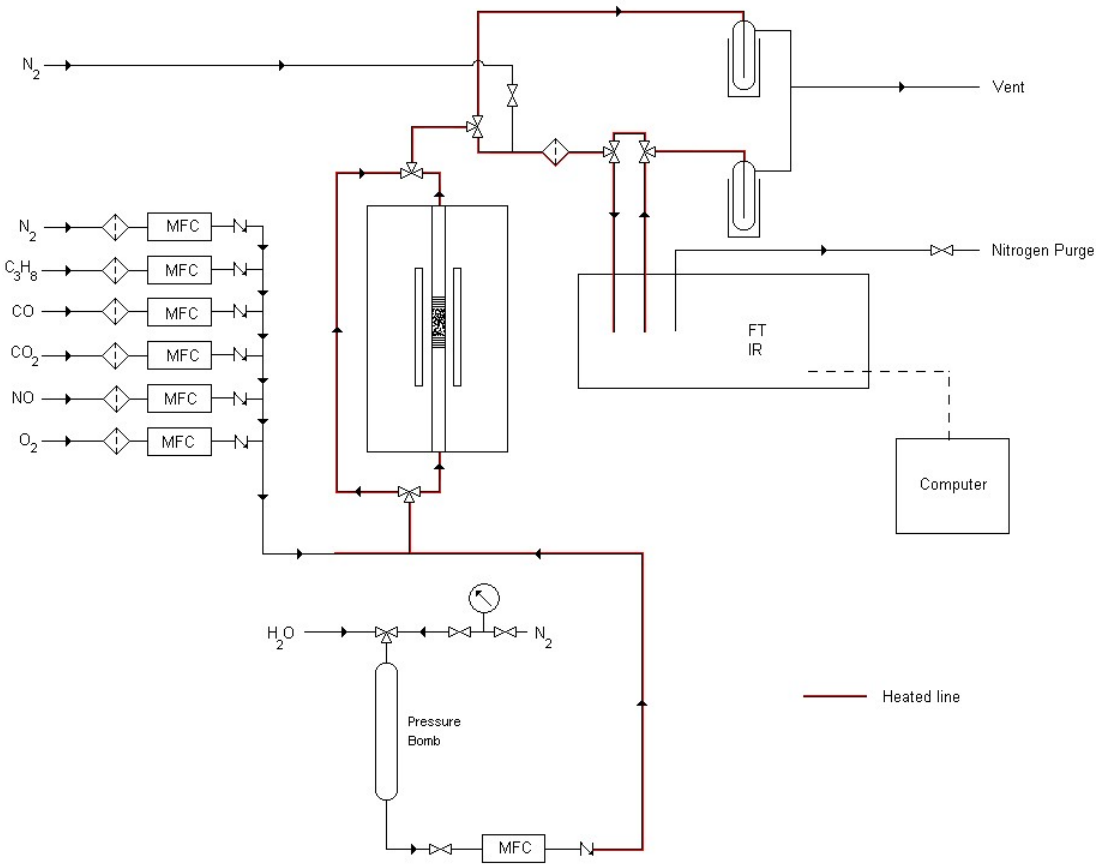

Figure 3. Schematic diagram of reactor setup, ¼" tubing, heated lines at 150 °C

All catalysts were tested on a synthetic exhaust gas rig designed to emulate the conditions found in a petroleum exhaust stream (Figure 3). MFCs modulate the output of N_2 (balance), O_2 (1-8%), H_2O (8%), CO_2 (6%), CO (1%), C_3H_8 (0.1%) and NO (0.03%) with an overall flow rate of 200 mL min^{-1}. Specific gas concentrations were changed and/or eliminated where required. The reactor consists of a 12.7mm OD stainless steel tube passing through an 800W furnace. Inside the tube, 0.3cc of the catalyst in powder form was held between 2 quartz wool plugs to give a space velocity of 40,000 h^{-1}. Gas lines are

heated with cord to 148 °C and insulated with fiberglass tape. The analysis was carried out with a Gasmet DX4000 portable FTIR gas analyser and subsequently vented.

Table 1. Reactor gas mixtures

Lean gas mixture		Stoichiometric gas mixture	
O_2	8%	O_2	1%
CO	1%	CO	1%
C_3H_8	0.1%	C_3H_8	0.1%
NO	0.03%	NO	0.03%
CO_2	6%	CO_2	6%
H_2O	8%	H_2O	8%
N_2	balance	N_2	balance

2.2.1.1 Gasmet™ DX4000 FTIR gas analyser

The FTIR gas analyser consists of a 0.4l rhodium coated aluminium sample cell heated to 180 °C. The IR laser passes into the sample cell and is reflected through by gold coated mirrors to a path length of 5 m. The gas cell is connected to the reactor feed and gives the average composition in the cell, rather than a time specific sample as with GC analysis, the implication of this being that readings must be allowed to stabilise before measurements are taken.

The software for carrying out the analysis is Calcmet™ which is a tool for multicomponent analysis of gases passing through the cell. A scan is carried out every 0.1 seconds, with a minimum scan duration of 1 second, and all scans are averaged to form a 'sample'. For all experiments presented in this document, a scan duration of 60 seconds was used (600 scans). Each sample was then subtracted from a background spectra (5 minutes, 3000 scans of N_2 gas) to give a gas phase rotational vibrational spectra, the theory of which is described in more detail in 2.3.4. These spectra were then compared to internal calibrations to determine the concentration in ppm or percent and a residual (conformity of signal to the calibration file). Three separate scans are averaged to give the final concentrations at a given temperature reported unless stated otherwise.

2.2.1.2 Fourier transform infrared spectroscopy theory

Infrared spectroscopy is the analysis of the adsorption of IR radiation by a sample in order to obtain information about the vibrational modes present in a molecule. Samples that exhibit a change in permanent dipole moment across the molecule are capable of adsorbing an IR photon to change vibrational state. This adsorption wavelength is then characteristic of the particular vibrational mode (Figure 4).

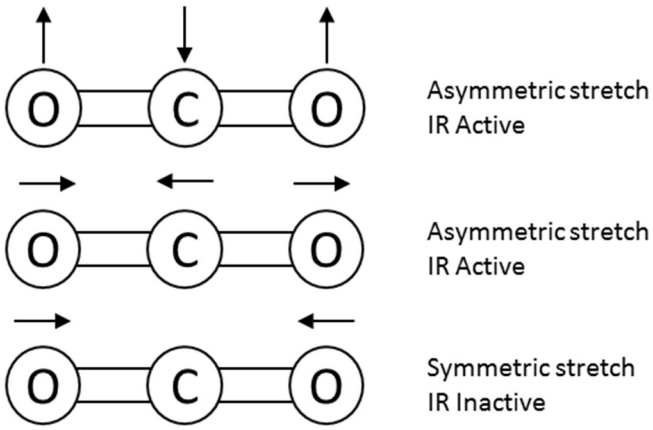

Figure 4. Vibrational modes of CO_2

In the gas phase IR spectroscopy has added complexity from the influence of a molecules rotation despite the fact that rotational modes adsorbs in the microwave region. This complexity arises because the rotational and vibrational energies change simultaneously with the adsorption of IR radiation, resulting in a fine band structure. The more modes of rotation and vibration, the higher the number of peaks and the complexity of the spectra. As a result of this, molecules like H_2O with 3 modes of rotation (due to C_{2v} symmetry) give a very extensive rotational fine structure, whereas CO_2 ($D_{\infty h}$ point group) will have band splitting to a lesser degree. In a multi component gas mixture this has implications for interference.

The selection rules for rotational-vibrational spectroscopy observes a simultaneous change in rotational (J) and vibrational (V) energy, Figure 5 details the transitions which give rise to the origins of each branch. The Q-branch is the transition $\Delta J = 0$, $\Delta V = +1$, in Figure 6, the Q branch is the central peak, individual bands are not resolved. The P branch is $\Delta J = -1$, $\Delta V = +1$ and thus is a lower energy transition,

therefore lying in the lower energy portion of the spectra. The R branch is $\Delta J = +1$, $\Delta V = +1$ and thus occurs at a higher energy region than the Q branch.

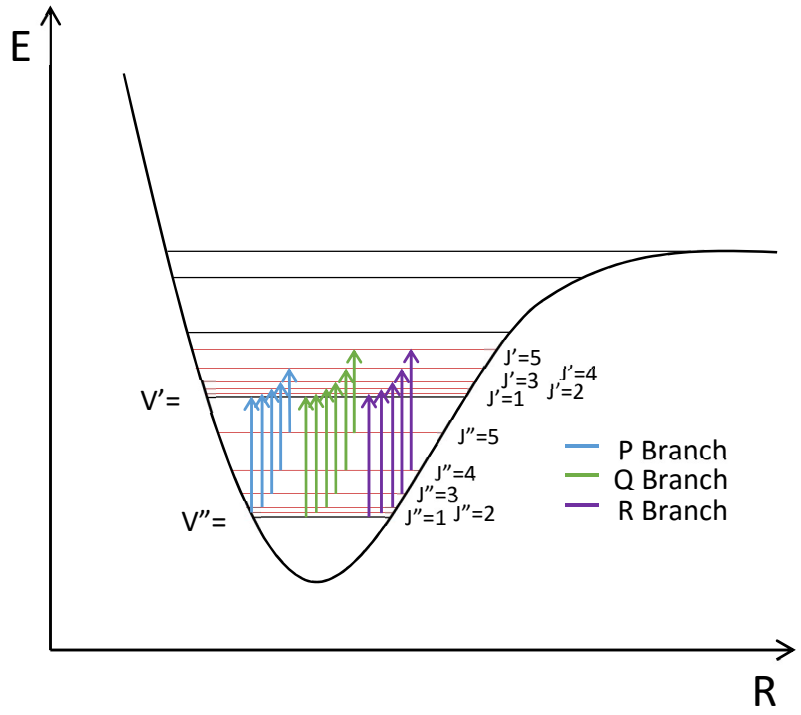

Figure 5 A simplified anharmonic oscillator Energy diagram for linear molecule detailing the transitions that can occur and the single letter names of their branches

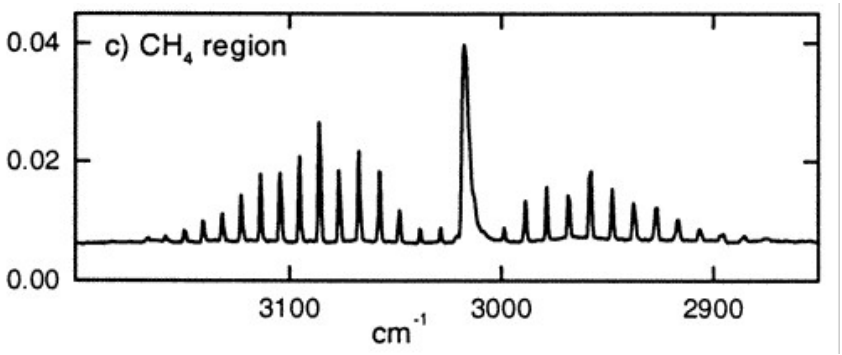

Figure 6 Rotational vibrational spectrum of methane[11], The Q-branch is central, the P-branch on the left side and the R-branch on the right.

For the purposes of exhaust gas analysis, the precise nature of the rotational fine structure is not important, peak intensity is used to determine the concentration of the component gases. The peak intensities were compared against calibration values to give

a concentration value of the particular species in the spectra. Analysis regions were chosen in areas of the spectrum with as little peak overlap as possible in order to give the most accurate possible data. However the effect of interfering peaks can be deconvoluted with post processing algorithms carried out by the analysis software.

2.3 Characterisation

2.3.1 BET surface area Aanalysis and pore size analysis

Brunauer–Emmett–Teller[9] (BET) is the primary technique used for the determination of surface area[9]. BET theory is based on Langmuir theory, while Langmuir theory describes monolayer adsorption, BET compensates for multi-layer adsorption. To do this the BET model makes 3 assumptions.

- At saturation pressure the number of adsorption layers tend to infinity
- Interaction between adsorption layers is negligible
- Langmuir theory can be applied to each layer

The resulting equation derived from Langmuir theory is given in equation 1.

$$\frac{p}{v(p_0-p)} = \frac{1}{v_m c} + \frac{c-1}{v_m c}\frac{p}{p_0} \qquad (1)$$

Where:

p = Equilibrium pressure

p_0 = Saturation pressure

v = Adsorbed gas volume

v_m = Adsorbed monolayer volume

c = BET constant (2.2)

$$c = e^{\left(\frac{E_1 - E_L}{RT}\right)} \qquad (2)$$

Equation 1 can then be used to determine the adsorbed monolayer volume. Typically this analytical technique is carried out using nitrogen as the adsorbate. In order to approach saturation pressure the analysis is carried out at -195.8 °C where the number of layers adsorbed tends to infinity. The BET constant is used as an indicator value, if the number is negative then the data does not fit the model.

2.3.2 Chemisorption[10]

Chemisorption is a technique for measuring the surface area of an active metal species by gas phase titration.

The catalyst is reduced via a hydrogen atmosphere heat treatment, typically for 1h at 200 °C. The sample is then cooled to room temperature and flushed with helium. The catalyst is then exposed to a known volume of an adsorbing gas and the effluent passed over a TCD detector, the process is repeated until the metal surface is saturated. The area under the titration peaks when compared to the reference signal corresponds to the total quantity of gas adsorbed. With an understanding of how the gas adsorbs to the surface of the metal, the surface area can be determined (Equation 3), along with dispersion (Equation 4) and average particle size (Equation 5).

$$MSA = \frac{N_a V_m}{S_f S_d} \qquad (3)$$

Where:

MSA = Metal surface area (m^2 per g)

N_a = Avogadro's number

V_m = Gas adsorbed at monolayer (mol per g of sample)

S_f = Stoichiometric factor of reaction (mol ratio of CO to surface metal atoms)

S_d = Metal surface density (metal atoms per m^2)

$$MD = \frac{V_m A_w 10^4}{wt\%\ S_f} \qquad (4)$$

Where:

MD = Metal dispersion (Percentage)

V_m = Gas adsorbed at monolayer (mol per g of sample)

A_w = Metal Atomic Weight (grams per mol)

wt% = Metal weight Percent

S_f = Stoichiometric factor of reaction (mol ratio of CO to surface metal atoms)

$$D_a = \frac{10^4\ F}{MSA\ D_m} \qquad (5)$$

Where:

D_a = Metal nanoparticle diameter (Angstroms)

F = Shape Factor

MSA = Metal surface area (m^2/g)

D_m = Metal density (grams per metal volume unit)

2.3.2.1 Experimental

Unless stated otherwise in the text, the conditions used are as follows. A known quantity of catalyst, typically between 100 and 500mg depending on density, was reduced under a stream of 10% H_2 in Ar at 200 °C for 1 hour. The sample was then

purged with helium until a static TCD reading was achieved. The sample is then exposed to pulses of CO of a known quantity until readings are stable. The quantity of CO adsorbed in the titration is used to calculate the metal surface area, average particle size and dispersion.

2.3.3 Scanning electron microscopy and energy dispersive X-ray analysis

Scanning electron microscopy (SEM) is a technique to produce an image of a sample from a beam of electrons rather than light (Figure 7), this allows for a significant improvement in resolution over optical microscopes which are limited by the wavelength of visible light at 390 to 700 nm, an electron microscope however is capable of significantly lower resolutions, down as low as a single nanometre.

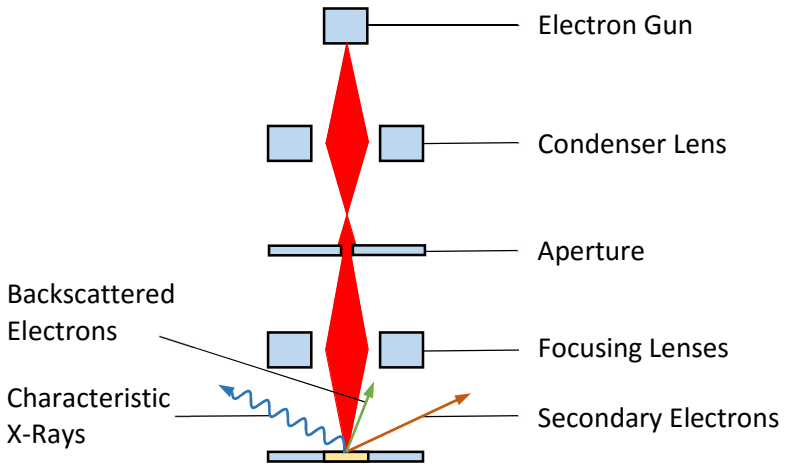

Figure 7 Simplified diagram of scanning electron microscope

The fundamental principles of an electron microscope are much the same as an optical one. The incident radiation is focused by magnets to produce an optimally shaped beam, the focal point of which is manoeuvred to the point of interest on the sample. There are two modes of interaction with the sample, elastic and inelastic scattering. Inelastic scattering con occur by many different processes, including phonon excitation,

continuum X-ray emission, secondary electron emission and core electron ejection while elastic scattering is the source of backscattered electrons.

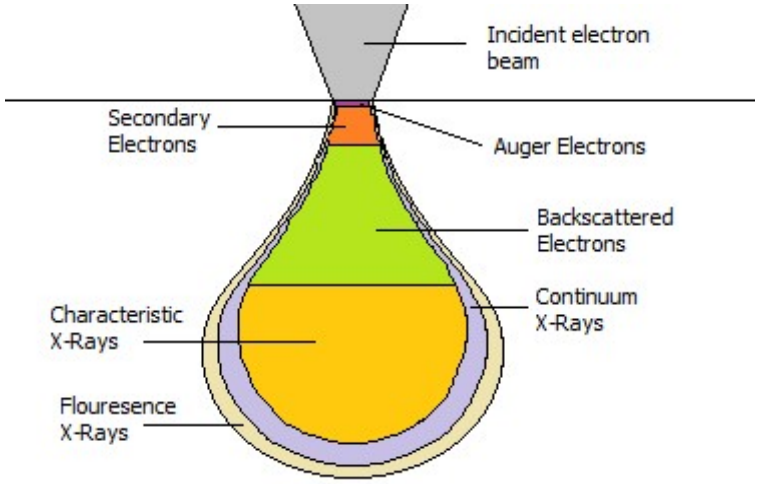

Figure 8 Interaction volume of electron beam with sample, exact size of volume varies with beam voltage and current.

Principally, two main types of electron event are detected in SEM microscopy. Secondary electron emission typically occurs close to the surface (Figure 8) and as result of ionisation events from the beam. Backscatter electrons are electrons deflected almost 180° back in the direction of the incident beam. These are picked up by a circular detector surrounding the beam, electrons are more likely to be deflected in this manner by atoms with a high atomic number, as a higher electron density will make the deflection event more likely; backscatter electrons can be used to identify regions of high electron density (for example, a platinum particle).

Energy dispersive X-ray analysis (EDX) is a technique for investigating the elemental composition of a sample. An incident electron beam of sufficient energy will eject core electrons from the atoms in the sample, creating an electron hole. Electrons from higher energy shells relax into the hole and emit an X-ray of a specific wavelength equal to the energy of the transition which is in turn characteristic of individual elements. (Figure 9) X-ray emissions can then be taken from a series of areas and averaged, or

surfaces can be mapped to reveal the locations of X-ray events from specific areas of a material.

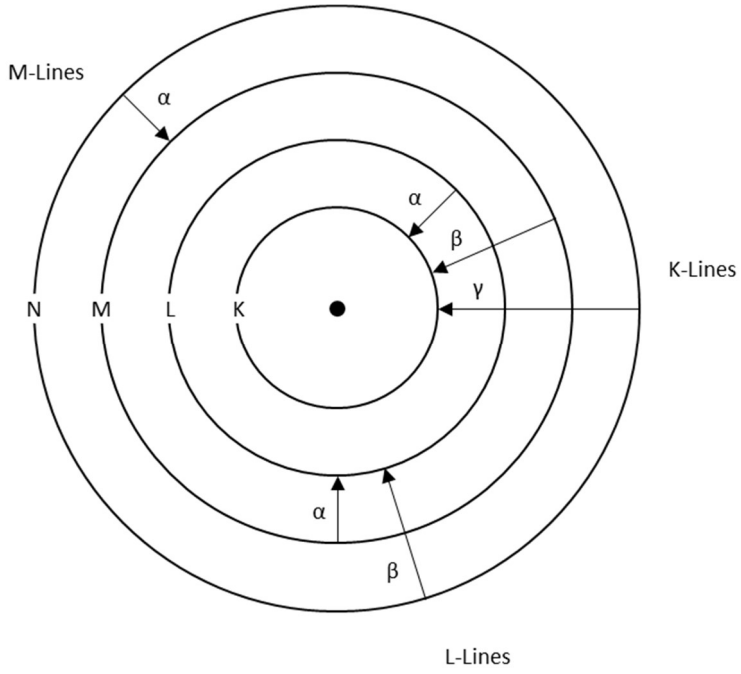

Figure 9 Orbital energies showing origin of X-ray emissions and their labels, K_α wavelengths are of principal interest. X-ray wavelengths are labelled after the shell in which the vacancy initially occurs and the shell from which the electron drops from.

Light elements ($Z < 11$) are difficult to analyse by EDX. Atoms $Z < 2$ have no characteristic X-rays due to having a single orbital, Lithium's K band X-rays are of a very low energy and difficult to detect. Elements from $4 > Z < 11$ do emit characteristic X-rays however they are of low energy and are subject to adsorption by surrounding elements, additionally the outer electrons typically involved in X-ray generation are also involved in chemical bonding causing a shift in the energy of the detected peak which can vary from compound to compound. As a result, effective quantitative analysis starts from sodium in the periodic table. Accuracy is influenced by overlapping peaks where resolution is insufficient to distinguish between two species and peak doubling, where two photons of equal intensity hit the detector at the same time, giving a false reading for a different element of twice the energy of the incident photons.

2.3.3.1 Experimental

All conditions for SEM are listed below unless stated otherwise in the results. A Carl Zeiss EVO 40 scanning electron microscope was used for imaging and EDX. All samples were mounted in a thin layer on carbon discs. For imaging, secondary electron and backscatter detectors are used. Beam conditions vary sample to sample and were selected to give the best possible images. For EDX analysis the beam conditions are kept consistent. A fixed EHT value of 25 keV and current of 25 nA were required in order for optimal X-ray production to occur and the working distance was fixed to 9mm min order to maximise exposure of generated X-rays on the detector. A cobalt standard was used and an Oxford EDX analyser was used to process the results.

2.3.4 Temperature programed reduction

Temperature programed reduction (TPR) is an analytical technique for determining the precise temperature of reduction of a material under an atmosphere of hydrogen. Using the reducibility of a catalyst as a characterisation technique was first proposed by Holm and Clarke[12]. By measuring the TCD signal of a reference flow against the flow over the catalyst the quantity of hydrogen consumed or in excess can be determined, and hence the reducibility of the catalyst determined. The peaks of H_2 consumption curves are taken as the reduction temperature of a species and can be compared with other catalysts and analytical techniques in order to gain an insight into oxidation states of the present elements. The area under the curve can be used to determine the quantity of hydrogen consumed and thus the quantity of reduced material on a catalyst.

2.3.4.1 Experimental

All conditions for TPR are listed below unless stated otherwise. Analysis was carried out using a Thermo TPDRO1100. Approximately 50mg of sample was pre-treated at 120 °C under a 20 mL min^{-1} flow of argon for 45 minutes at 20 °C min^{-1}. For analysis a temperature range of 30 °C to 900 °C in an atmosphere of 10% H_2 in Ar at 10 mL min^{-1} was used with a heating ramp of 10 °C min^{-1}. Integration was carried out in Origin 9.0.

2.3.5 Thermogravimetric analysis

Thermogravimetric analysis is the analysis of a samples mass as it is heated under a specific atmosphere, the weight as well as the change in temperature of the gas flow can be measured to give information about decomposition, sublimation, vapourisation desorption and phase changes in the sample. This information can be used to determine optimal conditions for heat treatment, or indicate chemical changes in the sample under reaction conditions

2.3.5.1 Experimental

All conditions for the dTGA are listed below unless otherwise stated. All dTGA was carried out on a SETARAM Labsys TG-DTA/DSC. The crucible was cleaned and dried thoroughly in air, the clean crucible is placed on the balance apparatus and the balance is tarred. The crucible was then removed from the balance, filled with a small quanitity of sample approximately 50 mg in weight and placed back onto the scales. The temperature and ramp rate is set to 900 °C and 10 °C min^{-1} respectively.

2.3.6 Transmission electron microscopy

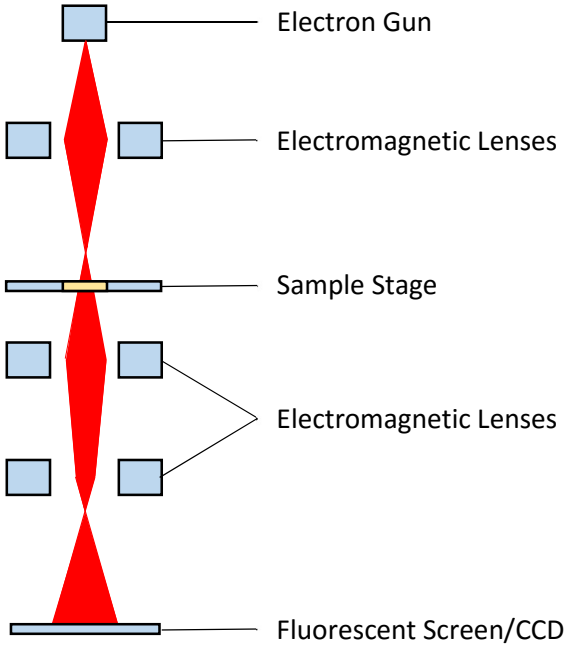

Figure 10. Simplified diagram of a TEM demonstrating the transmission through the sample as opposed to SEM which observes scattered electrons

Transmission electron microscopy is similar in principal to SEM, however it differs in that the image is formed from transmitted electrons as opposed to scattered electrons (Figure 10). The image focuses on single plane within a sample much in the same way as an optical microscope, but with a resolution many orders of magnitude higher, and significantly higher than SEM. Much the same as SEM, TEM can carry out EDX analysis with mapping, albeit at a lower resolution than imaging. This allows for the assignment of localised concentrations of elements but it can also gather information about d-spacing in crystalline samples in a manner similar to X-ray crystallography, the peak maxima and minima are visible as distinct rows, the average spacing of which is useful for identification of specific crystal planes.

2.3.6.1 Experimental

Unless otherwise stated in the results, analysis was carried out on a Jeol TEM 1210 transmission electron microscope. Samples were prepared from a sonicated suspension of material in water, a small volume of which was placed on a carbon mesh. As the water evaporated the solid material was deposited on the grid. Samples were placed in the path of the beam and the transmitted electrons detected by a CCD sensor or directly observed on a fluorescent plate. EDX analysis was also carried out where required.

2.3.7 Powder X-ray diffraction

X-ray diffraction is a bulk analysis technique for the determination of the crystalline phase, crystallite size and lattice strain.

The generation of X-rays is carried out by bombarding a metal source (typically Cu or Mo) with an electron beam. The incident electron ejects a core shell electron from the metal atom and leaves a vacant orbital. The transition of an electron from an outer shell to the vacant core shell results the emission of an X-ray, the energy of which is dependent on the energy lost by the electron in the transition and such energies are specific to the element as orbital transition energies are unique.

X-rays are electromagnetic radiation and so are subject to diffraction. The coherently scattered radiation from the crystal lattice is subject to constructive and destructive interference (Figure 11). Peaks as described by described by Bragg's law in equation 6.

$$n\lambda = 2dsi \qquad (6)$$

Where:

n = Order of reflection

λ = Wavelength of incident radiation

d = Spacing between atomic planes

Θ = Angle of incidence

Single crystal XRD looks at the X-ray diffraction pattern of a single crystal of a given material. The diffraction pattern is measured at all angles of Θ and the resulting spectra will appear as a series of maxima. Powder XRD operates on the principal that in a given powder sample the particles will be randomly oriented and will express all possible reflections at a given angle, the result being that instead of a single refracted beam at a given position, there is a diffraction cone at a given angle where constructive interference is occurring. A single 1D slice of these diffraction cones gives a graph of X-ray intensities against 2Θ, which is the standard method of representing a diffractogram.

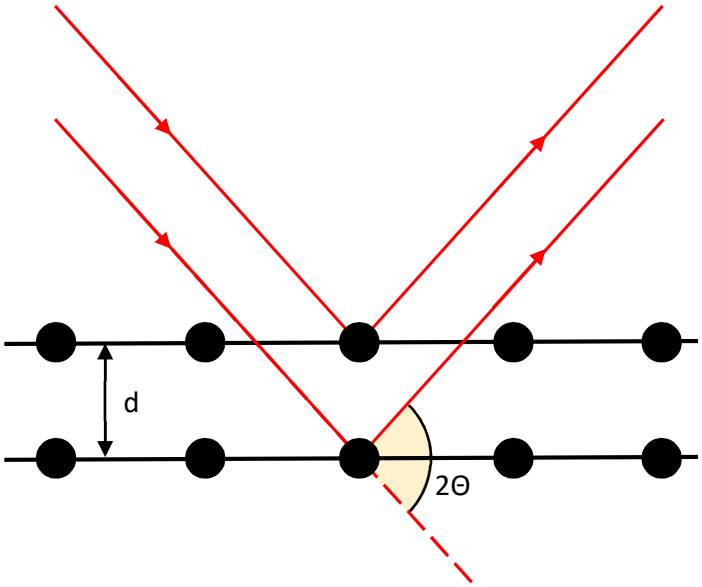

Figure 11. Reflection of X-rays from different atomic planes

Powder X-ray diffraction is principally used for the determination of phase of a material which is carried out by comparing an XRD spectra against database values. However, it can also be used for a number of analytical procedures. The Scherrer equation[13] can be used to determine the average crystallite size from the degree of line broadening and is described by equation 7.

$$\tau = \frac{K\lambda}{\beta cos\theta} \qquad (7)$$

Additionally a Williamson Hall plot[14] can be used to determine the lattice strain of a particular sample. This operates on the principal that size broadening and strain broadening varies independently with respect to the Bragg angle. The equation is analogous to a straight line and when reflections are plotted on a graph to give a Williamson-Hall plot the lattice strain can be determined from the slope of the graph as described in equation 8

$$\beta_{tot} cos\Theta = C\varepsilon \sin\theta + \frac{K\lambda}{L} \qquad (8)$$

Where

B_{tot} = Sum of strain broadening and size broadening

Θ = Angle of incidence

Cε = Lattice strain parameter

K = shape factor

λ = X-ray wavelength

L = Line broadening at half peak maximum

2.3.7.1 Experimental

The conditions used are given below, unless stated otherwise. Analysis was carried out on a PANalytical, XPERT Pro with CuK_α X-Ray source with a nickel filter to strip continuum X-rays from the spectra. The analysis was carried out over 20 minutes and a

2θ range of 10 to 80 ° with a tension and current of 40 Kv and 40 mA respectively. Data was compared against a database of published diffractograms using PanAnalytical's High Score software package in order to determine the crystalline phase. Any samples where crystalline size was calculated in the software using the Debye-Scherrer equation and where lattice strain information was required a Williamson-Hall analysis was carried out.

2.3.8 X-Ray photoelectron spectroscopy

X-ray photoelectron spectroscopy is a surface sensitive technique that measures the kinetic energy of ejected electrons from a sample irradiated with monochromatic X-rays (Figure 12). The energy of the ejected electrons allows insight into changes in electronic character on the surface. For example, it can be used to carry out quantitative analysis of surface atoms, probe the oxidation state of these atoms and give information about local bonding.

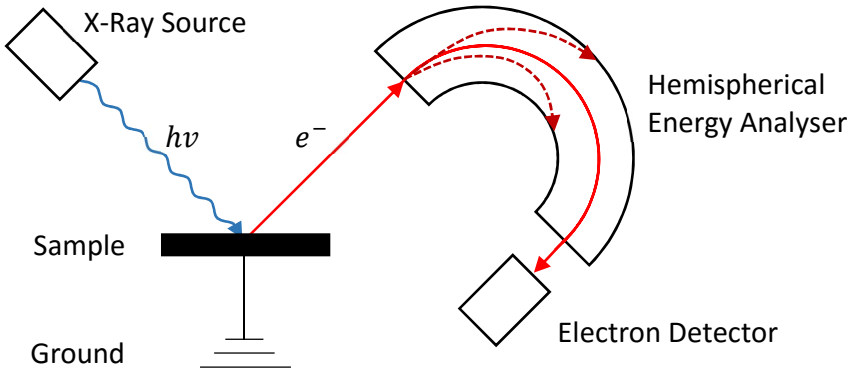

Figure 12. Schematic diagram of X-ray Photoelectron Spectrometer

2.3.8.1 Experimental

All XPS analysis was performed using a Kratos Axis Ultra DLD photoelectron spectrometer which utilises a monochromatic Al source for X-ray generation. A 700 µm x 300 µm was scanned at a pass energy of 40 eV for high resolution and 160 eV for

surveys. All spectra were calibrated with reference to the C 1s line of surface carbon species (typically CO_2)[15] which has a binding energy of 284.7 eV.

2.4 References

1. J. Knozinger, *Preparation of Solid Catalysts*, 1 edn., 1999.
2. Z. Y. Zhong, K. D. Chen, Y. Ji and Q. J. Yan, *Applied Catalysis A-General*, 1997, **156**, 29.
3. E. Manova, T. Tsoncheva, D. Paneva, I. Mitov, K. Tenchev and L. Petrov, *Applied Catalysis A-General*, 2004, **277**, 119.
4. S. Ohara, H. Abe, K. Sato, A. Kondo and M. Naito, *Journal of the European Ceramic Society*, 2008, **28**, 1815.
5. Q. W. Zhang, T. Nakagawa and F. Saito, *Journal of Alloys and Compounds*, 2000, **308**, 121.
6. Q. W. Zhang and F. Saito, *Journal of Alloys and Compounds*, 2000, **297**, 99.
7. S. A. Kondrat, G. Shaw, S. J. Freakley, Q. He, J. Hampton, J. K. Edwards, P. J. Miedziak, T. E. Davies, A. F. Carley, S. H. Taylor, C. J. Kiely and G. J. Hutchings, *Chemical Science*, 2012, **3**, 2965.
8. D. Sellick, PhD Thesis, Cardiff University, 2011.
9. S. Brunauer, P. H. Emmett and E. Teller, *Journal of the American Chemical Society*, 1938, **60**, 309.
10. M. Fadoni and L. Lucarelli, ed. A. Dabrowski, Elsevier, The Netherlands, 1st edn., 1999, vol. 1, ch. 196 - 225, p. 1064.
11. M. B. Esler, D. W. T. Griffith, S. R. Wilson and L. P. Steele, *Analytical Chemistry*, 2000, **72**, 206.
12. V. C. F. Holm and A. Clark, *Journal of Catalysis*, 1968, **11**, 305.
13. P. Scherrer, Springer Berlin Heidelberg, Kolloidchemie Ein Lehrbuch, 1912, pp. 387-409.
14. G. K. Williamson and W. H. Hall, *Acta Metallurgica*, 1953, **1**, 22.
15. D. J. Miller, M. C. Biesinger and N. S. McIntyre, *Surface and Interface Analysis*, 2002, **33**, 299.

Chapter 3. Modified lanthanum manganate catalysts for PGM-free catalysis of gasoline emissions.

3.1 Introduction

Lanthanum Manganite ($LaMnO_{3-\delta}$) has a disordered perovskite structure that results in defects that are important to catalysis. The structure can contain a mixture of Mn^{3+} and Mn^{4+}, which act as a redox couple, the difference in the ratio of these ions determines the degree of non-stoichiometry in the perovskite and hence the extent of disorder in the structure. Disordered perovskite structures are generally more useful for catalysis[1-4], the incidence of defects such as oxygen vacancies and strained structures enhance oxygen transport. Defects in the structure can be added by the addition of doping agents to the lattice or by changing the stoichiometric ratio of lanthanum to manganese.

The perovskites chosen as the subject of study were non stoichiometric lanthanum manganites and silver doped perovskites. The study of perovskites for catalysis has remained closely linked to preparation techniques such as sol gel and coprecipitation, while there is extensive literature on the use of mechanochemical preparative techniques[5-9] for the synthesis of perovskites, this has largely been from a materials perspective. The tests outlined below attempt to make non stoichiometric and silver doped perovskites via mechanochemical and reactive grinding techniques. The variables modified are discussed in detail below.

3.2 Reactive grinding

Perovskites with a PGM component are well established as oxidation catalysts for exhaust gas aftertreatment with Pd[10-13] and Ag[2, 14, 15]. The main method for the modification of perovskite was via changing the stoichiometry around the A-site and B-site cations. This was achieved by adding dopants or by simply using a non-stoichiometric

ratio of A:B to introduce lattice strain and defects. It may be possible to introduce metals that would otherwise be unstable in normal configurations due to their decomposition into less active forms or by inhibiting their sintering. Silver oxide was chosen as a candidate for testing as it is relatively cheap in comparison to platinum group metals and has established activity[15]; silver is a potent oxidation catalyst, however it is hindered by its tendency to sinter below the typical operating range of a three way catalyst due to a low Hüttig temperature[16]. The perovskite lattice could be a means of stabilising silver for application in demanding environments, in a similar method to the 'intelligent catalyst'[11, 13] which has been successful in extending the activity and lifespan of Pd on $LaFeO_3$ perovskite. The aim of this project was to produce a silver catalyst in a similar manner, but with a simple reactive grinding preparation.

A straightforward method for synthesising a perovskite catalyst was devised, the metal nitrates are combined in a pestle and mortar as described in 2.1.1, this technique reduced the requirement for solvents and produced an effective catalyst.

3.2.1 Initial investigation of loading

The first step was to identify how the loading of silver and calcination temperature might influence the formation of the catalyst and its activity, with the intent of finding a standard well performing catalyst for further testing. Silver loading is expressed in terms of a ratio to manganese, Ag 0.05 : Mn 0.95 or Ag 0.3 : Mn 0.7 for example, such that they always give a 1:1 ratio La : Ag-Mn. This way imperfect stoichiometry can be gradually introduced into the lattice to find an optimal loading. $Ag_{0.3}$ was chosen as a maximum, as this is at the boundaries of satisfying the equation laid out by Goldschmidt[17], which is based on atomic radii differences. Additional strain will be put on the perovskite lattice by having a significant quantity of +1 silver ions substituting the +3 manganese ions. The XRD powder patterns below show the different silver loadings on a Lanthanum Manganite. At lower weight loadings the silver formed a discreet phase and is not a part of the lattice when prepared by this technique. The silver phase was gradually seen increasing with weight loading as might be expected if the silver was not being incorporated into the lattice. At $Ag_{0.3}$ the perovskite was barely formed and the oxide phase was largely amorphous, which is likely because the non-stoichiometry is too great for the phase to form.

Table 1 shows EDX elemental analysis for the different weight loadings tested in the initial screening tests. The expected weight loadings are seen in these catalysts confirming incorporation of all the precursors. Figure 1 shows the powder XRD spectra of the perovskite catalysts with different silver weight loadings, the perovskite phase is denoted by the orange circles and the purple stars show silver, as can be seen incorporation of the silver is not complete.

Table 1 EDX data for silver doped $LaMnO_3$ catalyst with varying weight loading

	Atomic percentage				Weight Percentage			
Catalyst	La	Mn	Ag	O	La	Mn	Ag	O
$LaMnO_3$	20.69	19.81	0	59.49	58.48	22.15	0.00	19.37
$LaMn_{0.95}Ag_{0.05}O_3$	19.87	19.23	0.99	59.91	56.54	21.64	2.19	19.63
$LaMn_{0.9}Ag_{0.1}O_3$	20.13	17.98	2.41	59.48	55.97	19.77	5.20	19.05
$LaMn_{0.8}Ag_{0.2}O_3$	20.3	16.55	4.12	59.02	55.10	17.77	8.68	18.45
$LaMn_{0.7}Ag_{0.3}O_3$	19.87	14.36	5.11	60.66	54.43	15.56	10.87	19.14

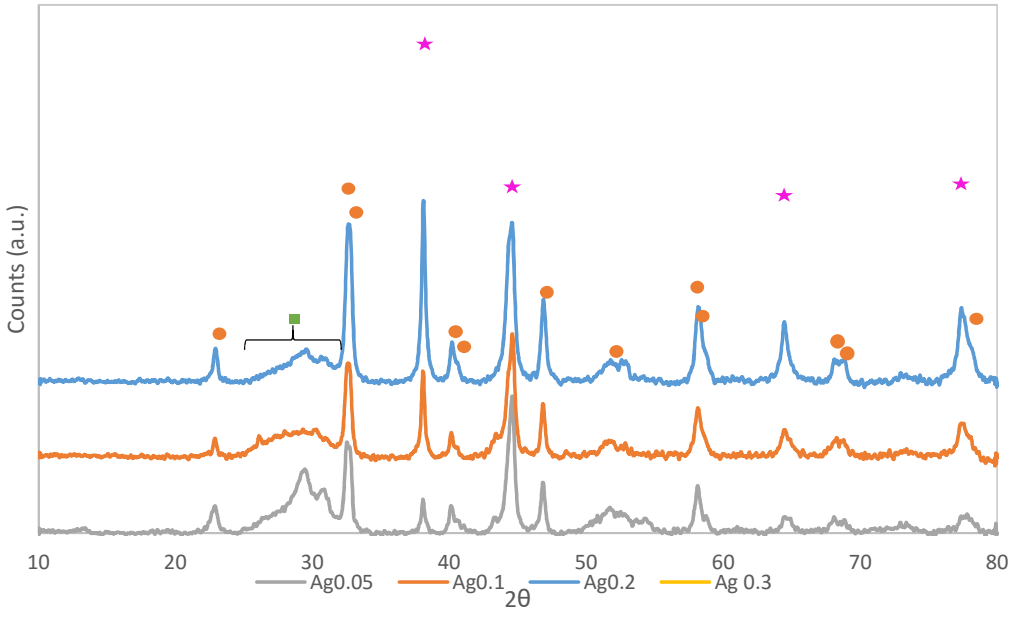

Figure 1. XRD patterns of varying stoichiometric ratio of silver to manganese. Top to bottom, $Ag_{0.3}$ (yellow line), $Ag_{0.2}$ (blue line), $Ag_{0.1}$ (orange line), $Ag_{0.05}$ (grey line $LaMnO_{3-\delta}$ (orange circle), $LaMn_2O_4$ (green square), Silver (purple star).

Table 2. BET surface area data

Sample	C value	BET surface area (m^2g^{-1})
$LaMnO_3$	58	16
$LaMn_{0.95}Ag_{0.05}O_3$	40	17
$LaMn_{0.9}Ag_{0.1}O_3$	48	16
$LaMn_{0.8}Ag_{0.2}O_3$	93	18
$LaMn_{0.7}Ag_{0.3}O_3$	107	18

Table 2 shows the BET surface area values for the catalysts; all of the catalysts display similar surface areas with no significant variation between them.

3.2.2 Activity data

The activity data for the different silver loadings as oxidation catalysts under stoich or lean conditions showed a general increase in activity with weight loading. Figure 2 shows the activity of the perovskite catalysts are clustered together with the $Ag_{0.3}$ catalyst more active with all silver catalysts being considerably more active than the perovskite phase formed by this method. There is a slight increase in the variation between the propane activities (Figure 3) where the trend was slightly clearer, showing an increase in silver gives an increase in activity with a large boost in activity for the $Ag_{0.3}$ catalyst.

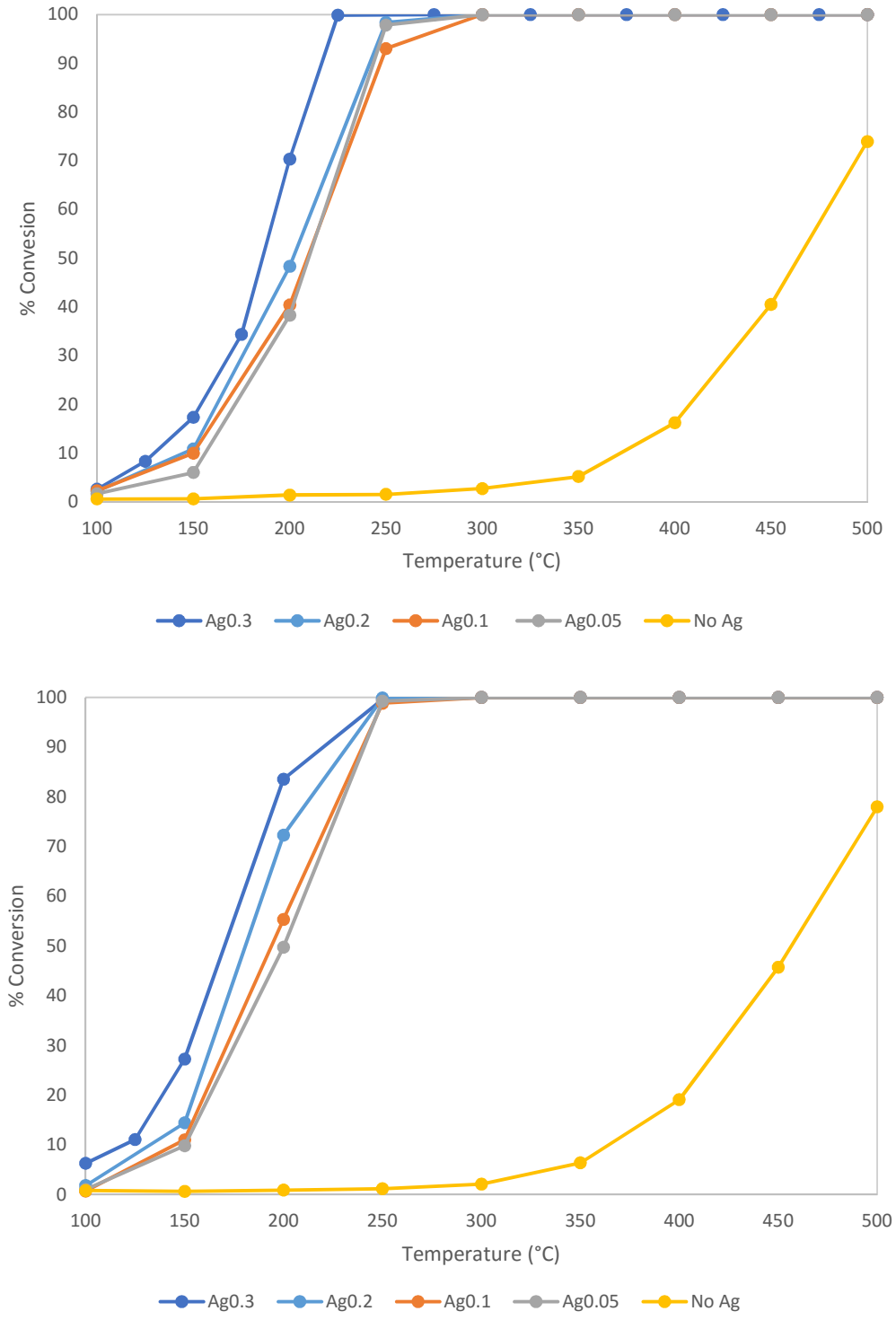

Figure 2 CO conversion under stoichiometric (top) and lean (bottom) conditions, 0.3 cm^3 catalyst, 40,000 h^{-1}, 1% CO, 0.1% C_3H_8, 300 ppm NO, 6% CO_2, 8% H_2O, 8%/1% O_2 for lean/stoichiometric.

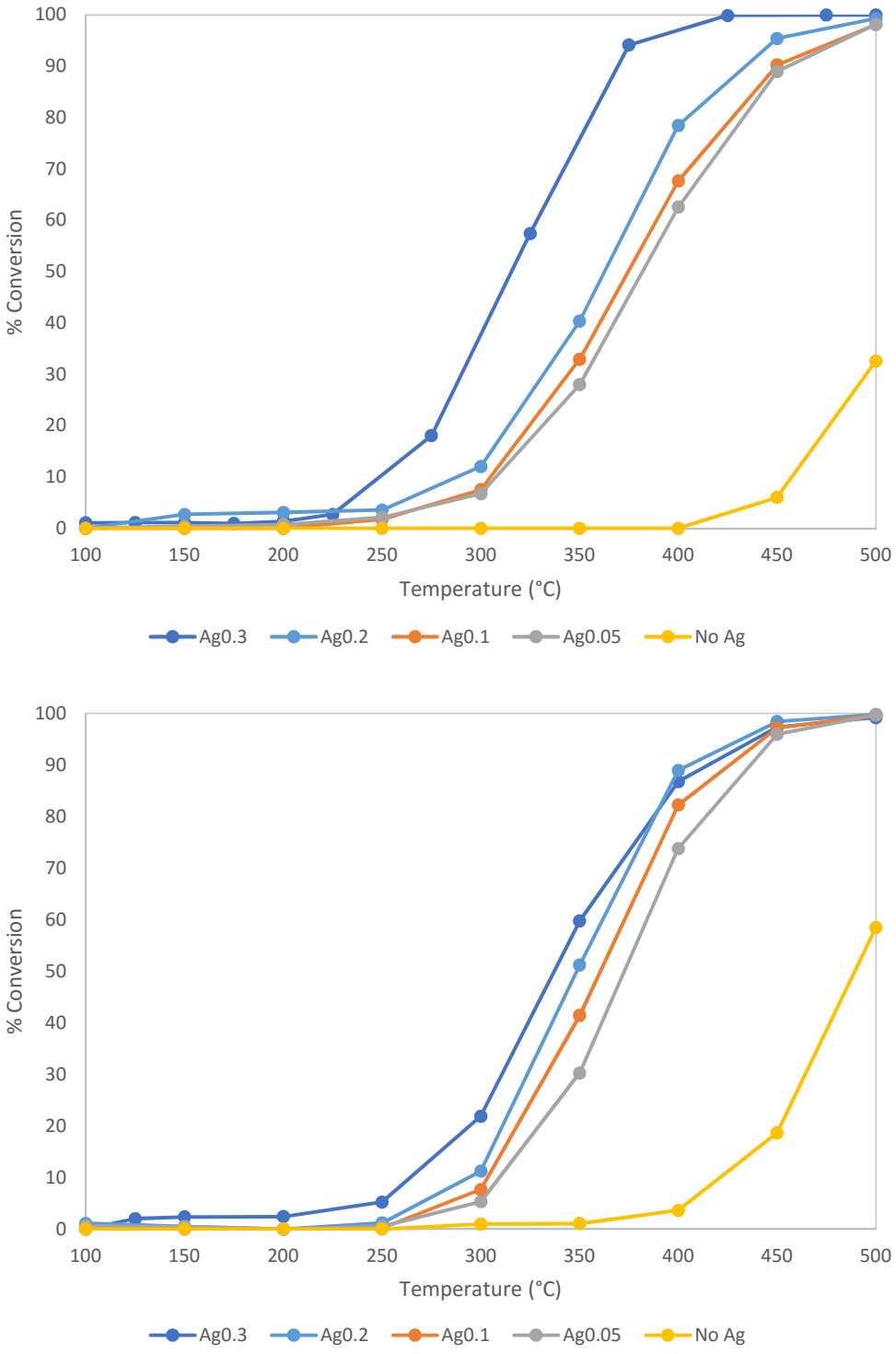

Figure 3 C_3H_8 conversion under stoichiometric (top) and lean (bottom) conditions, 0.3 cm^3 catalyst, 40,000 h^{-1}, 1% CO, 0.1% C_3H_8, 300 ppm NO, 6% CO_2, 8% H_2O, 8%/1% O_2 for lean/stoichiometric.

The stoichiometric and lean activity for CO conversion (Figure 4) and C_3H_8 (Figure 5) reveals the catalyst was considerably more active when prepared at 600 °C for C_3H_8 under lean conditions however the perovskite phase is still active and the catalysts heat treated at 700 °C and 800 °C have comparable activity under stoichiometric conditions. The reduction in activity from 800 °C to 900 °C could be a result of the phase change or a drastic reduction in surface area due to sintering that is often associated with perovskite formation at high temperatures. BET surface area analysis shows that sintering increases with increasing heat treatment (Table 3). When an excess of oxygen was provided the perovskite catalyst performed better and on par with the $Ag_{0.3}$ catalysts, an effect potentially explained by an increase in oxygen mobility in the amorphous catalyst, as lattice oxygen was more readily replenished in an oxygen deficient atmosphere

Table 3. BET results reactive grind varied temperature for $LaMnAg_{0.2}O_3$

Sample	C value	BET surface area (m^2g^{-1})
900	83	2
800	214	12
700	9	16
600	76	19

CO conversion was largely independent of oxygen concentration. On metallic silver surfaces CO oxidation is generally understood to proceed via a Langmuir-Hinshelwood mechanism,[18] while CO oxidation on the lanthanum manganite perovskite support would be a Mars van Krevelen (MVK) mechanism[19, 20]. An MVK reaction is quasi-zero order with respect to oxygen[21] which is replenished after the reaction has taken place. The difference in activity between C_3H_8 catalysts under stoichiometric and lean conditions indicates that the oxygen had a rate limiting role in the reaction, and potentially indicates a Langmuir-Hinshelwood mechanism while the lack of difference between CO activities under those same conditions may be indicative of an MVK mechanism. This seems to suggest that the CO oxidation was carried out by the perovskite and the propane oxidation took place on the silver, which would also explain the larger difference between propane activities at different silver weight loadings (Figure 4, 3).

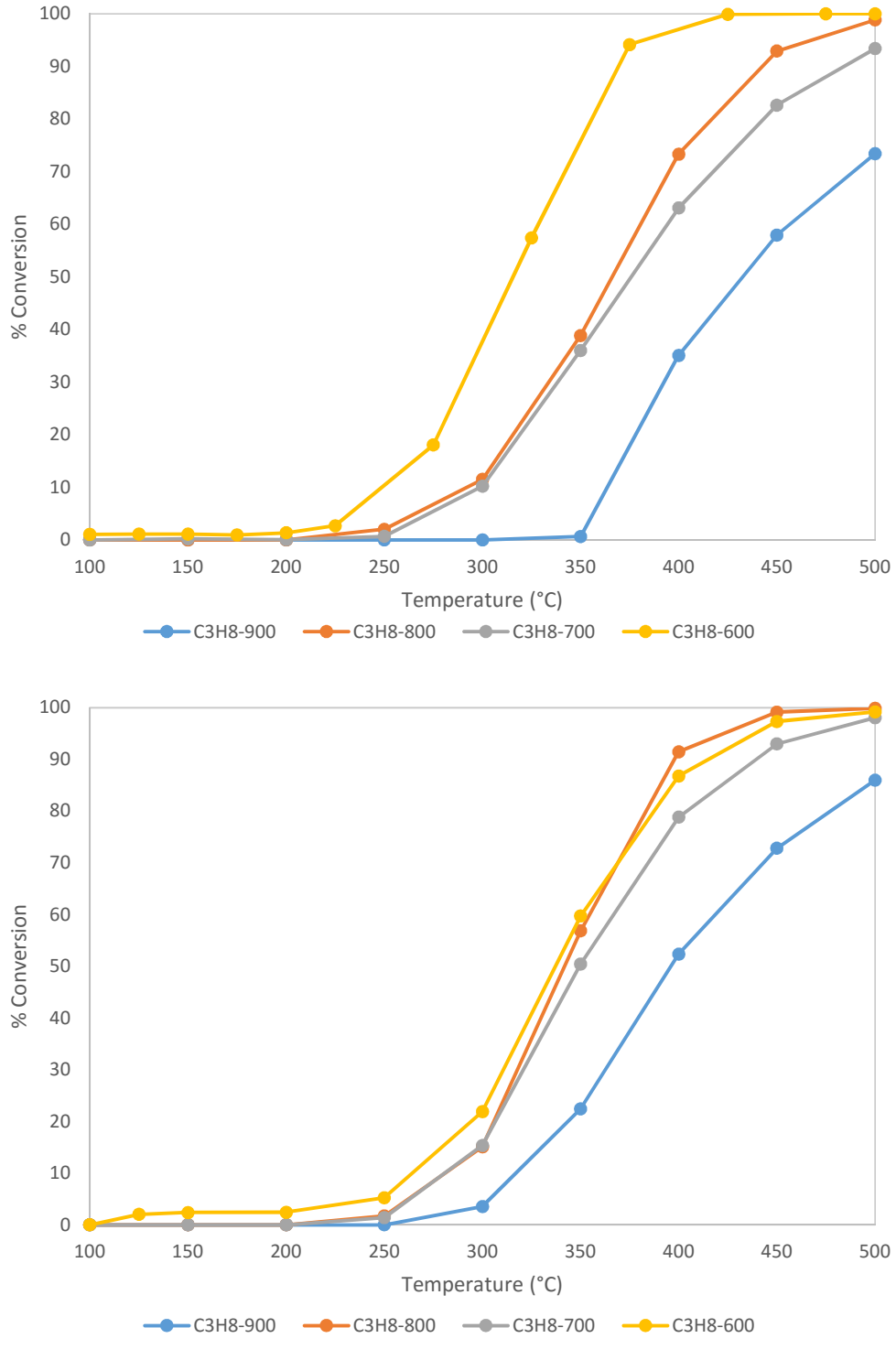

Figure 4. $LaMn_{0.8}Ag_{0.2}O_3$ testing C_3H_8 conversion under stoichiometric (top) and lean (bottom) conditions, 0.3 cm^3 catalyst, 40,000 h^{-1}, 1% CO, 0.1% C_3H_8, 300 ppm NO, 6% CO_2, 8% H_2O, 8%/1% O_2 for lean/stoichiometric.

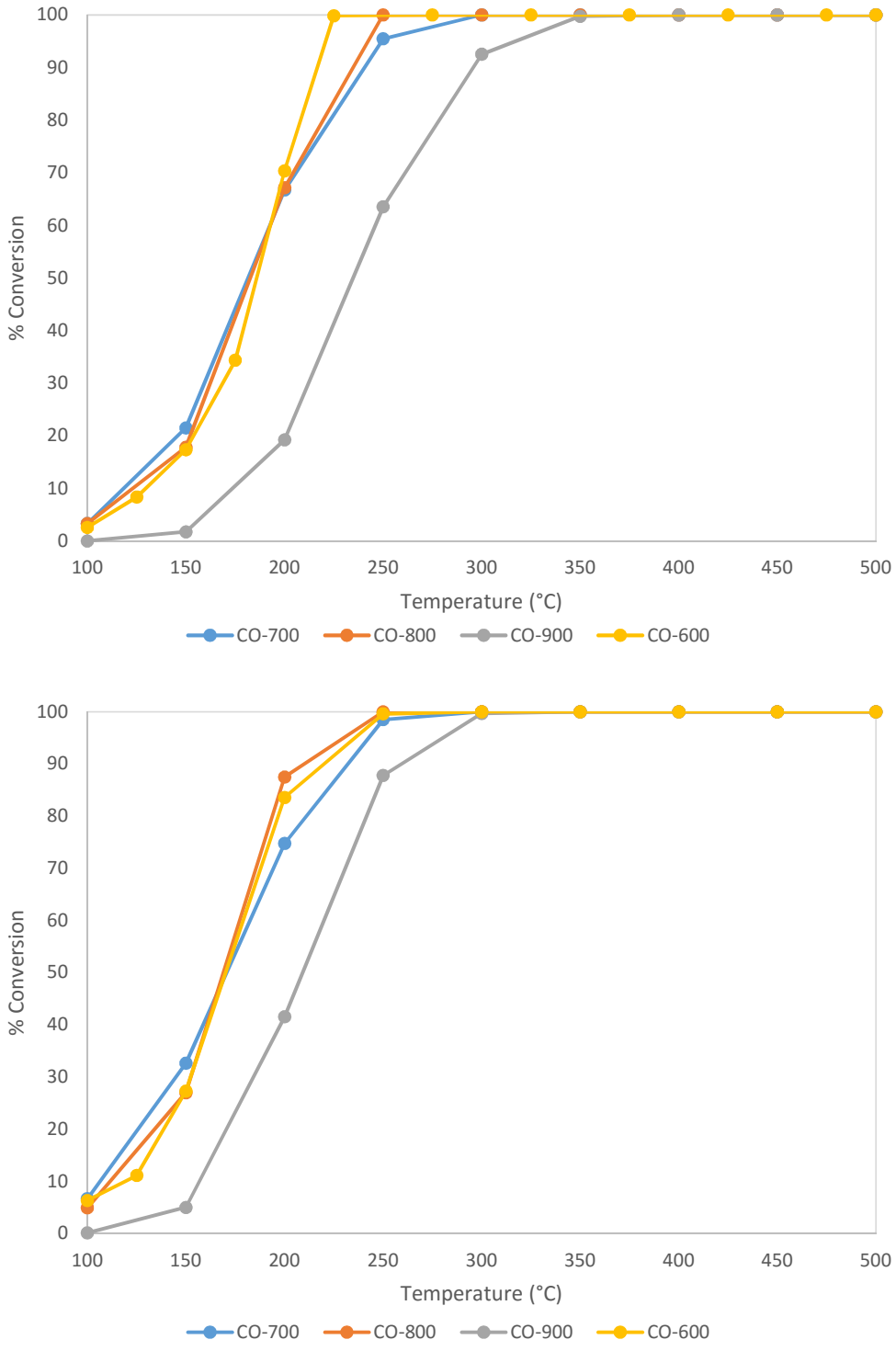

Figure 5. $LaMn_{0.8}Ag_{0.2}O_3$ testing CO conversion under stoichiometric (top) and lean (bottom) conditions. 0.3 cm^3 catalyst, 40,000 h^{-1}, 1% CO, 0.1% C_3H_8, 300 ppm NO, 6% CO_2, 8% H_2O, 8%/1% O_2 for lean/stoichiometric.

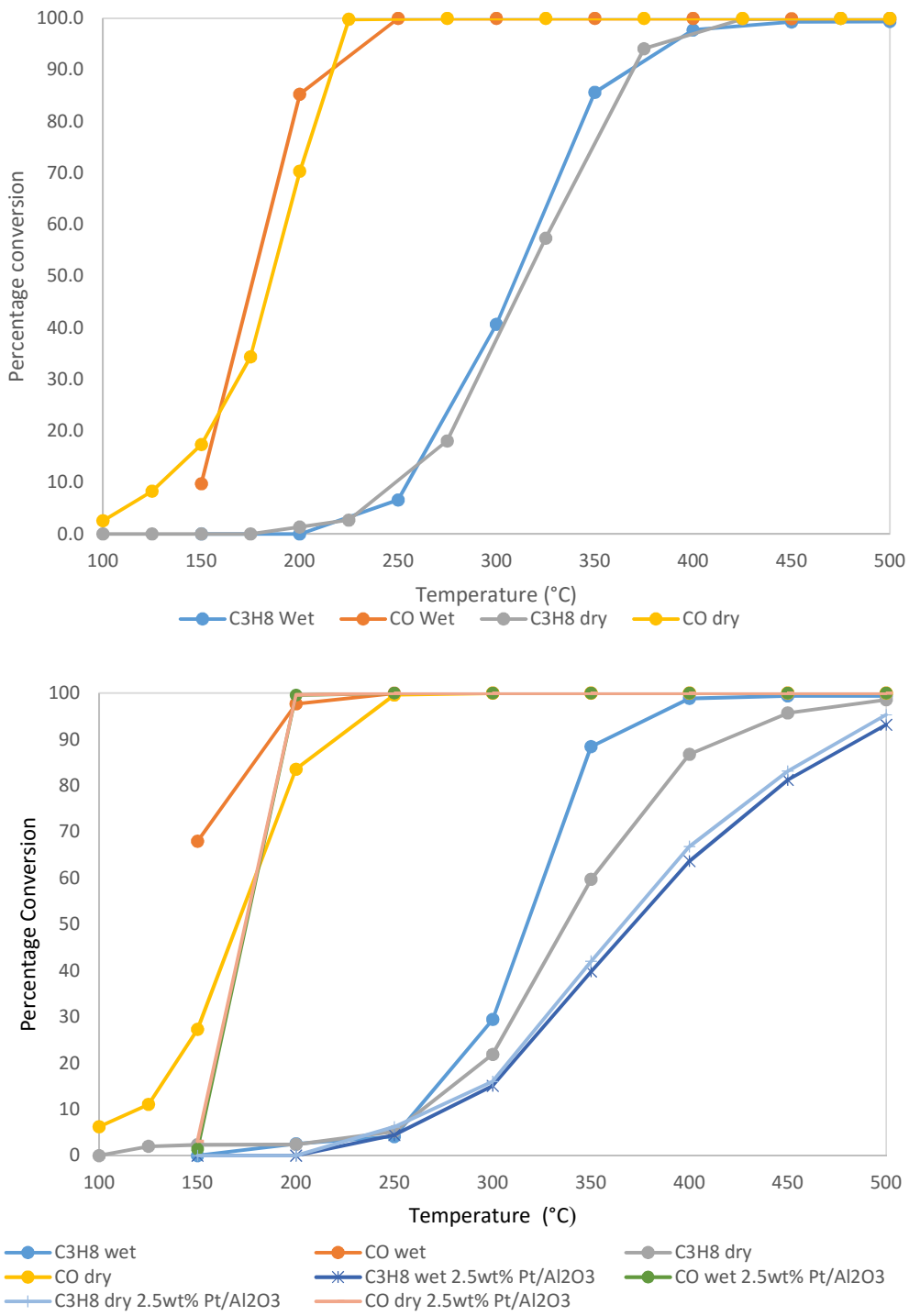

Figure 6. Water deactivation under stoichiometric (top) and lean (bottom) exhaust gas conditions. Included in the comparison was a standard 2.5 wt% Pt catalyst on alumina for comparative purposes. 0.3 cm^3 catalyst, 40,000 h^{-1}, 1% CO, 0.1% C_3H_8, 300 ppm NO, 6% CO_2, 8% H_2O, 8%/1% O_2 lean/stoichiometric.

Perovskites are susceptible to partial deactivation by water as it adsorbs to active sites and blocks the adsorption of CO and propane[22]. This is a reversible process and when steam is removed from the feed activity returns to its previous level. In vehicular applications water is an unavoidable component of exhaust gas so this deactivation is undesirable. The $LaMn_{0.7}Ag_{0.3}O_{3-\delta}$ catalyst showed no significant deactivation over 2 stoichiometric tests, with and without water as seen in Figure 6 and under a lean test showed a slight increase in activity over the duration of the experiment. One possible explanation is that this catalyst was particularly resistant to water deactivation due to the silver content, if the silver was acting as the active site or is modifying the supports affinity for the adsorption of water. Overall the performance of the catalyst is comparable to a standard 2 wt% Pt/Al_2O_3 catalyst (Figure 6) prepared by impregnation as described in 2.1.1, which represents a considerable reduction in catalyst cost in terms of precious metal content.

3.3 NO_x control with perovskites

For NO oxidation/reduction the data for each component has been represented as a concentration against temperature rather than as a selectivity value, the reason for this is that many catalysts exhibit a storage behaviour when exposed to NO. NO can be adsorbed to a support and desorbed as NOx at a higher temperature. This sto rage effect makes calculating conversion and selectivity problematic and so as not to misrepresent the data the actual measured concentrations of a gas are given rather than a value for conversion.

Increasingly soot combustion is being looked towards as a way to reduce particulate matter from exhaust emissions, diesel emissions are already heavily regulated and soon gasoline emissions will be regulated also. In diesel engines there is typically a large quantity of NO present and due to the nature of diesel engines the emissions are often lean, rendering NO emissions control difficult. A potential pathway for managing the increasingly strict NO emissions is to oxidise the NO to NO_2 and adsorb this to soot particulate trapped in a filter[23], As NO_2 is a strong oxidiser this lowers the ignition temperature and greatly increases the oxidation rate of the soot, while providing

a route for NO_x control. The $LaMn_{0.7}Ag_{0.3}O_{3-\delta}$ was especially effective for the oxidation NO, as silver and perovskite separately are known to be active for NO oxidation[24, 25]. Gasoline particulates are insufficiently characterised and current methods for generation are not proven as models for real world driving gasoline soot, however it is expected that NO_2 will also be useful in this role and can potentially be useful in a soot control application.

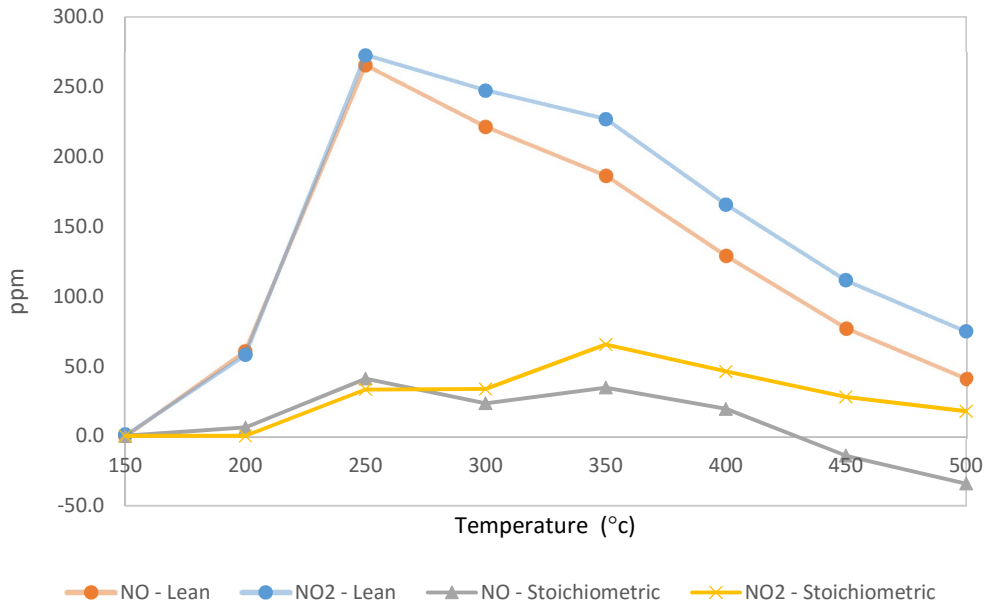

Figure 7. NO consumed compared against NO_2 produced under lean (top) and stoichiometric conditions (bottom). 0.3 cm^3 catalyst, 40,000 h^{-1}, 1% CO, 0.1% C_3H_8, 300 ppm NO, 1% O_2, 6% CO_2, 8% H_2O.

Figure 7 shows the NO production under lean and stoichiometric conditions. It can be seen that the excess of oxygen greatly enhanced NO oxidation over the course of the reaction, which is an important consideration for soot oxidation[26]. NO conversion can proceed by oxidation directly by oxygen or reduction by hydrocarbons[27] B site substituted perovskites such as $LaFeO_3$ and $LaMnO_3$ have been known to reduce NO via organo-nitrogen intermediates[28, 29], the silver catalyst in this instance though substituted in a similar way is a potent NO oxidation catalyst[30]. Silver (I) Oxide is known to oxidise NO to NO_2 while metallic silver carries out reduction even under oxidising conditions[31, 32], it can be inferred from this data that the active species was silver oxide as NO oxidation was occurring even under lean conditions, although without sufficient atmospheric oxygen the catalyst will not regenerate. The nitrogen imbalance seen was

likely a result of storage effects, a continuous ramp analysis reveals an adsorption and release. This is due to the fact that NO adsorbs to the perovskite surface and is released at higher temperatures as NO_2.

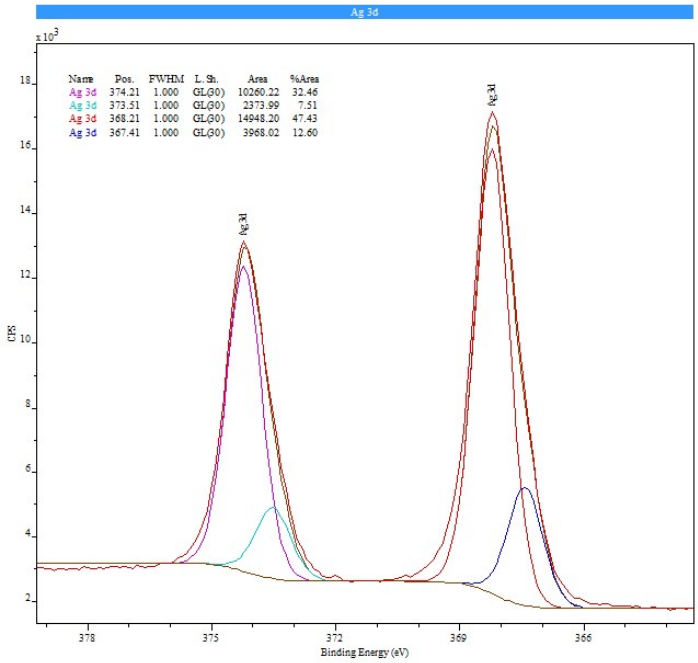

Figure 8. XPS spectra of $LaMn_{0.7}Ag_{0.3}O_3$ focused on the Ag 3d region, fresh catalyst.

In order to understand the nature of the surface silver species, XPS was carried out. Figure 8 shows an Ag 3d doublet corresponding to 3/2 and 5/2 high and low binding energy peaks respectively. From the spectra it was determined that there are two peaks present as there is a slight shoulder on the right side of each peak, one corresponding to 374.2eV and the other at 373.5eV. Literature reports Ag_2O 3d 3/2 has a binding energy of 373.9eV[33] while Ag(0) 3d 3/2 has a binding energy of 373.4eV[34], these could possibly correspond to the aforementioned peaks. If this was the case then the surface silver is in a predominantly oxidised state with the silver oxide species accounting for 81.2% of the atoms and metallic silver constituting the remainder. This answer is not definitive as there is the possibility of peaks being incorrectly attributed to the various oxidation states of silver and there is no information about the bulk oxidation state, but it agrees with the activity data that silver oxide was likely present on the fresh catalyst. Ag_2O is

unstable when heated above 200 °C and will decompose into Ag(0) and oxygen, over the course of a standard test where the temperature is brought up to 500 °C the activity for NO oxidation is not diminished and is reproducible over the range.

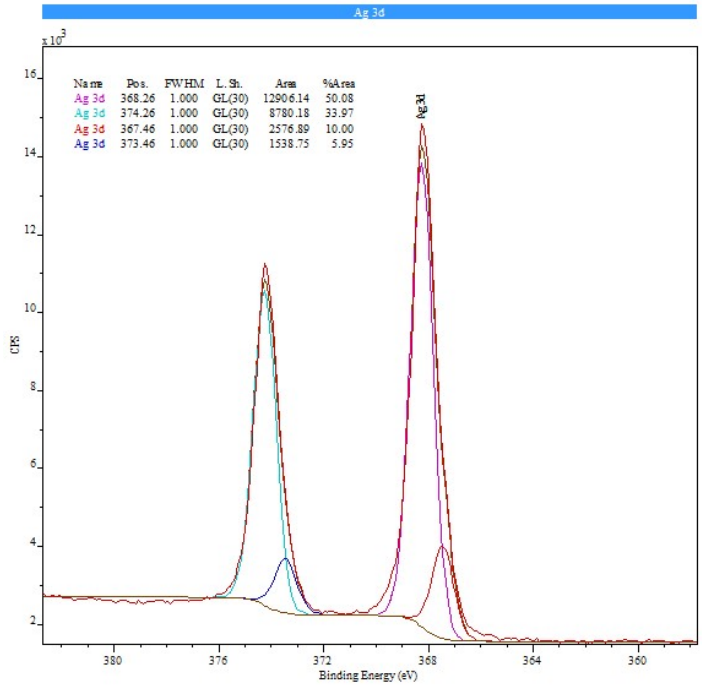

Figure 9. XPS spectra of $LaMn_{0.7}Ag_{0.3}O_3$ focused on the Ag 3d region, used catalyst after 2 tests.

The $LaMn_{0.7}Ag_{0.3}O_3$ catalyst was exposed to standard lean testing conditions, this catalyst was recovered and an XPS spectrum was acquired (Figure). The results showed that the silver oxide layer remains intact This could potentially mean that the silver oxide has been stabilised by the perovskite lattice, possibly by the formation of a solid state lattice. SEM imaging showed no obvious metallic particles (Figure) and for a catalyst of low surface area and relatively high metal loading this may have been expected if the silver was present in a metallic state.

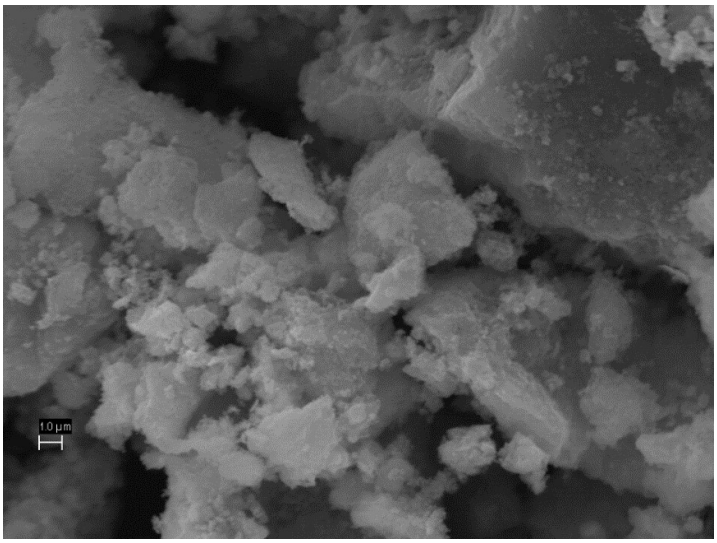

Figure 10. SEM secondary electron image of $LaMn_{0.7}Ag_{0.3}O_3$

3.4 High energy ball milling

As the objective of the previous work was to stabilise silver it was decided to try an alternative synthesis. Ball mills provide a mechanochemical route for metal oxide formation that allows the bypassing of high temperature heat treatments, reduces solvent waste and utilises 'greener' reagents. It has been established that the direct synthesis of perovskite from metal oxides[7-9] can be achieved. A procedure was devised to determine the optimum conditions for perovskite formation. It was known from literature that a sufficient grind time at 650 RPM would be 12 h for the synthesis of $LaMnO_{3-\sigma}$ and so an initial test was carried out to compare against a sample prepared by the reactive grinding technique outlaid earlier.

3.4.1 Characterisation

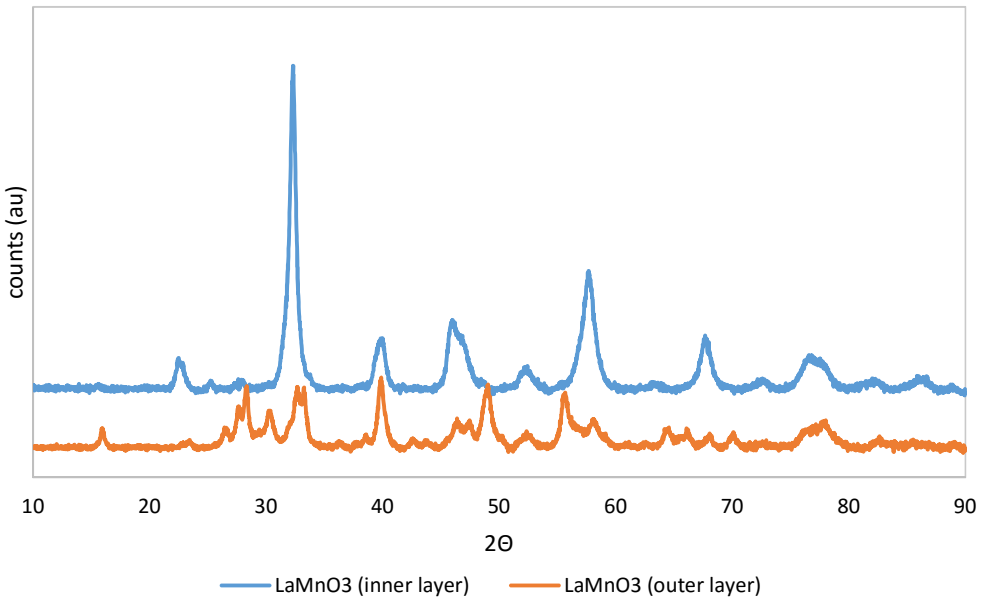

Figure 11. XRD powder diffraction comparison of material layers recovered from ball mill cell.

The sample recovered was not homogenous and consisted of 2 distinct layers, an easily recoverable inner surface and a hard, outer layer of unconverted oxides. An XRD comparison (Figure 11) reveals that the inner layer is a fully converted perovskite while the outside layer consists of a mixture of precursors and product. The overall yield of useful material was approximately 28%. The perovskite produced was compared against one prepared by pestle and mortar with powder XRD, immediately apparent is a shift in the peaks to a higher diffraction angle, this typically signifies a d-spacing increase and subsequently a larger unit cell, this could be due to compressive stress present in the lattice that might be associated with mechanochemical preparation. As a perovskite's activity is closely determined by lattice defects, oxygen vacancies and lattice strain[27, 35], this was a possible indicator that the catalytic activity might be improved. SEM imaging (Figure 12) shows sub-micron particles present in greater numbers in the ball mill sample and a smaller overall particle size was confirmed by the broadening XRD peaks seen in Figure 13 The increase in d-spacing associated with disordered lattice signified by the shift in peaks shown in Table 4. A Scherrer analysis[36] of the principal perovskite reflection

at 32 degrees showed the average crystallite size to be 12.5 nm for the mill perovskite and 15.2 nm for the pestle and mortar perovskite.

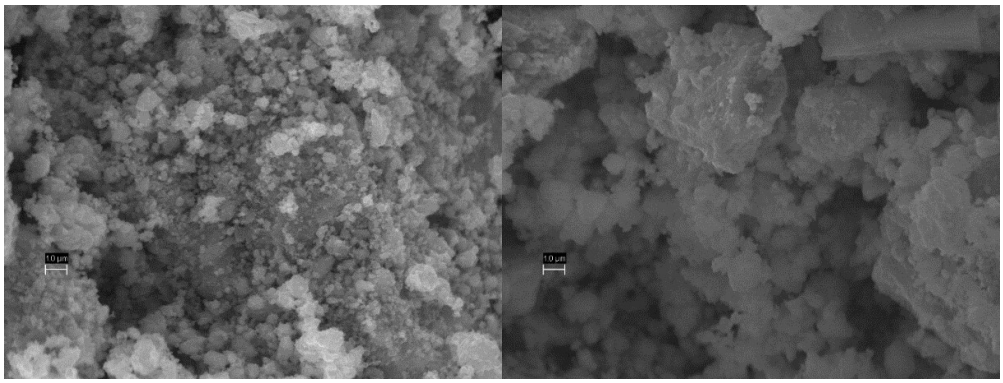

Figure 12. SEM Secondary electron image of ball mill $LaMnO_{3-\delta}$ (left) and pestle and mortar $LaMnO_{3-\delta}$ (right)

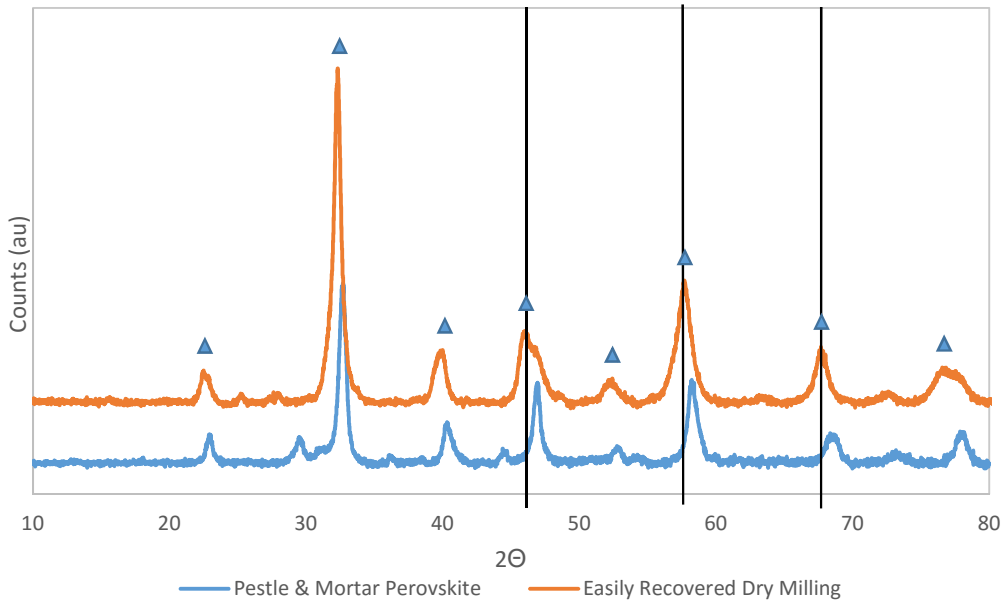

Figure 13. XRD powder diffraction comparison of $LaMnO_3$ as prepared by pestle and mortar and high energy ball milling. $LaMnO_3$ phase (blue triangles)

Table 4. Positions of perovskite reflections

Ball mill (2θ)	P&M prep (2θ)
22.64	22.96
32.33	32.70
39.87	40.68
46.078	46.95
52.34	58.29
57.753	58.29
67.64	68.55

3.4.2 Additives

In order to improve the yield, the addition of a small quantity of solvent was tested. Ethanol was chosen as the solvent as it is cheap and readily available as well as being simple to remove from the final product. As the concentration was increased, the recoverable sample went up markedly, however conversion to the perovskite phase dropped as the increasingly fluid nature of the system allowed the precursors to flow from the path of the balls (Figure 14).

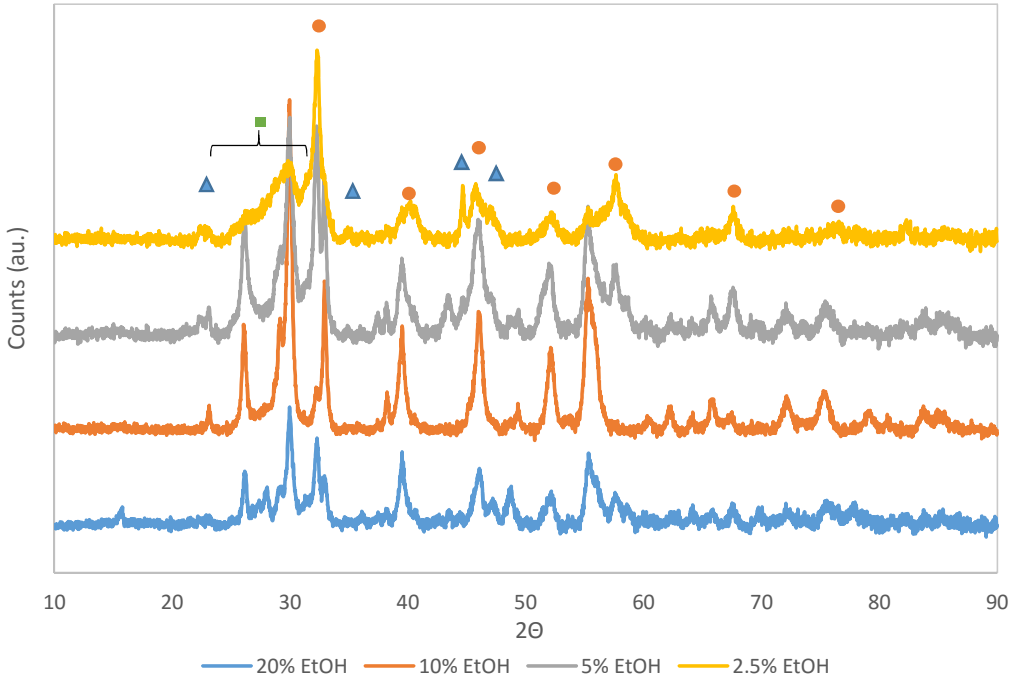

Figure 14. XRD powder diffraction comparison of $LaMnO_3$ prepared in the ball mill at 650 RPM for 6h with different percentage quantities by weight of EtOH present. $LaMnO_3$ (orange circles), Mn_2O_3 (blue triangles), $LaMn_2O_3$ (green square)

A small quantity of ethanol increased the yield from 28% to 57% without a significant impact on the final phase as shown by XRD patterns in Figure 10. A milling duration study was then carried out to determine the optimum duration of the grind. Intervals of 3h were used and 4 tests were carried out. In each instance, the recovered sample was removed from the vessel and powder XRD diffraction carried out. The phase progression over the course of the milling was similar to the solvent free grind, with the exception of a possible $LaMn_2O_4$ phase and Mn_2O_3 being present in small quantities (Figure 15).

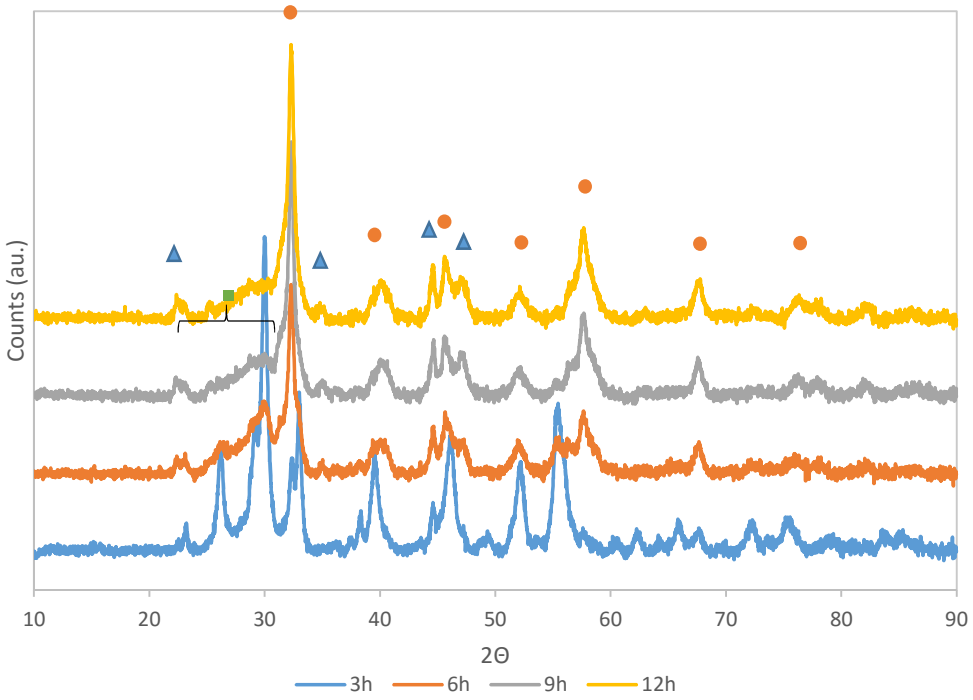

Figure 15. Powder XRD patterns of LaMnO3-δ with 2.5 wt% EtOH present over grinding duration in hours. LaMn2O4 (green square), Mn2O3 (blue triangle), LaMnO3-δ (orange circle).

This method was tested with the silver doped perovskite prepared using ball milling techniques and the activity data is given in Figure 16. Performance of this catalyst was poor in comparison to the catalysts prepared without a solvent present. To retain the benefits to yield, water was utilised as a lubricant as literature suggests that despite the basic nature of lanthanum in the presence of water. A small quantity of which can

be used to promote the formation of the perovskite phase[6]. It was suspected that this is due to the water adsorbing to the surface of the oxide materials and lowering the surface energy for bond breaking[6, 37, 38], thus making the oxides more reactive and speeding up the phase conversion for a given energy input.

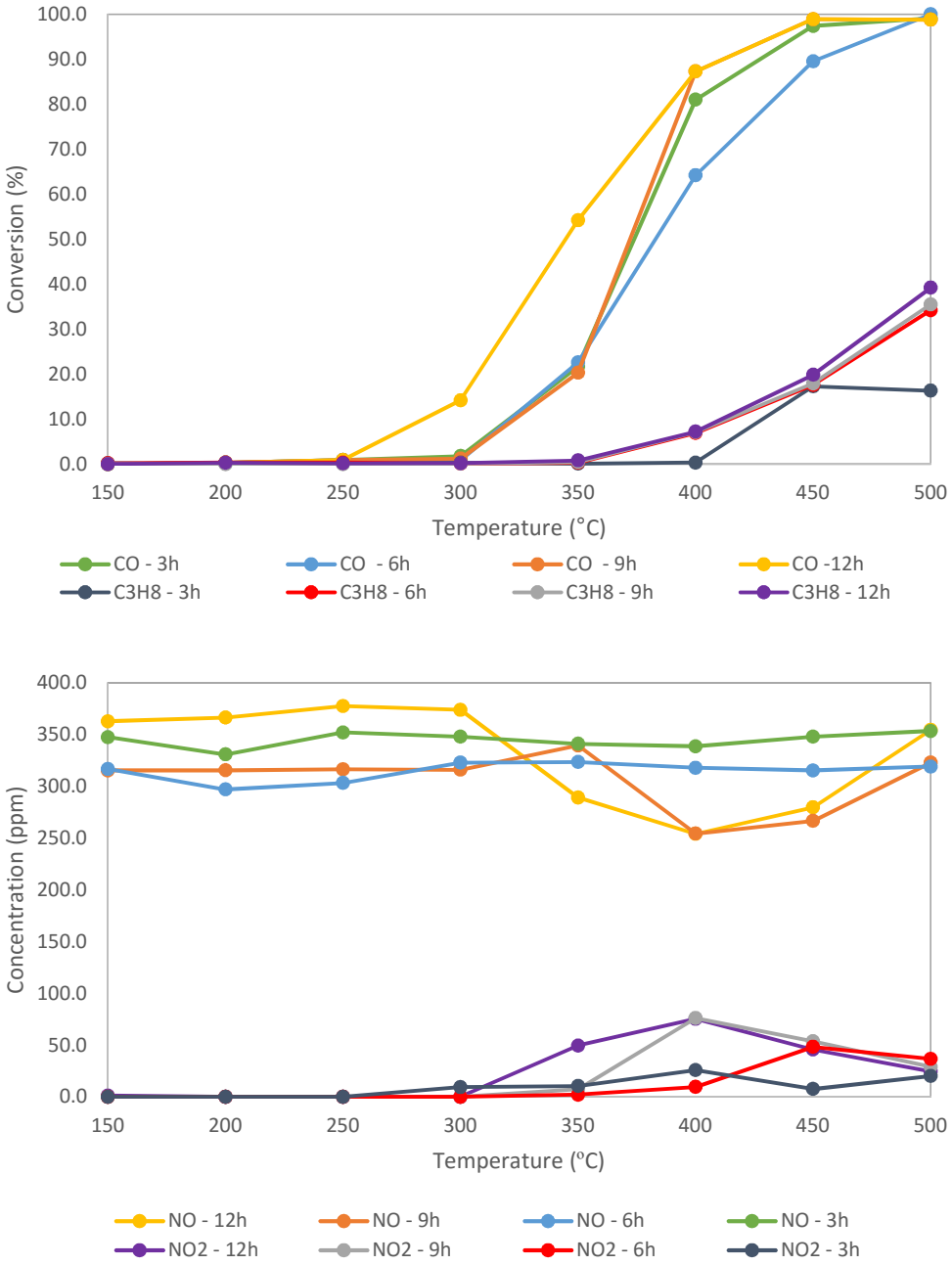

Figure 16 $LaMn_{0.8}Ag_{0.2}O_3$ testing C_3H_8 and CO conversion (top) and NO/NO_2 concentrations (bottom) under lean testing conditions at different grind durations. 0.3 cm^3 catalyst, 40,000 h^{-1}, 1% CO, 0.1% C_3H_8, 300 ppm NO, 6% CO_2, 8% H_2O, 8%/1% O_2 for lean/stoichiometric.

3.5 Statistical design

As the ball mill requires a relatively large quantity of material in each run, it was decided that a statistical design experiment would represent the most efficient use of resources when introducing silver. A 2 Level Factorial resolution 4 statistical design was devised using Design-Expert® 8 with the information gathered in the initial experiments. 7 variables were chosen for testing. The first 2 variables considered co-dependently were speed and duration, 600 RPM and 650 RPM and a duration of 9h or 12h, this is enough time and energy to convert precursors to the perovskite phase but enough of a difference to hopefully gauge the effect of these parameters on catalytic activity. As the next parameter was hydration, a change from ethanol was considered as water gave better initial results. The presence of water in the formation of $LaMnO_3$ perovskite from La_2O_3 and Mn_2O_3 is also a potential benefit, improving the milling action[6] despite the basicity of La_2O_3 making it likely that the water will quickly react to form lanthanum hydroxide species. An additional effect to consider is the gradual increase in temperature, the extremely high speeds and aggressive impacts within the cell produce elevated temperatures, a cool down period in the middle of a run allows the temperature to decrease and limits the thermal effects on the catalyst. The next two factors were the ion substituted from the lattice and the silver loading. Perovskites can be either A or B site substituted and either will introduce defects into the lattice to different degrees. $LaMnO_3$ often has a slightly increased oxygen content, if the La ion is substituted there will be an increasing ratio of Mn^{4+} to Mn^{3+} and vice versa for Mn substitution. By adjusting these two variables, the magnitude of both effects can be determined and because this is a resolution 4 study it also reveals 2 factor interactions between the effects, which may help to reveal the mechanisms at play. The final factor was a heat treatment, as the catalyst may benefit from a final annealing at 700 °C for 5 h under static air. An overview of all the standards are detailed in Table 5.

Table 5. All standards produced for statistical design

Std	Run	Factor 1 A:Speed RPM	Factor 2 B:Duration h	Factor 3 C:Hydration %wt	Factor 4 D:Halfway Pause m	Factor 5 E:Ion substituted	Factor 6 F:Silver loading equivs	Factor 7 G:Heat Treatment
1	1	600	9	3	0	La	0.15	No
8	2	650	12	6	0	Mn	0.15	No
14	3	650	9	6	30	La	0.15	Yes
6	4	650	9	6	0	La	0.3	No
11	5	600	12	3	30	Mn	0.15	Yes
10	6	650	9	3	30	Mn	0.3	No
12	7	650	12	3	30	La	0.15	No
2	8	650	9	3	0	Mn	0.15	Yes
9	9	600	9	3	30	La	0.3	Yes
4	10	650	12	3	0	La	0.3	Yes
13	11	600	9	6	30	Mn	0.15	No
16	12	650	12	6	30	Mn	0.3	Yes
15	13	600	12	6	30	La	0.3	No
3	14	600	12	3	0	Mn	0.3	No
7	15	600	12	6	0	La	0.15	Yes
5	16	600	9	6	0	Mn	0.3	Yes

3.5.1 Characterisation

All catalysts were characterised by XRD, BET, SEM/EDX, TPR and activity testing. The XRD patterns show that all samples were converted to a perovskite phase although many of the catalysts show the presence of additional phases, these secondary phases consist of La_2O_3, Mn_2O_3 and Ag_2O. As the heat treatment was likely to have a strong influence on the presence of non-perovskite phases and catalysts that underwent one were expected to show a lower abundance of these phases. EDX was carried out to confirm elemental compositions (Table 6). Catalysts showed the expected ratio of elements confirming that all the oxides had been incorporated into the final product.

Table 6. EDX Results for Statistical design

			Atomic percentage				Weight Percentage			
	Ion subbed	Ag equivs	La	Mn	Ag	O	La	Mn	Ag	O
std 1	La	0.15	17.62	18.80	2.55	61.0	51.7	21.8	5.81	20.6
std 2	Mn	0.15	18.60	14.28	2.25	64.8	55.5	16.8	5.22	22.3
std 3	Mn	0.3	20.10	13.92	5.21	60.7	54.8	15.0	11.0	19.1
std 4	La	0.3	12.68	16.86	4.69	65.7	41.4	21.8	11.9	24.7
std 5	Mn	0.3	18.99	14.36	5.21	61.4	53.0	15.8	11.3	19.7
std 6	La	0.3	15.10	19.22	5.81	59.8	44.2	22.2	13.2	20.2
std 7	La	0.15	16.80	18.98	2.89	61.3	49.9	22.3	6.68	21.0
std 8	Mn	0.15	20.32	16.88	2.50	60.3	56.6	18.6	5.41	19.3
std 9	La	0.3	12.48	16.58	4.52	66.4	41.3	21.7	11.6	25.3
std 10	Mn	0.3	19.19	14.37	4.83	61.6	53.7	15.9	10.5	19.8
std 11	Mn	0.15	21.10	16.64	2.65	59.6	57.6	17.9	5.62	18.7
std 12	La	0.15	17.80	19.30	3.52	59.3	50.8	21.8	7.81	19.5
std 13	Mn	0.15	20.01	17.65	2.45	59.8	55.9	19.5	5.32	19.2
std 14	La	0.15	16.87	19.45	2.99	60.6	49.8	22.7	6.85	20.6
std 15	La	0.3	15.01	20.31	6.23	58.4	43.3	23.2	13.9	19.4
std 16	Mn	0.3	19.60	15.50	5.70	59.2	53.0	16.5	11.9	18.4

BET testing data is given in table 7. This data shows a poor surface area in comparison the perovskites prepared by reactive grinding, however the materials that did not undergo a heat treatment show a surface area on par with the coperciptation catalysts.

Table 7. BET results statistical design

std	C value	BET SA (m^2g^{-1})
1	52	2
2	74	9
3	94	3
4	488	4
5	339	4
6	47	2
7	84	5
8	221	1
9	168	4
10	547	1
11	111	7
12	310	2
13	211	2
14	124	4
15	193	1
16	156	6

Figur 17 shows a powder XRD comparison of all 16 standards separated by whether or not they underwent a heat treatment step, immediately apparent is the decreased intensity of the reflections at 15, 27 and 49 degrees which correspond to lanthanum oxide. And an increasing intensity and sharpening of the peaks that correspond to the perovskite phase at 23, 33 and 47 A sample of standard 5 was preserved before heat treating in order to determine how the phase changes over a test, the powder XRD pattern in Figure 18 shows an increase in the perovskite reflections and a reduction in the precursor reflections. Although the perovskite phase is being formed in the ball mill it is less crystalline in this example, however this sample was low speed and low duration grind resulting in a poorer conversion to the perovskite phase.

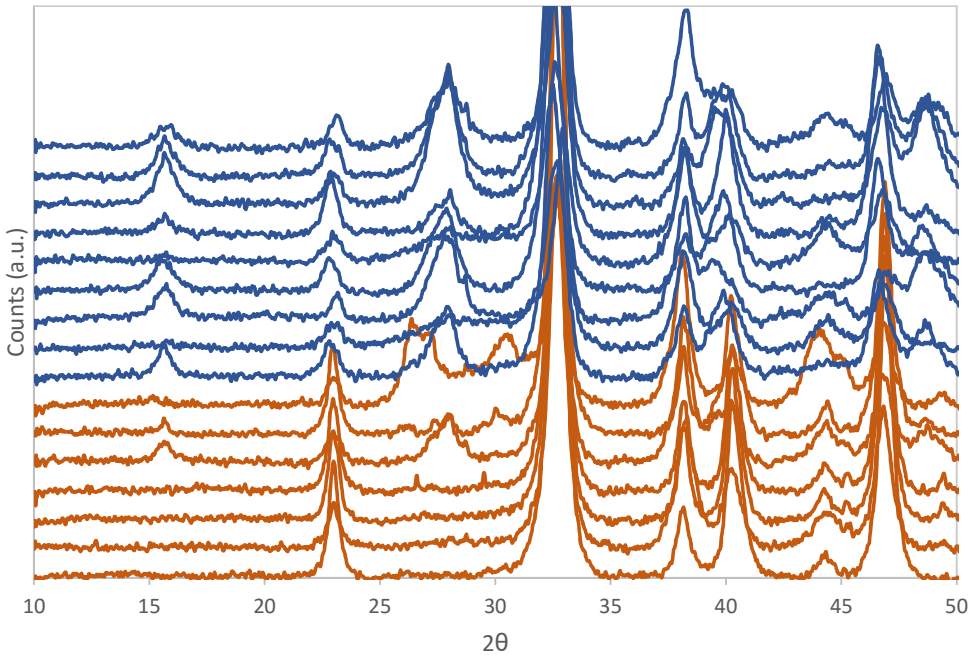

Figure 17. Heat treated catalysts (orange) vs non heat treated catalysts (blue). 700 °C for 5h in static air at a ramp rate of 10 °C/min.

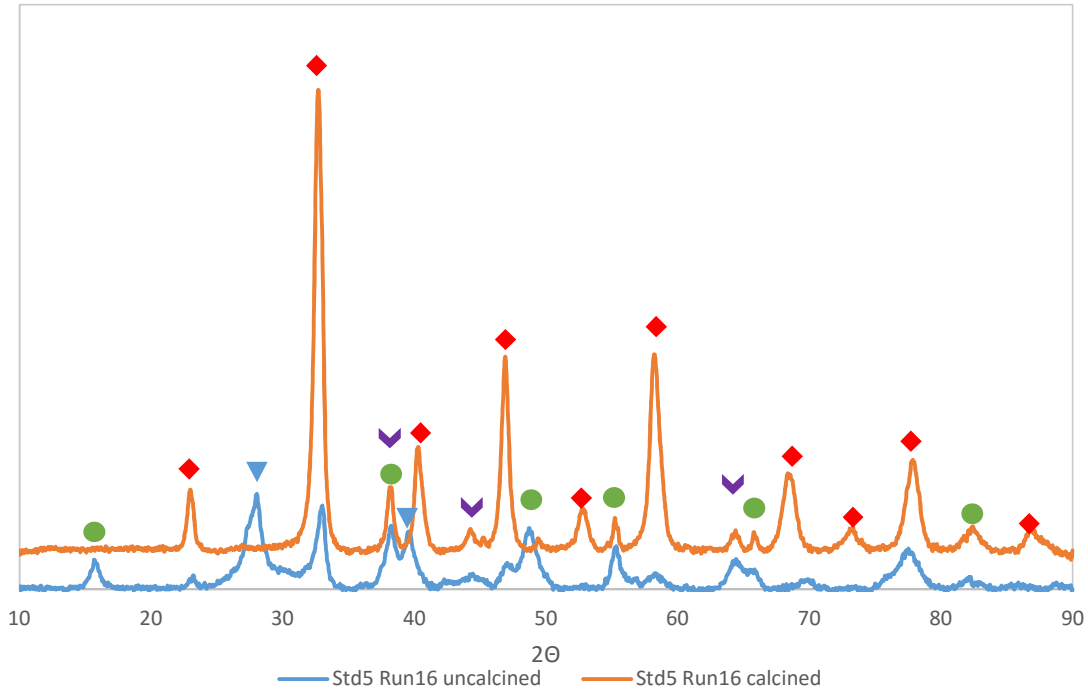

Figure 18. Standard 5 before and after a heat treatment at 700 °C for 5h in static air at a ramp rate of 10 °C/min. $LaMnO_{3-\delta}$ (red diamonds), Ag (purple chevrons), Ag_2O (green circles), La_2O_3 (blue triangles).

In summary, it can be seen the by far the most important factor in the formation of perovskites by this method is the calcination step, the crystallinity of the perovskite phase is enhanced in heat treated catalysts and the incidence of precursor phases such as La_2O_3 are reduced in the heat treated catalysts. Speed and duration are also key factors, with precursors left unincorporated during the grinding procedure.

3.5.2 Results

The catalytic activity was measured under lean testing conditions only as a means of screening the performance. As can be seen from Figure 19 to Figure 22which show the activity for CO, C_3H_8, NO conversion and NO_2 production, the variation between catalysts is great over the standardised testing conditions, none of the catalysts preformed as effectively as the catalyst prepared by the reactive grinding technique, however all catalysts are active. The data was assembled into a table under different response types, T10, T50 and T90 for CO oxidation, T10 for C_3H_8 oxidation, activity at specific temperature increments at 250 °C, 350 °C and 450 °C for C_3H_8, CO, NO, NO_2 and N_2O. The approximate error calculated for each measurement (δ) was added and the minimum signal response (σ) determined such as to give an acceptable resolving power for the statistical study, a table of these values is included in the appendix. The data is tabulated and the analysis can be carried out.

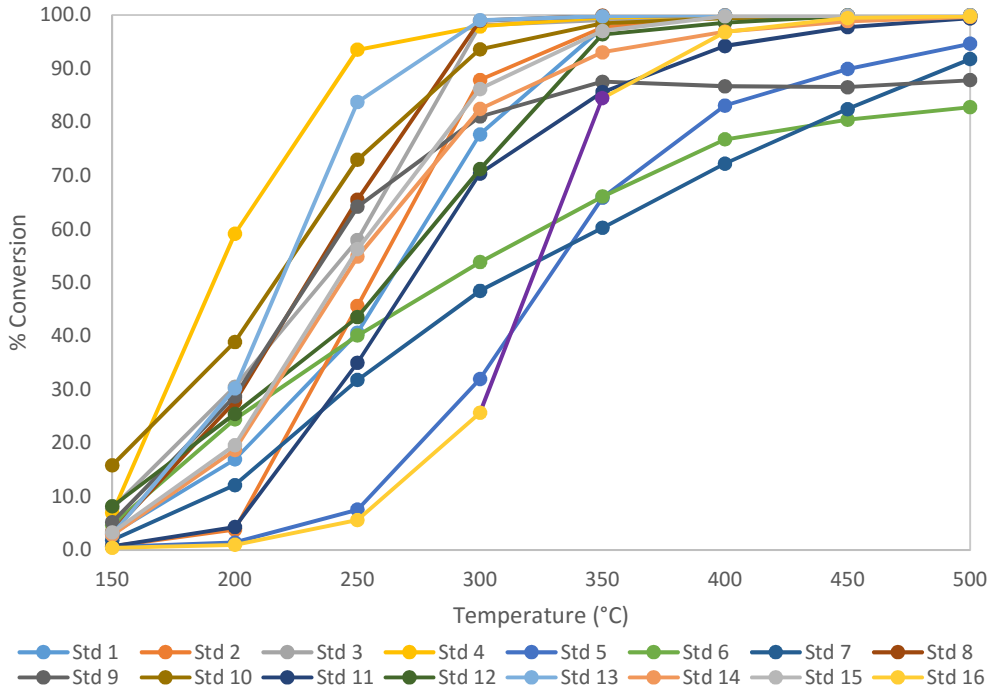

Figure 19. CO conversion over standard lean conditions, 0.3 cm^3 catalyst, 30,000 h^{-1}, 1% CO, 0.1% C_3H_8, 300 ppm NO, 8% O_2, 6% CO_2, 8% H_2O

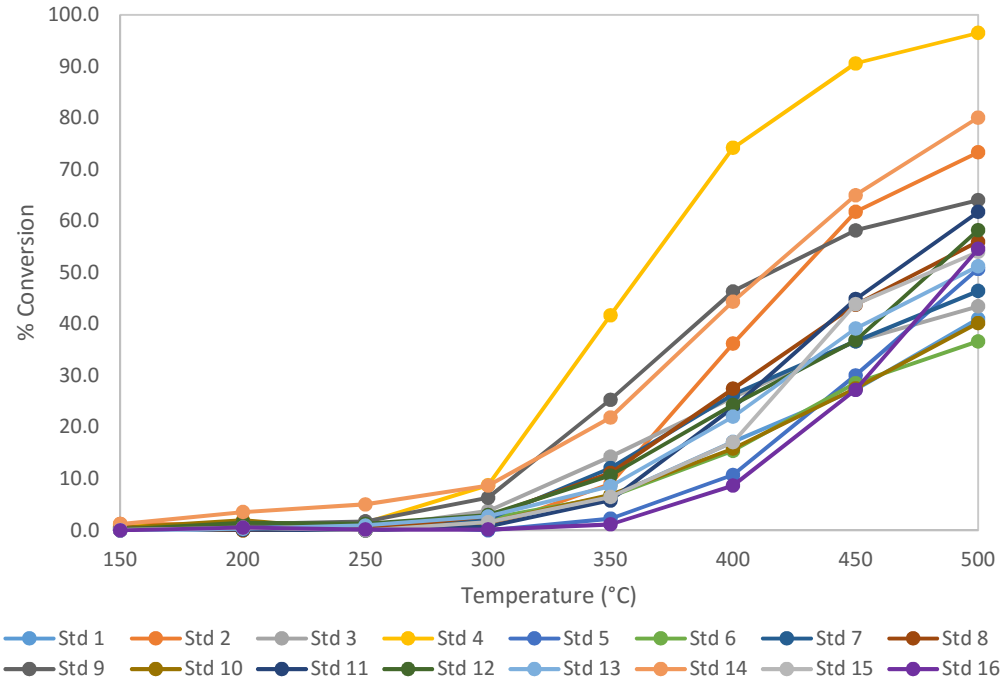

Figure 20. C_3H_8 conversion over standard lean conditions, 0.3 cm^3 catalyst, 30,000 h^{-1}, 1% CO, 0.1% C_3H_8, 300 ppm NO, 8% O_2, 6% CO_2, 8% H_2O

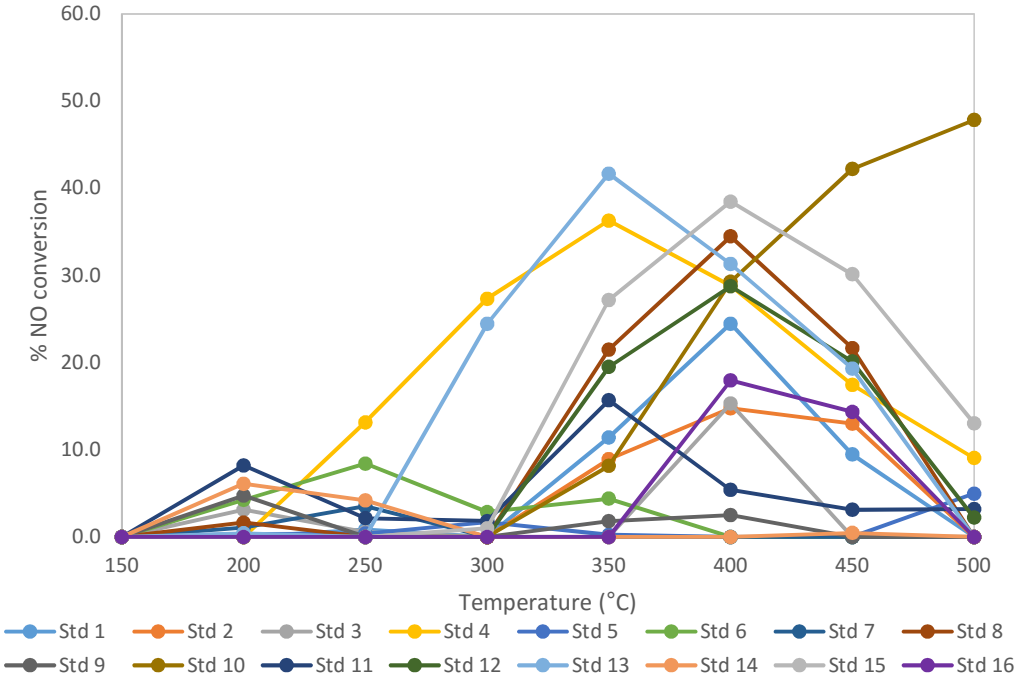

Figure 21. NO conversion over standard lean conditions, 0.3 cm^3 catalyst, 30,000 h^{-1}, 1% CO, 0.1% C_3H_8, 300 ppm NO, 8% O_2, 6% CO_2, 8% H_2O

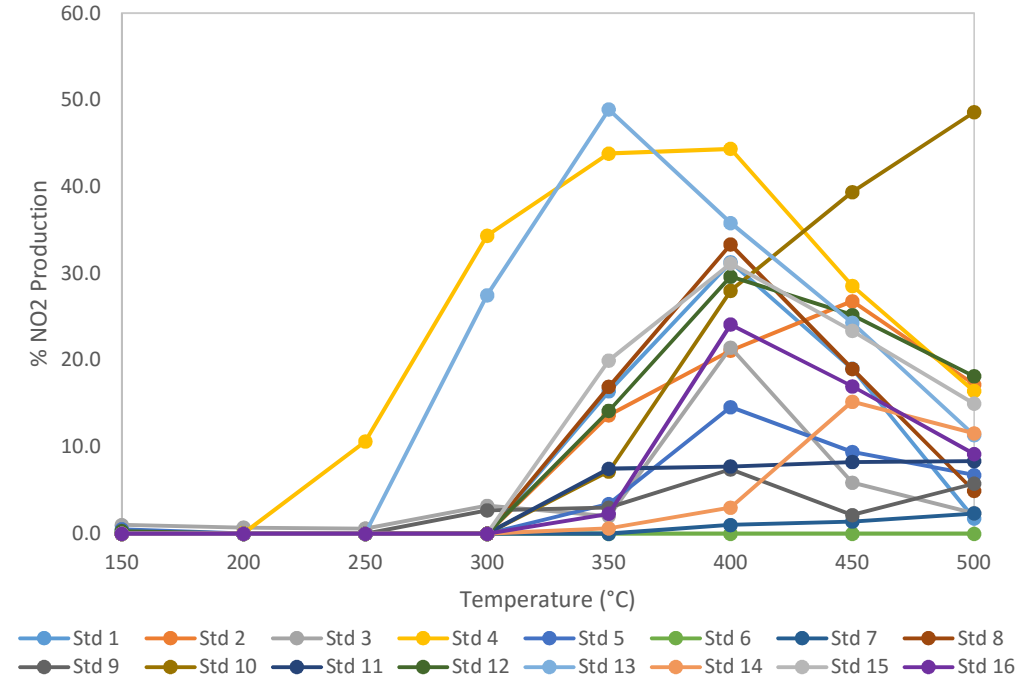

Figure 22. NO_2 production over standard lean conditions, 0.3 cm^3 catalyst, 30,000 h^{-1}, 1% CO, 0.1% C_3H_8, 300 ppm NO, 8% O_2, 6% CO_2, 8% H_2O

3.5.3 Analysis

The first step of the analysis is to select a response factor and perform a transform operation based on the ratio of maximum to minimum values. For ratios under 3, which constitute the majority of responses in this study, no transformation is required as it will have little effect, and generally values over 10 require transformation. Once the requirement for transformation was determined, a half-normal plot was used to identify the significant effects. Points were selected from the higher end of the x-axis until the non-significant factors closest to zero conform to a line of best fit. A Pareto plot was used to confirm the significance of the selected effects (example in figure 23). Values that appear above the t-value limit were possibly significant and for a screening analysis such as this one are still useful for identifying potentially important effects, while values exceeding the Bonferroni limit (where the individual significance level is divided by the number of experiments n) were considerably more likely to be significant and can be considered with confidence. The data was then assembled in an ANOVA table which provided the p-value for each effect, and the required p-value for a higher than 0.01% chance the effects are due to noise.

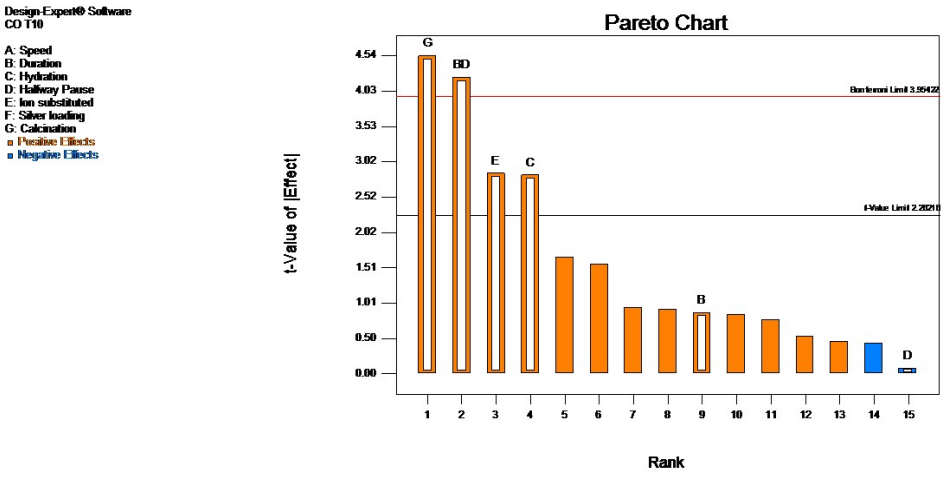

Figure 23. Example of a Pareto plot for CO T10, significant values and those involved in significant two factor interactions appeared hollowed out, t-value limit (grey line) and Bonferroni limit (red line) are marked

For CO conversion the most significant single factor was calcination, the catalysts that did not undergo a heat treatment procedure were more active for CO Oxidation at T10 (Figure 24).

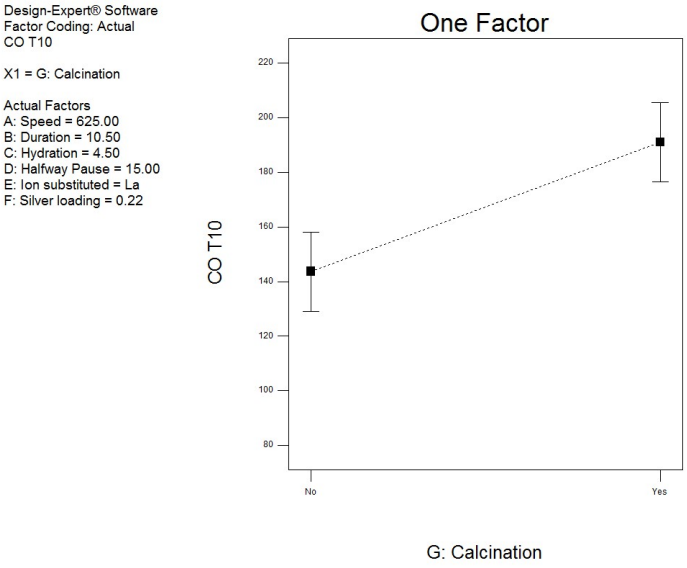

Figure 7. CO T10 effect of calcination

There are several possibilities for this effect, the first being that as imperfections and deformity in the lattice are important for catalysis on perovskites, the heat treatment process allows the lattice to reorganise and some of these defects are lost, thus reducing the catalytic capability of the catalyst. This rearrangement can also lead to a loss of surface area as the perovskites sinter, which can be seen from the BET data in Table 8, although no effect was seen in the experimental data. A second possibility is that the heat treatment step is reducing the silver oxide to silver, which is less active for CO oxidation than Ag^{+}. [39]

Table 8. Five point BET surface area of catalysts

Test	Heat treatment	C Value	Surface area (m^2g^{-1})
Std 14 Run 3	Yes	388	1
Std 14 Run 3	No	124	4
Std 11 run 5	Yes	288	1
Std 11 run 5	No	111	7
Std 2 run 8	Yes	524	3
Std 2 run 8	No	74	9
Std 9 run 9	Yes	158	1
Std 9 run 9	No	168	4
Std 4 Run 10	Yes	102	4
Std 4 Run 10	No	488	4
Std 16 Run 12	Yes	44	2
Std 16 Run 12	No	156	6
Std 7 Run 15	Yes	366	2
Std 7 Run 15	No	84	5
Std 5 Run 16	Yes	216	3
Std 5 Run 16	No	339	4

When the T50 data was considered, a few trends presented themselves. Once more the calcination had a significant effect on the activity of the catalysts, but it is this time it is involved in a 2 factor interaction with speed (Figure 25). When the speed is low at 600 RPM the effect of calcination has a much larger detrimental effect on activity, increasing the average CO T50 by approximately 50 °C. Whilst at a higher milling speed the effect of heat treatment is lessened and has no effect. It was expected that while a higher speed would produce the perovskite faster it would generate the higher temperatures by friction that might reduce the surface area. A possibility is that the higher speeds produce a more intimately mixed oxide, this stabilises the Ag2O in the perovskite lattice and so preserves the activity after a heat treatment.

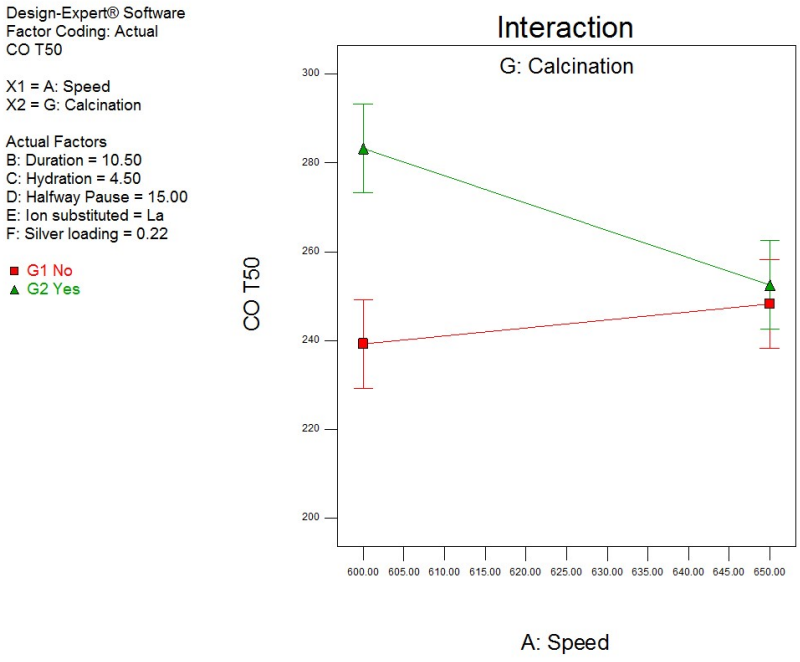

Figure 25. Two factor interaction between the heat treatment step and speed.

Comparing the EDX data of two samples in table 9, std9 was milled at low speed and Std2 at high speed with both samples before and after the heat treatment step. If the high speed milling stabilised the silver oxide then it would be expected to see a simultaneous decrease in oxygen and a subsequent increase in silver in the low milling speed sample and no such significant change for the high speed samples. Assuming a decomposition of Ag_2O to Ag(0) then for the decomposition of $Ag_{0.3}$ and $Ag_{0.15}$ perovskite it would be expected to see a decrease in oxygen mass of approximately 0.62 wt% and 0.31 wt% respectively. Std9 saw a drop of well over this amount a possible factor being oxygen loss from the perovskite lattice while undergoing heat treatment. A slight increase in silver is seen but within the error of the measurement.

Table 9. EDX quantification of elements on ball mill samples before and afterheat treatment for both weight and atomic percent.

	Std9		Std9 after heat		Std2		Srd2 after heat	
Element	wt%	at%	wt%	at%	wt%	at%	wt%	at%
O K	25.33	66.42	23.09	63.8	22.32	64.86	24.77	65.76
Mn K	21.71	16.58	21.92	17.64	16.88	14.28	21.82	16.86
Ag L	11.61	4.52	11.71	4.80	5.23	2.25	11.92	4.69
La L	41.34	12.48	43.28	13.77	55.57	18.60	41.49	12.68

TPR would reveal if there is a reduction peak from the silver oxide present in the sample, if the perovskite support stabilises the oxide phase then a peak shift would be expected. Silver oxide was tested under standard TPR conditions as laid out in chapter 2, this produced a large reduction peak at approximately 150°C with a shoulder visible at approximately 180 °C. These peaks may correspond to a crystalline Ag_2O phase and a dispersed Ag_2O respectively as the dispersed phase is thought to be more stable.[40]

Figure 26 shows a TPR of oxides milled for increasing intervals to make $LaMn_{0.7}Ag_{0.3}O_{3-\delta}$, there is a decrease in the magnitude of the silver reduction peaks and shift to higher temperatures up to 4h. The shift to a higher temperature indicates that the silver oxide is becoming more difficult to reduce and the reduction in magnitude of the peak indicates less reducible material available. The reduction in available reducible material could be due to the silver being reduced under milling conditions. Table 10 displays the peak positions and areas.

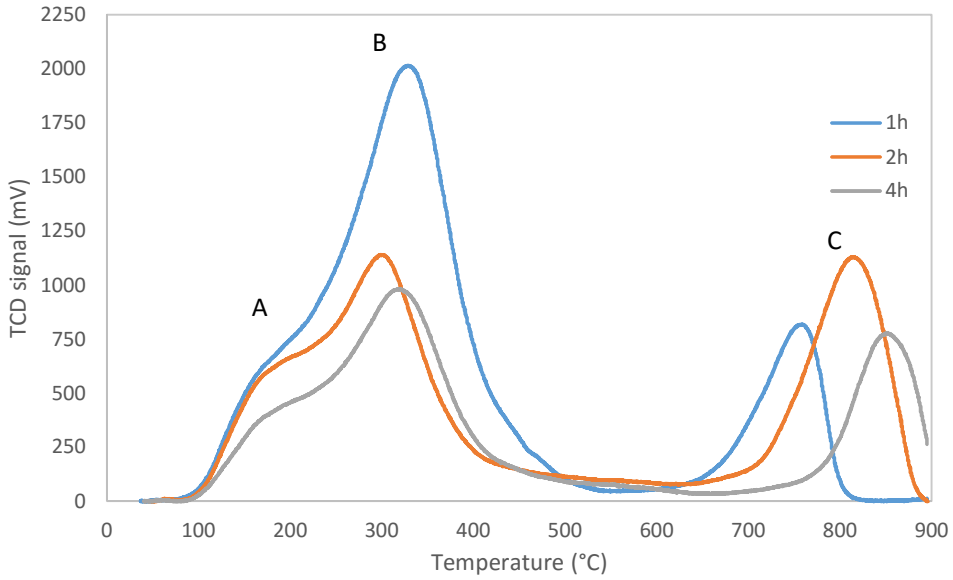

Figure 26. TPR of La_2O_3, Mn_2O_3 and Ag_2O milled at increasing intervals showing 3 peaks labelled A, B and C

Table 10. Peak positions and areas of TPR data of catalysts tested by grind time

	A (°C)	Mag	H2 (mol)	B (°C)	Mag	H2 (mol)	C (°C)	Mag	H2 (mol)
1h	188	70320	$4.154x10^{-5}$	324	267665	$1.58x10^{-4}$	745	57075	$3.37x10^{-5}$
2h	188	40245	$2.3774x10^{-5}$	295	130232	$7.69x10^{-5}$	808	101003	$5.97x10^{-5}$
4h	189	32798	$1.9375x10^{-5}$	315	120594	$7.12x10^{-5}$	850	61630	$3.64x10^{-5}$

Also showing a significant effect was the interaction between the halfway pause and the duration of the grind. As the perovskite forms during the longer grinds the long

sustained temperature on a grind without a pause improved activity, while the precursors, which still show activity, benefit from a pause. While temperature may have had an impact of phase formation, it can also have physical effects on the system as well. As the oxides being ground cooled they may have cracked, this could expose lower layers of unconverted material, which may then become incorporated into outer layers upon resumption of grinding. This in effect reduces the overall activity of the catalyst. The pause being beneficial to the activity of the shorter grind may be explained by looking at previous data collected for the reactive grind. In earlier experiments it was determined that the most active species was the amorphous material produced before the perovskite phase had a chance to form. A possibility is that the short grind is hindered in its conversion to a perovskite phase by this pause, which is not detrimental to initial activity but may not provide long-term stability, especially under the demanding conditions required in three way catalysis. Further testing is required to determine if this is the case.

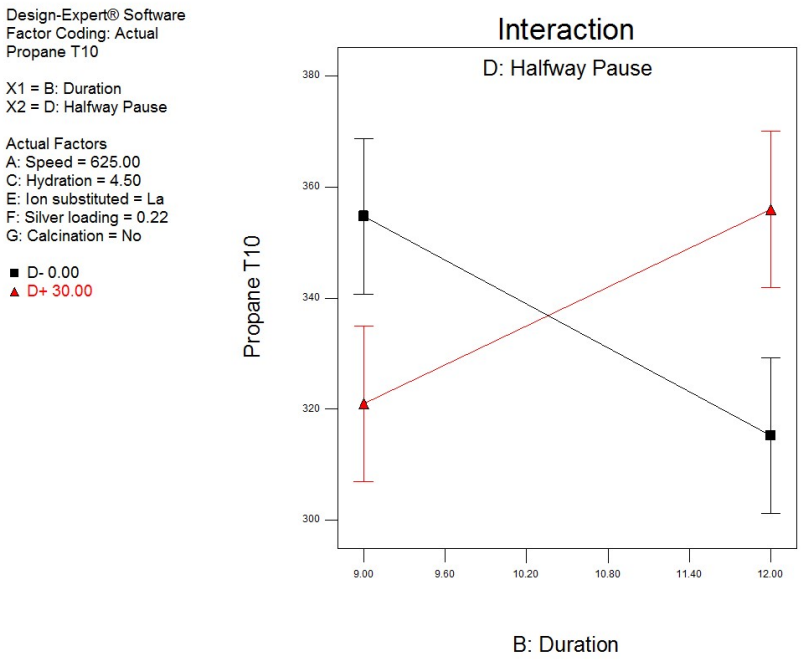

Figure 8. 2 factor interaction between the halfway pause and grind duration and its effect on T10 propane conversion

When comparing the XRD patterns separated into these 4 categories as in Figure 28 we can see some differences that may account for the effect. The catalysts that undergo a pause at 9h have more secondary phases than those that do not undergo a pause. The catalysts milled for 12h however showed a greater incidence of secondary phases when the pause occurred in comparison to no pause. This is possibly a result of the hypothesised effect that during a longer grind, a rest period allows the hardened outer layers consisting of unconverted precursors to incorporate into the perovskite phase, possibly due to contraction on cooling of both the material and the vessel. The 12h grind catalysts with a 30 minute pause show a greater incidence of Ag_2O, La_2O_3 phases with less consistency between them. The 12h grind with no pause shows a better conversion with no La_2O_3 phase seen and more consistent signal for the perovskite phase and for the presence of Ag. When comparing the 9h grinds, it was seen that the consistency within tests is reduced generally, with greater variation between tests, strong responses were seen for lanthanum phases in some samples and variable responses for silver oxide and metallic silver also. Between the pause and no pause tests however there is an important difference between the perovskite phases, the catalysts with a pause show a consistent perovskite phase, however the catalysts with no pause showed two tests with a better defined perovskite phase and two on par with the paused grinds. Because of the nature of statistical studies direct comparisons are difficult, however the general shift was towards greater consistency at long grinds with a pause which is possibly resulting in the improved activity. Analysis of the XRD for the short grinds was inconclusive, a possibility is that there was an amorphous transition between the precursor oxides and the final perovskite phase that is more active.[12] Looking at the comparison in Figure 29 it was seen that the more active catalysts generally had more crystalline perovskite phases.

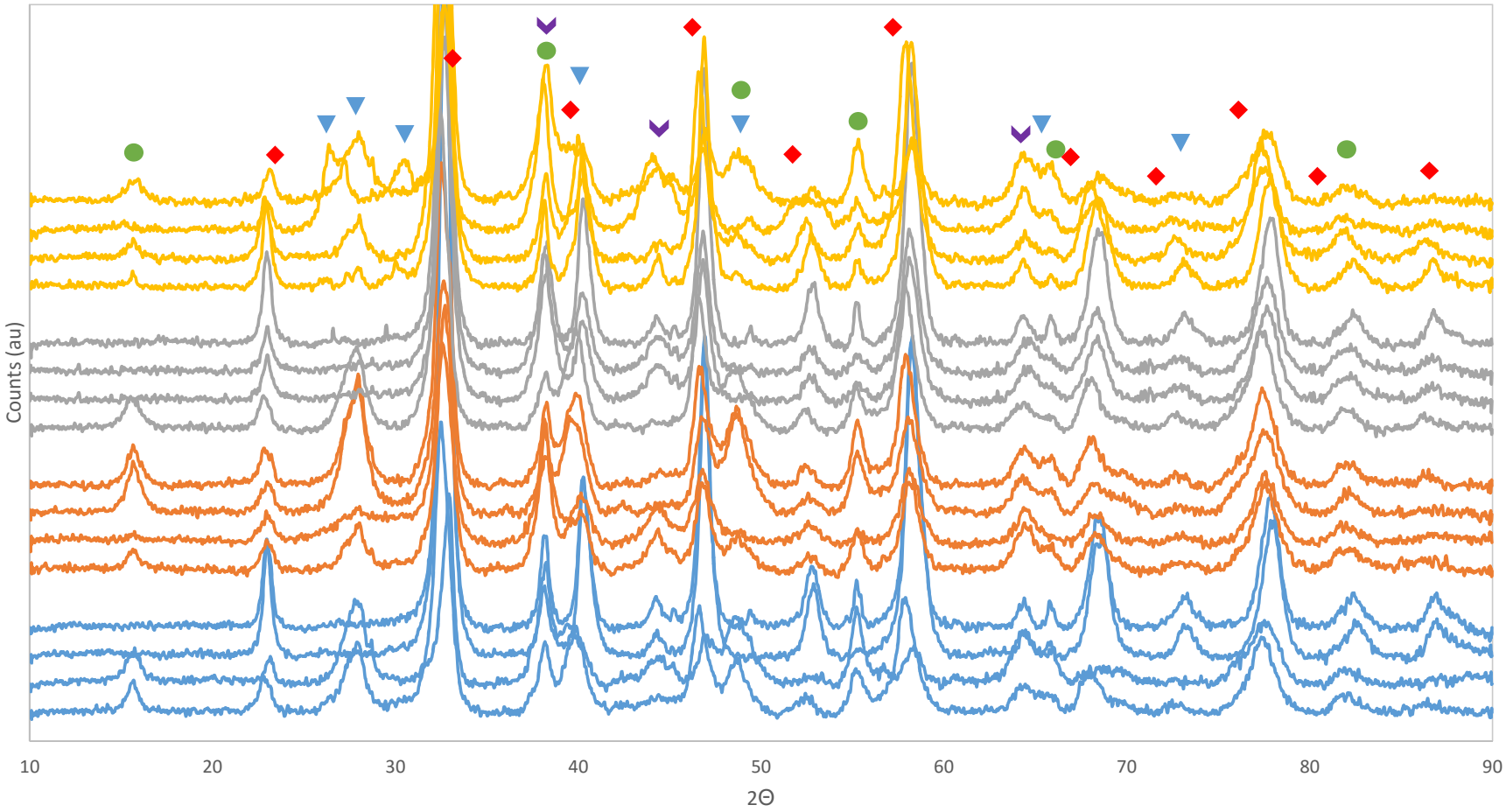

Figure 28. Powder XRD patterns of lanthanum manganese perovskite separated by duration and pause. From top to bottom; 12h with 30 minute pause (yellow), 12h with no pause (grey), 9h with 30 minute pause (red), 9h with no pause (blue). Markers indicate phases of materials present; $La_{1-x}Mn_{1-y}O_{3-\delta}$ (red diamond), La_2O_3 (blue triangle), Ag_2O (green circle), Ag^0 (purple chevron)

Table 11. Position of principal perovskite reflection and crystallite size.

Std	Peak pos. [°2Th]	B struct. [°2Th]	Crystallite size [Å]
1	32.5	0.951	87
2	32.676	0.665	124
3	32.569	1.06	78
4	32.675	0.653	127
5	32.833	0.661	125
6	32.606	0.556	149
7	32.451	0.889	93
8	32.6	0.61	136
9	32.553	1.02	81
10	32.649	0.727	114
11	32.501	0.785	105
12	32.502	0.766	108
13	32.597	1.101	75
14	32.508	0.83	100
15	32.819	0.82	101
16	32.491	0.8	103

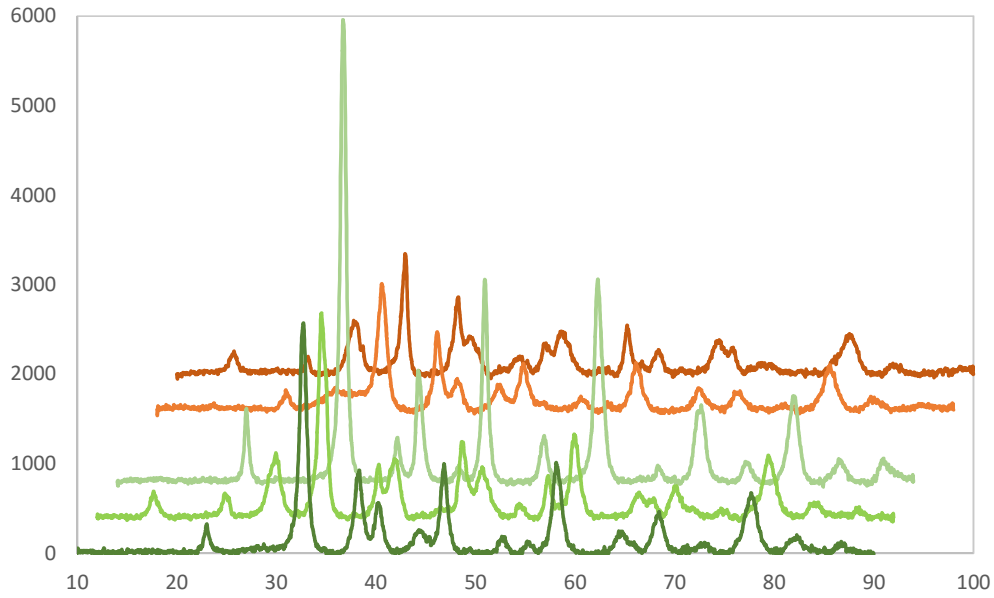

Figure 9. Powder XRD comparison of 3 best performing catalysts (bottom, green) and 3 worst performing catalysts (top, red) for C_3H_8 oxidation.

The effect of the pause is also seen for the T10 of C_3H_8 conversion, while the effect that the calcination stage had on the CO T50 conversion is not conclusively seen in this case. The T10 propane results also indicate that the ion exchanged from the perovskite lattice has an effect (Figure 30). The catalysts with La exchanged are more active for propane oxidation, suggesting that the perovskite plays more of a role in propane oxidation than the Ag or Ag_2O, additionally it suggests that the defects introduced via La substitution are more important for propane oxidation. As the Mn^{3+} to Mn^{4+} ratio is changed when either ion is substituted. When the lanthanum ion is substituted with silver then there are more Mn^{4+} ions present to make up for the lack of positive charge in the A-site. This may indicate that the redox couple of both oxidation states is responsible for the increased activity for propane oxidation and is irrelevant for CO oxidation. A possibility is that with A site substitution more of the B site ions were left to carry out the catalysis while retaining the oxygen vacancies and defects that are important for catalysis on perovskites[35].

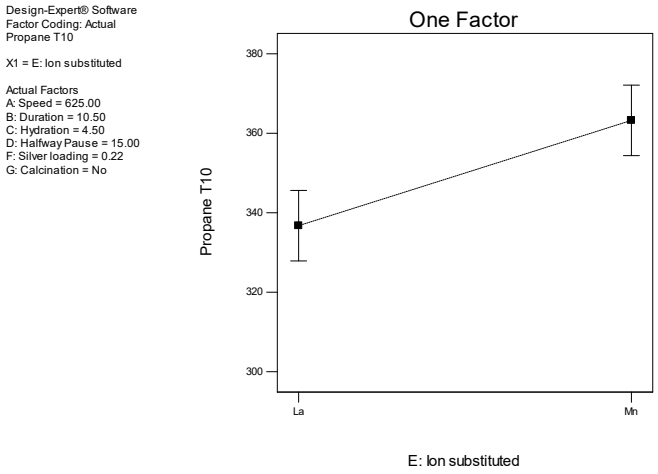

Figure 30. One Factor plot of the effects of ion substitution on propane conversion visible at T10

The only significant effect is detected for NO conversion which is the heat treated stage, Figure 31 shows that after a calcination step the NO conversion drops. This is likely due to the calcination decomposing any Ag_2O present into metallic Ag which is less active for NO oxidation or as a result of the increased selectivity for the perovskite phase of the heat treated catalysts. However, the utility and accuracy of this information is distorted by the absence of N_2 quantification and NO storage effects.

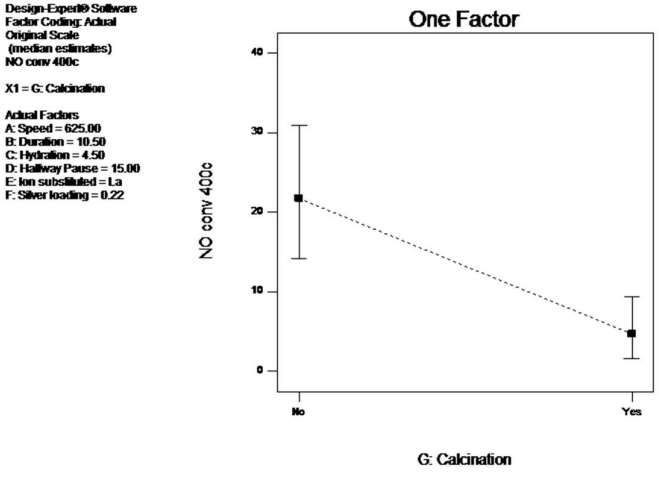

Figure 31. One factor effect of calcination on NO conversion.

3.6 SO_2 resistance

A concern for perovskite catalysts is their stability in the presence of sulphur dioxide, the lanthanum ion is very basic and strongly adsorbs SO_2 from the gas feed. This adsorption gradually degrades the perovskite structure and thus deactivates the catalyst. Additionally, SO_2 can poison metallic particles by blocking the surface and so can also deactivate metallic silver, this is a major consideration in exhaust gas applications because although sulphur emissions are low in developed countries, emerging markets have considerably more sulphur present in fuels and still represent a significant challenge for automotive catalysis.

In order to test the effects of SO_2 poisoning on $LaMn_{0.8}Ag_{0.2}O_{3-\delta}$ A sample was exposed to 15 ppm of SO_2 at 10,000 h^{-1} and a flow rate of 100 mL/min, the concentration is elevated over typical levels found in gasoline exhausts of <5 ppm to accelerate the aging effects on the catalyst. The SO_2 is flowed over the catalyst bed for ten minutes at room temperature before it is heated to 500 °C at a rate of approximately 20 °C min^{-1}. The catalyst was held at 500 °C for approximately 6 h before being cooled to room temperature under continuous flow. The sample was then recovered for testing.

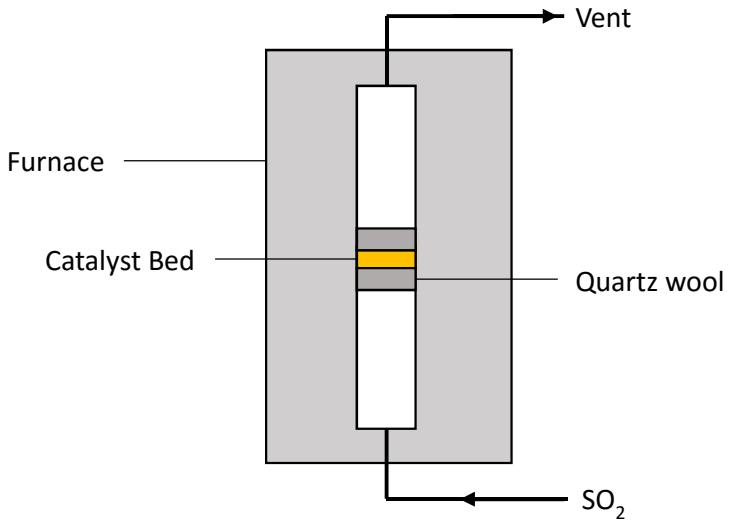

Figure 32. Diagram of SO_2 treatment process

The effects of SO_2 poisoning on catalytic activity are significant (Figure 33), there is a ≈50 °C increase of the CO T50 and a larger increase of 75 °C for the T50 of propane. There is a flatter light-off curve after SO_2 poisoning which indicates that the reaction may have become mass transfer limited, this is likely because Ag active sites are being blocked or by adsorbed SO_2[41] limiting the reaction rate or the perovskite phase is being destroyed by the reaction of La with SO_2[42]. The deactivation of these catalysts is irreversible under heating under both flowing nitrogen and lean exhaust conditions at 500 °C for 6h.

The resistance to SO_2 can be improved by the addition of a sacrificial agent, as in current catalysts there is a barium oxide component that also plays a role on SO_x control. As group 2 oxides are relatively basic in character[43] it preferentially adsorbs SO_2 to form barium sulphate. It has been shown that SO_2 resistance varies significantly between different perovskite compositions[44, 45], a more resilient A site cation would be desirable, however, lanthanum is integral to the activity of the catalyst and is not easily replaced, future work could investigate partial or whole A site substitutions to find a more robust catalyst that does not sacrifice activity.

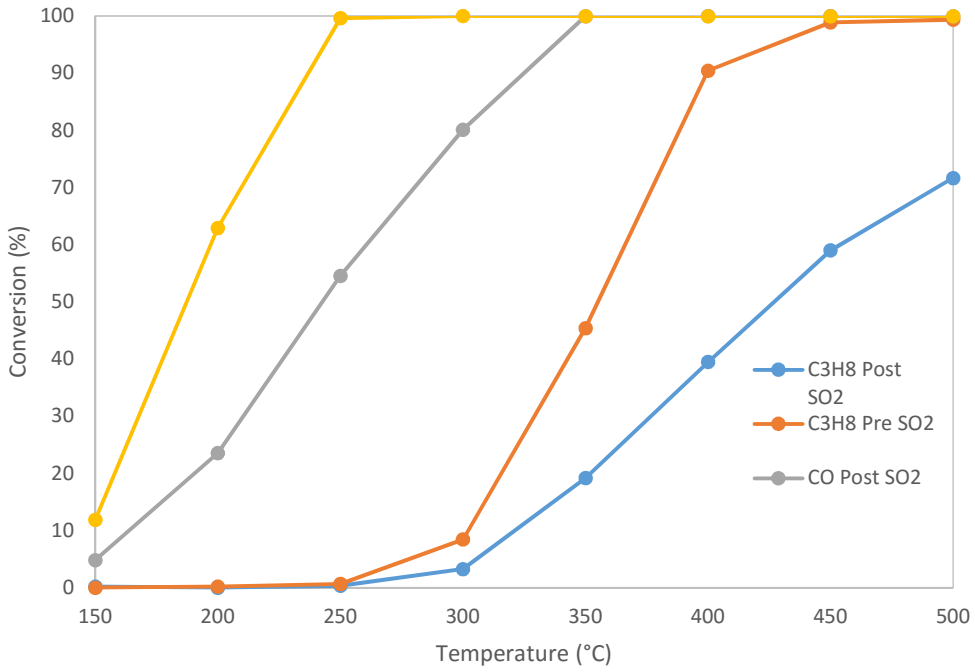

Figure 33. The effects of SO_2 on the $LaMn_{0.8}Ag_{0.2}O_{3-\delta}$ catalyst as prepared by the pestle and mortar reactive grinding technique.

3.7 Comparison with conventionally prepared catalysts

The final step was a comparison with the more conventionally prepared catalyst, from Figure 34 shows a comparison of the catalysts synthesised in this chapter for CO oxidation. Taking the best performing catalyst from the statistical design, we can see that the catalyst prepared in the ball mill is at least as effective as a perovskite prepared by copreciptation. The most active catalyst of these is the catalyst prepared by the reactive grind process.

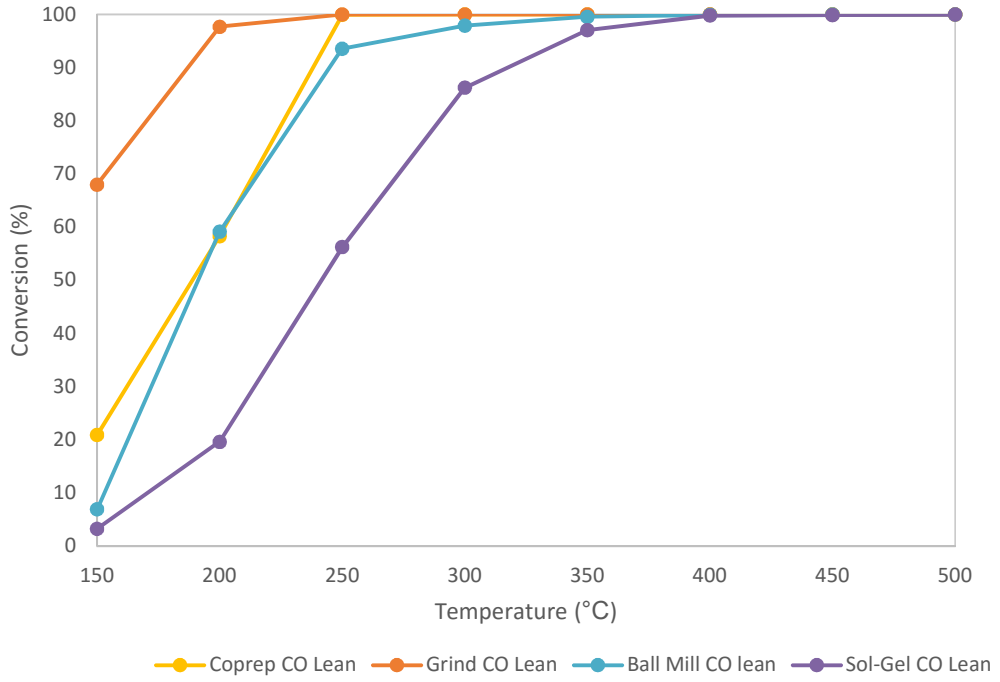

Figure 34. Comparison of $LaMn_{0.7}Ag_{0.3}O_3$ as prepared by coprecipitation, reactive grinding, high energy ball milling under lean testing conditions for CO oxidation.

Similarly, performance differences were seen for propane oxidation (Figure 36), the main difference being that the coprecipitation catalyst outperformed the catalyst prepared in the ball mill. The top performing catalyst once again prepared by reactive grinding and the least active is the sol-gel preparation.

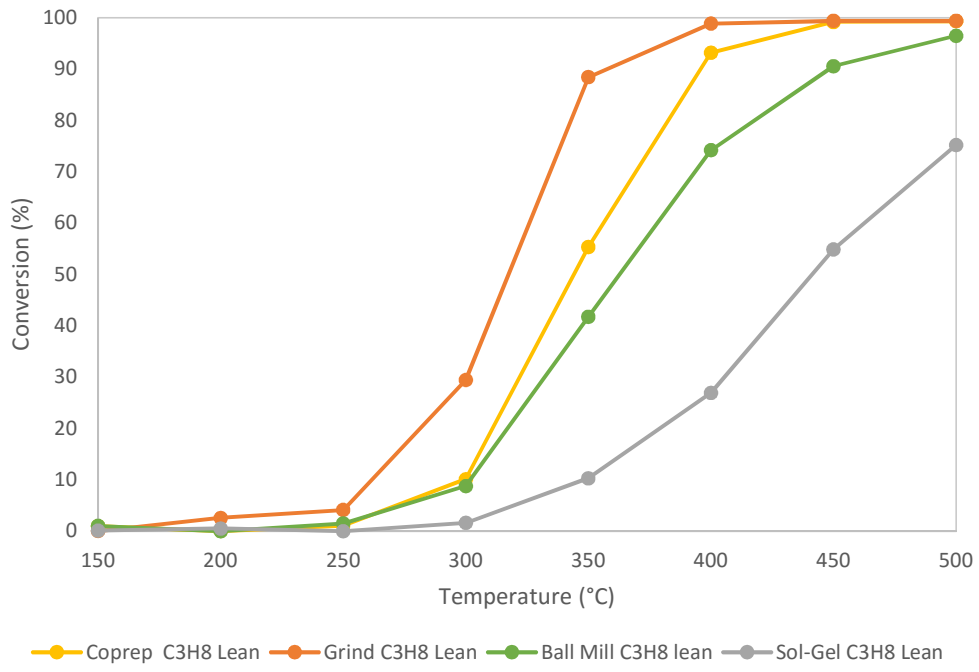

Figure 35. Comparison of $LaMn_{0.7}Ag_{0.3}O_3$ as prepared by coprecipitation, reactive grinding, high energy ball milling under lean testing conditions for propane oxidation.

For NO activity (Figure 36), generally the more active the catalyst for the oxidation of CO and NO, the more active it was for the oxidation of NO. More often than not, this is an undesirable reaction. The only use it has in exhaust after treatment is as an oxidising agent for soot. As these tests were not carried out under real world conditions, where the exhaust output oscillates around the stoichiometric point, these catalysts may still be capable of performing adequately under exhaust conditions and with other components present in the catalyst may be capable of carrying out reduction. The NO activity data (Figure 36) shows that the catalysts that display the most activity for NO oxidation are the catalysts prepared by reactive grind and coprecipitation. The catalyst prepared by sol-gel produced the least NO_2 of all the catalysts.

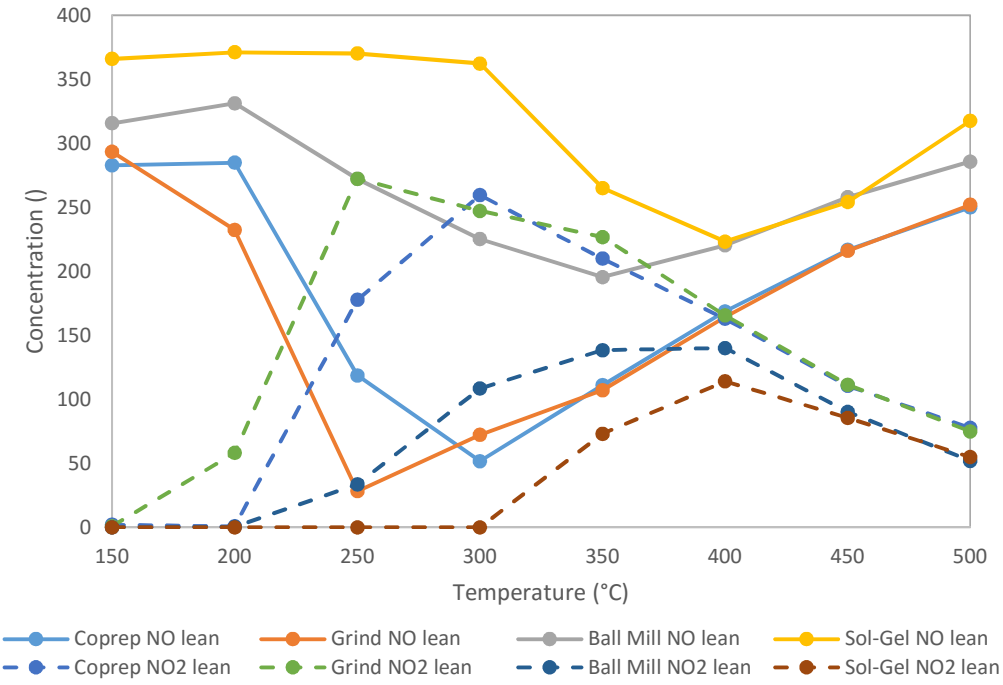

Figure 36. Comparison of $LaMn_{0.7}Ag_{0.3}O_3$ as prepared by coprecipitation, reactive grinding, high-energy ball milling under lean testing conditions for NO activity.

Surface area is a critical aspect of perovskites, as they are extremely prone to sintering. The catalysts prepared by reactive grinding showed a significantly improved surface area (Table 12) compared to the other supports. While this may not be important for the activity of the perovskite itself, it has implications for the support of materials on the perovskite surface that may carry out reduction, NO_x storage or other secondary functions in the catalyst.

Table 12. BET results varied techniques for synthesis of $LaMnO_3$

Sample	C value	BET surface area
Coprecipitation	58	1
Sol-gel	193	9
Pestle and mortar	141	19
Ball mill	32	5

3.8 Conclusions

The application of milling in the synthesis of mixed metal oxides provides an interesting avenue of research for future catalysts, the system allows many of the downsides of traditional synthesis to be avoided while still producing active materials. However, the mechanochemical synthesis of materials is not fully characterised in the literature and the effects of this alternative synthesis on catalysts is not fully understood. The silver doped $LaMnO_3$ catalysts prepared in this chapter all show good activity for the treatment of exhaust gases and have established activity already, however these techniques use traditional methods such as coprecipitation and sol-gel preparations. The samples produced by reactive grinding dramatically reduce the solvents required for production and still produce very active catalysts. The catalysts prepared by ball milling have an incredibly simple synthetic procedure that almost entirely eliminates solvent requirements and totally eliminates solvent waste, industrially this would reduce costs and cut the environmental risks associated with waste stream disposal.

The technique is not without issues however, optimisations need to be performed on yield and for consistent phase conversion. The effects of all possible factors influencing final catalytic activity and physical properties need to be studied more closely and some of the interesting effects investigated directly such as the factors outlined in the statistical study discussed earlier in this chapter. High energy ball milling are not as scalable to the degree coprecipitation or sol-gel procedures are and may present safety hazards of their own. Energy requirements increase proportionally to the scale up ratio to the power of 4.87 and so for very large scale reactions may become unfeasible[46]. Additionally, scale may introduce different problems such as the practicality and cost of cell materials. However, the mechanochemical synthesis of catalysts is a growing field and the potential for new and exciting synthetic procedures for highly active catalysts will undoubtedly spur further research in the future.

3.9 References

1. M. Alifanti, J. Kirchnerova and B. Delmon, *Applied Catalysis a-General*, 2003, **245**, 231.
2. A. Machocki, T. Ioannides, B. Stasinska, W. Gac, G. Avgouropoulos, D. Delimaris, W. Grzegorczyk and S. Pasieczna, *Journal of Catalysis*, 2004, **227**, 282.
3. J. J. Zhu and A. Thomas, *Applied Catalysis B-Environmental*, 2009, **92**, 225.
4. Z. J. Sui, L. Vradman, I. Reizner, M. V. Landau and M. Herskowitz, *Catalysis Communications*, 2011, **12**, 1437.
5. M. Muroi, R. Street and P. G. McCormick, *Journal of Applied Physics*, 2000, **87**, 3424.
6. S. Ohara, H. Abe, K. Sato, A. Kondo and M. Naito, *Journal of the European Ceramic Society*, 2008, **28**, 1815.
7. B. D. Stojanovic, *Journal of Materials Processing Technology*, 2003, **143**, 78.
8. Q. W. Zhang, T. Nakagawa and F. Saito, *Journal of Alloys and Compounds*, 2000, **308**, 121.
9. Q. W. Zhang and F. Saito, *Journal of Alloys and Compounds*, 2000, **297**, 99.
10. M. J. Koponen, T. Venalainen, M. Suvanto, K. Kallinen, T.-J. J. Kinnunen, M. Harkonen and T. A. Pakkanen, *Journal of Molecular Catalysis A-Chemical*, 2006, **258**, 246.
11. Y. Nishihata, J. Mizuki, T. Akao, H. Tanaka, M. Uenishi, M. Kimura, T. Okamoto and N. Hamada, *Nature*, 2002, **418**, 164.
12. Z. Say, M. Dogac, E. I. Vovk, Y. E. Kalay, C. H. Kim, W. Li and E. Ozensoy, *Applied Catalysis B-Environmental*, 2014, **154**, 51.
13. H. Tanaka, I. Tan, M. Uenishi, M. Kimura and K. Dohmae, *Topics in Catalysis*, 2001, **16**, 63.
14. S. Kumar, Y. Teraoka, A. G. Joshi, S. Rayalu and N. Labhsetwar, *Journal of Molecular Catalysis A: Chemical*, 2011, **348**, 42
15. B. Kucharczyk and W. Tylus, *Applied Catalysis a-General*, 2008, **335**, 28.
16. A.E.B. Presland, G.L. Price, D.L. Trimm, *Journal of Catalysis*, 1972, **26**, 313
17. V. M. Goldschmidt, *Naturwissenschaften*, 1926, **14**, 477.
18. R. J. Baxter and P. Hu, *Journal of Chemical Physics*, 2002, **116**, 4379.
19. P. Mars, D.W. van Krevelen, *Chemical Engineering Science*, 1954, **3, Supplement 1**, 41
20. C. Doornkamp and V. Ponec, *Journal of Molecular Catalysis A-Chemical*, 2000, **162**, 19.
21. S. Colonna, S. De Rossi, M. Faticanti, I. Pettiti and P. Porta, *Journal of Molecular Catalysis A-Chemical*, 2002, **187**, 269.
22. R. Zhang, H. Alamdari and S. Kaliaguine, *Applied Catalysis B-Environmental*, 2007, **72**, 331.
23. A. Setiabudi, M. Makkee and J. A. Moulijn, *Applied Catalysis B-Environmental*, 2004, **50**, 185.
24. N. Tang, Y. Liu, H. Wang and Z. Wu, *Journal of Physical Chemistry C*, 2011, **115**, 8214.
25. N. Bogdanchikova, F. C. Meunier, M. Avalos-Borja, J. P. Breen and A. Pestryakov, *Applied Catalysis B-Environmental*, 2002, **36**, 287.

26. M. V. Twigg, *Applied Catalysis B-Environmental*, 2007, **70**, 2.
27. M. B. Gunther, R. Zhang and S. Kaliaguine, *Heterogeneous Catalysis Research Progress*, Nova Science Publishers, New York, 2008.
28. C. J. Blower and T. D. Smith, *Zeolites*, 1993, **13**, 394.
29. R. H. H. Smits and Y. Iwasawa, *Applied Catalysis B-Environmental*, 1995, **6**, L201.
30. K. Otsuka, R. Takahashi and I. Yamanaka, *Journal of Catalysis*, 1999, **185**, 182.
31. F. C. Meunier, J. P. Breen, V. Zuzaniuk, M. Olsson and J. R. H. Ross, *Journal of Catalysis*, 1999, **187**, 493.
32. K. Eranen, L. E. Lindfors, F. Klingstedt and D. Y. Murzin, *Journal of Catalysis*, 2003, **219**, 25.
33. L. H. Tjeng, M. B. J. Meinders, J. Vanelp, J. Ghijsen, G. A. Sawatzky and R. L. Johnson, *Physical Review B*, 1990, **41**, 3190.
34. G. B. Hoflund, J. F. Weaver and W. S. Epling, *Surface Science Spectra*, 1994, **3**, 157.
35. M. A. Pena and J. L. G. Fierro, *Chemical Reviews*, 2001, **101**, 1981.
36. P. Scherrer, Springer Berlin Heidelberg, Kolloidchemie Ein Lehrbuch, 1912, pp. 387-409.
37. J. H. Gong and C. S. Du, *Materials Science and Engineering A-Structural Materials Properties Microstructure and Processing*, 2000, **283**, 76.
38. N. J. van der Laag, A. J. M. van Dijk, N. Lousberg, G. de With and L. Dortmans, *Journal of the American Ceramic Society*, 2005, **88**, 660.
39. S. K. Megarajan, S. Rayalu, M. Nishibori, Y. Teraoka and N. Labhsetwar, *ACS Catalysis*, 2015, **5**, 301.
40. M. F. Luo, X. X. Yuan and X. M. Zheng, *Applied Catalysis A-General*, 1998, **175**, 121.
41. S. Xie, J. Wang and H. He, *Journal of Molecular Catalysis A-Chemical*, 2007, **266**, 166.
42. R. Zhang, H. Alamdari and S. Kaliaguine, *Applied Catalysis A-General*, 2008, **340**, 140.
43. M. Kosmulski, *Chemical Properties of Material Surfaces*, CRC Press, 2001.
44. M. Alifanti, R. Auer, J. Kirchnerova, F. Thyrion, P. Grange and B. Delmon, *Applied Catalysis B-Environmental*, 2003, **41**, 71.
45. H. Xian, X. W. Zhang, X. A. Li, L. Y. Li, H. H. Zou, M. Meng, Q. A. Li, Y. S. Tan and N. Tsubaki, *Journal of Physical Chemistry C*, 2010, **114**, 11844.
46. H. Mio, J. Kano and F. Saito, *Chemical Engineering Science*, 2004, **59**, 5909.

Chapter 4. Physical grinding for the preparation of Low PGM catalysts for lean exhaust gas after treatment.

4.1 Introduction

One of the main drives in automotive catalysis research is towards a reduced requirement for platinum group metals (PGMs)[1-3] or even their elimination[4-6], however, despite much research it has been difficult to produce a catalyst with the stability and performance of PGMs. In light of this, methods for promoting the activity of current catalysts to reduce any requirement for high loaded monoliths are generating interest, especially for reactions such as deep methane oxidation, where the commercial answer to stricter hydrocarbon legislation is to increase loading, with some commercial solutions having higher than 7% Pd.

Another pressure is towards simpler, greener preparations to reduce costs and the environmental impact of the industrial processes involved in making catalysts. Solid state preparation methods could reduce solvent use, thus significantly reducing waste streams from production. The preparations outlined in this chapter aimed to do this by grinding organic metallic salt precursors onto catalyst supports and decomposing in a furnace as described by Kondrat *et al*.[7], the procedure of which is outlined in 2.1.7, resulting in highly dispersed catalysts.

4.1.1 Metals

The precious metals chosen to investigate were platinum and palladium. Platinum is an active and relatively stable metal, however it has become increasingly expensive and its oxide is less stable at the elevated temperatures found in three way catalysis[8]. Palladium, while less active, is significantly more stable under exhaust conditions and can carry out reduction as well[9], which reduces the requirement for expensive rhodium. Platinum and palladium are typically the oxidation components in

automotive catalysis and have well established high activity and durability. As palladium can carry out reduction processes as well, combined with its relatively low cost and improved durability, it has recently become the favoured metal for many vehicle after treatment systems. Rhodium is the reduction catalyst in a TWC and is added in order to carry out the reduction of NO to N_2 and O_2. Rh like Pt and Pd has proven difficult to replace in TWCs and is still used commercially for NO after treatment.

The base metals investigated are cobalt(II), iron(II), and iron(III). The base metals are added to fulfil a number of roles, firstly they can promote the activity of the precious metals or augment their activity with their own catalytic properties, ceria[10] and cobalt oxide are particularly well described oxidation catalysts. Ceria in close contact with palladium is a particularly good oxidation catalyst for the deep oxidation of short chain hydrocarbons. These materials can also provide oxygen to the precious metals, a property known as oxygen storage/transport, these oxygen atoms can be available to the metal to carry out reactions allowing the cerium atom to reoxidise[11-13]

4.1.2 Supports

Alumina has become the *de facto* standard for autocatalysis[14] and so research often focuses on this material. Alumina shows fantastic long term hydrothermal stability under exhaust conditions, is cheap, abundant and has a high surface area in its gamma phase. Other potentially suitable materials are discussed later in chapter 5, but due to its established utility as well as other properties such as its free flowing, static-free behaviour is ideally suited to this preparation procedure and so is the main subject of this study.

4.1.3 Composition of catalysts

Catalysts were prepared to the procedure described in 2.1.7. A 0.5 wt% loading of Pt or Pd on Al_2O_3 was used as a standard precious metal loading and the quantity of base metal oxide was varied accordingly. The compositions were chosen to give a cross

section of catalysts to probe for important factors. A study on grind duration found that there was no improvement in catalytic activity after a grind time of 5 minutes, as this was sufficient to disperse the Pt across the surface of the support. An analysis of crystallite size by CO chemisorption (Table 1) showed that there was no change in metal surface area from 5 minutes onwards and that the maximum metal particle size remained no larger than 1.2 nm. dTGA (Figure 1) also shows little significant change in the combustion temperature after 5 minutes, that the precursor is evenly spread on the alumina surface and little benefit is obtained from further mixing.

Table 1. CO chemisorption data of 1 wt% Pt/Al_2O_3 catalyst prepared by physical grinding

Grind duration (min)	Dispersion (%)	Crystalite size (Å)
2.5	49.6	22.8
5	96.49	11.7
10	95.23	12.0
20	96.01	11.9
30	94.06	12.1

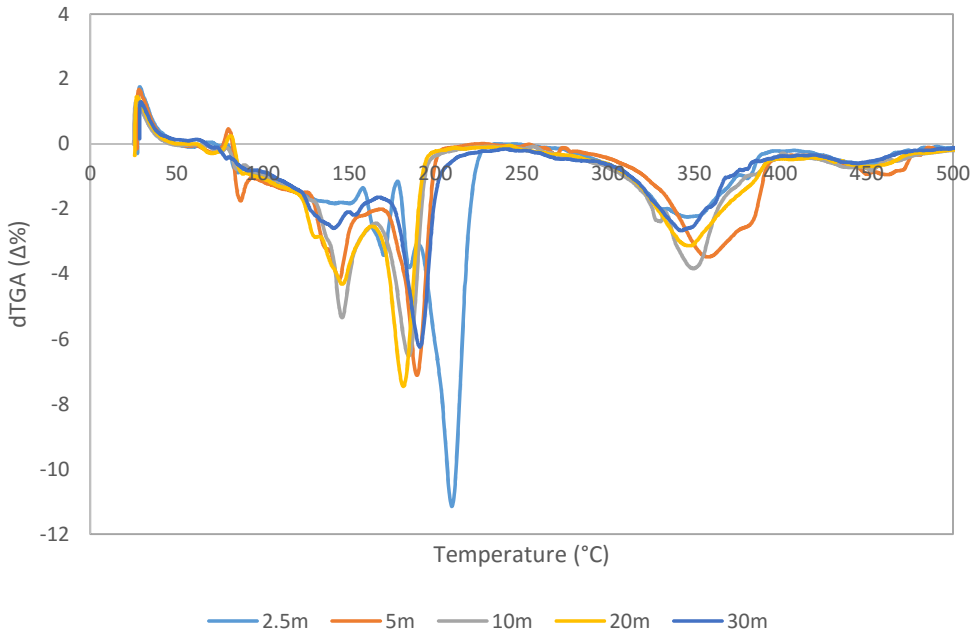

Figure 1. dTGA of 0.5 wt% Pt/Al_2O_3 catalyst prepared from $Pt(acac)_2/Al_2O_3$

Catalyst testing was carried out in 2 cycles as it was noted that a single test run can significantly change the activity of the catalyst with regards to NO reduction or oxidation. This process is likely to be a result of the oxidation of metal species at higher temperatures.

4.2 Pt and Co catalysts

For CO conversion, it can be seen from the graph in Figure 2 that the optimum level of cobalt loading lies between 0.125 wt% Co and 0.5 wt% Co, though all catalysts perform similarly and are significantly more effective than a 0.5 wt% Pt/Al_2O_3 prepared by a similar method. The higher cobalt loading of 1 wt% had no positive effect on activity, and both cycles of the test closely follow the platinum only catalyst. This effect could be

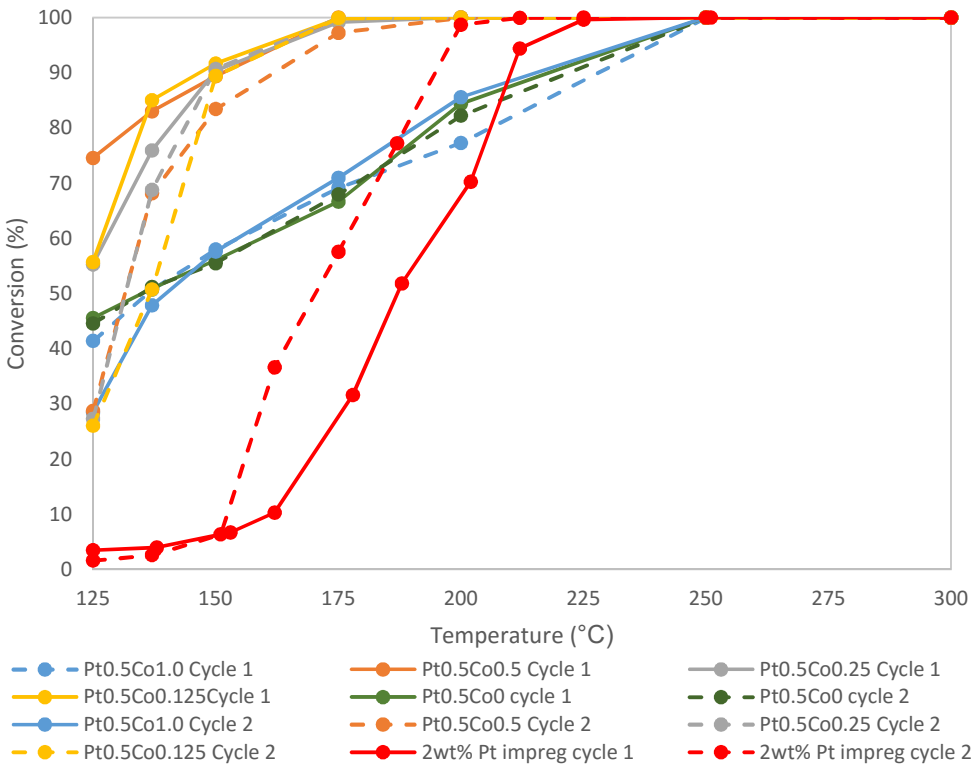

Figure 2. CO conversion after two cycles for platinum-cobalt samples supported on alumina, compared against a 0.5 wt%Pt/Al_2O_3 prepared by grinding and a 2 wt%Pt/Al_2O_3 catalyst prepared by impregnation. 0.3 cm^3 catalyst, 40,000 h^{-1}, 1% CO, 0.1% C_3H_8, 300 ppm NO, 6% CO_2, 8% H_2O, 8% O_2 stoichiometric.

due to the particle size of the cobalt oxide affecting its oxygen storage capacity, or it could be due to the catalytic behaviour of the cobalt oxide itself. All the catalysts that were prepared by the grinding procedure compared favourably to a 2 wt% platinum on alumina prepared by impregnation with a chloroplatinic acid precursor. The impregnation catalyst however increases in activity with a test cycle, as opposed to the grinding catalyst which lost activity. As commercial three way catalysts are prepared in a similar manner to this, the effect could be down to a degreening effect[15].

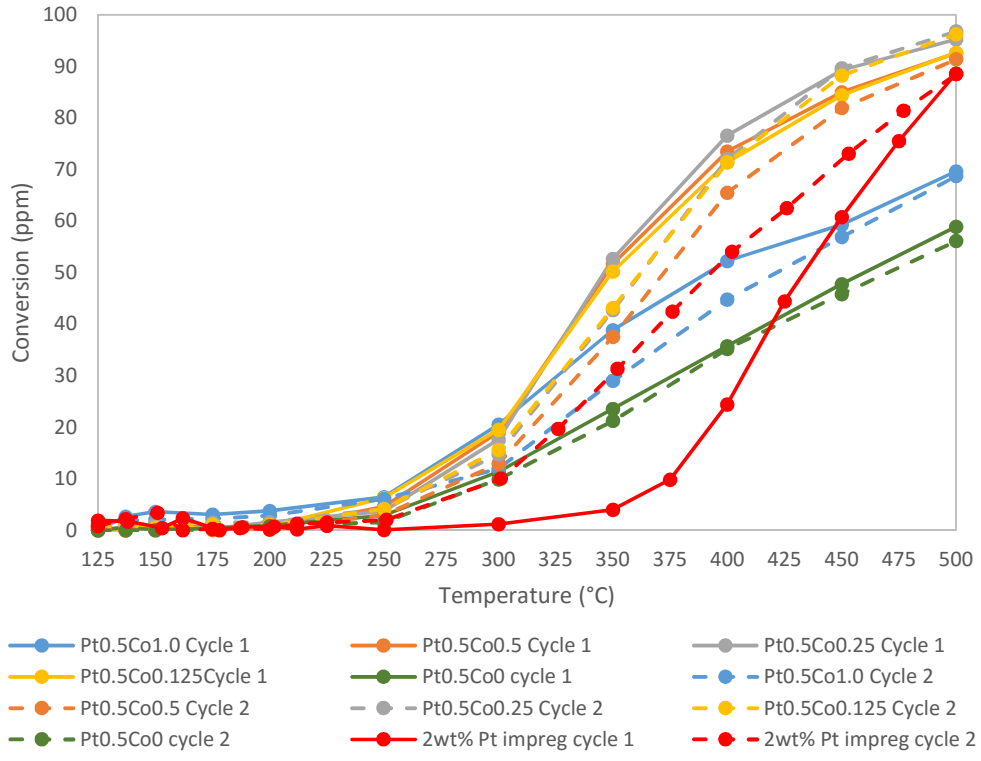

Figure 3. Propane conversion after two cycles for platinum-cobalt samples supported on alumina, compared against a 0.5 wt%Pt/Al_2O_3 prepared by grinding and 2 wt% impregnation catalyst a 0.3 cm^3 catalyst, 40,000 h^{-1}, 1%CO, 0.1% C_3H_8, 300 ppm NO, 6% CO_2, 8% H_2O, 8% O_2 N_2 balance.

Table 2. BET surface are of 0.5 wt%Pt/Al_2O_3 catalysts with cobalt

Co loading wt%	C value	BET surface area (m^2g^{-1})
0.125	59	112
0. 25	182	120
0.5	115	115
1.0	56	115

From the testing for propane oxidation (Figure 3) it can be seen that the cobalt doped catalysts performed better than the catalyst without, and significantly better than the 2 wt% platinum catalyst prepared by impregnation when metal loading is considered. Due to the linear light off of the 0.5 wt% platinum on alumina, it can be inferred that this reaction was mass transfer limited, where diffusion of gas to the catalyst surface is the rate limiting step[16]. The catalysts with cobalt present in quantities lower than 1 wt% however showed a classic light off curve indicating that mass transfer was less limiting in these tests. This could possibly indicate that oxygen transport to the platinum nanoparticles had improved. As was seen with the CO testing, the impregnation catalyst improved after an initial test cycle and the catalysts prepared by grinding show no change or a slight decrease in activity, though the effect is less pronounced than in the carbon monoxide testing.

For NO oxidation/reduction the data for each component has been represented as a concentration against temperature rather than as a selectivity value, the reason for this is that many catalysts exhibit a storage behaviour when exposed to NO. NO can be adsorbed to a support and desorbed as NOx at a higher temperature. This sto rage effect makes calculating conversion and selectivity problematic and so as not to misrepresent the data the actual measured concentrations of a gas are given rather than a value for conversion.

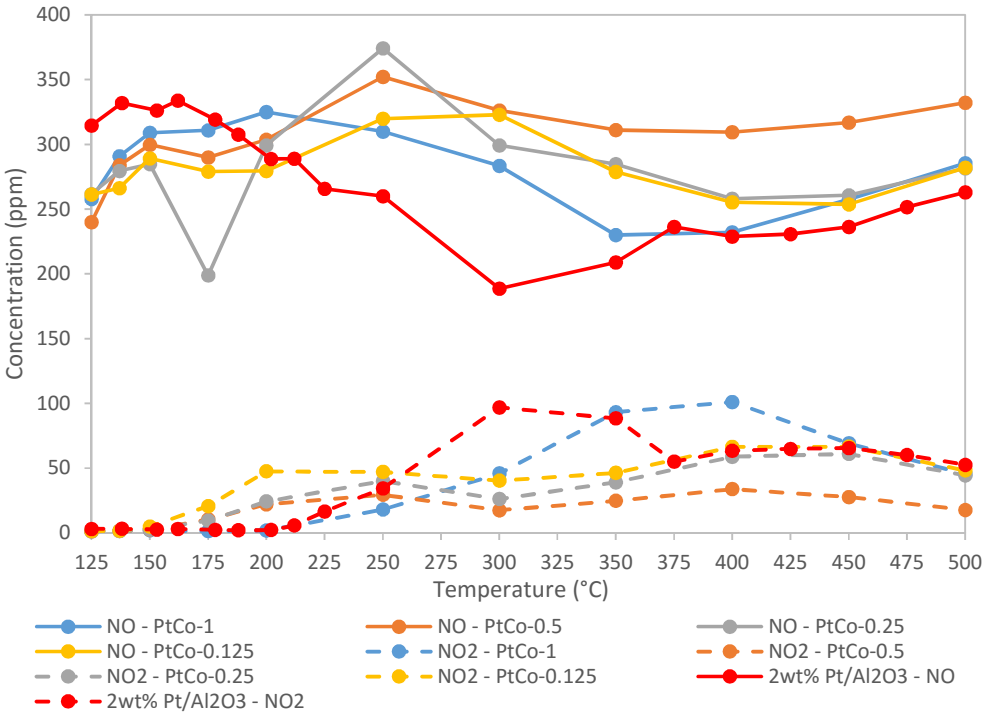

Figure 4. NO and NO_2 concentrations for platinum-cobalt samples supported on alumina, compared against a 0.5 wt%Pt/Al_2O_3 prepared by grinding and a 2 wt%Pt/Al_2O_3 prepared by impregnation, over the first cycle. 0.3 cm^3 catalyst, 40,000 h^{-1}, 1% CO, 0.1% C_3H_8, 300 ppm NO, 6% CO_2, 8% H_2O, 8% O_2 N_2 balance.

During the first cycle the NO activity was fairly low and mostly oxidative in character (Figure 4). There were some small NO adsorption and release events with many of the samples although the degree of this was difficult to determine by the analysis method used. There was also a little NO conversion to NO_2 at higher temperatures, which is greatly increased during the second test cycle, indicating a change in the degree of oxidation of the platinum species is likely[17]. When the activity of the low loading cobalt doped catalyst was compared with the 2 wt% Pt/Al_2O_3 catalyst a decrease in activity for NO oxidation was seen, both the standard and the cobalt containing catalyst display the increase in NO oxidation on the second test cycle, this suggests that the platinum was carrying out the catalysis. It is also worth noting that storage effects are greater on the cobalt containing catalyst, indicating that the cobalt could have assisted in a NO_x storage and release mechanism, possibly on the cobalt oxide itself or via a spillover mechanism on to the alumina[18].

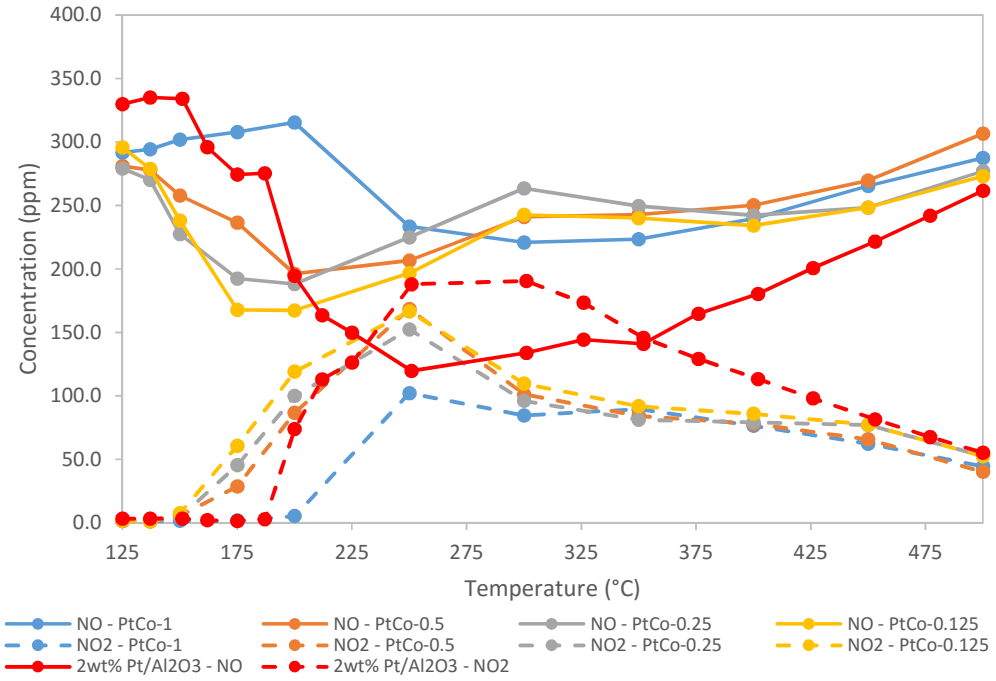

Figure 5. NO and NO_2 concentrations for platinum-cobalt samples supported on alumina, compared against a 0.5 wt%Pt/Al_2O_3 prepared by grinding and a 2 wt%$Pt/A_{l2}O_3$ prepared by impregnation, over the second cycle, 0.3 cm^3 catalyst, 40,000h^{-1}, 1% CO, 0.1% C_3H_8, 300 ppm NO, 6% CO_2, 8% H_2O, 8% O_2 N_2 balance.

In the first cycle an increase in NO_2 was observed, while NO had remained relatively static, this is likely due to NO adsorbing at lower temperatures, oxidising and desorbing at higher temperatures. During the second cycle (Figure 5) there continues to be a lag between NO absent from the gas feed and NO_2 evolved, this is likely because NO was being adsorbed and stored and released later as NO_2. Without the means to detect the concentration of nitrogen in the gas feed it is extremely difficult to separate any catalytic decomposition from NO storage, however it is worth noting that N_2O was formed early on and tails off as NO_2 is produced/released, possibly indicating that reduction was taking place at lower temperatures. The catalysts with a lower quantity of cobalt tend to demonstrate an increased capability to oxidise NO to NO_2, this was

possibly due to the smaller cobalt oxide particles having an increased oxygen mobility, increasing the oxidising power of the platinum or directly oxidising the NO itself.

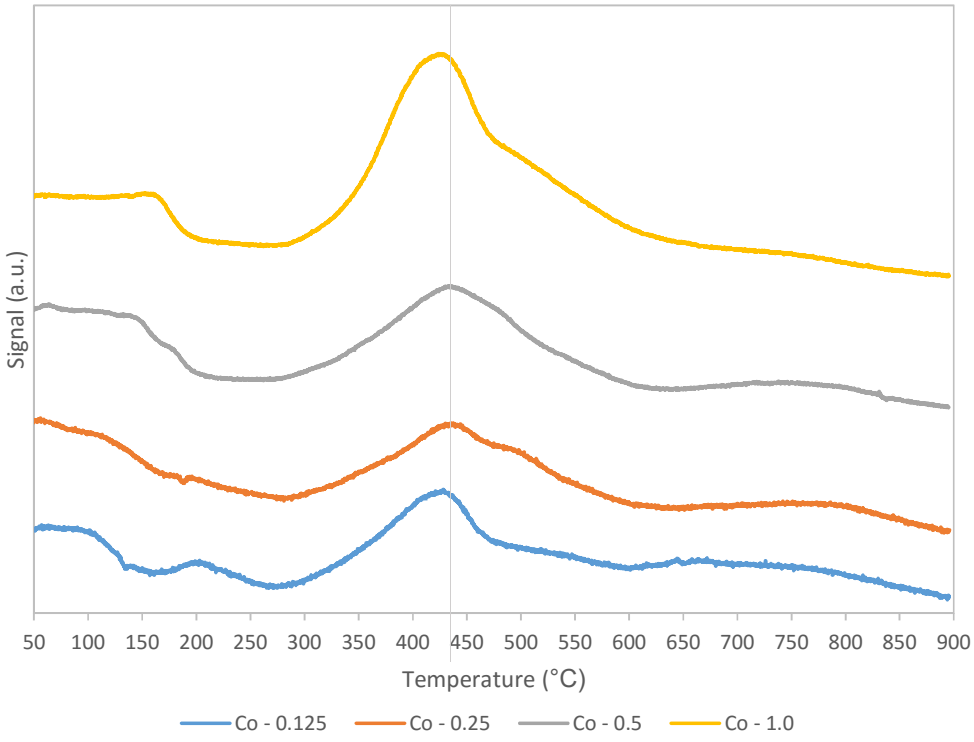

Figure *6*. TPR analysis of 0.5 wt% Pt and Cobalt (II) oxide of varied weight loadings.

Table 3. Integration of TPR in Figure 6

Composition	mass (g)	Cobalt (mg)	Temp (°C)	Peak Area	moles H2	Co reduced
Co1	0.1009	1.009	426	43474.1	2.568E-05	1.0089
Co0.5	0.1034	0.517	436	13288.3	7.849E-06	0.3084
Co0.25	0.1017	0.25425	444	8176.9	4.831E-06	0.1897
Co0.125	0.1022	0.12775	428	12486.1	7.37E-06	0.2897

There are a number of possibilities for the reduction in activity over the course of two tests, the first is that any precious metal present in the sample is sintering under

the high heat. Since sintering is expected to occur at half-melting point of a metal in Kelvins (mp. Pt = 2041.4°K) and the range of experimental temperatures present in these tests is 398.15 °K to 773.15 °K then sintering should not be the presumed method of deactivation.

The reducibility of the catalyst changes very little with wt% composition of cobalt (Figure 6). There was a slight shift to higher temperature and broadening of the reduction peaks from 0.125 wt% to 0.25 wt% which reverses on an increase in loading, with respect to NO oxidation, the 0.25 wt% cobalt sample was the lower performing catalyst (with the exception of the 1 wt% cobalt, which was possibly a particle size effect). Upon integration, it can be seen that the peak area at 426 in the 1 wt% cobalt sample corresponds to the quanitity of cobalt expected and so this peak can be assigned to cobalt oxide. However, approaching the lower loadings there are issues with sensitivity and the error becomes too great to quantify the material adequately. The extremely small loading differences will be convoluted by any slight difference in sample preparation. Integration of the peaks correlates approximately to the cobalt presenty in the samples, with the exception of 0.125 wt% which possibly hs too low a loading for a relaiable signal. EDX results are given in table 4. They show that the cobalt concentration in the sample is increasing as intended, the precise value is effected by the error inherent in EDX analysis when large amounts of light atoms (oxygen) are present. Table 5 shows the BET surface area results which show little difference between the samples.

Table 4. EDX analysis of 0.5 wt%Pt/Al_2O_3 catalysts with cobalt

	Atomic percentage				Weight Percentage			
Co (wt%)	Al	Co	Pt	O	Al	Co	Pt	O
0.125	33.34	0.05	0.04	66.24	45.65	0.14	0.39	53.80
0.25	33.18	0.11	0.05	66.29	45.39	0.32	0.33	53.78
0.5	36.37	0.28	0.04	62.97	47.49	0.80	0.38	51.33
1.0	33.84	0.62	0.05	65.19	45.60	1.82	0.48	52.09

Table 5. BET surface are of 0.5 wt%Pt/Al_2O_3 catalysts with Cobalt

Co loading wt%	C value	BET surface area (m^2g^{-1})
0.125	173	116
0. 25	107	118
0.5	150	113
1.0	120	114

Changes to the nanoparticles present on the surface were investigated by TEM (Figure 7), a sample of Pt and Pt/Co on alumina was analysed by a particle size count and the information was compiled into a histogram. Particle size was found to average slightly higher for the samples with cobalt present. Chemisorption analysis (Table 6) revealed that the cobalt had a significant effect on the average crystallite size and dispersion. EDX analysis shows no evidence of alloying, even when the sample was heat treated under reducing conditions to encourage its formation. What was observed was a well dispersed cobalt with discrete platinum nanoparticles. Particle size difference will have an important impact on activity, the ideal size of Pt particles on gamma alumina for CO oxidation is reported at approximately 0.7 nm[19], however the testing regime represents significantly different conditions seen in these particle size analyses, which operate 1:1 ratios of CO to O_2. Additionally if the cobalt added was acting as an oxygen storage component then the Pt particle size may have had an important effect on oxygen availability. Research by Fernández-García *et al.* demonstrated that ceria assisted in activating both carbon monoxide and oxygen on Pd[10], and Gorte *et al.* demonstrated that this relationship applies to other precious metals also[20] and that metal particle size has a significant effect.[21]

Table 6. CO chemisorption of 0.5 wt%Pt on alumina with varied cobalt loading

Cobalt loading (wt%)	Dispersion (%)	Crystalite size (Å)
1.0	60.8	20.3
0.5	22.3	50.1
0.25	30.9	38.2
0.125	45.2	24.7

Figure 7. STEM image with EDX map of catalyst heat treated catalyst under inert (top left) and reducing (bottom left) atmospheres. TEM images of 1 wt%Pt supported on γ-Alumina showing Pt nanoparticles (top right) and 0.5 wt%Pt/0.5 wt%Co supported on γ-Alumina with inlaid histrogram of nanoparticle sizes (bottom right).

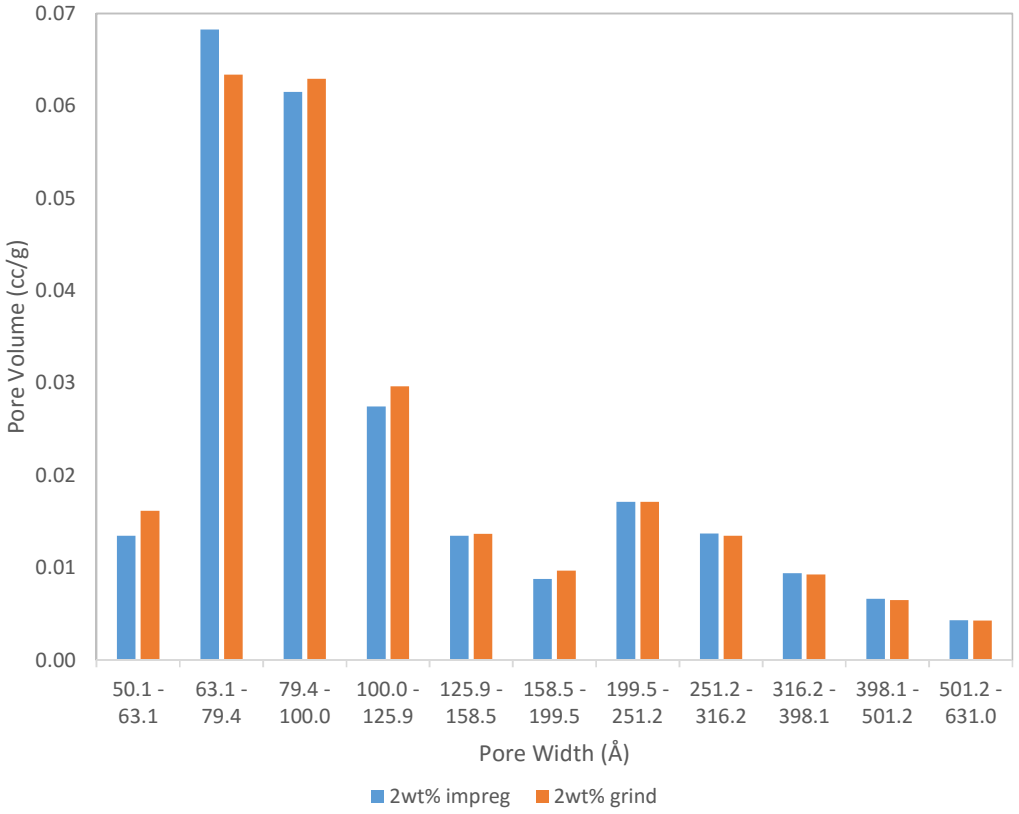

Figure 8. Mesopore volume histogram of 2 wt% Pt on alumina synthesised by impregnation and grinding preps.

The change in activity could also be a result of a change in pore volume, a pore volume analysis (Figure 8) shows a slight difference between the 2 wt%Pt/Al_2O_3 catalyst prepared by impregnation and by grinding, 2 wt% was used to allow for a direct comparison with a typical commercial weight loading and also to accentuate effects. From 200Å pore structure was identical between the catalysts indicating very little interference with large pores, below this however there were some differences, the impregnated catalyst has more pore volume in the 63.1-79.5 range, possibly indicating pore blockage on the grinding prep catalyst that correlates to the average particle size. The pore volume data suggests that the impregnation catalyst having an overall lower pore volume over a larger range of pore widths.

Figure *9*. Depiction of oxidation state change of platinum over course of test.[17]

Another potential reason for the activity of the doped catalyst is in how the cobalt may affect the oxidation of the Pt surface; the NO activity discussed previously seems to suggest the modification of the active species over the course of a test cycle. Literature suggests that in the presence of NO and oxygen the platinum surface will gradually become oxidised (Figure 9)[17], as the catalyst was heat treated in an inert atmosphere and due to the auto reduction effects[7], the Pt was likely to be in a more reduced state than if it was simply calcined in air. This platinum would gradually oxidise over the course of a test and if a significant quantity of platinum oxide was present after a test than at temperatures below 200 °C then platinum oxide will be reduced readily by any NO present, an effect that would not be present in the first test cycle. The reduction in activity as the temperature ramps could be explained by this mechanism, however it would be hidden by the NO/NO_2 equilibrium whereby NO_2 reduces to NO and O_2 which is kinetically limited at lower temperatures.

4.3 Pd and Co catalysts

To determine if the promotional effect on activity is a physical property of the cobalt oxide present or a synergistic effect with the platinum, the catalyst was synthesised with Pd as an alternative to Pt.

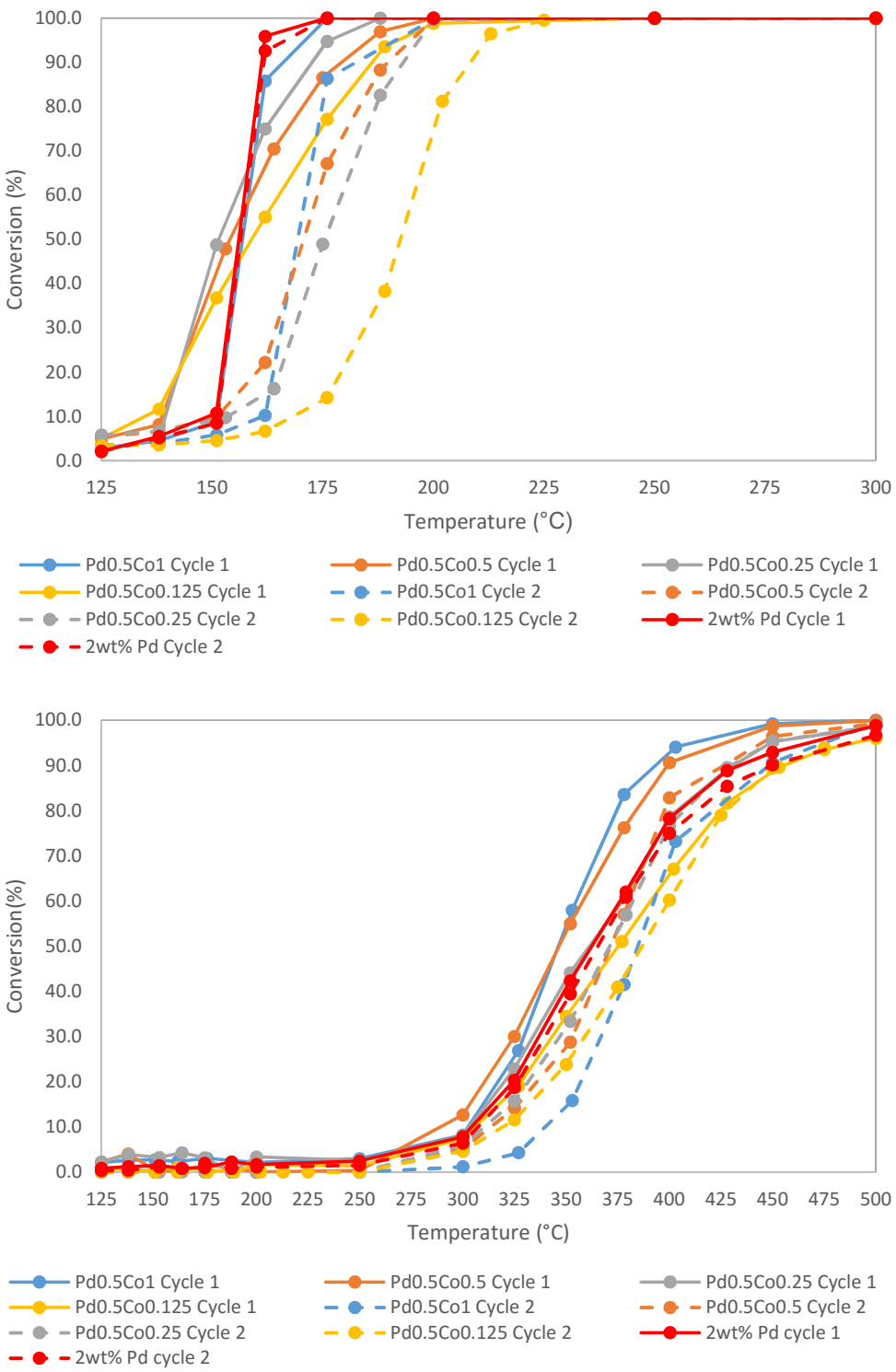

Figure 10. CO conversion (top) and C_3H_8 conversion (bottom) for platinum-cobalt samples supported on alumina, compared against a 0.5 wt%Pd/Al_2O_3 prepared by grinding and a 2 wt%Pd/Al_2O_3 standard prepared by impregnation over 2 cycles. 0.3 cm^3 catalyst, 40,000h^{-1}, 1% CO, 0.1% C_3H_8, 300 ppm NO, 6% CO_2, 8% H_2O, 8% O_2 N_2 balance.

If the enhancement in activity was due to an oxygen storage or transport component then it might be expected to see a similar promotion in activity with the Pd catalyst. The catalyst was synthesised with the same percentage weight loadings as the Pt catalyst. What we see in Figure 10 is a promotional effect with increasing Co loading, this seems to suggest a property of the cobalt nanoparticles is responsible for improving the activity of the precious metal species. In an oxygen storage/transport model the cobalt oxide that is in close contact with the metal species can provide a source of oxygen that is more available. Oxygen is removed from the cobalt oxide lattice and dissociated onto the metal surface, which carries out oxidation, the oxygen deficient lattice then readily re-oxidises with atmospheric oxygen[13, 22, 23]. Potentially these effects could be seen in other, cheaper base metals such as iron. Comparing the activity against the Pt catalysts, we do not see the same degree of improvement over the impregnation standard catalyst. The palladium samples are less active than the platinum catalysts for CO oxidation, however palladium exhibits superior hydrocarbon conversion under these testing conditions. The CO curves in figure 10 suggest that on the catalysts prepared by grinding are more diffusion limited that the 2wt% Pt Standard, this is likely due to the lower number of active sites. On the second cycle, overall activity has dropped, however the light off curve is sharper, this could be due to the catalyst transforming and producing more active sites for the CO oxidation to take place.

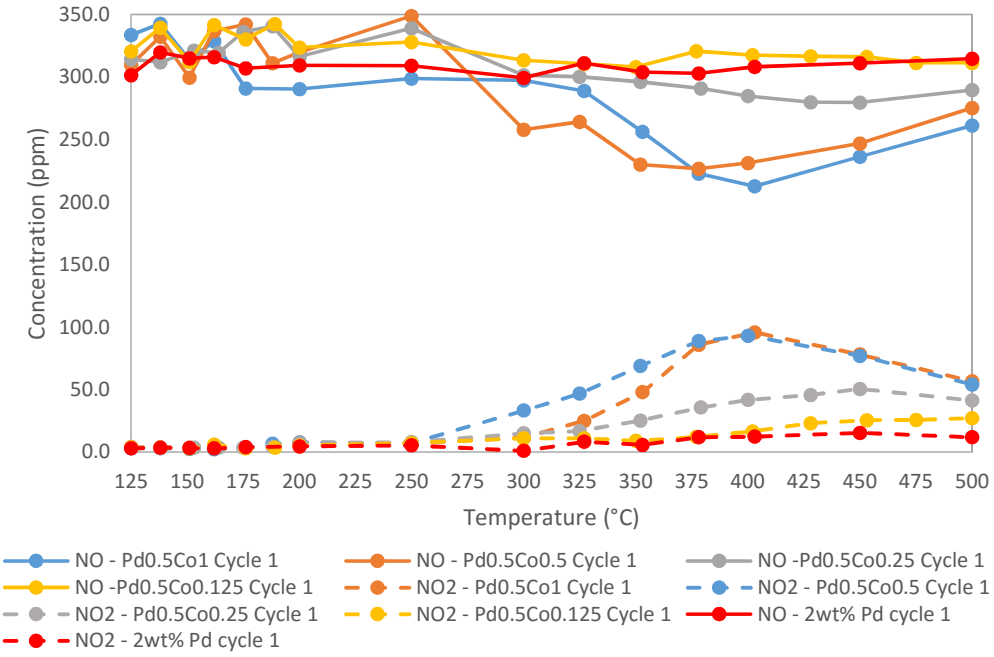

Figure 11. NO and NO_2 for palladium-cobalt samples supported on alumina, compared against a 0.5 wt%Pd/Al_2O_3 prepared by grinding and a 2 wt%Pd/Al_2O_3 over the first cycle. 0.3 cm^3 catalyst, 40,000 h^{-1}, 1% CO, 0.1% C_3H_8, 300 ppm NO, 6% CO_2, 8% H_2O, 8% O_2, N_2 balance.

Palladium exhibits different chemistry to platinum[24] and doesn't typically carry out NO oxidation[25]. Despite this there was a small level of NO oxidation occurring on some of the cobalt samples (Figure 11), with the most active species being 1 wt% and 0.5 wt% Co, the activity of these in relation to the loading suggesting that this oxidative character is linked to the size of the nanoparticles produced. During the second cycle (Figure 12), the NO oxidation had decreased significantly with only very minor quantities produced at high temperatures. Storage and release also appears to have diminished after the initial test.

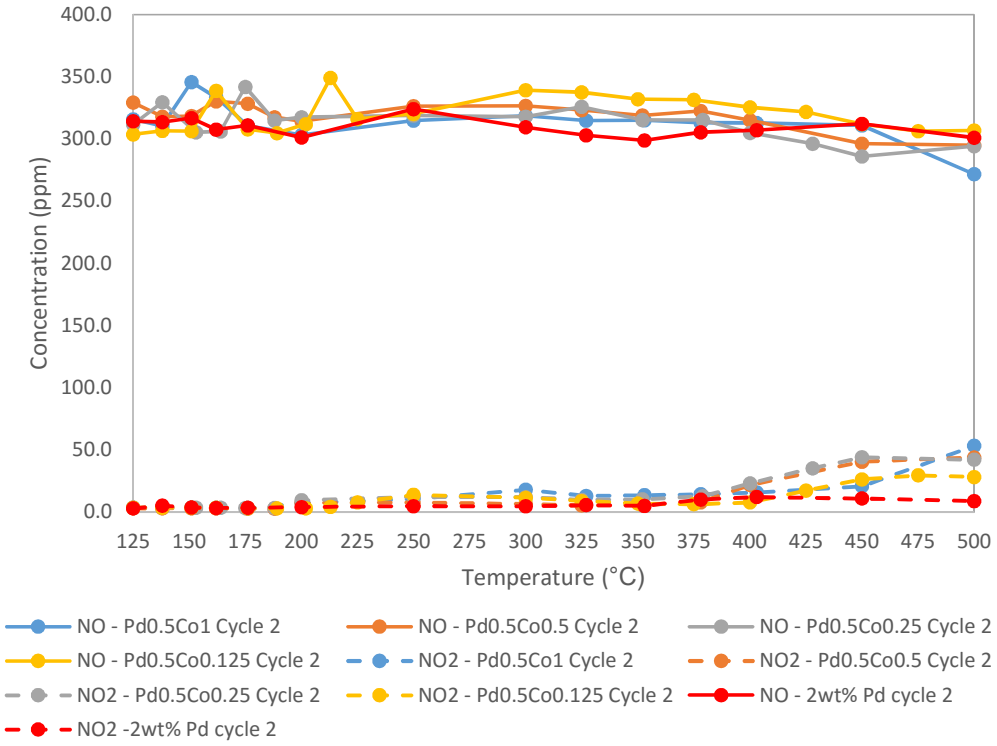

Figure 12. NO and NO_2 for palladium-cobalt samples supported on alumina, compared against a 0.5 wt%Pd/Al_2O_3 prepared by grinding and a 2 wt%Pd/Al_2O_3 impregnation over the 2nd cycle. 0.3 cm^3 catalyst, 40,000 h^{-1}, 1% CO, 0.1% C_3H_8, 300 ppm NO, 6% CO_2, 8% H_2O, 8% O_2 N_2 balance.

Table 7. EDX analysis of 0.5 wt%Pd/Al_2O_3 catalysts with cobalt

	Atomic percentage				Weight Percentage			
Co loading (wt%)	Al	Co	Pd	O	Al	Co	Pd	O
0.125	33.14	0.04	0.11	65.47	45.71	0.12	0.59	53.56
0.25	34.1	0.12	0.10	65.70	46.26	0.36	0.54	52.85
0.5	33.36	0.27	0.09	66.32	45.30	0.80	0.48	53.41
1.0	38.1	0.66	0.11	64.19	48.82	1.85	0.56	48.78

EDX analysis in table 7 shows the increasing cobalt loading between samples relative to the static quantity of Pd and confirmed the presence of these elements in the sample. A CO Chemisorption was carried out on the catalyst, this revealed a similar relationship between the cobalt to precious metal loading as the platinum catalyst (table 8). With the platinum samples the highest and lowest cobalt loadings showing a smaller particle size compared to the intermediate loadings. With palladium, the performance of the catalysts is shifted with the best performing catalysts being the 1.0 and 0.5 wt% cobalt materials. This indicates a particle size effect is important in this catalyst. CO chemisorption on palladium is less accurate than with platinum, this is due the tendency of CO to form bridging species on the palladium surface.

Table 8. CO chemisorption of palladium cobalt catalysts.

Cobalt loading (wt%)	Dispersion (%)	Crystalite size (Å)
1.0	21.9	48.2
0.5	22.3	47.3
0.25	30.9	38.2
0.125	45.2	24.7

Overall the improvements are not as great as those that were seen in the platinum/cobalt system, however they display a marked improvement over the 2 wt% impregnation catalyst. A comparison of cobalt loading with no Pt present (Figure 13) shows that the relative activity of the cobalt is poor with respect to the catalysts with either the Pd or Pt present.

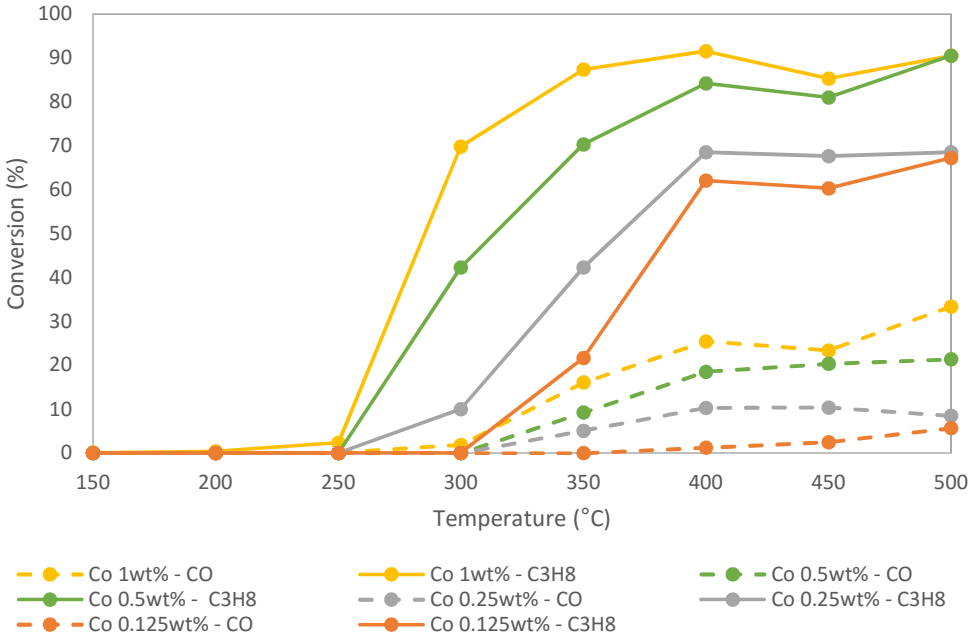

Figure 13. comparison of Co/Al_2O_3 catalysts of varied weight loading. 0.3 cm^3 catalyst, 40,000 h^{-1}, 1% CO, 0.1% C_3H_8, 300 ppm NO, 6% CO_2, 8% H_2O, 8% O_2 N_2 balance.

4.4 Pt and Fe Catalysts

Iron is a cheap and abundant element and its oxides are established oxidation catalysts. Iron has 2 principal oxidation states +2 and +3 and has oxides that can be formulated from a mixture of both of these. Iron (II, III) oxide is a particularly interesting material as it can form a redox couple[26] and it is formed readily from iron (II) oxide under typical exhaust conditions. By taking the principles discussed previously for forming a highly dispersed Co doped alumina surface we attempted to produce a highly dispersed Fe catalyst with iron acetylacetonates. As FeO is thermodynamically unstable, upon heating under testing conditions it will decompose to Fe_3O_4 and metallic iron[27] (which will quickly reoxidise).

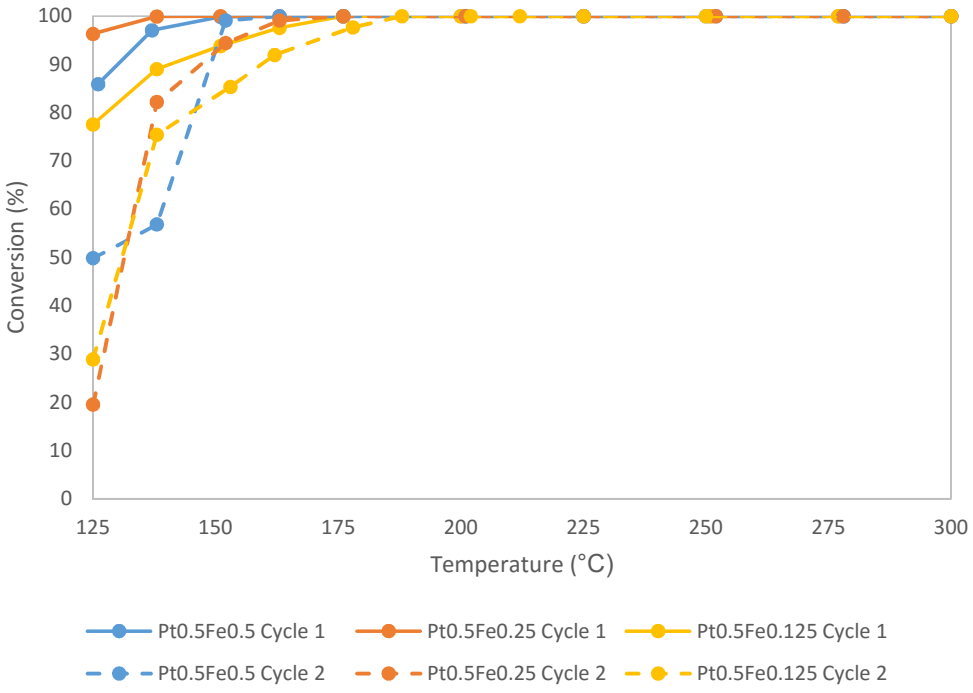

Figure 14. CO conversion for iron (II) acetylacetonate precursors for platinum-iron catalysts supported on alumina

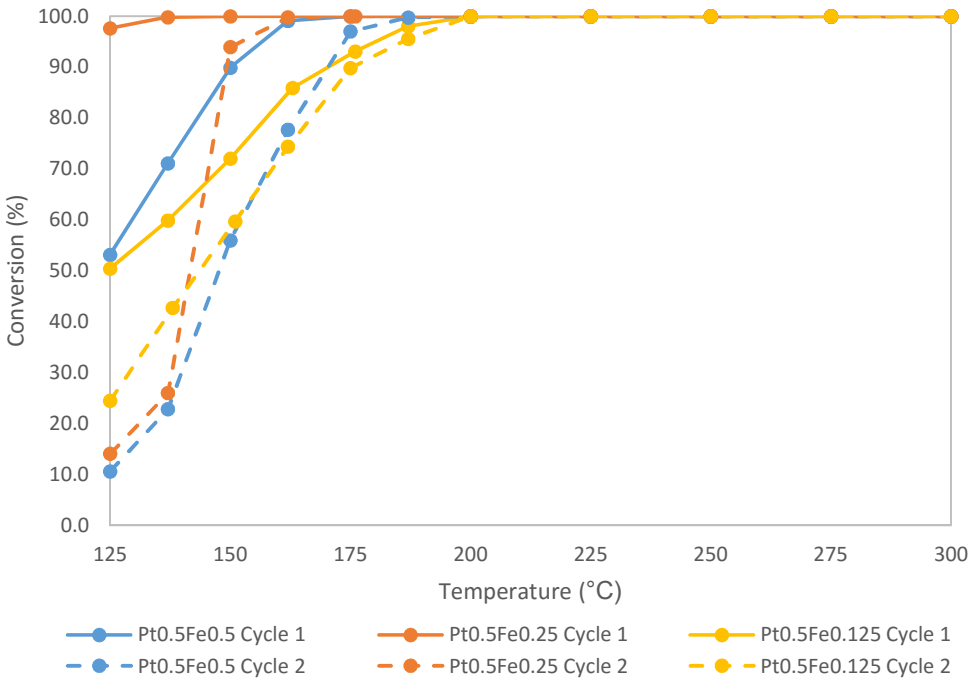

Figure 15. CO conversion for iron (III) acetylacetonate precursors for platinum-iron catalysts supported on alumina

If Iron (II, III) oxide is a more capable oxygen storage component then we would expect to see increased oxidation activity from the $Fe(acac)_2$ precursor catalyst on the second cycle (after an appreciable quantity of the FeO had decomposed). Comparing the Fe^{2+} catalysts (Figure 14, 15) with the cobalt catalysts discussed earlier (Figure 2, 3) a substantial improvement can be seen, with a considerably more active catalyst for the first cycle and yet still superior oxidation activity on the next cycle. Propane activity was reduced from the first cycle to the second but not to the same degree. Direct comparisons between the catalysts are difficult when looking at CO oxidation, T10 reveals kinetic limitation, T50 pore diffusion and T90 is generally indicative of differences in mass transfer[16]. Increased loading results in a more effective catalyst in the case of iron (III) with less of a difference between the iron (II) precursors, however the iron (II) samples retain a higher overall activity than the iron (III) precursors on the second cycle. Both sets of samples compare favourably against a 2 wt% platinum standard prepared by impregnation as seen in Figures 2 and 3.

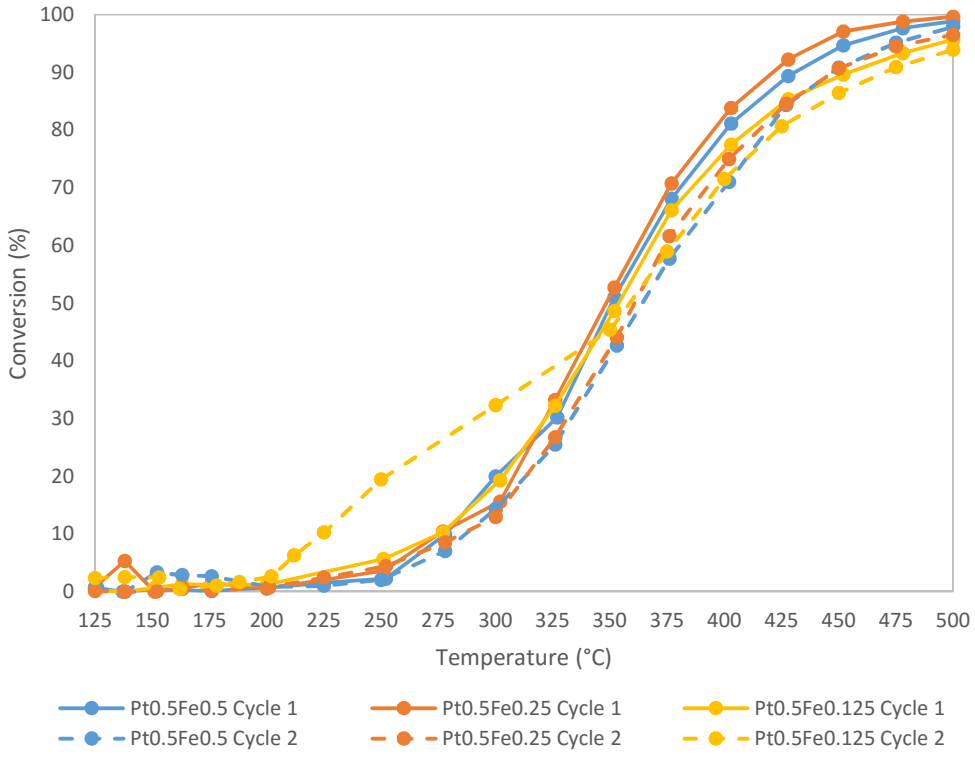

Figure 16. C_3H_8 conversion for iron (II) precursor platinum-iron catalysts supported on alumina, compared against a 0.5 wt%Pt/Al_2O_3 prepared by grinding.

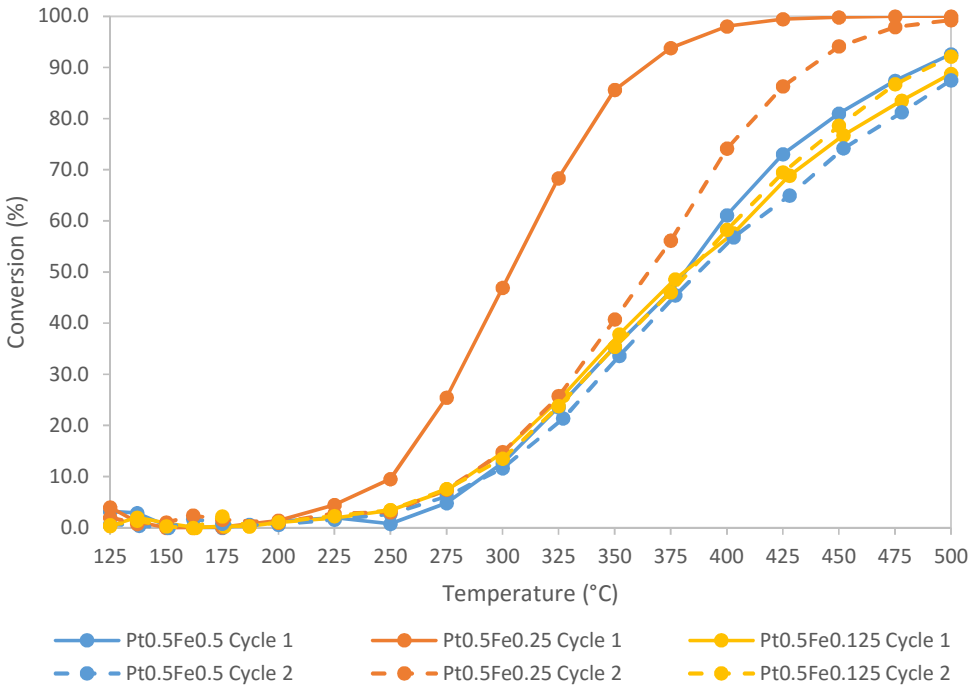

Figure 17. C_3H_8 conversion for iron (III) precursor platinum-iron catalysts supported on alumina, compared against a 0.5 wt%Pt/Al2O3 prepared by grinding.

As discussed earlier the oxidation state of the surface platinum is likely to have an effect here, with PtO being less active for CO oxidation. As the platinum catalyst starts in a reduced state, the gradual oxidation of the surface will reduce activity. When looking at the propane combustion (Figure 16, 17) we can see some important differences, the first being that the average catalytic activity of the iron (II) acac precursor catalysts is comparable to the cobalt catalysts (Figure 2, 3), with the exception of $Pt_{0.5}Fe_{0.25}$ which shows good low temperature activity on the first cycle. The precise reason for $Pt_{0.5}Fe_{0.5}$'s early increase in activity is unclear, however the catalyst underwent an equally significant deactivation before the second test. The differences between iron (II) and iron (III) however seem to be more distinct with T50 values of 350-360 °C and 380-390 °C respectively. This is a large improvement over platinum alone on alumina as prepared by impregnation and a similar grinding prep. Potentially this could be evidence that the Fe(II) precursor catalyst underwent a decomposition from an iron (II) oxide to an iron

(II)(III) oxide, this redox couple may account for the general increase in activity using an iron(II) precursor.

Looking to the activity with regards to NO (Figure 18) we see a large difference between first cycle and second cycle activity, given that the degree of NO oxidation is dependent on the surface oxidation of platinum (Figure 9), this would seem to indicate that the platinum surface is oxidised over the course of a test. A comparison between the iron II and iron III precursor catalysts reveals some important details. It would be expected that an oxidised platinum catalyst would be more active for NO oxidation as NO more readily reduces PtO. As PtO is not considered the active phase[17] then we might expect a less active catalyst to appear more active for NO oxidation. The oxygen may be replaced via a Mars-Van Krevelen style mechanism retaining the poor activity for the other catalysts. Since the average performance of the Fe(II)acac precursor catalysts is better than the performance of Fe(III)acac catalysts (Figure 19), we would expect to see the Fe(III) catalysts being better performing for NO oxidation to NO_2. Looking at the results we can see an indication that this may be the case. A larger quantity of NO is converted to NO_2 on the second cycle which is to be expected if the platinum is in a somewhat reduced state due to the nature of the heat treatment procedure. Because the only variable factor between the two tests is the oxidation state of the iron precursor, it may be that the different iron oxides present are assisting in the oxidation of the platinum surface to varying degrees. This effect may coincide with an optimal iron oxide particle size to produce the non-linear change in activity between different iron loadings.

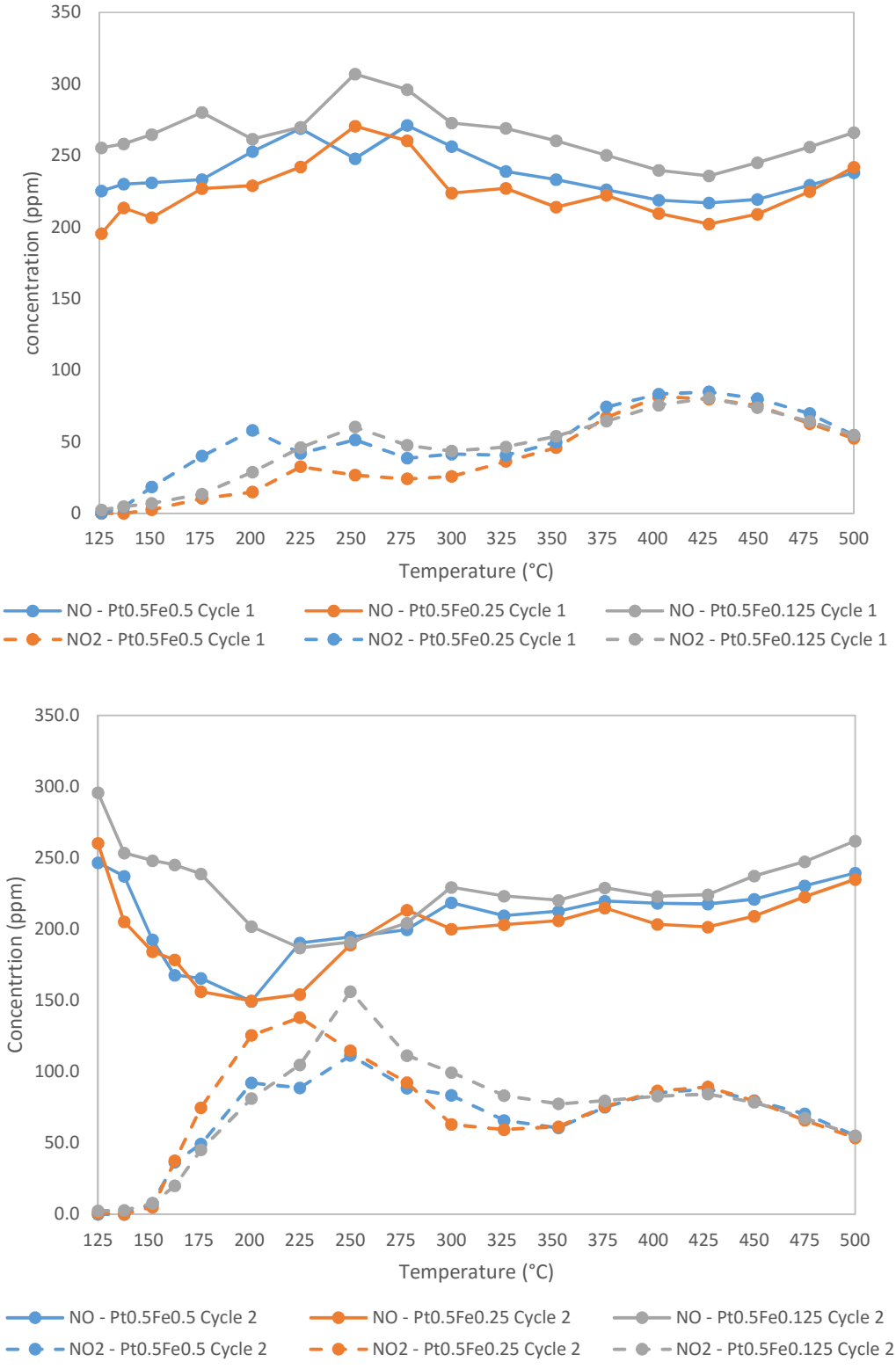

Figure 18. NO oxidation to NO_2 over iron (II) acetylacetonate precursor catalysts containing platinum catalysts over two cycles, first cycle (top), second cycle (bottom)

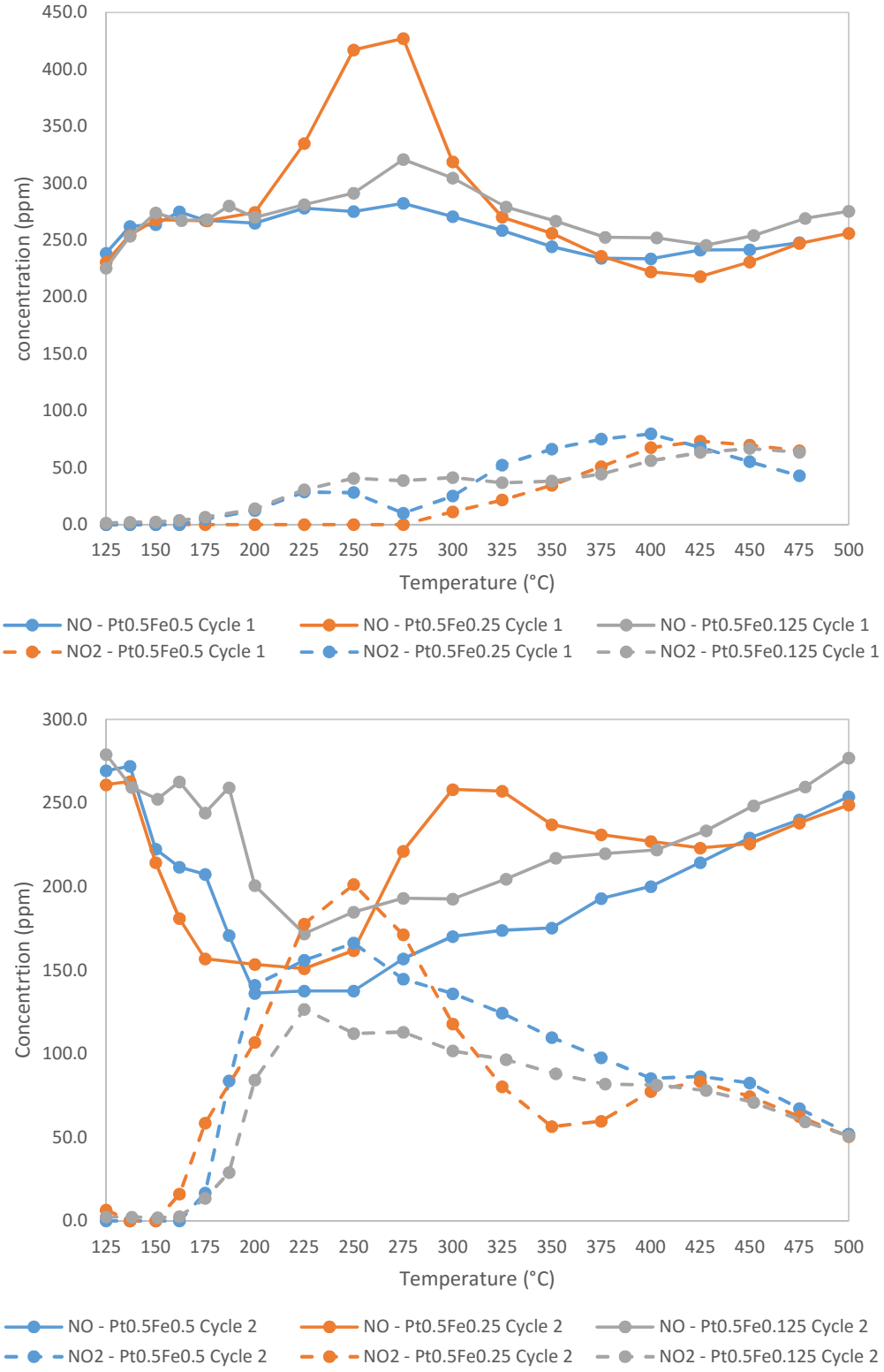

Figure *19*. NO oxidation to NO_2 over iron (III) acetylacetonate precursor catalysts containing platinum catalysts over two cycles, first cycle (top), second cycle (bottom)

EDX analysis was carried out to confirm correct loadings of the iron (II) (Table 9) and iron (III) precursors (Table 10), the EDX showed a static platinum weight loading with gradually increasing iron loading.

Table 9. EDX analysis of 0.5 wt%Pt/Al_2O_3 catalysts with Fe(II) precursors

	Atomic percentage				Weight Percentage			
Fe loading (wt%)	Al	Fe	Pt	O	Al	Fe	Pt	O
0.125	33.94	0.05	0.04	65.98	46.28	0.14	0.22	53.36
0.25	34.19	0.09	0.05	65.63	46.52	0.25	0.27	52.96
0.5	33.99	0.17	0.04	65.79	46.24	0.48	0.21	53.07
1.0	32.78	0.25	0.04	66.91	44.82	0.71	0.22	54.26

Table 10. EDX analysis of 0.5 wt%Pt/Al_2O_3 catalysts with Fe(III) precursors

	Atomic percentage				Weight Percentage			
Fe loading (wt%)	Al	Fe	Pt	O	Al	Fe	Pt	O
0.125	32.71	0.04	0.04	67.18	44.94	0.11	0.22	54.73
0.25	34.19	0.08	0.05	65.68	46.52	0.23	0.27	52.99
0.5	33.84	0.19	0.05	65.88	46.04	0.54	0.27	53.16
1.0	31.62	0.31	0.04	68.02	43.46	0.88	0.22	55.44

BET analysis for iron (II) (Table 11) and iron (III) (Table 12) show little variation between them, The iron (II) catalysts seem to have a higher average surface area at lower loadings, however this isn't outside of experimental error for BET measurements and so it is inconclusive.

Table 11. BET surface are of 0.5 wt%Pt/Al_2O_3 catalysts with the iron (II) precursor

Fe loading wt%	C value	BET surface area (m^2g^{-1})
0.125	69	120
0. 25	158	119
0.5	115	118
1.0	56	116

Table 12. BET surface are of 0.5 wt%Pt/Al_2O_3 catalysts with the iron (III) precursor

Fe loading (wt%)	C value	BET surface area (m^2g^{-1})
0.125	52	115
0. 25	50	118
0.5	108	113
1.0	89	117

Analysis of catalysts by CO chemisorption showed a similar relationship to the cobalt catalysts for both Fe^{2+} (Table 13) and Fe^{3+} (Table 14), where the intermediate iron loadings, which are typically the more active catalysts, show a larger average crystallite size and lower dispersion.

Table 12. CO chemisorption of 0.5 wt%Pt/Al_2O_3 catalysts with the iron (II) precursor

Iron loading (wt%)	Dispersion (%)	Crystalite size (Å)
1.0	50.3	48.2
0.5	47.15	47.3
0.25	27.86	38.2
0.125	43.82	24.7

Table 13. CO chemisorption of 0.5 wt%Pt/Al_2O_3 catalysts with the iron (III) precursor

Iron loading (wt%)	Dispersion (%)	Crystalite size (Å)
1.0	49.2	23.5
0.5	18.7	46.3
0.25	24.3	42.2
0.125	45.1	25.1

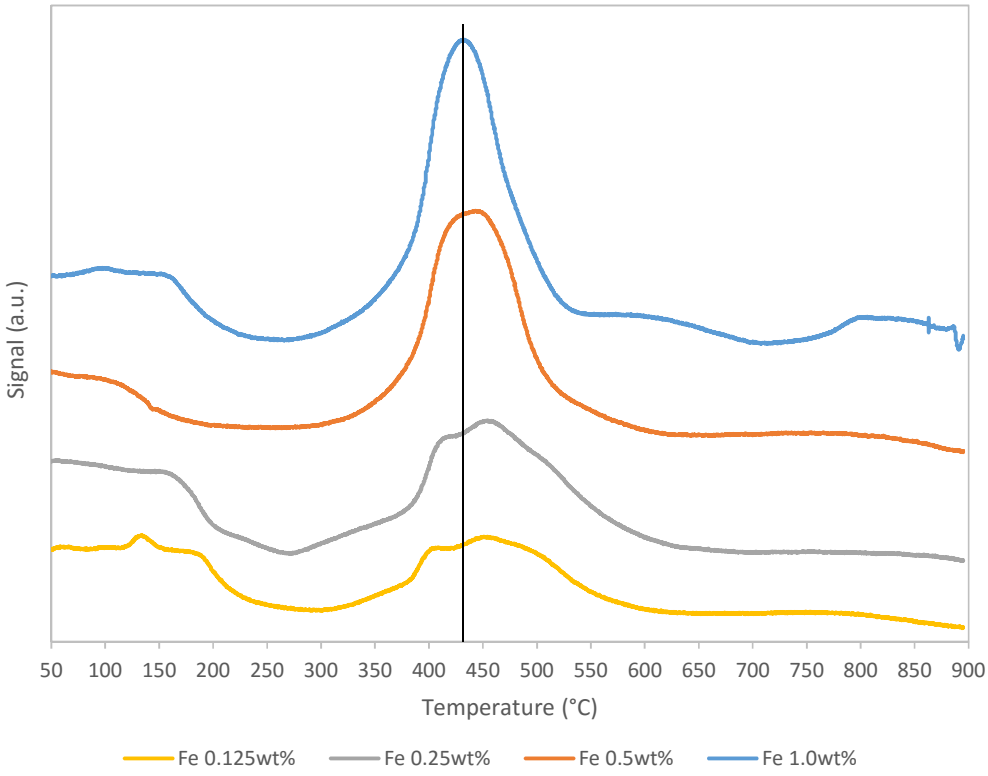

Figure *20.* TPR analysis of 0.5 wt% platinum and iron II acetylacetonate precursor catalysts on gamma alumina

Table 15. Integration of TPR peaks in Figure 19.

Composition	mass (g)	Fe present (mg)	Peak Pos (°C)	Peak Area	moles H_2 ($x10^{-5}$)	FeO (mg of Fe)	Fe_3O_4 (mg of Fe)	Fe_2O_3 (mg of Fe)
Fe1	0.1219	1.219	433	42113	2.49	1.3893	1.1114	0.9262
Fe0.5	0.1074	0.537	443	42749	2.53	1.4102	1.1282	0.9401
Fe0.25	0.1047	0.26175	458	20919	1.24	0.6901	0.5520	0.4600
Fe0.125	0.1064	0.133	454	1858.4	0.11	0.0613	0.0490	0.0408

To investigate if the iron oxide might be influencing the reducibility of the Pt catalyst, TPR analysis was carried out on the Fe (II) (Figure 20) and Fe (III) (Figure 21). Because of the low weight loadings, the differences can be subtle in effect. The samples were tested after heat treatment and so as a result the platinum is likely in a fairly reduced state, the peak(s) seen from 400-450 °C are likely due to iron oxide content and the large negative region is likely due to hydrogen release from the alumina surface. Integration of the peaks (table 15) shows approximately the expected quanitity of iron, though it is unclear which phase from this data. The data suggests that FeO is there phase present asuming 100% oxidation, but the noise in the data makes it difficult to analyse lower loadings correctly Literature indicates that the reduction of Fe(II) proceeds via the pathway detailed in equation 1 rather than by direct reduction of Fe(II) to Fe(0).[28] Either process however should produce 1 major reduction peak, the split could possibly be due to surface/bulk reduction differences or may indicate the presense of Fe(III).

$$4\mathrm{FeO} \rightarrow 3\mathrm{Fe_3O_4} + \mathrm{Fe} \qquad (1.1)$$

$$Fe_3O_4 + 2H_2 \rightarrow 3Fe + 4H_2O \qquad (1.2)$$

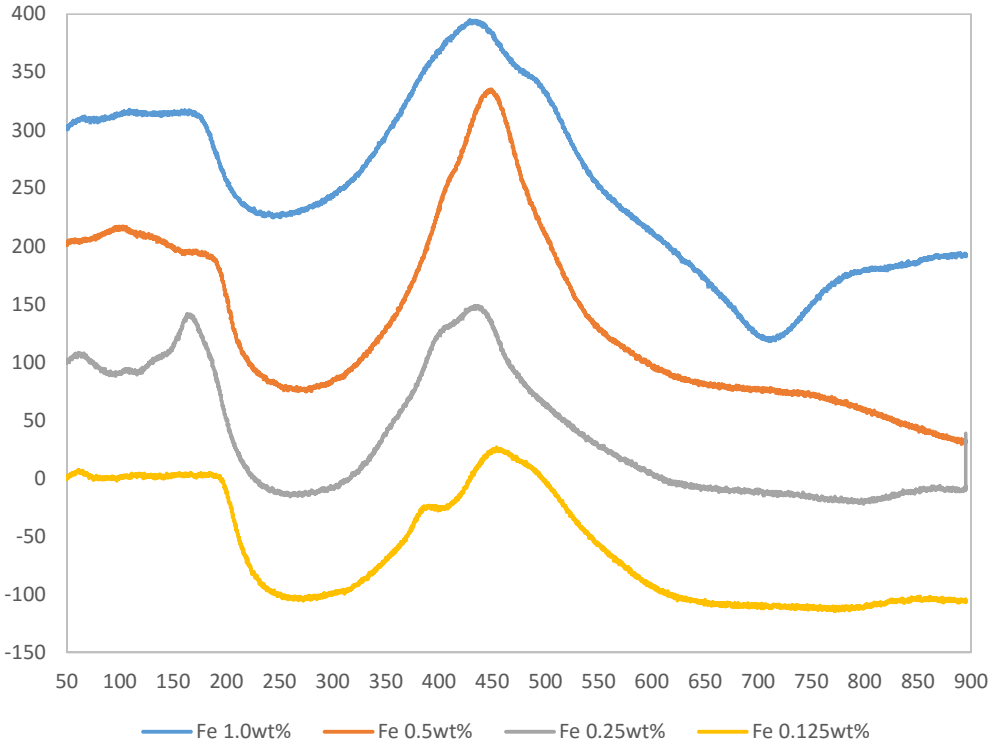

Figure *21*. TPR analysis of 0.5 wt% platinum and iron III acetylacetonate precursor catalysts on gamma alumina

Table 16. Integration and peak positon data of TPRs from Figure 20.

Composition	mass (g)	Fe (mg)	Peak Pos (°C)	Peak Area	moles H_2 ($x10^{-5}$)	FeO (mg of Fe)	Fe_3O_4 (mg of Fe)	Fe_2O_3 (mg of Fe)
Fe 1	0.1030	1.03	434	18965	1.12	0.625	0.500	0.417
Fe 0.5	0.1030	0.51	449	22046	1.30	0.727	0.581	0.484
Fe 0.25	0.1049	0.26	437	7873.2	0.46	0.259	0.207	0.173
Fe 0.125	0.1015	0.12	454	7303.3	0.43	0.240	0.192	0.160

For the Fe(III) catalysts, a 2 peak structure is expected and this can be seen as a shoulder on the peaks in Figure 21, again literature suggests[28] that the reduction pathway for Fe(III) is that shown in equation 2.

$$3Fe_2O_3 \rightarrow 2Fe_3O_4 \quad (2.1)$$

$$2Fe_3O_4 + 2H_2 \rightarrow 6FeO + 2H_2O \quad (2.2)$$

$$6FeO + 6H_2 \rightarrow 6Fe + 6H_2O \quad (2.3)$$

Comparing the two samples, the key difference was that the reducibility of the Fe (III) catalyst appeared lower. There are a few possible explanations for this, with the starting precursor being $Fe(acac)_3$ instead of $Fe(acac)_2$ there was a greater quantity of acetylacetonate present during the heat treatment. Since the decomposition of this compound resulted in a reducing atmosphere[7] it could possibly have reduced the Fe(III) species further than Fe(II) in the presence of a small oxygen impurity in the helium supply. If the starting precursor had little effect on the final oxidation state of the Fe species, then this is a possible reason for the difference in reducibility. Practically this would have no effect on the catalyst, as under testing conditions the iron would quickly reoxidise. A second possibility is that iron (III) was migrating into the alumina lattice, a potential test for this is the comparison of the background levels in XRD (Figure 22). If iron or cobalt was dissolving into the alumina then a gradual increase in background may be seen as the alumina becomes less crystalline, as observing the cobalt or cobalt aluminate directly is beyond the detection limits of powder XRD at these weight loadings. alumina then a gradual increase in background may be seen as the alumina becomes less crystalline, as observing the cobalt or cobalt aluminate directly is beyond the detection limits of powder XRD at these weight loadings.

This can be demonstrated with the XRD powder patterns in Figure 23. In these patterns we can see that as the cobalt loading increases there is an increase in background, possibly indicating a decrease in the long range order in the alumina lattice, possibly due to the formation of cobalt aluminate. This however is of limited utility as Co fluoresces under copper X-ray sources and so this may simply be due to that effect. The Iron compounds however did not display this effect, despite the tendancy to fluoresce under copper source X-rays which may be expected. Comparing the Fe(II) (Figure 23) and Fe(III) (Figure 24) powder XRDs, we can see little real difference between each other and the cobalt samples, there is possibly more difference between samples synthesised with

Fe(III) precursors as there appears to be a non-linear relationship with the 0.25 wt% Fe displaying the lowest background signal, however the signal to noise ratio is poor compared to the trend seen in the cobalt samples.

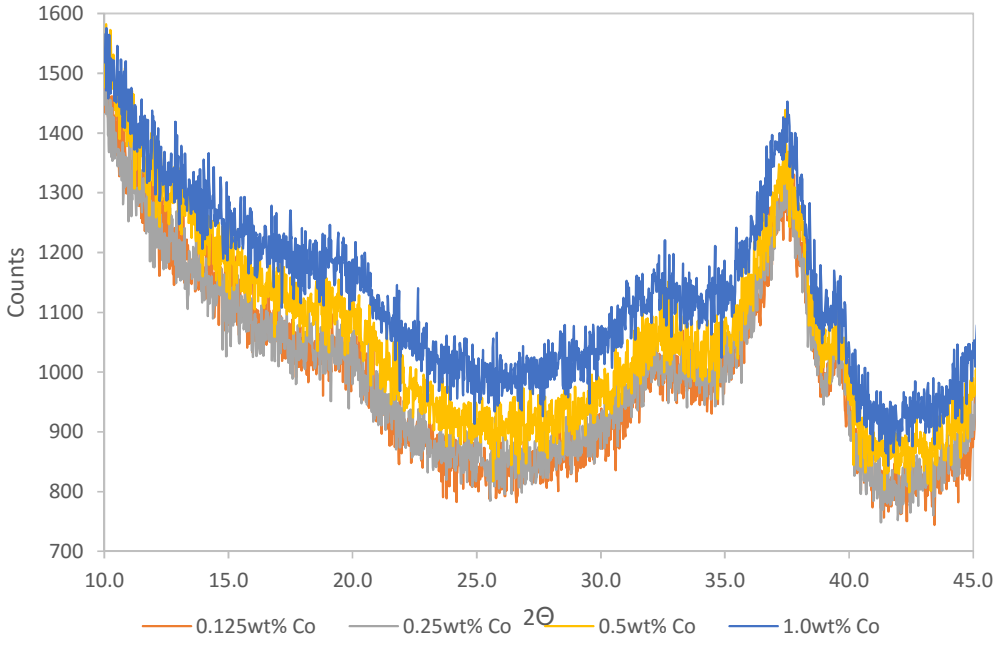

Figure 22. Expanded view of XRD powder patterns of 0.5 wt%Pt and Co catalysts supported on γ-alumina demonstrating increasing disorder with higher Co loading.

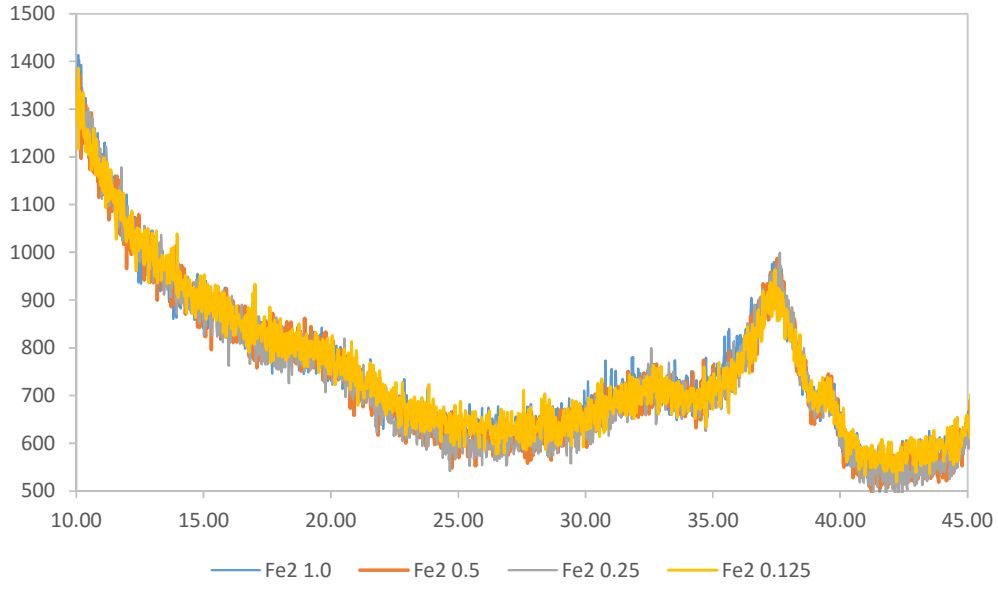

Figure 23. XRD powder patterns of 0.5 wt%Pt and Fe^{2+} catalysts supported on γ-alumina, not showing the same decrease in disorder as the cobalt catalysts.

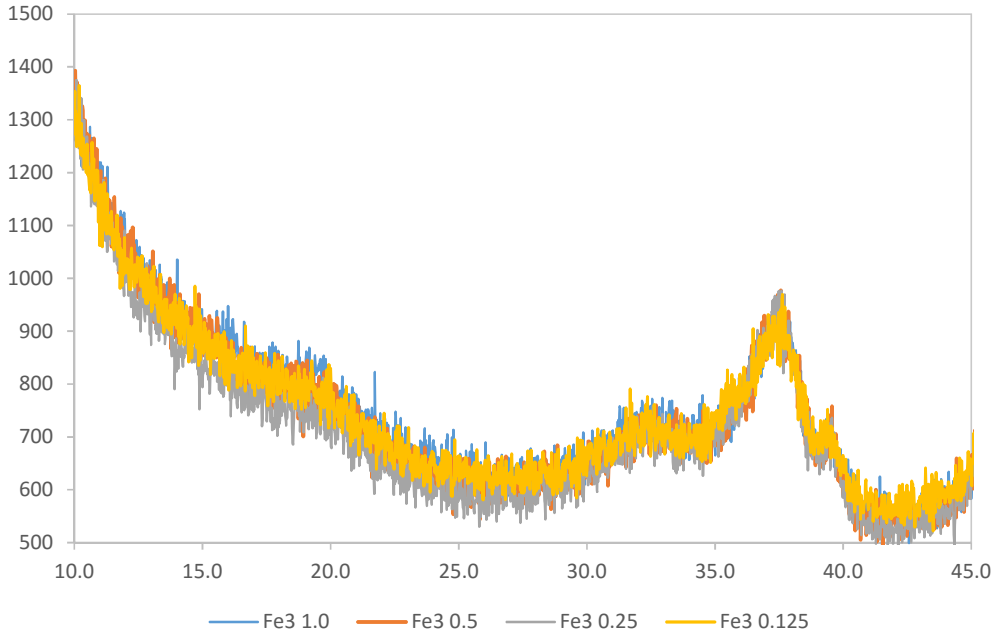

Figure 24. XRD powder patterns of 0.5 wt%Pt and Fe^{3+} catalysts supported on γ-alumina, not showing the same decrease in disorder as the cobalt catalysts.

A post mortem TEM analysis of the cobalt containing samples shows that over the course of two tests, the catalyst had experienced no platinum sintering and the small, discreet nanoparticles remained unchanged, however the cobalt oxide had started to show some sintering under testing. Figure 25 demonstrates with EDX that the samples started to show concentrated regions of cobalt present, this gradual sintering of the cobalt oxide could potentially have been the deactivation mechanism for the cobalt catalysts. The iron catalysts however appear to be more resilient over time and did not form concentrated regions of iron (Figure 26), maintaining its dispersion over the course of the test, despite showing a similar deactivation over time. The iron catalysts have possibly been deactivated by a change in oxidation state from a more active phase. TEM analysis is a powerful technique, however due to the limitations of viewing extremely small areas of the catalyst surface, there is always the possibility that the analysis of the samples fell under a selection bias with the microscopist selecting areas that may not be representative of the entire sample.

Figure 25. Post mortem TEM analysis of cobalt catalysts prepared by physical grinding, all samples are 0.5 wt%Pt/Al_2O_3 with (clockwise from top left) 1.0 wt% Co, 0.5 wt% Co, 0.25 wt% Co, 0.125 wt%Co.

Figure 26 Post mortem TEM analysis of iron (III) catalysts prepared by physical grinding, all samples are 0.5 wt%Pt/Al_2O_3 with (clockwise from top left) 1.0 wt% Fe, 0.5 wt% Fe, 0.25 wt% Fe, 0.125 wt%Fe.

4.5 Conclusions

Catalysts with only platinum present were less active and the presence of iron and cobalt significantly enhances activity, so there are a few possibilities. Firstly, that the cobalt and iron is acting as an oxygen storage material, providing oxygen for carrying out oxidation. Secondly that the metals are dissolving into the support and changing the nature of the metal support interaction (MSI)[13, 29] a very well documented effect by which the electronics of the support influence the electronics of the platinum, the effect of which can be seen during chemisorption. Where the strength of adsorption can be linked to the MSI, as the interaction between platinum and support increases the affinity for adsorbing hydrogen or CO decreases. This strength of adsorption has a direct influence on the catalytic activity of the material. The possibility of an MSI effect is a potential avenue for future enquiry.

This reactive grinding method of catalyst production with iron and cobalt is extremely simple and produces active catalysts, the precursors are commercially available and the technique requires very little in the way of specialist equipment to carry out. It uses industrially proven materials and builds on their effectiveness. There is however more to be gained from understanding the underlying cause of the increase of activity. Experiments could be devised that would take advantage of modern analysis techniques. The nature of the cobalt and iron in the sample can be determined by XPS, this would give insight into the oxidation state of the metals, possibly providing evidence for a redox couple mechanism 2 different oxidation states are observed, it could also be used to further test the solid state solution hypothesis and complement the XRD data. A deeper understanding of the mechanisms taking place on the surface might provide details on the activity; different pathways could be favoured by adding different dopants and thus produce different intermediates on the catalyst surface. DRIFTS can provide information about various species present on the surface[30], details on intermediate formation can be particularly useful for CO and NO as these have various different pathways for oxidation and reduction that are interdependent such as CO NO, ie direct NO reduction, CO/NO redox and direct oxidation of CO. For an experiment with a multicomponent feed such as exhaust gas analysis there will be a considerable number

of peaks, a simpler gas feed must be used to differentiate effectively between different intermediates and importantly to overcome the significant interference that arises from gas phase water. This information could be used to propose and test other candidate materials potentially opening the door for more candidate materials to research.

4.6 References

1. J. Kaspar, P. Fornasiero and N. Hickey, *Catalysis Today*, 2003, **77**, 419.
2. Y. Nishihata, J. Mizuki, T. Akao, H. Tanaka, M. Uenishi, M. Kimura, T. Okamoto and N. Hamada, *Nature*, 2002, **418**, 164.
3. H. Tanaka, M. Uenishi, M. Taniguchi, I. Tan, K. Narita, M. Kimura, K. Kaneko, Y. Nishihata and J. i. Mizuki, *Catalysis Today*, 2006, **117**, 321.
4. H. Tanaka, N. Mizuno and M. Misono, *Applied Catalysis A-General*, 2003, **244**, 371.
5. Suresh Kumar, Y. Teraoka, Amish G. Joshi, S. Rayalu and N. Labhsetwar, *Journal of Molecular Catalysis A: Chemical*, 2011, **348**, 42
6. H. Iwakuni, Y. Shinmyou, H. Yano, H. Matsumoto and T. Ishihara, *Applied Catalysis B-Environmental*, 2007, **74**, 299.
7. S. A. Kondrat, G. Shaw, S. J. Freakley, Q. He, J. Hampton, J. K. Edwards, P. J. Miedziak, T. E. Davies, A. F. Carley, S. H. Taylor, C. J. Kiely and G. J. Hutchings, *Chemical Science*, 2012, **3**, 2965.
8. M. V. Twigg, *Applied Catalysis B-Environmental*, 2007, **70**, 2.
9. H. Muraki, K. Yokota and Y. Fujitani, *Applied Catalysis*, 1989, **48**, 93.
10. M. Fernandez-Garcia, A. Martinez-Arias, L. N. Salamanca, J. M. Coronado, J. A. Anderson, J. C. Conesa and J. Soria, *Journal of Catalysis*, 1999, **187**, 474.
11. C. Bozo, N. Guilhaume and J. M. Herrmann, *Journal of Catalysis*, 2001, **203**, 393.
12. G. Groppi, C. Cristiani, L. Lietti, C. Ramella, M. Valentini and P. Forzatti, *Catalysis Today*, 1999, **50**, 399.
13. A. Trovarelli, *Catalysis Reviews-Science and Engineering*, 1996, **38**, 439.
14. A. Fathali, L. Olsson, F. Ekstrom, M. Laurell and B. Andersson, *Topics in Catalysis*, 2013, **56**, 323.
15. X. Auvray, T. Pingel, E. Olsson and L. Olsson, *Applied Catalysis B-Environmental*, 2013, **129**, 517.
16. *Preparation of Catalysts VII*, Elsevier, 1998.
17. K. Hauff, U. Tuttlies, G. Eigenberger and U. Nieken, *Applied Catalysis B-Environmental*, 2012, **123**, 107.
18. L. Olsson, H. Persson, E. Fridell, M. Skoglundh and B. Andersson, *Journal of Physical Chemistry B*, 2001, **105**, 6895.
19. J. Singh and J. A. van Bokhoven, *Catalysis Today*, 2010, **155**, 199.
20. T. Bunluesin, E. S. Putna and R. J. Gorte, *Catalysis Letters*, 1996, **41**, 1.
21. T. Bunluesin, H. Cordatos and R. J. Gorte, *Journal of Catalysis*, 1995, **157**, 222.
22. G. Kim, *Industrial & Engineering Chemistry Product Research and Development*, 1982, **21**, 267.
23. V. P. Zhdanov and B. Kasemo, *Applied Surface Science*, 1998, **135**, 297.
24. A. Obuchi, A. Ohi, M. Nakamura, A. Ogata, K. Mizuno and H. Ohuchi, *Applied Catalysis B-Environmental*, 1993, **2**, 71.

25. H. S. Gandhi, G. W. Graham and R. W. McCabe, *Journal of Catalysis*, 2003, **216**, 433.
26. A. Khan and P. G. Smirniotis, *Journal of Molecular Catalysis A-Chemical*, 2008, **280**, 43.
27. S. K. Sharma, J. M. Vargas, K. R. Pirota, S. Kumar, C. G. Lee and M. Knobel, *Journal of Alloys and Compounds*, 2011, **509**, 6414.
28. W. K. Jozwiak, E. Kaczmarek, T. P. Maniecki, W. Ignaczak and W. Maniukiewicz, *Applied Catalysis a-General*, 2007, **326**, 17.
29. S. Sharma and M. S. Hegde, *Journal of Chemical Physics*, 2009, **130**.
30. T. Baidya, P. Bera, B. D. Mukri, S. K. Panda, O. Kroecher, M. Elsener and M. S. Hegde, *Journal of Catalysis*, 2013, **303**, 117.

Chapter 5: Hydrophobic materials as catalytic supports.

5.1 Introduction

Aftertreatment catalysts have been extensively developed since their introduction and many of the commercial products available are still fundamentally based on platinum, palladium and rhodium. In lieu of alternatives, much effort has been carried out into improving the performance of Pt with additives such as Ce/Zr[1-3] and BaO[4] to adjust its activity and resistance to poisoning, but the support is typically alumina as it has been effective and stable and has remained unchanged for some time. H_2O is a ubiquitous exhaust component in any form of hydrocarbon combustion and it is largely seen as detrimental. Hydrothermal ageing can be extremely aggressive in car exhausts with 10% steam reaching temperatures of 1,000 °C, this has serious implications for catalyst lifetime. One method to guard against these detrimental effects may be to use hydrophobic supports such as silicon carbide and silicon nitride, allowing a window into the behaviour of the support and its interaction with water while potentially opening up a new class of supports for the commercial three-way catalyst.

Hydrophobic supports do not express terminating groups on their surfaces that interact with water. In addition, hydrophobic materials often exhibit different physical properties such as electronic interaction with the metallic support. This can change factors such as the metal support interaction (MSI) which is crucial for modifying the chemisorption properties of reactants on the surface of the metal. Hydrophobic supports may also interact more favourably with non-polar gas components such as uncombusted hydrocarbons and polyaromatics that are often found in exhaust gases[5]. A few materials were chosen that display hydrophobic character. These included silicon carbide[6], silicon nitride[7-9], tin oxide[5] and boron nitride[10-12]. The metal used for all of the activity tests was platinum.

Hydrophobic materials typically do not express the high surface areas of classic catalytic supports such as zeolites and have for a long time not been available due to limitations of technology or a simple lack of demand. The situation is changing and now many high surface area morphologies are becoming available. β-SiC was chosen as a

relatively high surface area analogue to the more common α-SiC, and commercially available nanopowders were chosen for SnO_2 and Si_3N_4 and BN, BET surface areas are presented in table 1. The surface areas for all hydrophobic samples are comparable. This allows us to say with greater certainty what effects the supports are having on the chemistry of the Pt surface and how it influences particle size rather than attributing greater activity to enhanced surface area.

All of the catalysts in this section were prepared using the modified impregnation procedure outlined in 2.1.5. For testing, all the catalysts in this chapter were tested under oxidising exhaust gas conditions as laid out in chapter 2 unless stated otherwise.

Table 1. BET surface areas of 1 wt% and 2.5 wt% Pt catalysts

Catalyst	Surface Area (m^2g^{-1})	C value
1 wt%Pt/SnO_2	46.6	84
1 wt%Pt/SiC	35.6	312
1 wt%Pt/Si_3N_4	48.2	234
1 wt%Pt/Al_2O_3	123.9	31
2.5 wt%Pt/SnO_2	48.0	332
2.5 wt%Pt/SiC	38.1	248
2.5 wt%Pt/Si_3N_4	43.6	153
2.5 wt%Pt/Al_2O_3	121.4	93

Metal surface area and dispersion measurements were taken using CO chemisorption. The samples were pre-treated at 200 °C for 1h in an atmosphere of pure H_2. 2.5 wt% Pt/Al_2O_3 was used as a standard for comparison as this is the most commonly used support in the automotive Industry. The experimental data shows 2.5 wt% Pt/Al_2O_3 had a greater dispersion and higher metal surface area than the similarly loaded hydrophobic supports. The poorer dispersion and lower metal surface area for SnO_2

suggests that Pt is more inclined to form larger particles with smaller surfaces. Pt/SiC proved difficult to reduce, even at temperatures of 300 °C for 2 hours, as the catalyst didn't display a signal in the titration, the CO chemisorption data is unavailable. A low metal surface area resulting in a poor TCD signal was ruled out by titrating with 10% CO rather than pure CO gas. This was investigated further in section 5.4.

Table 2. CO Chemisorption data

Catalyst	Crystallite size (nm)	Dispersion (%)
1 wt%Pt/SnO_2	222.0	6
1 wt%Pt/SiC	N/A	N/A
1 wt%Pt/Si_3N_4	89.7	13
1 wt%Pt/Al_2O_3	35.3	32
2.5 wt%Pt/SnO_2	312.1	4
2.5 wt%Pt/SiC	N/A	N/A
2.5 wt%Pt/Si_3N_4	102.7	12
2.5 wt%Pt/Al_2O_3	41.1	26.92

5.2 Tin oxide

The testing conditions were as laid out in chapter 2, gases removed were balanced with N_2. The CO activity data (Figure 1) for tin oxide shows moderate activity at higher weight loadings under a standard exhaust gas mixture without water. With increased weight loading, there is an additional increase in activity with light offs improving by very large values, with the T50 of CO decreasing by approximately 75 °C. Likewise, the propane also has a very large increase in activity from an increase in weight loading up to 2.5 wt% of just less than 50 °C. In order to investigate the effects of a hydrophobic support, a further test was carried out under identical conditions with the

exception of the addition of 8vol% water. The introduction water has a few effects, firstly in the 1 wt% Pt catalyst (Figure 2), a decrease in activity can be seen. CO is slow to start lighting off after 200 °C rather than between 100-150 °C, but the catalyst under wet conditions has a sharper curve with T50 being approximately 20 °C more and the time to reach T100 has been increased somewhat more significantly, possibly indicating some mass transfer limitation on the catalyst under water vapour. The T10 value for propane was not heavily modified under the atmosphere of steam. T10 is typically more indicative of the catalytic activity and so for propane oxidation the catalyst performs similarly, however, as T50 was approached, the catalysts diverge a little and the activity becomes more distinct. Since T50 tends to reveal pore structure effects and T90 mass transfer, this shows that for propane, the water may be having an influence on the catalyst support, despite its apparent lack of interaction.

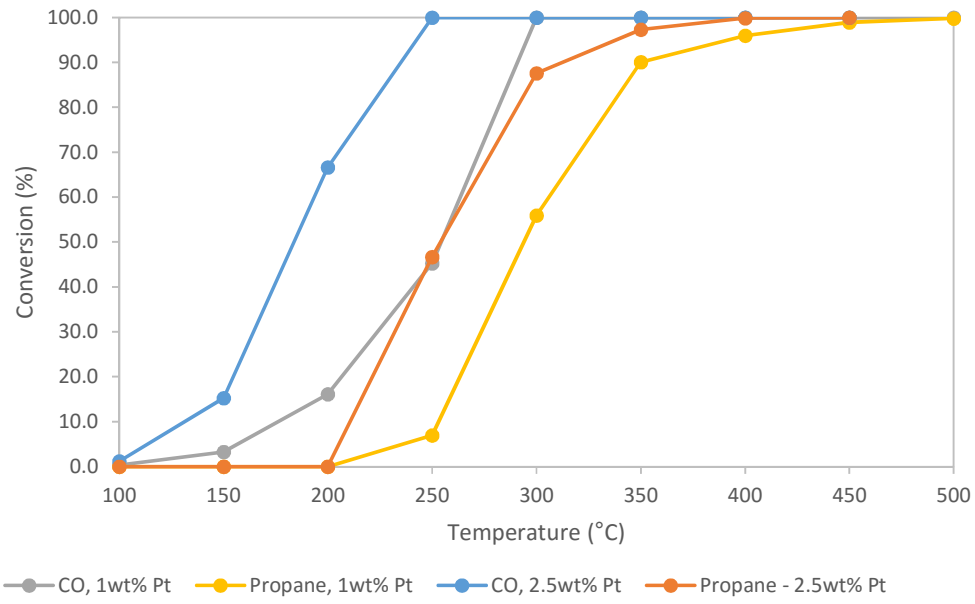

Figure 1. Comparison of weight loadings of Pt supported on tin oxide tested under a dry exhaust gas mixture

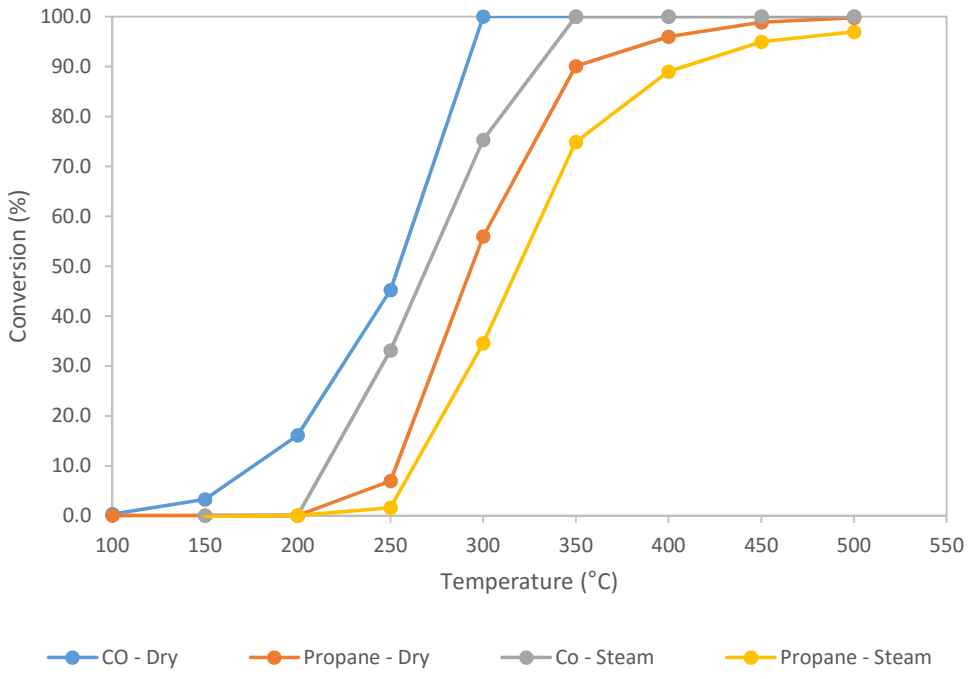

Figure 2. Activity of 1 wt% Pt supported on tin oxide in the presence of steam

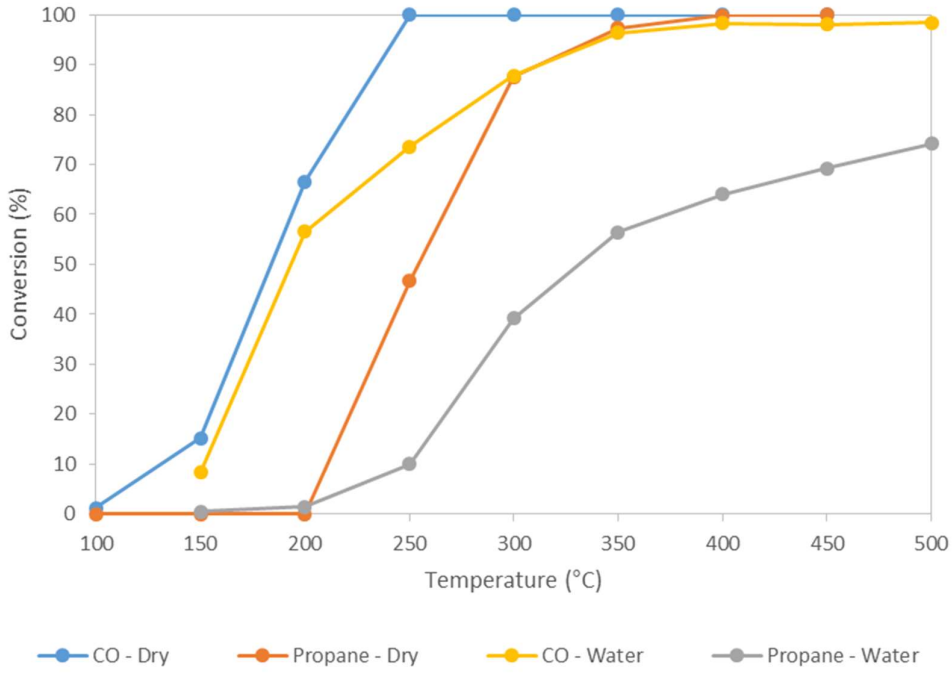

Figure 3. Activity of 2.5 wt% Pt supported on tin oxide in the presence of steam

The inhibition of the 2.5 wt% Pt catalyst was considerably more pronounced than its 1 wt% analogue (Figure 3) and shows a few features of interest. The CO activity showed a significant mass transfer limitation when steam was present in the gas feed. This is very likely a sign of competitive inhibition of the catalyst surface with the CO and H_2O competing for active sites on the platinum This results in less available space on the catalyst surface for carrying out oxidation, the reaction then becomes controlled by the diffusion of the CO to the remaining active sites. The propane activity again shows this difference, but it is considerably greater than the effect seen in the 1 wt% catalyst and the mass transfer limitation means that activity after 60% conversion is supressed significantly. The reason for the large difference between the 2.5 wt% catalysts and the 1 wt% catalysts is likely the difference between particle size distribution discussed earlier. The 1 wt% catalysts have smaller nanoparticles present on the surface, while the 2.5 wt% will have limited room on a support with such a low surface area, and thus more energetically favourable to form large particles with a lower surface area available for catalysis. Such large particles may have a greater affinity for water, and thus the effect on activity is greater.

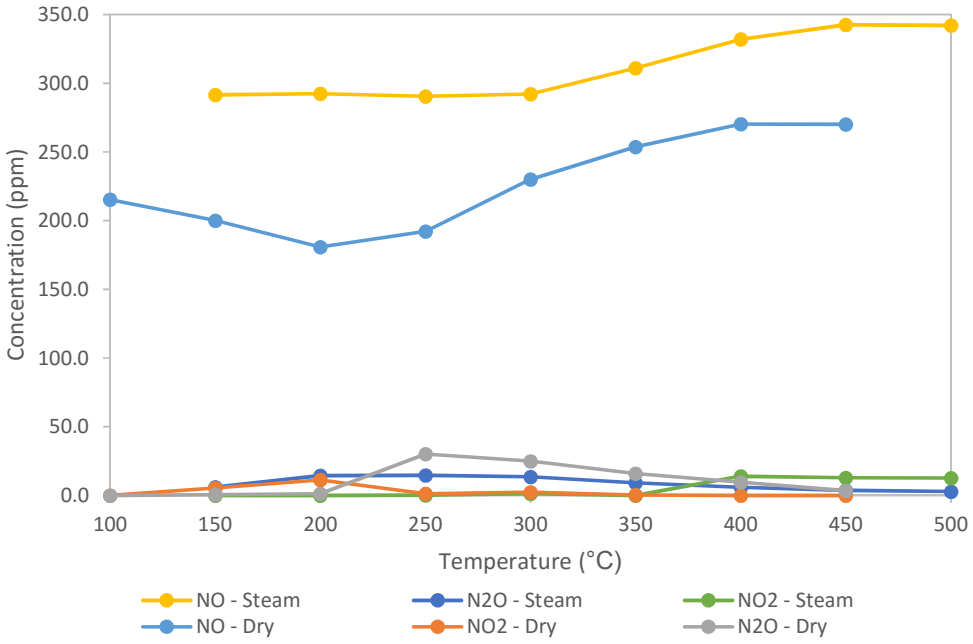

Figure 4. NOx concentrations after 2.5 wt% Pt supported on tin oxide in the presence of steam

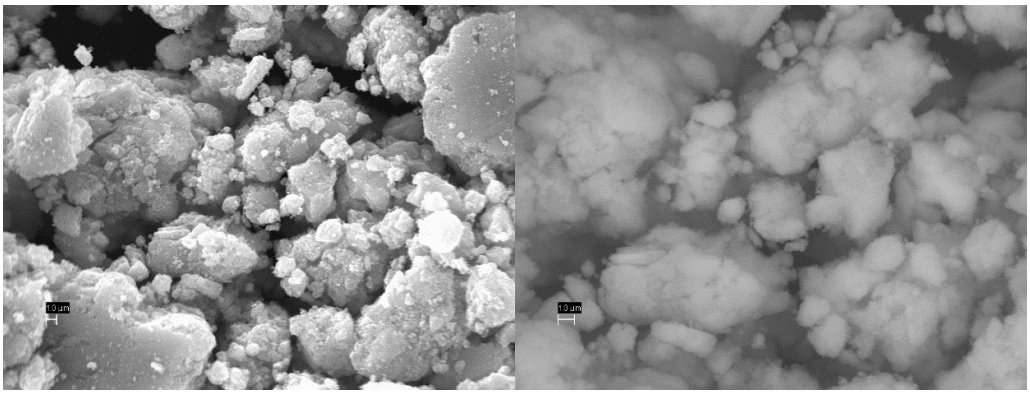

Figure 5. SEM secondary electron image of 2.5 wt%Pt/SnO_2 (left) and backscatter (right)

The effect on NO of water in the gas stream is straightforward. The presence of water almost completely inhibits activity (Figure 4). The NO reduction reaction is known to be very sensitive to inhibition from oxygen[13] and so it may also be inhibited by the adsorption of water species to the surface. The catalyst under dry conditions however, appeared to be an effective reducing catalyst, as N_2 cannot be analysed by FT-IR it is possible that a strong storage effect could be responsible for the drop in NO concentration. However, no significant release event was seen through the course of the test. This is of interest as Pt is more commonly considered an NO oxidation catalyst without a reducing agent such as ammonia present, and could be a result of the lack of a strong MSI between the SnO_2 than seen in Pt/Al_2O_3. Figure 5 shows and SEM image of the 2.5 wt% catalyst, no distinctive Pt nanoparticles can be seen on the surface of the tin oxide. TPR analysis does not show a distinctive reduction peak for the Pt before the large SnO_2 reduction peak (Figure 6). Whilst it is possible the Pt peak is poorly resolved. the likely scenario is that the materials were reduced.

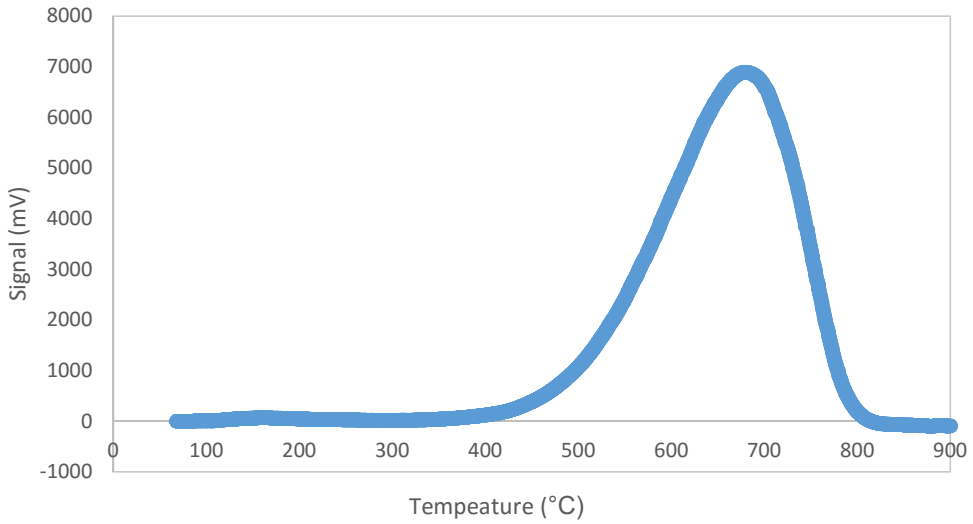

Figure 6. TPR of 1 wt% Pt/SnO_2. 10vol% H_2 in Ar at 10 °C min^{-1}

To ascertain the oxidation state of the surface Pt, XPS was carried out on the sample (Figure 7), the Pt 4f 7/2 signal is a peak at 75.17eV, a signal which is characteristic of PtO_2[14, 15], so indicating the presence of the oxide phase. The O 1s has two peaks at 530.63 and 531.52, characteristic of SnO_2[16] and PtO_2[17] respectively. The XPS data would suggest that the Pt oxide surface is oxidised, though this does not necessarily translate to the bulk properties that would be seen with TPR.

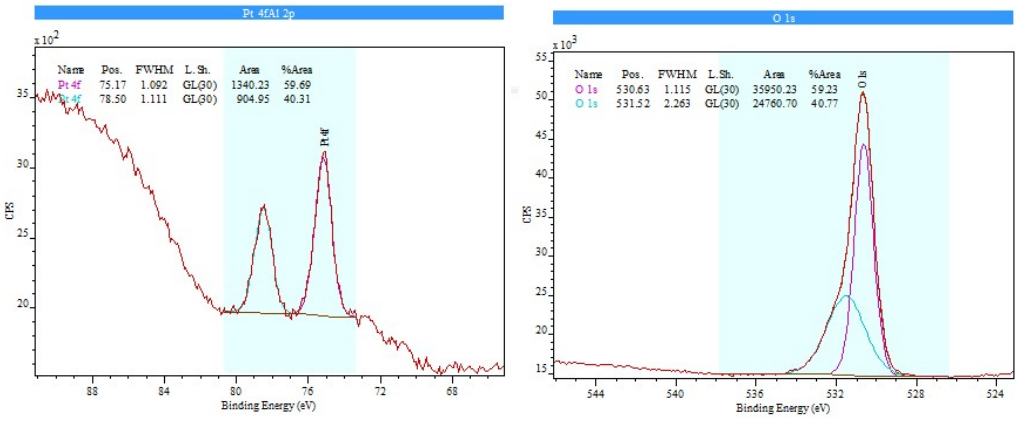

Figure 7. XPS spectra of 2.5 wt% Pt/SnO_2, O 1s spectra with a peak position at 530.63eV and 531.52eV, Pt 4f 7/2 at 75.17eV and Pt 4f 5/2 at 78.50eV.

5.3 Silicon nitride

Si_3N_4 is a material of particular interest as it has a relatively high MSI effect with platinum. MSI interactions can stabilise nanoparticles and encourage the formation of smaller, more dispersed molecules. However, Si_3N_4 has a lower surface area than a typical catalytic support and so this may be counteracted with space limitations at higher loadings.

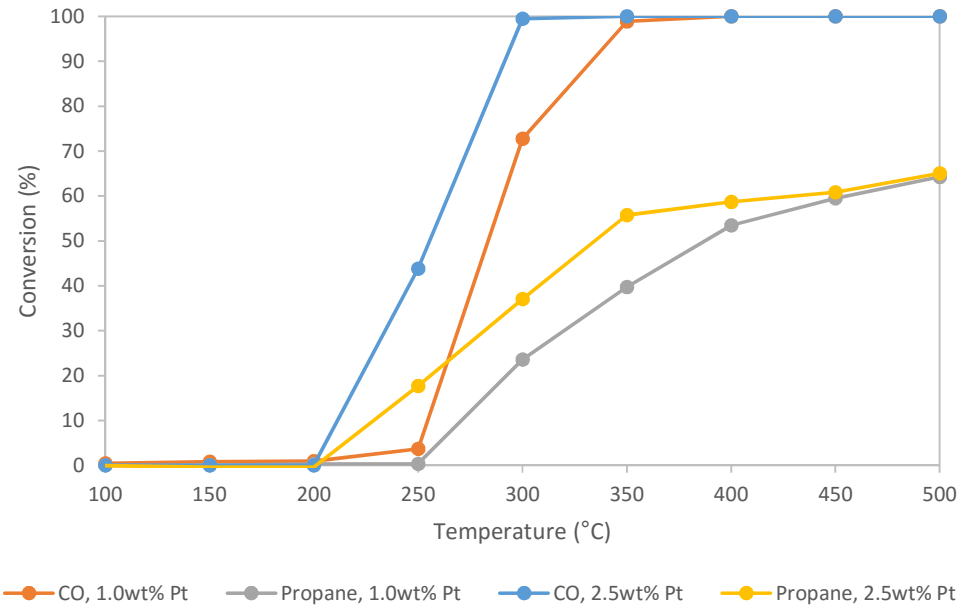

Figure 8. Comparison of weight loadings of Pt supported on silicon nitride tested under a dry exhaust gas mixture

Figure 8 shows a comparison of 1 wt% and 2.5 wt% Pt supported on Si_3N_4. The 2.5 wt% catalyst shows an increase in activity for CO oxidation and propane oxidation, however in comparison to the tin oxide catalyst discussed earlier, the catalyst doesn't show exceptional activity. The 2.5 wt% catalyst shows an increase in T50 of approximately 25 °C for CO oxidation but the propane oxidation is less impressive. The 2.5 wt% catalyst shows an initial improvement however, the flat light off curve eventually converges with the 1 wt% catalyst. The implication is that severe mass transfer limitations exist for this catalyst under the artificial exhaust gas mixture. Literature shows

that Si_3N_4 is a good support for hydrocarbon oxidation[7, 9], therefore there it's likely that a component of the gas mixture is inhibiting the activity of the catalyst. As some studies show that water can be a promotor in the exhaust, steam was introduced to the exhaust gas mixture to observe the effects. On the 1 wt% catalyst (Figure 9), the catalyst showed a large decrease in CO activity in the presence of steam with T50 values dropping from 280 °C to 349 °C also with propane significant deactivation was observed, and the light off curve begins flattened greatly well before reaching T50.

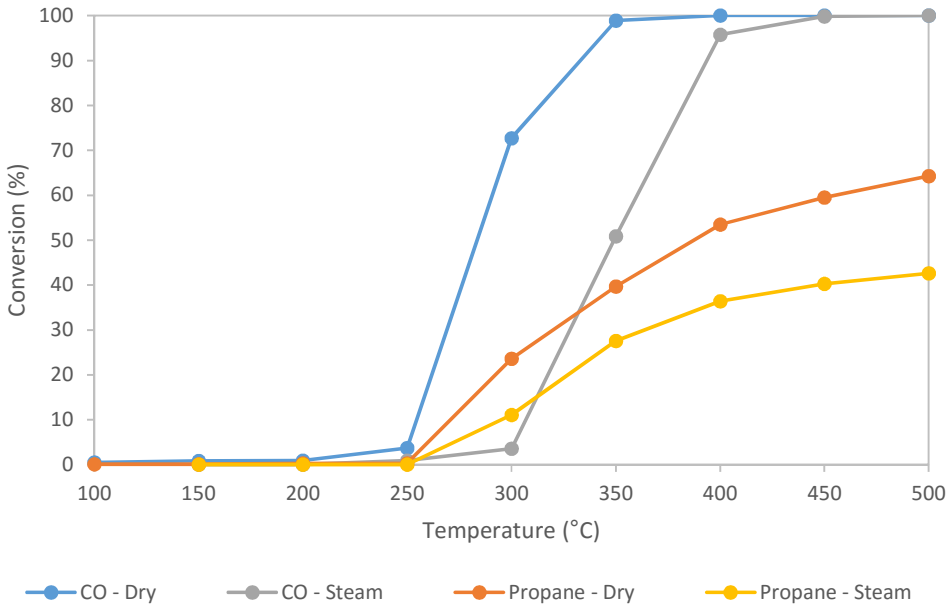

Figure 9. 1 wt% Pt supported on Si_3N_4 in the presence of steam

The 2.5 wt% catalyst (Figure 10) however did not see as significant a decrease. With CO T50 increasing from 255 °C to 305 °C. The propane activity, while lessened, eventually converged on the catalyst tested under dry conditions and may, with extrapolation, show better activity than the dry catalyst at higher temperatures. Though further testing would be required to validate this, as it goes beyond the capabilities of the current testing apparatus. The poor activity of this catalyst could be due to larger Pt particle sizes that are less active for oxidation. SEM analysis (Figure 11) shows large clusters of electron dense material which is likely platinum.

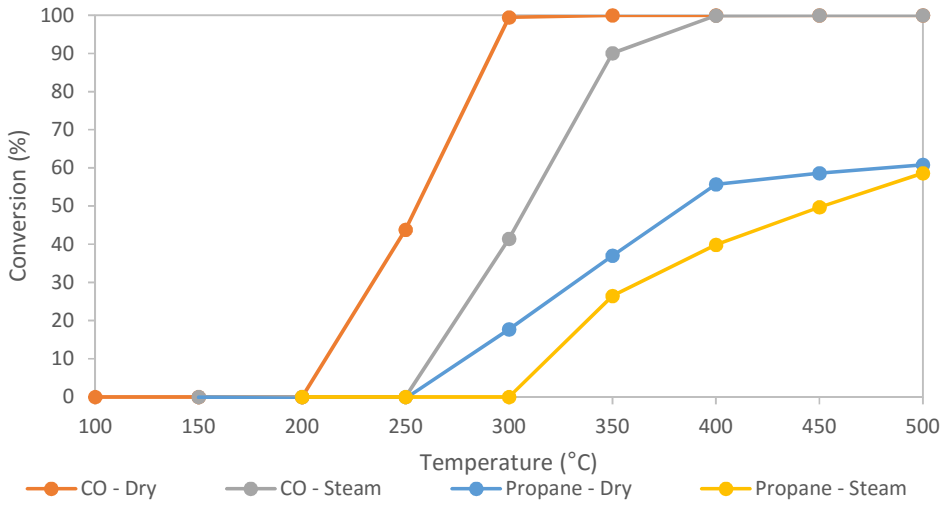

Figure 10. 2.5 wt% Pt supported on Si_3N_4 in the presence of steam

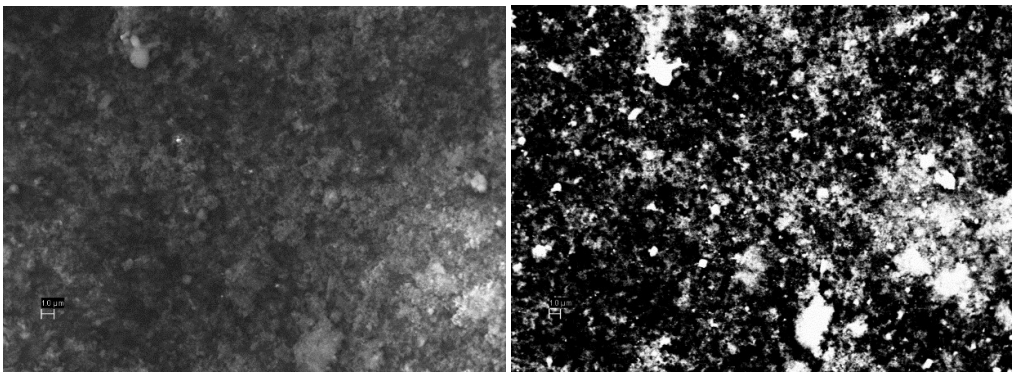

Figure 11 SEM secondary electron image of 2.5 wt%Pt/SnO_2 (left) and backscatter (right)

To determine the oxidation state of the surface Pt on Si_3N_4, XPS was carried out (Figure 12). The Pt 4f 7/2 signal is a peak at 71.3 2 eV, a signal which is characteristic of a metallic platinum surface species[15] so indicating the presence of the metallic phase, Pt 4f 7/2 for Pt in PtO_2 is approximately 75 eV. Indicating platinum bonded to oxygen on the surface. The O 1s has one peak at 532.74 eV, this indicates the presence of silicon bonded to oxygen[18]. No response was seen for the oxygen in PtO_2. The XPS data then indicates the presence of metallic and oxidic platinum supported on an oxidised Si_3N_4 surface.

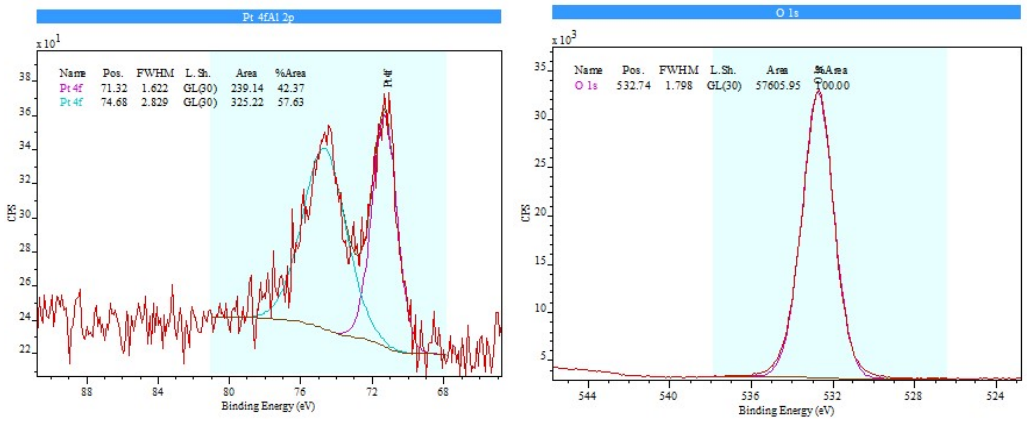

Figure 12. XPS spectra of the O 1s spectra with a peak position at 532.74 ev, Pt 4f 7/2 at 71.32 ev and Pt 4f 5/2 at 74.68 ev

5.4 Silicon carbide

SiC is an interesting support material. It is usually used in reactors as an inert bedding material in its α-SiC phase and exhibits good thermal properties that allow it to distribute heat efficiently over the catalyst bed. SiC is very resistant to oxidation but will start to oxidise at temperatures over 800 °C. Whilst catalyst bed temperatures in gasoline exhausts can exceed 1000 °C, the thermally conductive properties of these supports may help to mitigate the effects of temperature spikes and if the catalyst is effective, then steps could be taken to reduce the temperature in the exhaust through changes to the engine cycle or engineering solutions to the exhaust system.

SiC has been used as a support previously for exhaust gas, however the phase used was lower surface area α-phase[19]. In this project the higher surface area β-SiC was used as an alternative.

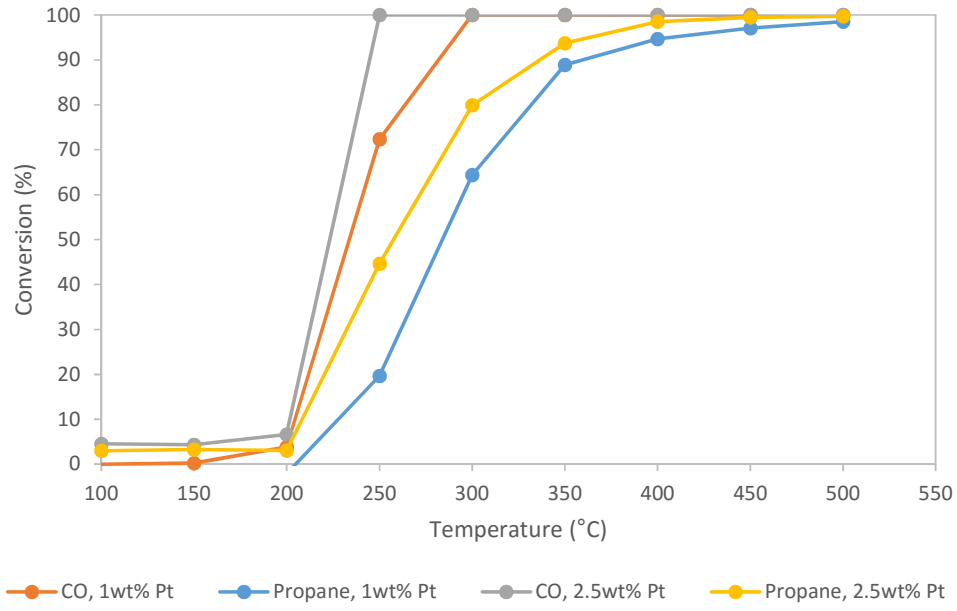

Figure 13. Comparison of weight loadings of Pt supported on silicon carbide tested under a dry exhaust gas mixture.

The activity data (Figure 13) showed that the weight loading had little effect on the activity of SiC, whilst there was some improvement going from 1 to 2.5 wt%, the improvement was nowhere near as great as the SnO_2 and Si_3N_4 catalysts that were tested previously. This may have been as a result of particle size distribution being significantly different compared to the previous supports. Unfortunately, CO chemisorption failed to reduce the nanoparticles effectively and up to the safe operating limits of the equipment and so it is difficult to say with certainty if this is an effect. The difficulty in reducing the Pt present on the SiC catalyst however indicated that there may be a resilient oxide present on the surface of the nanoparticles. As smaller nanoparticles of Pt are more prone to oxidation than bulk platinum, there may be very small nanoparticles present on the surface. SEM analysis (Figure 14) shows a comparison between 1 wt% Pt/SiC and 1 wt% Pt/Al_2O_3. What can be seen from these images is the presence of large visible nanoparticles of Pt on the alumina catalyst that are not as prevelant on the SiC catalyst. There are a few bright regions on the SiC catalyst, but not on the same scale as seen in the Pt/Al_2O_3. If the metal surface area was lower than the detection limits of the CO chemisorption test then very large particles of platinum would be expected.

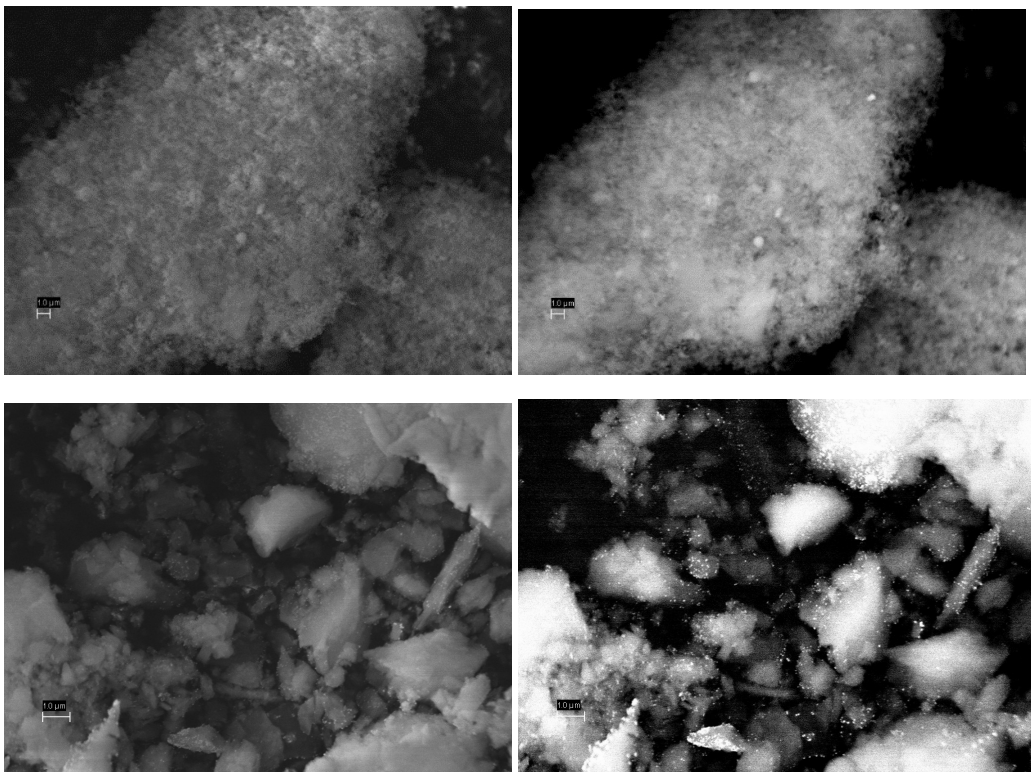

Figure 14. SEM secondary electron image of 1 wt% Pt/SiC (top left) and a backscatter image of the same area (top right), and a secondary electron image of 1 wt% Pt/Al_2O_3 (bottom left) with backscatter image of the same area (bottom right).

If a resilient oxide phase is present at the surface preventing the reduction under the relatively mild conditions used in chemisorption then there are several tests that could be done to characterise it. TPR shows a reduction peak at approximately 100 °C that corresponds to a reduction of Pt (Figure 15), this indicates that there is reducable material present that should interact with CO in CO chemisorption. XPS analysis is a

highly sensitive surface technique that can reveal the oxidation state of the materials on the surface. A platinum oxide phase could be revealed by this method.

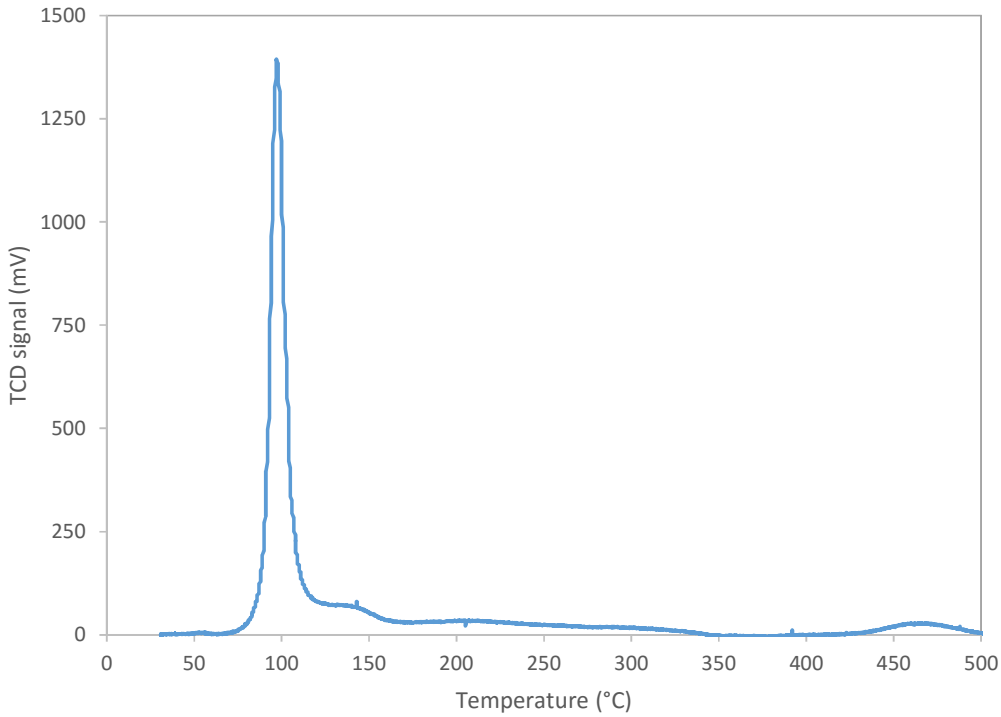

Figure 15. TPR of 2.5 wt% Pt/SiC. 10vol% H_2 in Ar at 10 °C min^{-1}

The XPS data (Figure 16) revealed the following. The signal for the O 1s signal was given at 532.84eV which is characteristic of the oxygen bond to a silicon atom in SiO or SiO_2[18]. The Pt 4f 7/2 signal would be expected to be at approximately 74eV for PtO[20, 21], 75eV for PtO_2[14, 15] or 71eV for metallic Pt[22]. The signal shown for 4f 7/2 was at 71.14 which would indicate that the Pt seen on the SiC is actually metallic Pt and that the reason for no response was a pre reduced catalyst. This result means that if the Pt was reduced in the CO chemisorption test, then the CO was failing to interact with the metal, evidence that contradicted the CO activity data if a Langmuir-Hinshelwood mechanism is presumed to be taking place[23].

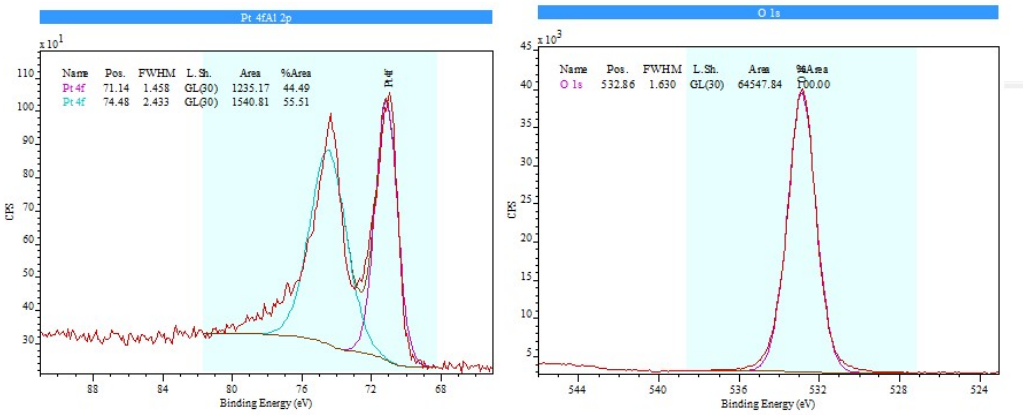

Figure 16 XPS spectra of the O 1s spectra with a peak position at 532.84, Pt 4f 7/2 at 71.14 and Pt 4f 5/2 at 74.48

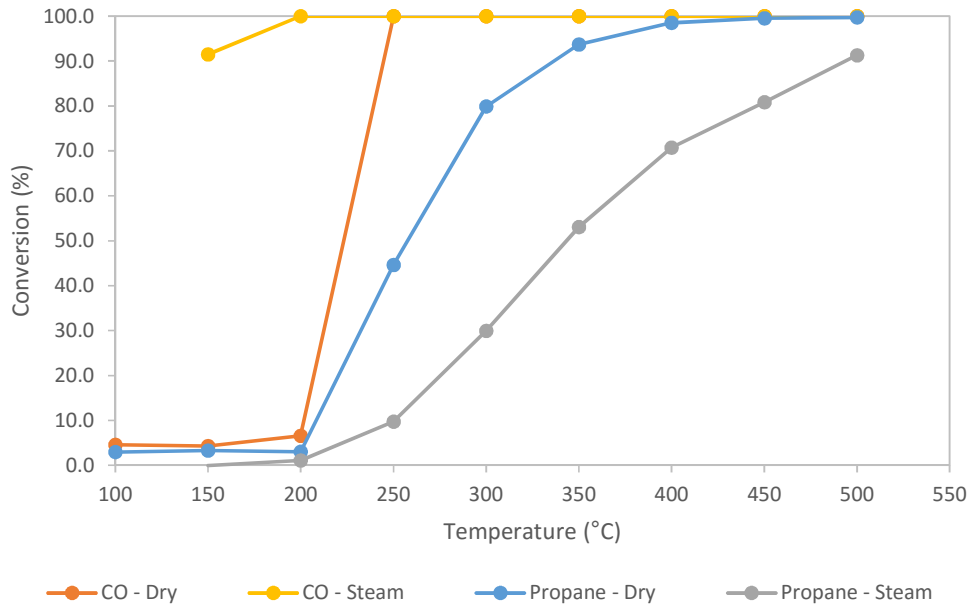

Figure 17. Activity of a 2.5 wt% Pt catalyst supported on Si_3N_4 in the presence of steam

When tested under an atmosphere of water, the SiC catalysts were the only ones tested to see an improvement in activity for CO oxidation. The effect of water on propane oxidation remains inhibitory. The CO oxidation promotion effect of H_2O shows that the H_2O is interacting with the metallic nanoparticles in a significant way. One potential way the SiC could be promoting the activity of the catalyst is by an oxygen promoted water gas shift reaction (equation 1)[24]. To test this, a 2.5 wt% Pt/SiC catalyst was tested under 3 sets of conditions outlined in Figure 17. The catalyst tested under 1% CO and 1%H_2O

showed no low temperature activity and from 300 °C the CO starts to convert to CO_2 and C. The catalyst tested with 8% H_2O present however, showed what appeared to be an equilibrium process taking place at temperatures lower than 350 °C with total oxidation by O_2 later. When compared against a catalyst tested in a dry atmosphere, we can see that the WGS component may account for this increase in activity.

$$H_2O + CO \rightleftharpoons H_2 + CO_2 \qquad (1)$$

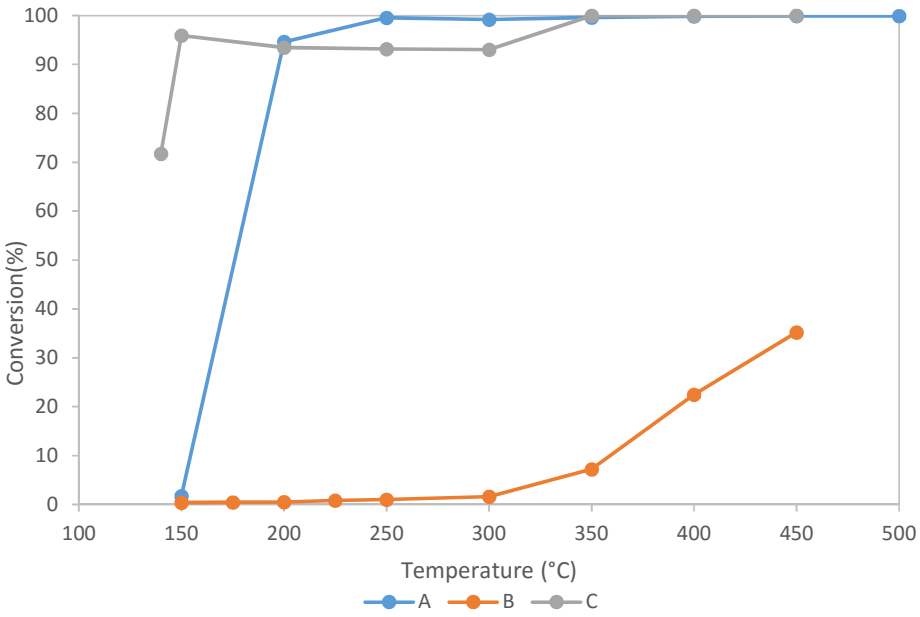

Figure 18. Activity data for water gas shift over a 2.5 wt% Pt/SiC catalyst, Catalyst A tested under the standard conditions without H_2O, B in CO 1%, H_2O 1%, N_2 balance, and C in CO 1%, H_2O 8%, 1% O_2, N_2 balance, all tests at 40,000 h^{-1}.

WGS could also go some way to explain why Pt/SiC partially reduces NO to N_2O instead of oxidising the NO as the Pt/Al_2O_3 does (Figure 18, 19). It is possible that in the presence of a hydrogen pathway exists for the NO to reduce. Hamada *et al.*[25] showed that the selective catalytic reduction of NO to N_2O and N_2 can take place in the presence of hydrogen on a platinum catalyst. This further adds weight to the prospect of a water gas shift reaction taking place at low temperatures that acts as this H_2 source. Shibata *et*

al. theorised that the oxidation state of the platinum was the important factor for reduction, but for selectivity the availability of acid sites was important also. They state that more acidic supports have a higher selectivity for N_2 over N_2O[26]. The explanation given is that the NH_4^+ intermediate in the reaction of NO with H_2 is a similar pathway to ammonia SCR, which is known to be highly selective for NO reduction in comparison to H_2 SCR. SiC interacts poorly with water by virtue of its lack of acid sites on the surface and likely leads to the poor selectivity for N_2 over N_2O.

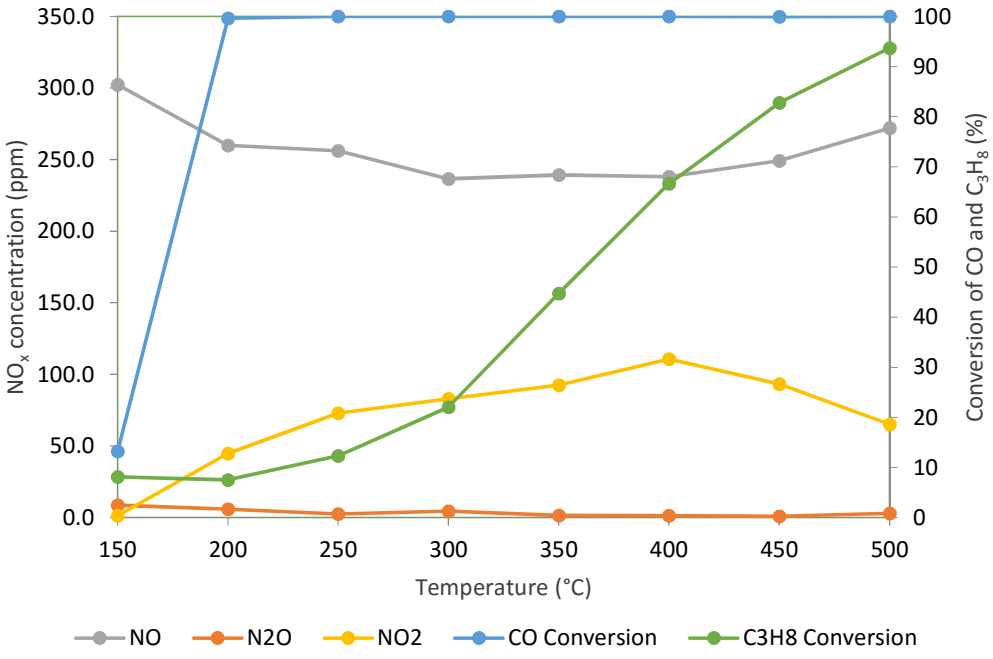

Figure 19. Activity data for 2.5 wt% Pt/Al_2O_3 in the presence of steam

It is thought that H_2O is dissociating on the surface of the Pt to form hydroxyl species. Such species are normally thought to have lower binding energy of CO to the Pt surface, thus increasing the rate at which the surface is renewed. However it has been demonstrated by Caporali *et al.*[5] with the isotopic labelling of H_2O with ^{18}O that CO oxidation does not necessarily proceed with molecular oxygen preferentially. CO was shown to almost exclusively react with $H_2{}^{18}O$ on 2 wt%Pd/Al_2O_3 and a similar mechanism could be occurring here.

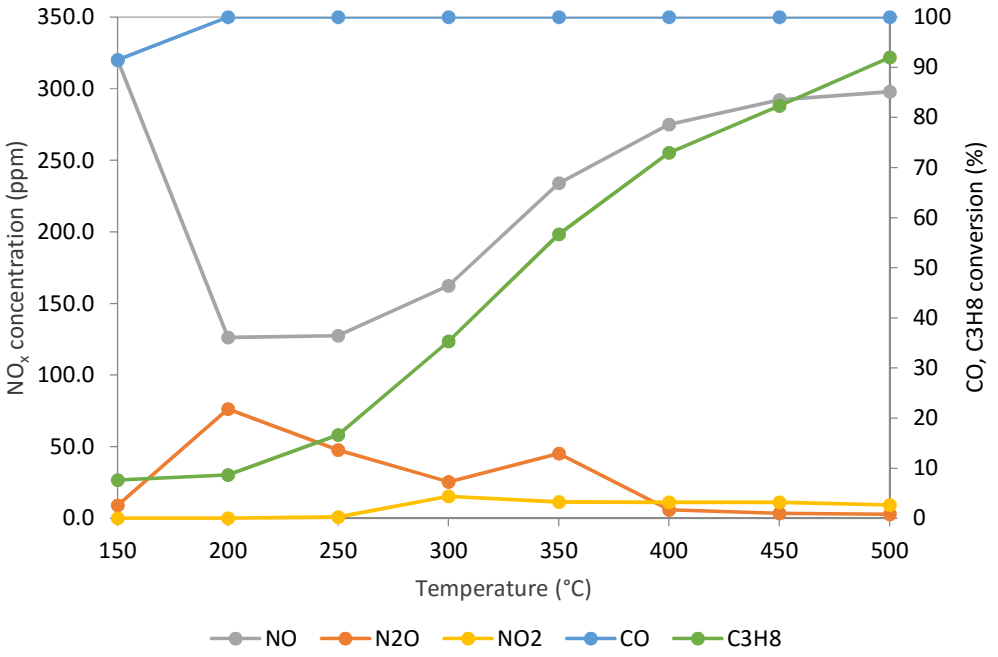

Figure 20. Activity data for 2.5 wt% Pt/SiC in the presense of steam

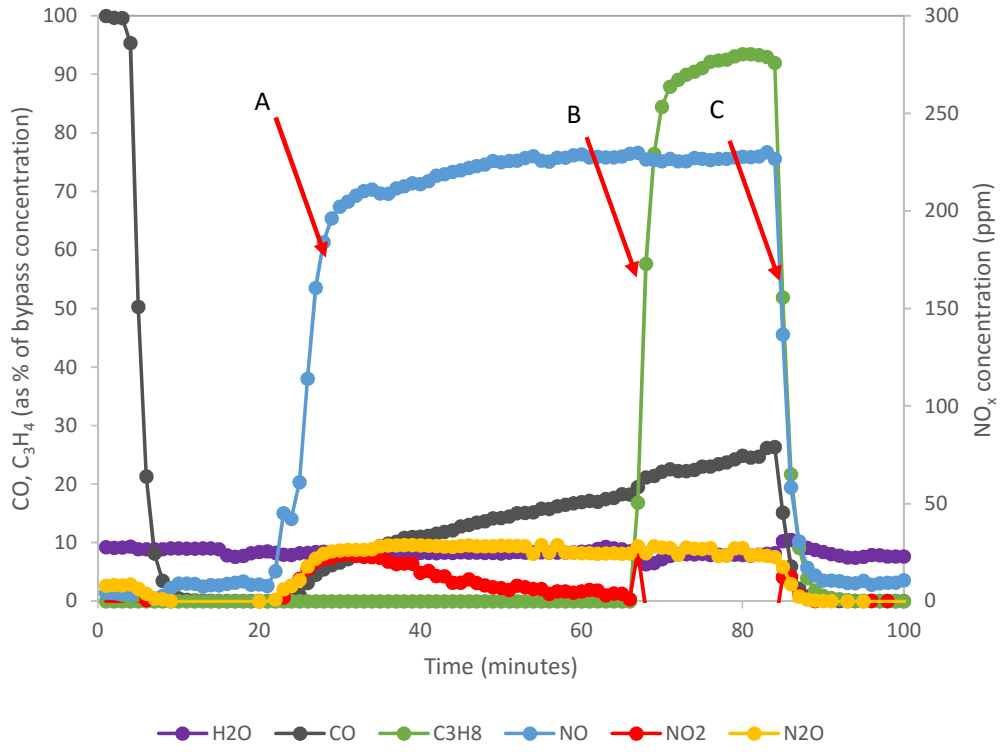

Figure 21. TOL study at 200 °C of 2.5 wt% Pt/SiC with exhaust gas mixture initially omitting NO, and propane, and then introducing procedurally. A = introduction of NO, B = introduction of propane, C = both propane and NO stopped.

In order to understand the relationship between the various gas components and gain some insight into the activity, a TOL test was carried out where NO and propane were omitted as potential inhibitors and reintroduced into the gas mixture (Figure 21). Upon the introduction of NO, it was noted that that there is a gradual decrease in the catalyst's activity for CO oxidation, as the NO competes with the CO for surface sites on the catalyst. Also seen is that immediately NO is reduced to N_2O and oxidised to NO_2 simultaneously, with the oxidation to NO_2 peaking approximately 10 minutes after NO's introduction to the gas feed and then tailing off, N_2O remains at a constant level until the NO is removed from the gas feed. The reason for this is unclear, but a likely answer is that the NO is reacting with any small amount of platinum oxide[28] either present from the start or generated during the test until it has been consumed. As soon as the supply of platinum oxide is depleted, the NO_2 is formed at the rate that platinum oxide forms. As the peak of NO_2 production is reached, there is a slight drop in the rate of change in CO activity. NO_2 is also likely a competitive inhibitor for the CO oxidation reaction.

The selectivity for the reduction of NO to N_2O rests at approximately 25% with the rest being either stored or converted to nitrogen. It is likely that in this incidence the NO was converted to N_2 and O_2 as there is not a significant adsorption event or release of anything other than a small quantity of NO_2 at the initial switch over. Further testing with a different analytical technique is required to confirm. The switch in of propane has subtler effects than the NO. Firstly, what little NO_2 is present before the switch is completely removed, additionally the CO oxidation rate of deactivation increased slightly at first, however this could have been an artefact of switching gas feeds. Upon the removal of both NO and propane, CO oxidation is immediately restored to total conversion as is expected if the competitive inhibition is an equilibrium process, with no gas to replenish surface NO species. This also rules out the possibility of a stable NCO intermediate inhibiting the surface[29].

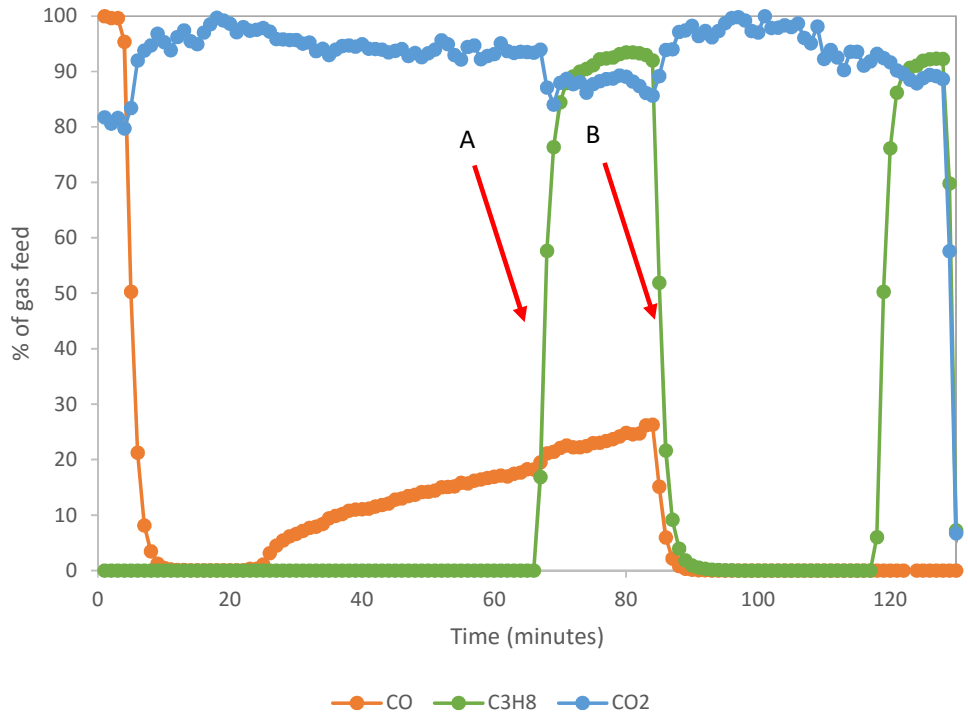

Figure 22. Alternative view of TOL study at 200 °C of 2.5 wt% Pt/SiC with exhaust gas mixture initially omitting NO and Propane. The graph has had NO_x removed and CO_2 for clarity. A = Propane started, B = Both propane, NO stopped.

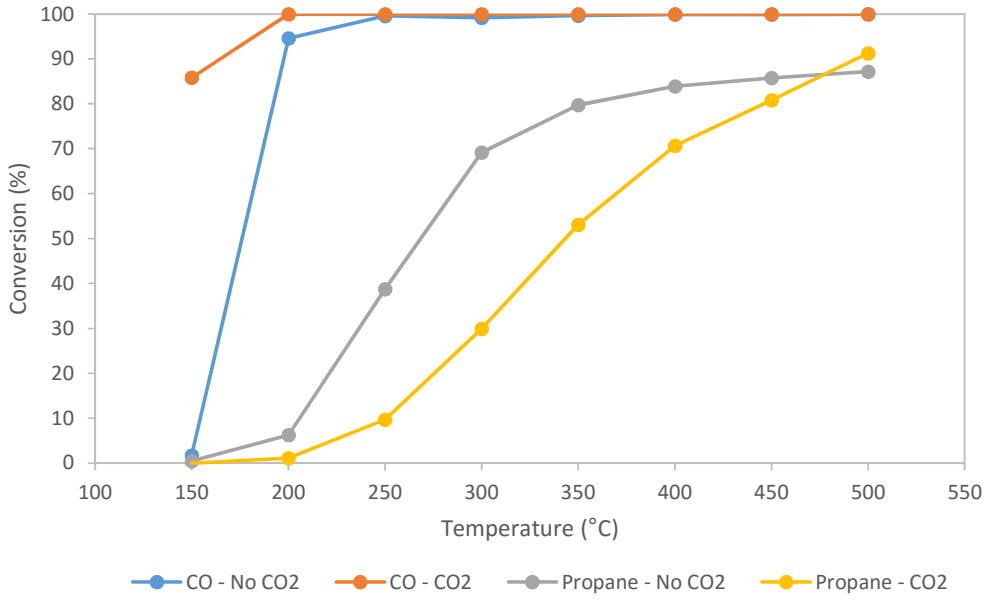

Figure 23. Depicting the effects of CO_2 promotion of CO oxidation and inhibition of propane oxidation over a 2.5 wt% Pt/SiC catalyst.

It was also noted that CO_2 was having an effect on the Pt/SiC catalyst for CO oxidation. Figure 21 shows an alternative view of the same process, with the switch in of propane at A to the switch out at B, a slight increase in the CO but a greater decrease in CO_2 was seen, to investigate this effect the catalyst was tested under a standard exhaust gas mix with, and without CO_2 present (Figure 23). What can be seen is an increase in CO activity for the catalyst tested with CO_2 present and an inhibitory effect for the propane oxidation. CO_2 is a known inhibitor of CO oxidation on many catalysts[30-32] but has also been reported as a potential promotor by Liang *et al*[33] for palladium supported on ceria-titania catalyst. There are no references of the effect being demonstrated for platinum. The aforementioned route for CO_2 promotion on a metal by Liang *et al.* was theorised to be a result of CO_2 dissociation at low temperatures and switched to become inhibitory carbonate formation at high temperatures. This could explain why the catalyst was promoted for CO at lower temperatures; however the carbonate aspect of that explanation is unlikely in this catalyst system due to a lack of suitable material for its formation.

5.5 Boron nitride

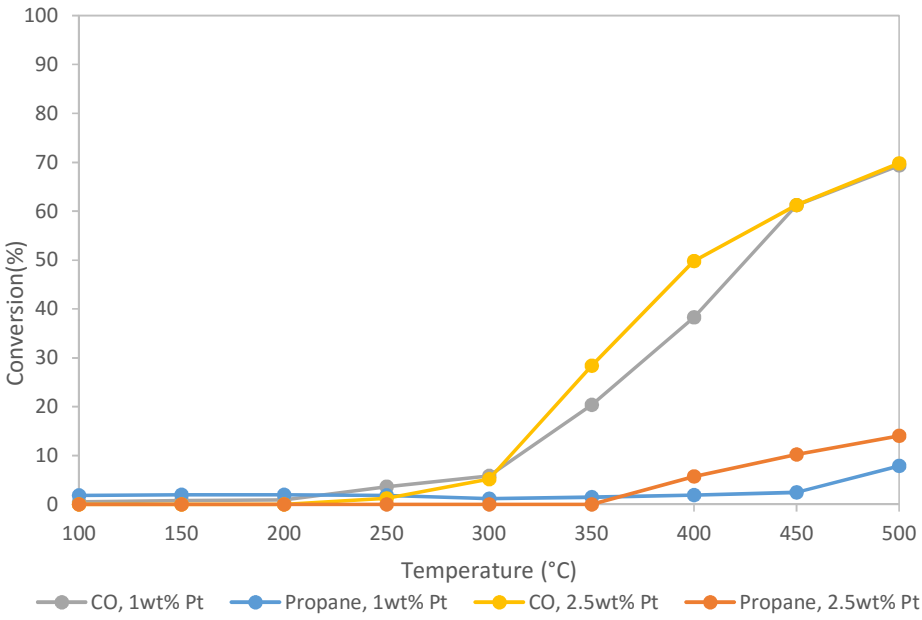

Figure 24. Comparison of weight loadings of Pt/ BN tested under a dry exhaust gas mixture.

Boron nitride was initially considered a promising support material, however initial testing (Figure 24) indicated that it was significantly worse performing than the other hydrophobic supported catalysts. CO oxidation activity is extremely limited for both weight loadings and propane activity was low compared to the other catalyst of this type. The catalysts were further tested under wet conditions to ascertain if there was a promotion effect from the water and improvements to activity may have been seen. The result however was that the catalyst was further inhibited by the presence of gas phase water. Figure 25 shows the extent of the deactivation on the 1 wt% catalyst. What little activity was present for propane oxidation had almost entirely been inhibited. CO oxidation additionally was badly affected by the addition of water. The 2.5 wt% catalyst (Figure 26) also suffered from a similar deactivation, however the extent was lessened slightly.

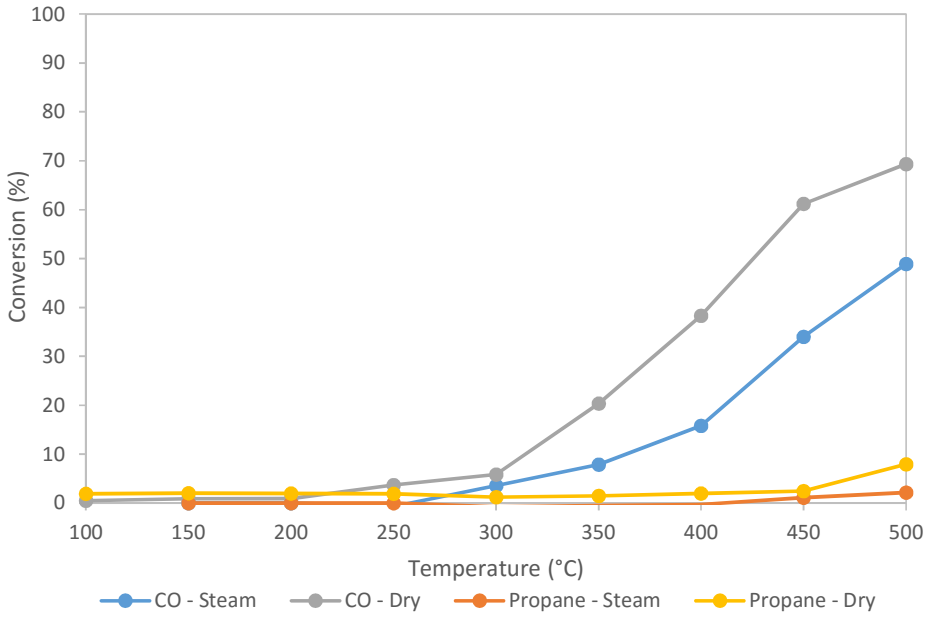

Figure 25. Effect of steam on 1 wt% Pt/BN tested under standard exhaust conditions

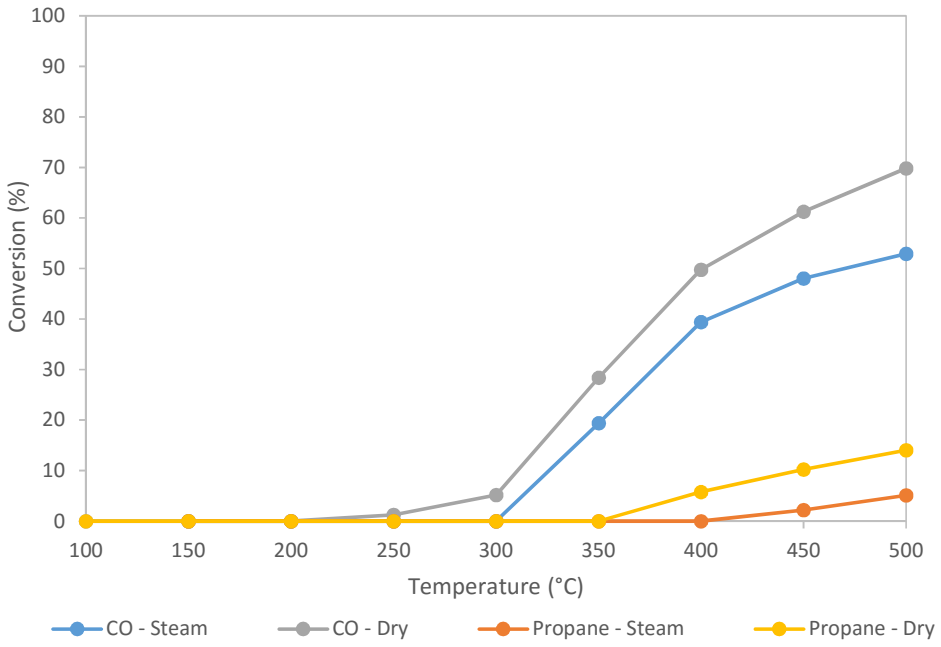

Figure 26 Effect of steam on 2.5 wt% Pt supported on BN tested under standard exhaust conditions.

TPR shows (Figure 27) a hydrogen desorption and adsorption peak at approximately 145 °C and 170 °C respectively. The precise nature of the adsorption is unknown, but the TPR indicates that there is less reducible material than the the other materials, indicating the presence of metallic platinum. This agrees with the low metal support interaction hypothesised to influence the chemistry of this support.

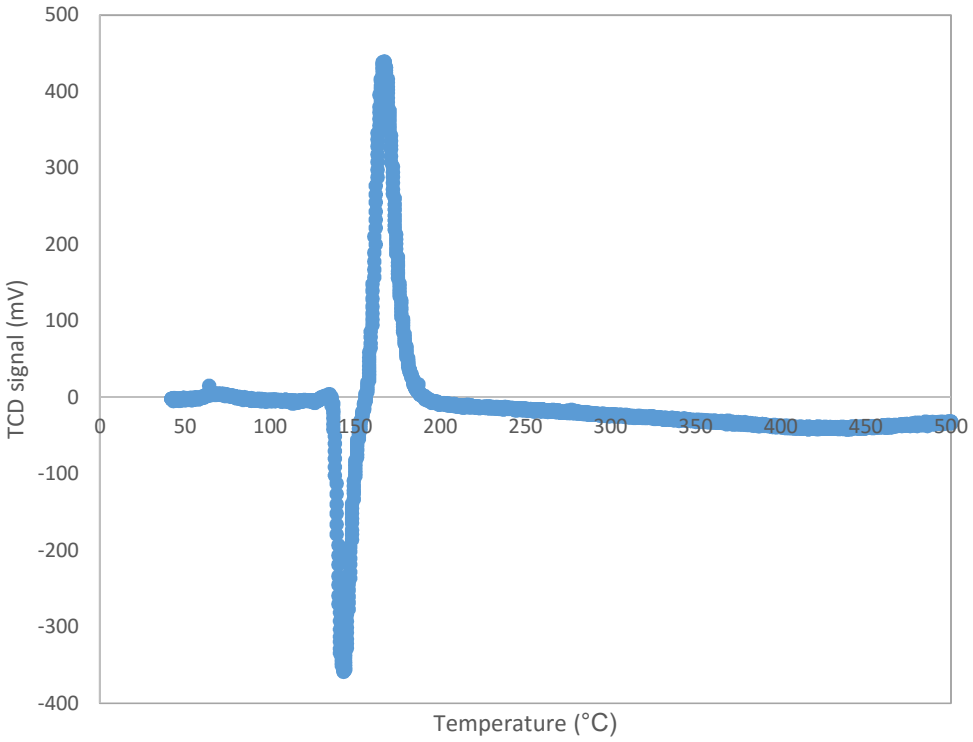

Figure 27. TPR of 2.5 wt% Pt/SiC. 10vol% H_2 in Ar at 10 °C min^{-1}

5.6 Comparison with Pt/Al_2O_3

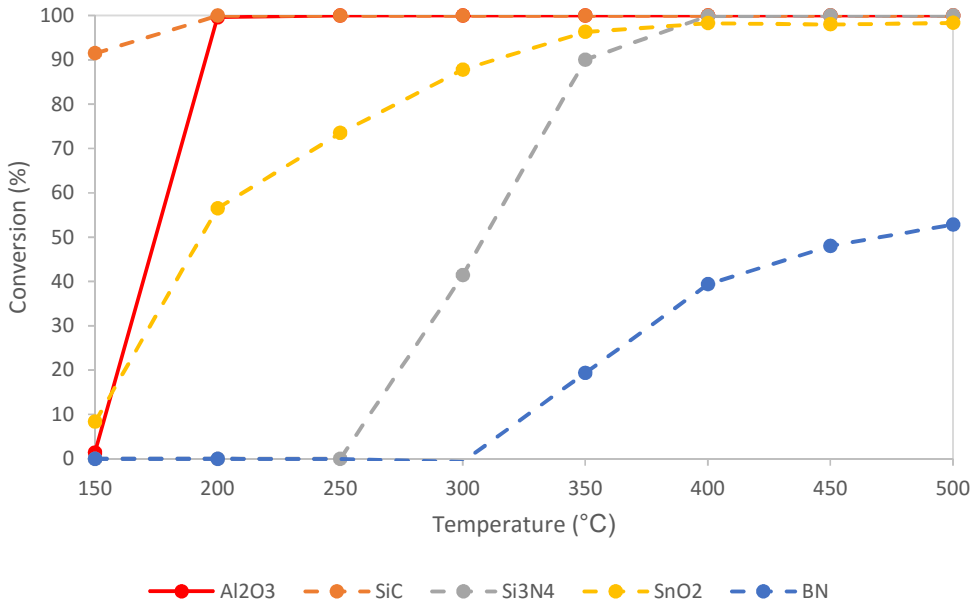

Figure 28 Comparison of the CO activity data for 2.5 wt% supported on various supports

The performance the hydrophobic catalysts was compared against a standard 2.5 wt% Pt/Al_2O_3 catalyst for reference purposes. For CO oxidation (Figure 27) the results were highly variable. Pt/Al_2O_3 is a very effective catalyst for CO oxidation and only one catalyst exceeded the platinum standard. The SiC catalyst was very active at low temperatures on account of its simultaneous water and CO_2 promotion. As SiC was the only catalyst that displayed greater activity, it can be inferred that the hydrophobicity of the support is not the crucial factor in determining the performance of the final catalyst for CO oxidation. The results for propane oxidation were fairly different from the CO in that the activity of the hydrophobic catalysts was more in line with the standard catalyst (Figure 28). Here we see that the SiC, Si_3N_4 and SnO_2 catalysts all initially outperform the Al_2O_3 catalyst, however the light off curves are shallower and so the standard exceeds the activity of the Si_3N_4 and SnO_2 catalyst. Once more the SiC supported platinum has been the most active for propane oxidation and its lower temperature activity may be useful in the control of cold start emissions.

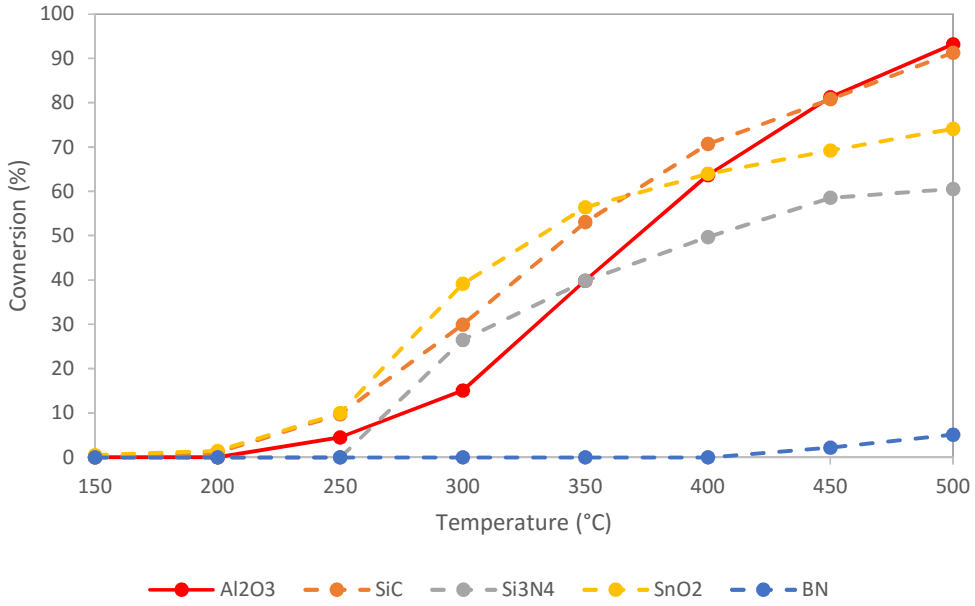

Figure 29 Comparison of the propane activity data for 2.5 wt% Pt supported on various materials.

NO activity was varied with Si_3N_4, BN and SnO_2 being relatively inert in comparison to SiC and Al_2O_3 (Figure 30). Al_2O_3 showed a classic oxidation of NO to NO_x which is seen on Pt catalysts. The reaction proceeded until it became thermodynamically controlled above 400 °C[34]. SiC demonstrated a more interesting behaviour as it converted NO to N_2O at approximately 75% selectivity at 200 °C with 25% N_2 assumed as the secondary product, and showed some NO oxidation character at higher temperatures also. This was likely due to partially oxidised platinum species formed under reaction conditions or storage effects on the catalyst or support surface. Si_3N_4 showed very little reduction.

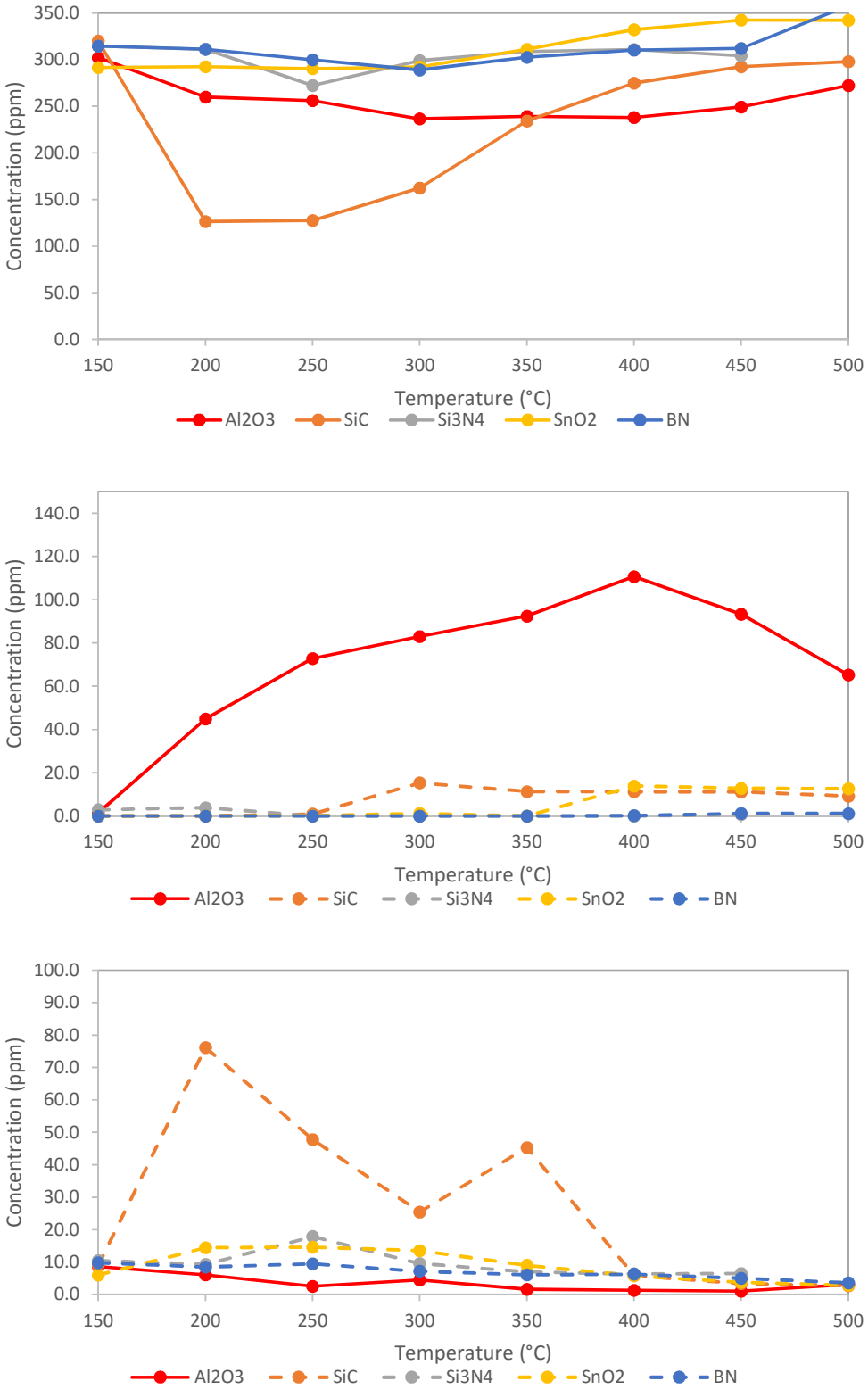

Figure 30 Comparison of the NO activity data for 2.5 wt% Pt supported on various supports, NO (top), NO_2 (middle) and N_2O (bottom)

5.7 Conclusions

The results of this chapter leave some interesting avenues left to explore. The CO_2 promotion effect on Pt/SiC is something not yet described in the literature for a Pt catalyst in these reactions and could provide insight into behaviour of Pt in a catalyst exhaust. This effect could potentially be utilised by modification of existing catalysts to help reduce cold start emissions as much as possible. Of all the catalysts tested, only SiC showed a significant improvement transitioning from dry to wet conditions and was the only catalyst to demonstrate activity that competes with Pt/Al_2O_3. Temporal analysis of products could be used with isotopically labelled carbon dioxide to identify whether the CO_2 is activated and carrying out/assisting through an unknown reaction pathway, the oxidation of CO at low temperatures. The same could be tested with water to determine the extent of the water gas shift reaction, if it takes place and the temperatures at which it is outstripped by direct oxidation.

In the case of SiC, there are unanswered questions about the nature of the platinum on the surface of the catalyst. It appears to be reduced but also, for the purposes of chemisorption, CO does not seem to interact with the platinum on the surface of the catalyst. TEM/TEAM could be utilised to directly observe the surface and determine if there are large or small particles of Pt present. The NO reduction through to N_2O is undesirable and therefore before this catalyst could be used commercially this must be addressed. There are a few ways this could be achieved. Future work could focus on how this reaction could be supressed in some way through modification of the synthesis of these catalysts or the addition of dopants to promote fully the reduction of NO to N_2. If indeed reduction is facilitated by the hydrogen produced in the water-gas shift reaction then the suppression of this side reaction may be important, however to do so would also likely prevent any reduction from taking place on the platinum surface. A more fruitful path may be to introduce acid sites to the surface of the catalyst, though this may affect the hydrophobic character of the support.

5.8 References

1. A. Trovarelli, *Catalysis Reviews-Science and Engineering*, 1996, **38**, 439.
2. H. C. Yao and Y. F. Y. Yao, *Journal of Catalysis*, 1984, **86**, 254.
3. H. S. Gandhi, G. W. Graham and R. W. McCabe, *Journal of Catalysis*, 2003, **216**, 433.
4. L. Olsson, H. Persson, E. Fridell, M. Skoglundh and B. Andersson, *Journal of Physical Chemistry B*, 2001, **105**, 6895.
5. N. N. Edwin, A. F. Carley and S. H. Taylor, *Catalysis Today*, 2008, **137**, 362.
6. C. Pham-Huu, N. Keller and M. J. Ledoux, *Actualite Chimique*, 2002, 8.
7. F. Aires and J. C. Bertolini, *Topics in Catalysis*, 2009, **52**, 1492.
8. R. Shang, W. Sun, Y. Wang, G.-Q. Jin and X.-Y. Guo, *Catalysis Communications*, 2008, **9**, 2103.
9. I. A. Kurzina, F. J. Cadete Santos Aires, J. C. Bertolini and Ieee, *Silicon nitride supported platinum catalysts for the total oxidation of methane*, 2004.
10. G. Postole, M. Caldararu, N. I. Ionescu, B. Bonnetot, A. Auroux and C. Guimon, *Thermochimica Acta*, 2005, **434**, 150.
11. C. A. Lin, J. C. S. Wu, J. W. Pan and C. T. Yeh, *Journal of Catalysis*, 2002, **210**, 39.
12. J. C. S. Wu, Y. C. Fan and C. A. Lin, *Industrial & Engineering Chemistry Research*, 2003, **42**, 3225.
13. F. Kapteijn, J. R. Mirasol and J. A. Moulijn, *Applied Catalysis B-Environmental*, 1996, **9**, 25.
14. J. L. G. Fierro, J. M. Palacios and F. Tomas, *Surface and Interface Analysis*, 1988, **13**, 25.
15. J. Escard, B. Pontvianne, M. T. Chenebaux and J. Cosyns, *Bulletin De La Societe Chimique De France Partie I-Physicochimie Des Systemes Liquides Electrochimie Catalyse Genie Chimique*, 1975, 2399.
16. A. W. C. Lin, N. R. Armstrong and T. Kuwana, *Analytical Chemistry*, 1977, **49**, 1228.
17. J. P. Contour, G. Mouvier, M. Hoogewys and C. Leclecq, *Journal of Catalysis*, 1977, **48**, 217.
18. J. A. Taylor, G. M. Lancaster, A. Ignatiev and J. W. Rabalais, *Journal of Chemical Physics*, 1978, **68**, 1776.
19. P. H. Cuong, S. Marin, M. J. Ledoux, M. Weibel, G. Ehret, M. Benaissa, E. Peschiera and J. Guille, *Applied Catalysis B-Environmental*, 1994, **4**, 45.
20. T. H. Fleisch and G. J. Mains, *Journal of Physical Chemistry*, 1986, **90**, 5317.
21. K. S. Kim, N. Winograd and R. E. Davis, *Journal of the American Chemical Society*, 1971, **93**, 6296.
22. C. J. Powell, *Journal of Electron Spectroscopy and Related Phenomena*, 2012, **185**, 1.
23. R. J. Baxter and P. Hu, *Journal of Chemical Physics*, 2002, **116**, 4379.
24. J. Kugai, J. T. Miller, N. Guo and C. S. Song, *Journal of Catalysis*, 2011, **277**, 46.
25. H. Hamada and M. Haneda, *Applied Catalysis A-General*, 2012, **421**, 1.
26. J. Shibata, M. Hashimoto, K. Shimizu, H. Yoshida, T. Hattori and A. Satsuma, *Journal of Physical Chemistry B*, 2004, **108**, 18327.
27. M. Konsolakis, M. Vrontaki, G. Avgouropoulos, T. Ioannides and I. V. Yentekakis, *Applied Catalysis B-Environmental*, 2006, **68**, 59.

28. K. Hauff, U. Tuttlies, G. Eigenberger and U. Nieken, *Applied Catalysis B-Environmental*, 2012, **123**, 107.
29. D. K. Captain and M. D. Amiridis, *Journal of Catalysis*, 1999, **184**, 377.
30. T. Davran-Candan, S. T. Tezcanli and R. Yildirim, *Catalysis Communications*, 2011, **12**, 1149.
31. J. Yan, J. X. Ma, P. Cao and P. Li, *Catalysis Letters*, 2004, **93**, 55.
32. K. E. Uguz and R. Yildirim, *Turkish Journal of Chemistry*, 2009, **33**, 545.
33. F. Liang, H. Zhu, Z. Qin, G. Wang and J. Wang, *Catalysis Communications*, 2009, **10**, 737.
34. P. Granger, C. Dathy, J. J. Lecomte, L. Leclercq, M. Prigent, G. Mabilon and G. Leclercq, *Journal of Catalysis*, 1998, **173**, 304.

Chapter 6: Conclusions

Emissions control is one of the greatest achievements of modern day legislation. The drastic drop in airborne pollutants in the countries that have implemented such controls has improved general public health as well as air quality, reducing the severity of smog events and transforming the public image of motor vehicles. It has truly been a silent revolution passing unnoticed under the public eye precisely because they are so effective at controlling pollution.

As the general shift of consumer focus is to more fuel efficient vehicles, gasoline emission control faces a challenging future, the increasing requirements for lean burn conditions, stop start engines and ever toughening government regulation of emissions. Engineering the solutions to these problems will be a multidisciplinary affair with chemists and engineers designing new systems to cope with these demands. For the chemistry aspect of this, there is still much left to research and many demands for practical implementation. The holy grail of this being the invention of a PGM free catalyst that is as, if not more, effective than current leading commercial PGM catalysts. While there have been varied approaches to this problem in the literature, there has as not yet been a commercial success story for PGM free catalysts in exhausts. The dynamic conditions experienced within an exhaust combined with punishing conditions have limited the use of metal oxides for example, or cheaper yet effective metals such as silver. Approaches to the problem of expensive TWCs has been to improve the activity of PGM catalysts through alternative preparative procedures, dopants and novel supports. The catalysts for example were revolutionised by the introduction of ceria/zirconia in the monolith this allowed the catalyst to retain oxidation activity during rich periods in the exhaust and boosted oxygen availability for oxidation in general.

With the introduction of lean burn engines to meet increasing demand for fuel efficiency, car exhausts will be expected to cope with longer periods of lean exhaust gas. This means a more efficient catalyst for oxidation, however NO emissions will still have to be managed and likely under increasingly strict legislation. This represents a huge problem for gasoline and the solution will possibly utilise the technologies being developed for diesel vehicles. Technologies such as selective catalytic reduction (SCR) of

NO_x with urea and lean NO_x traps might become a part of gasoline emissions control in the future. The challenge for chemists will be to utilise a catalyst that can efficiently reduce NO even under oxidising conditions.

The efficacy of PGM based catalysts is such that they have been unrivalled in practical application since their inception in the 1970's. Great strides have been made in improving these materials whilst little in the way of PGM free catalysis has been a commercial success. The starting point was to boost the activity of PGM based catalysts with a view to reducing the loading requirements. There were a few potential paths to research. Firstly the preparation. Catalysts are often extremely sensitive to their preparative conditions, slight changes in procedure can result in large changes in activity. The second area is to modify the catalyst with a dopant, this could be a small quantity of another material in an effort to modify system. This could be through the use of another metal to boost activity (for example), or the addition of a metal oxide to provide OSC.

The ultimate approach in this work was to combine these two methods. The preparation was adapted from a technique used to highly disperse gold over a catalyst support. Base metal components were added in to the procedure to see the effects of a highly dispersed dopant on the resulting small and tightly distributed nanoparticles of platinum and palladium. The result was a marked improvement of activity for CO and C_3H_8 oxidation for both iron and cobalt doped systems. Analysis revealed a very finely distributed cobalt oxide over the catalyst with discreet nanoparticles of approximately 5nm in size. These catalysts also produced more NO_2 compared to standard catalysts and whilst this is considered an undesirable reaction, with the move towards soot particle control in gasoline emissions, NO_2 can play an important role in the oxidation of soot. These catalysts showed an interesting promotion of activity and further research is required to determine the root cause. Analysis of different weight loading of cobalt and iron catalysts could be analysed by Transmission Electron Aberration-Corrected Microscopy to better resolve any small oxide particles if they are present and a potential correlation between particle size and activity could be explored. Additionally a temporal analysis of products with isotopically labelled oxygen could be useful in determining the oxygen source on these catalysts. If they exist in a fairly reduced state and the base metal oxides are providing oxygen for oxidation rather than the dissociated oxygen reacting directly with the CO/propane, this would allow that to be seen directly.

The introduction of gasoline particulate regulations will also see a shift in the technologies used in vehicles. Gasoline particulate filters (GPFs) will eventually be introduced, with the potential to load these filters with catalysts that not only carry out the catalytic reactions traditionally dealt with in a TWC, but will also be required to catalyse the reaction of soot. Such catalysts may utilise silver doped perovskite as described in Chapter 4. As space for these catalysts becomes increasingly tight in vehicles, dual purpose catalysts like these become extremely attractive provided they meet regulations. Perovskites have already seen commercial use in some vehicles when doped with palladium as in the case of the intelligent catalyst. They show very good activity and catalyst lifetime. The intelligent catalyst is a particularly elegant solution to the problem of catalyst resilience. The self-regenerating nature of this material was of interest, as it could potentially be applied to a material that is less resilient but that shows high initial activity. The material chosen to be studied was silver, as there is precedence in the literature for silver modified perovskites.

Ultimately the mechanochemical synthesis of perovskites proved to be less effective than other techniques for the formation of active catalytic phases in the silver doped lanthanum manganite catalysts. The catalysts themselves unfortunately, proved to be heavily susceptible to sulphate poisoning. Further work must be carried out to boost the resilience of these catalysts to poisoning. Scale up is an issue with high energy ball milling, while the low energy milling of nitrates is a much more viable step for scale. It still has issues with reproducibility on account of the affinity of nitrates for atmospheric water. However the catalysts did show some activity and the study did not comprehensively explore every facet of their synthesis. Further research could optimise and explore the possibilities for these methods with different ions or modifications to the procedure to improve existing formulations.

Exhaust gas is charged with catalytic poisons such as SO_2, ash and inhibitors such as water. One way to boost catalyst lifetime and reduce the effect of these substances on the active species is to reduce the amount present in the exhaust, or use sacrificial agents such as BaO to sulphate preferentially. Water however presents a different challenge, whilst it is not overwhelming in its effect, it does reduce the activity somewhat, and in a test cycle the difference of 10 degrees in light off can mean the difference in passing or failing a regulator test. If a catalyst can be protected from the

short term inhibition of steam and long term rigors of hydrothermal aging, then it may prove to be a more robust alternative to current materials. To approach this problem we utilised hydrophobic materials such as SiC, and BN with phases of relatively high surface areas compared to their more commonly encountered polymorphs. Such materials do not easily interact with water, due to a lack of hydroxyl species terminating on the surface with which water can hydrogen bond. Pt supported on SiC showed particularly interesting results. It was capable of lighting off propane at a lower temperature than its alumina based analogue and showed interesting properties such as the promotion of activity by CO_2 and H_2O. A closer look revealed that the Pt/SiC catalysts carried out a water gas shift reaction which would have produced hydrogen, which may have been responsible for the improved activity. A temporal analysis of products could reveal which oxygens from which reactants are ultimately carrying out this chemistry. Ultimately issues with consistency between batches of precursors have left a few unanswered questions, and further research is required upon this system to discover the precise nature of the improvement in activity and why it is so dependent on the support.

As the world moves into the 21st century, society is looking towards replacements for fossil fuels. Promising technologies are emerging with lithium batteries, hydrogen storage and fuel cells that may one day see gasoline becoming obsolete. However these technologies are not yet effective enough to see widespread adoption in the near term future. Gasoline and diesel therefore are still going to be relevant for some decades to come. The standards imposed on gasoline vehicles will continue to tighten as the world becomes less tolerant of pollution and novel solutions will be required to meet these targets. New areas of research in chemical catalysis are opening doors that were previously closed to industry. Novel supports allow the utilisation of materials that would otherwise be unable to cope with the extreme stress put on them in hydrothermal conditions exceeding 1,000 °C. The one thing that is certain is that the last gasoline vehicle to go into commercial production will implement many ideas that have yet to be conceived and even in an area dominated by extensive industrial and academic research there is still a large body of research left to be explored.

Appendix I

Statistical design IR spectra

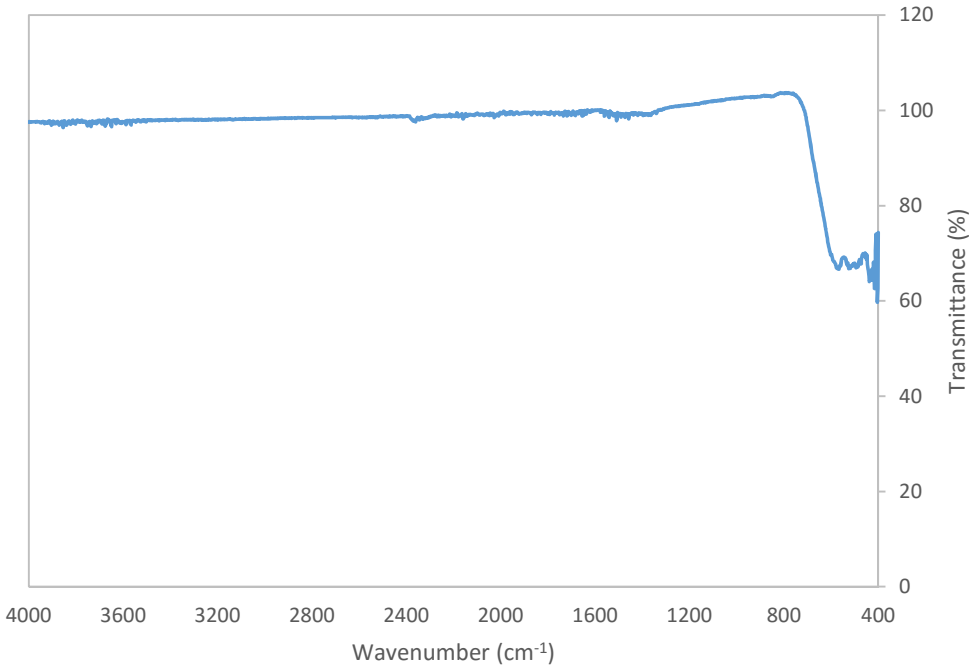

Figure 1 Std 1 run 11

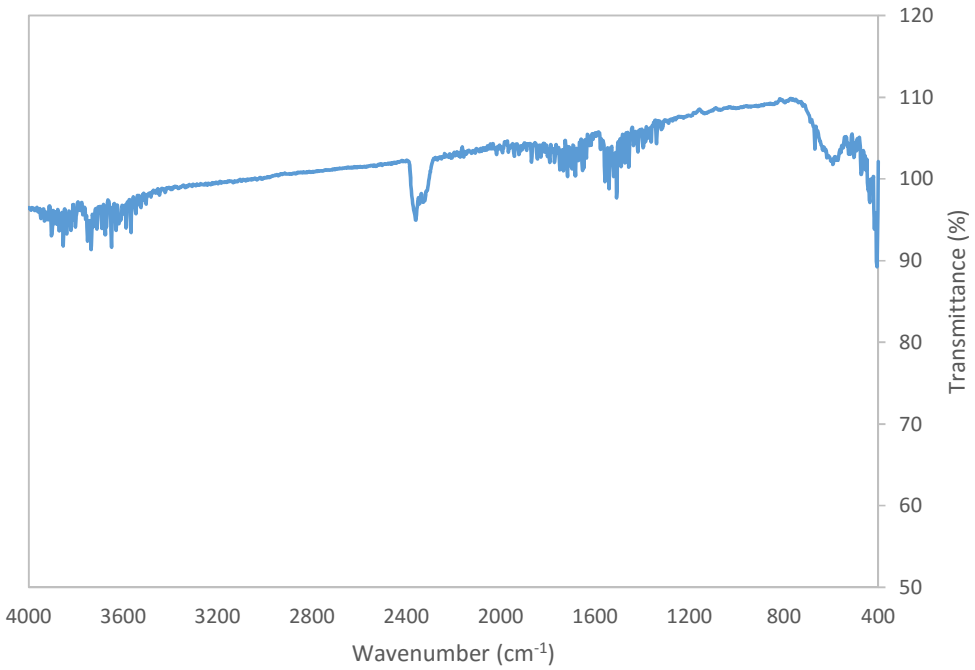

Figure 2. Std 2 run 8 uncalcined

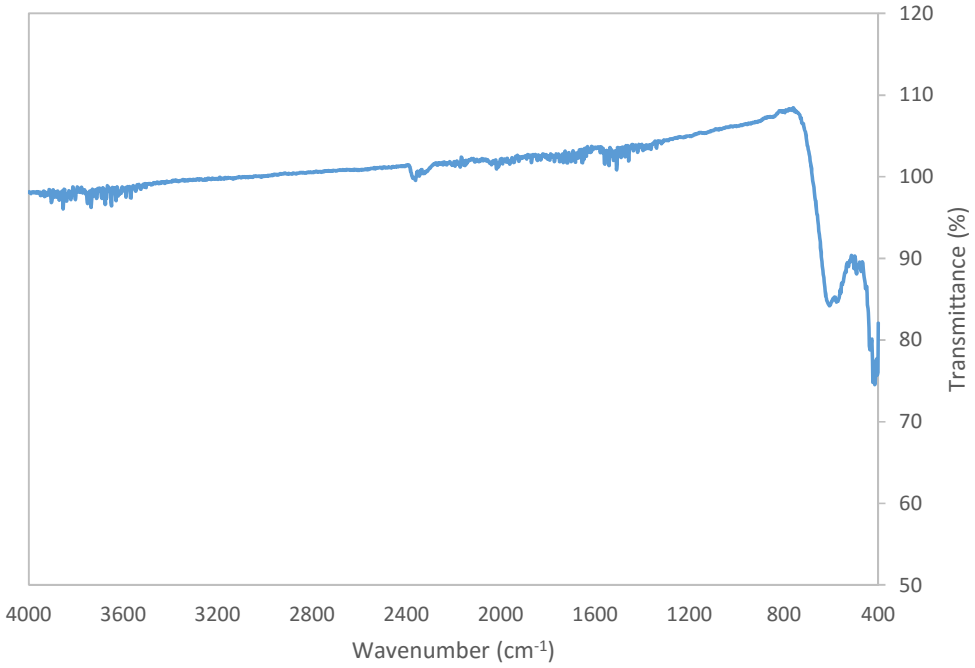

Figure 3. Std 2 run 8 heat treated

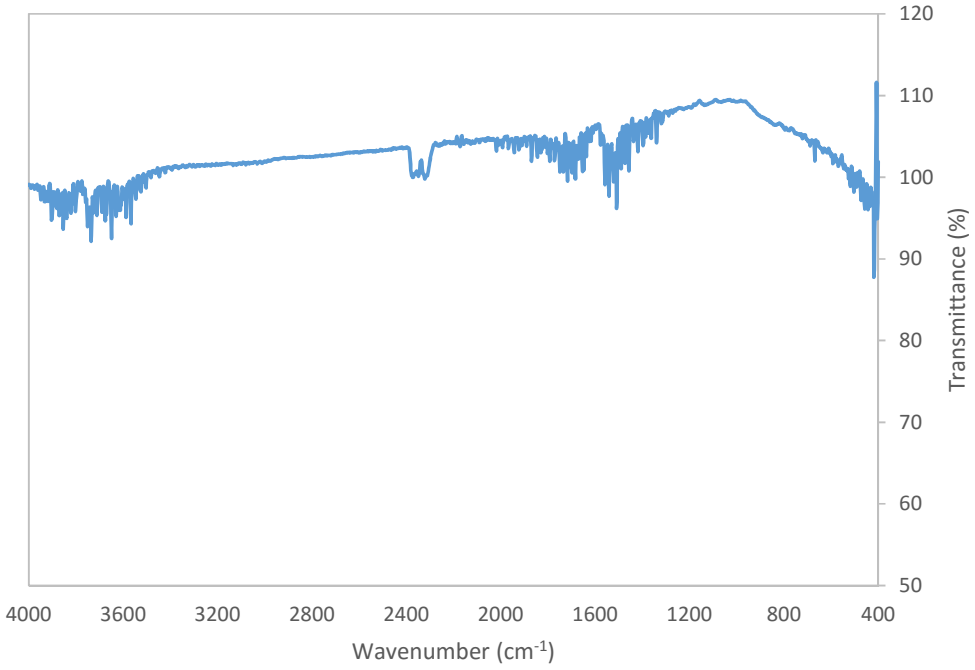

Figure 4. Std 4 run 10 uncalcined

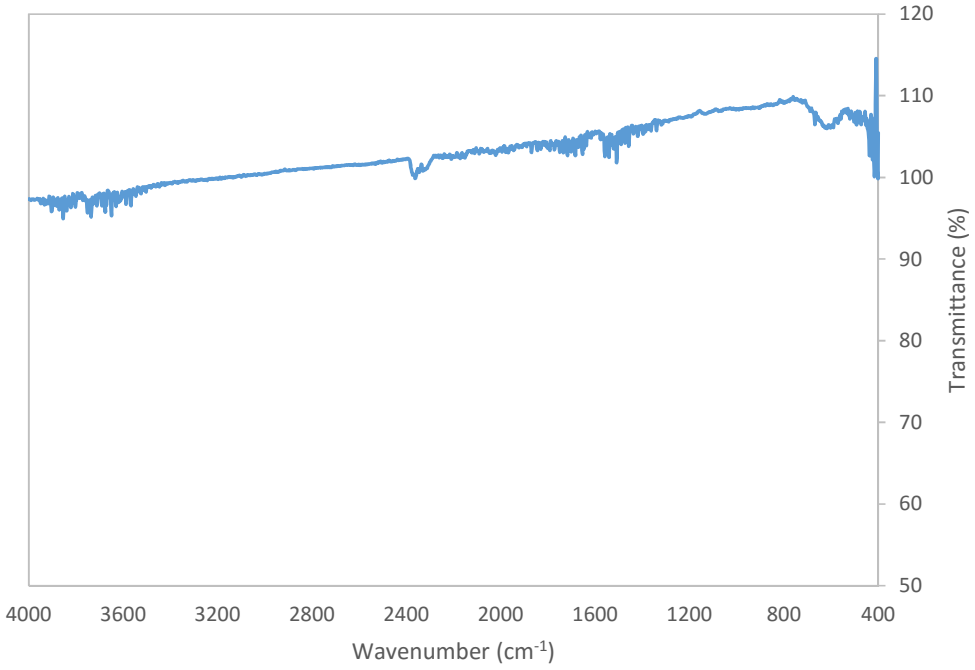

Figure 5. Std 4 run 10 heat treated

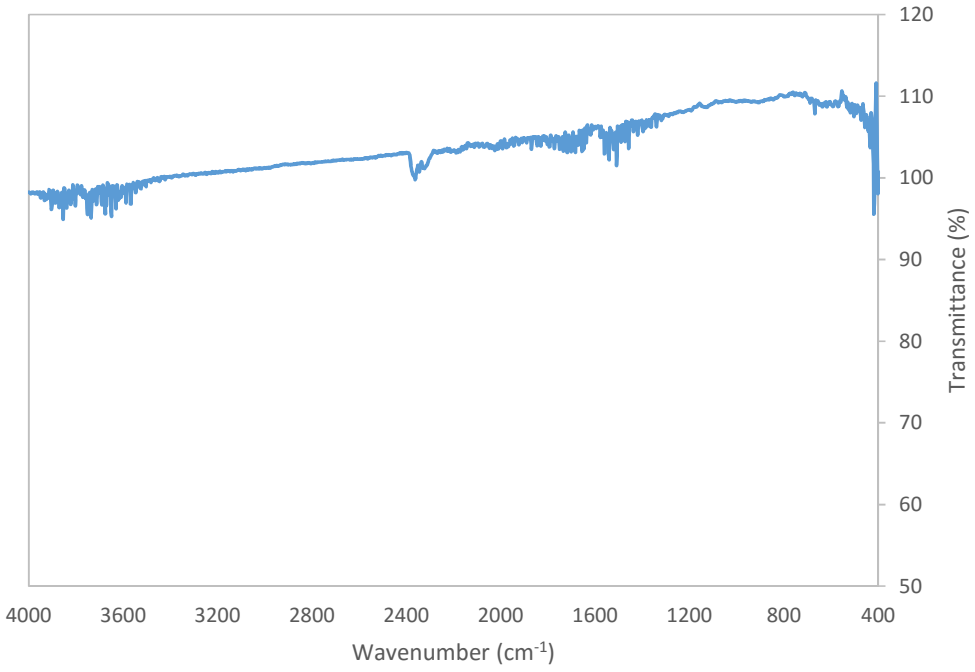

Figure 6. Std 5 run 16 uncalcined

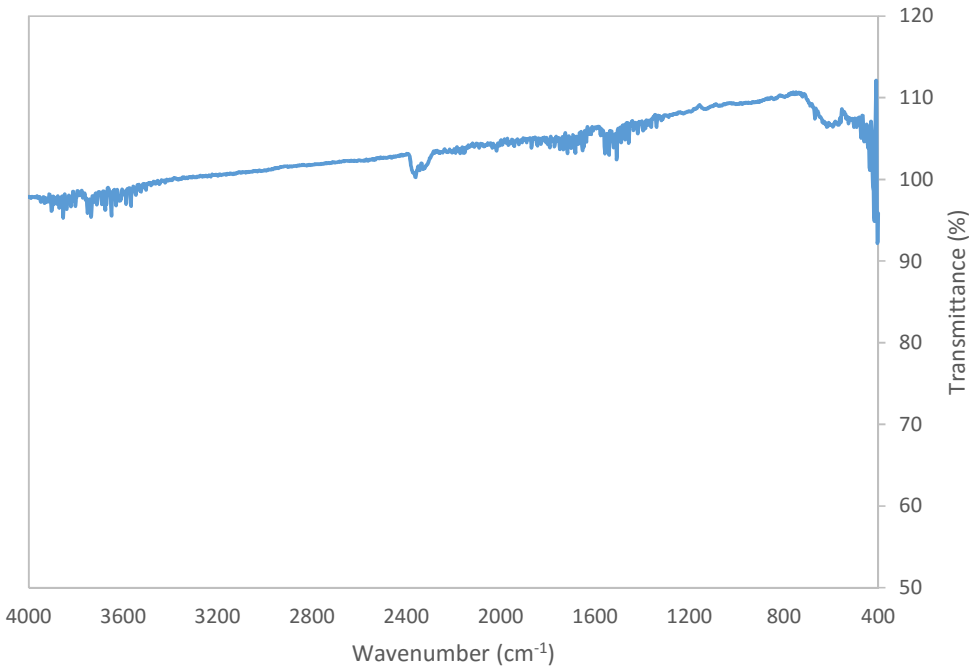

Figure 7. Std 5 run 16 heat treated

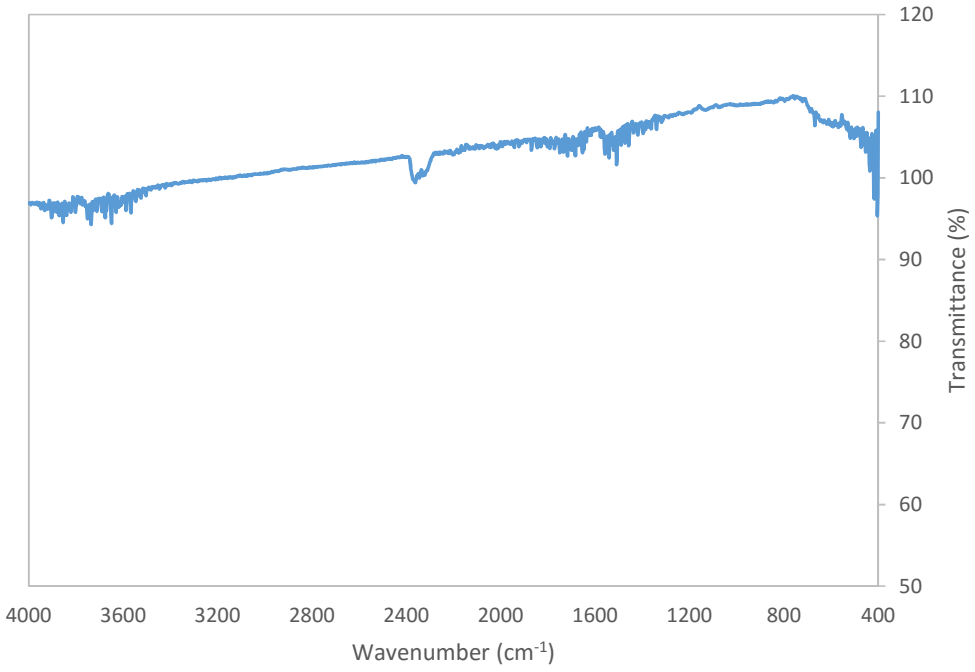

Figure 8. Std 6 run 4

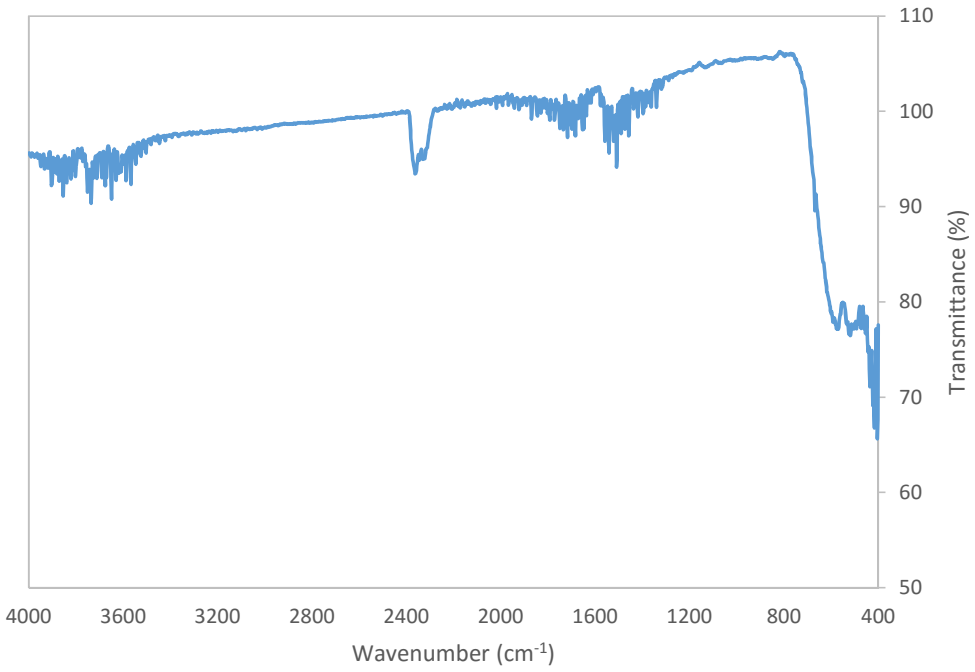

Figure 9. Std 7 run 15 uncalcined

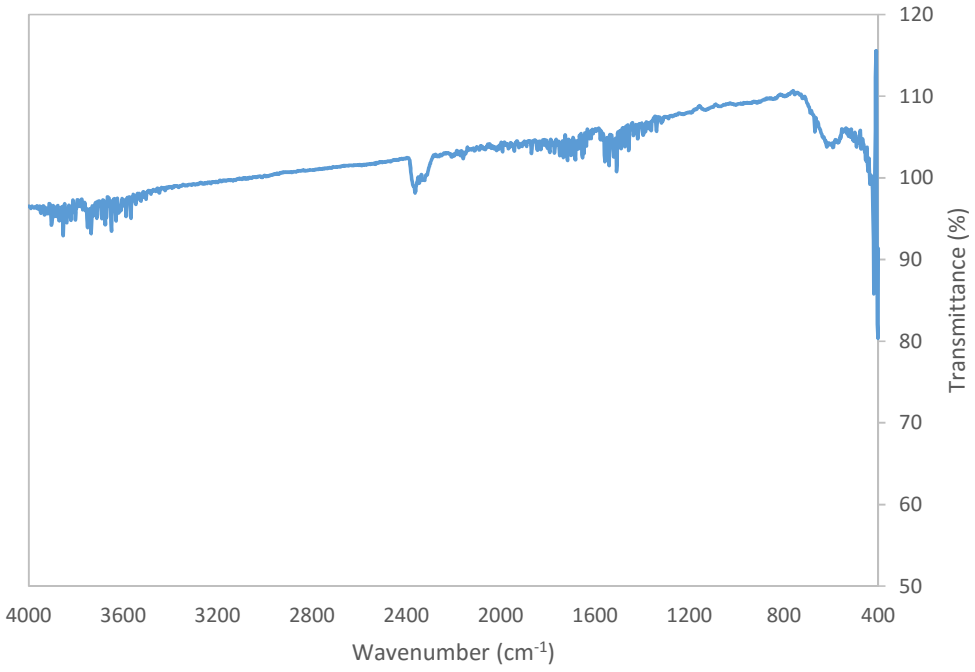

Figure 10. Std 7 run 15 calcined

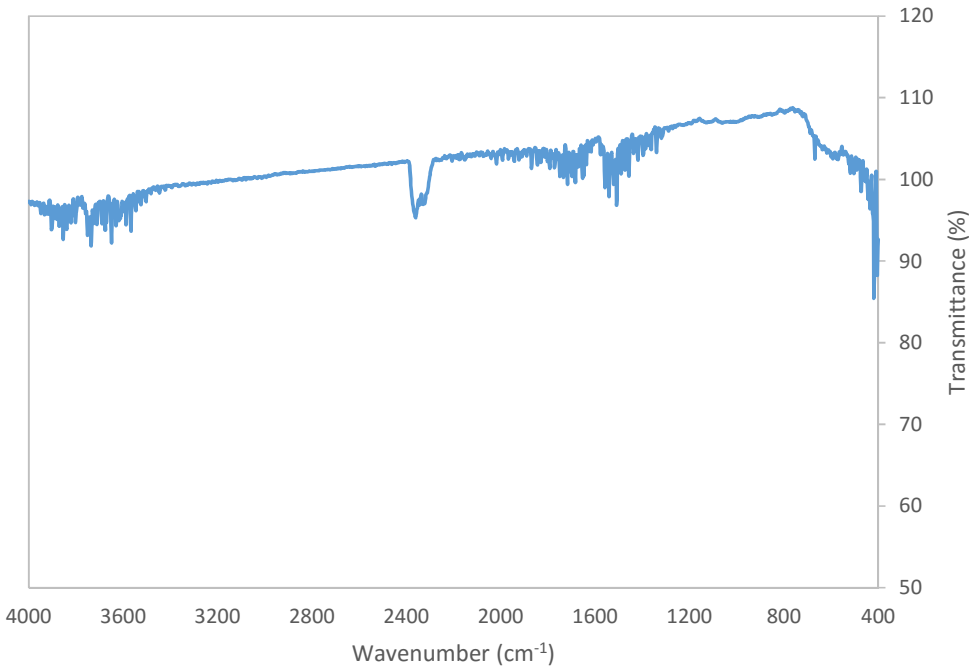

Figure 11. Std 9 Run 9 uncalcined

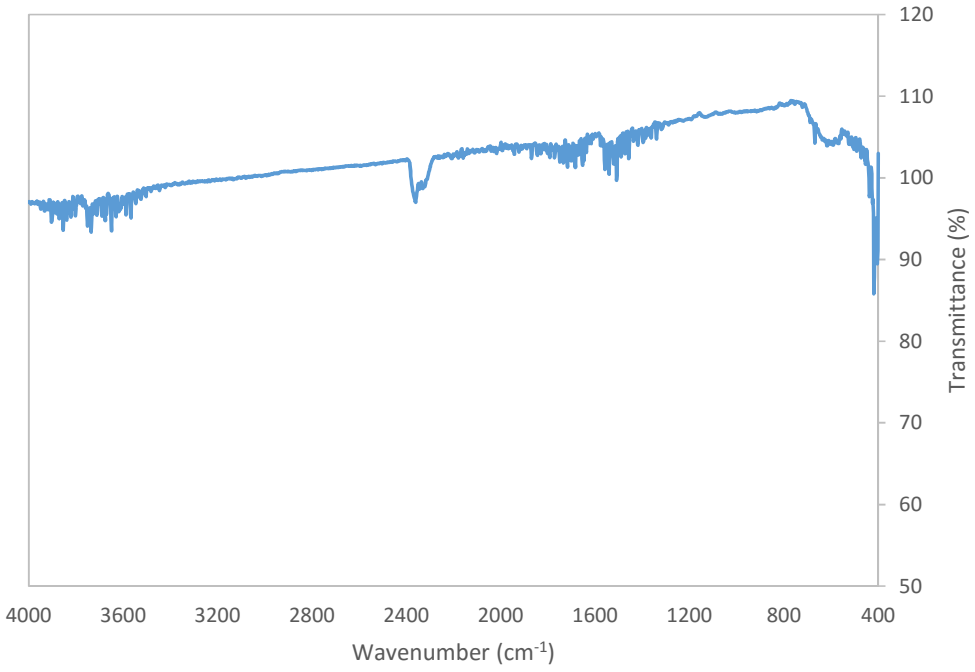

Figure 12. Std 9 run 9 heat treated

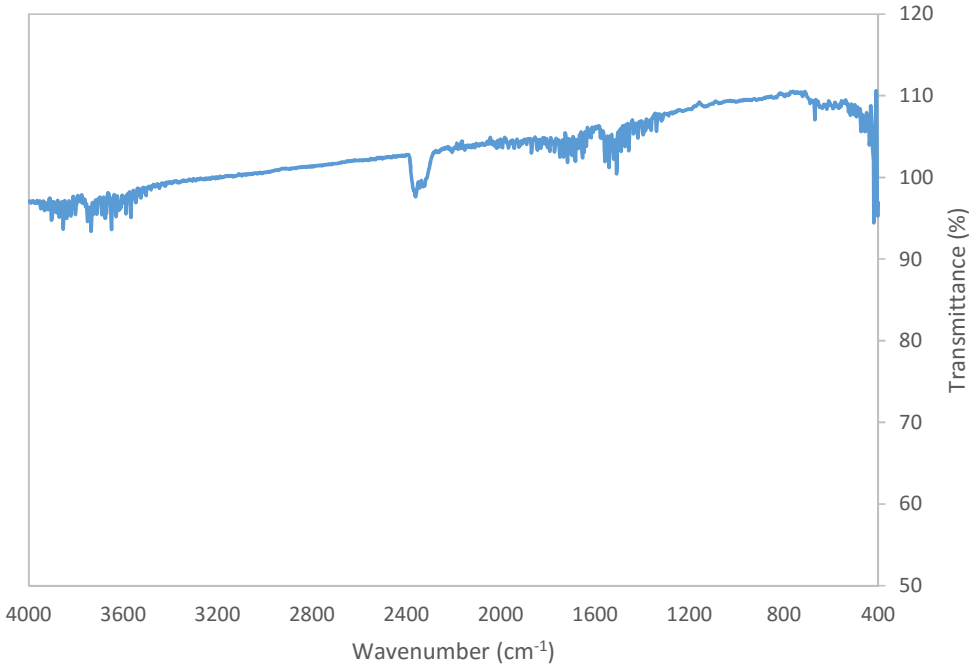

Figure 13. Std 10 run 6

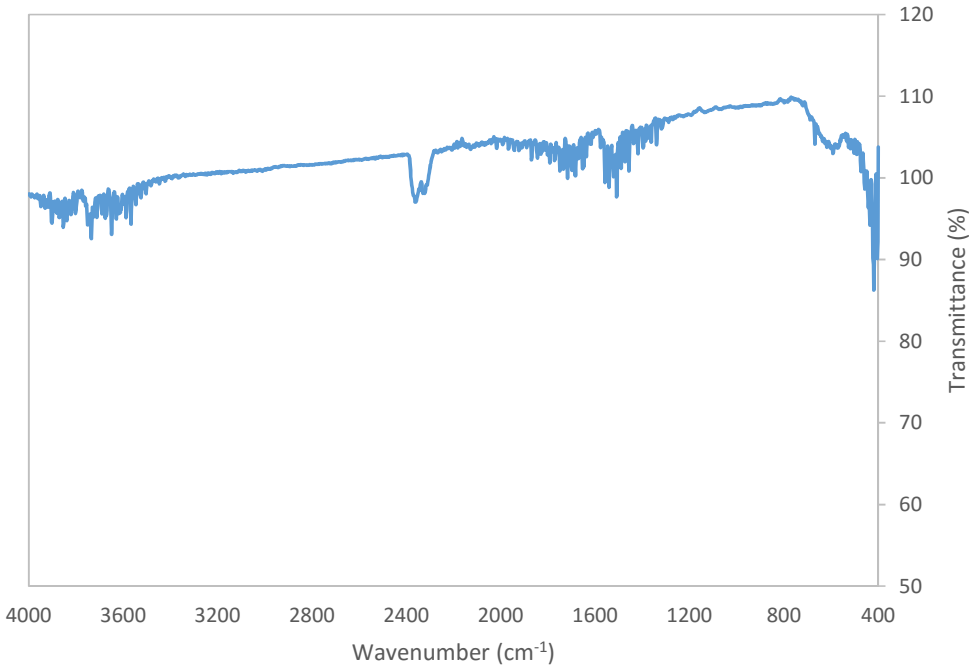

Figure 14. Std 11 run 5 uncalcined

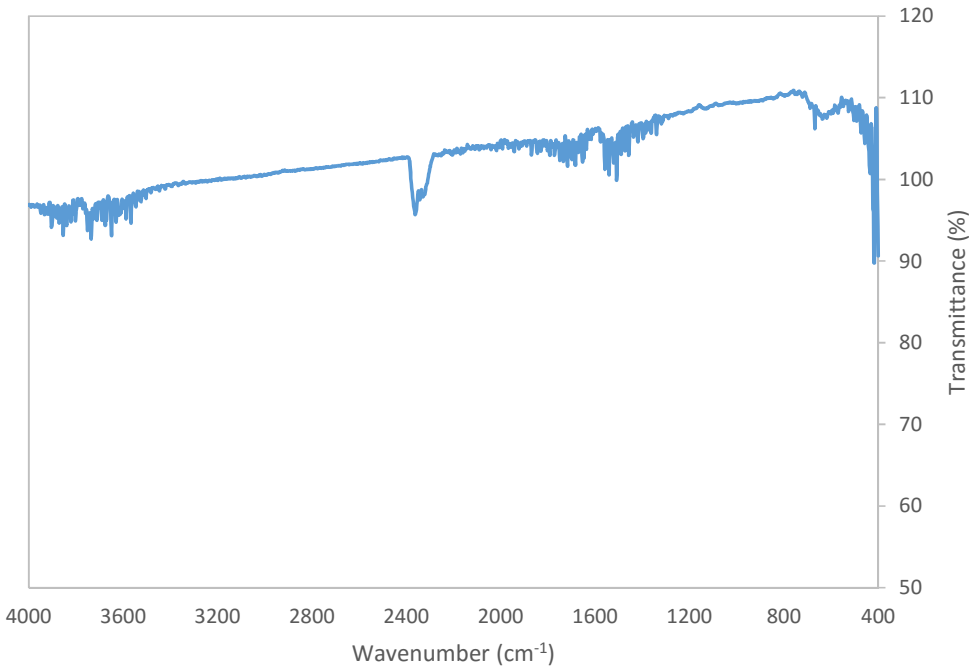

Figure 15. std 11 run 5 heat treated

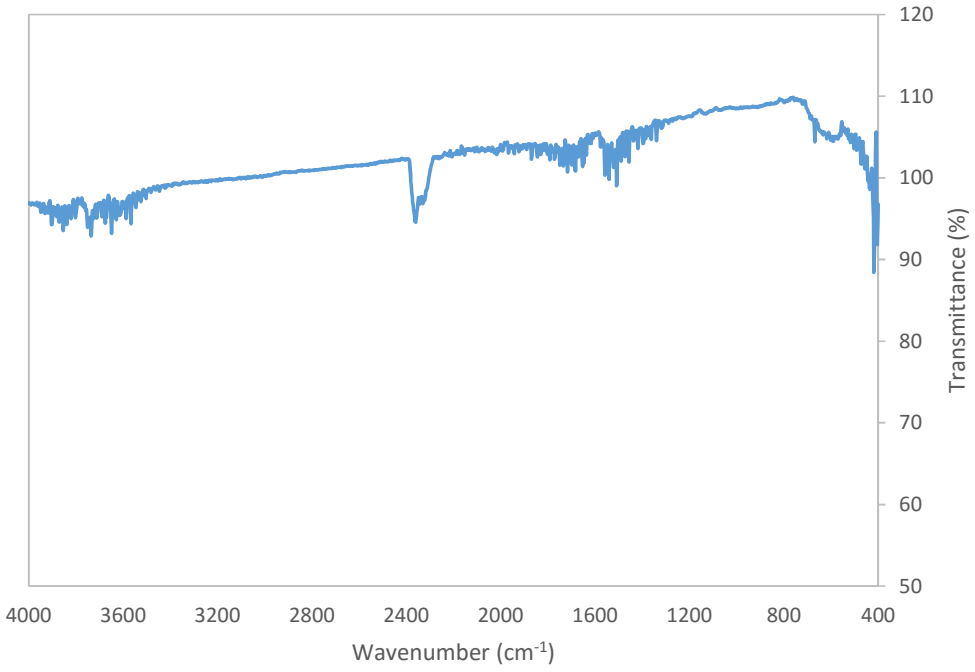

Figure 16. Std 12 run 9

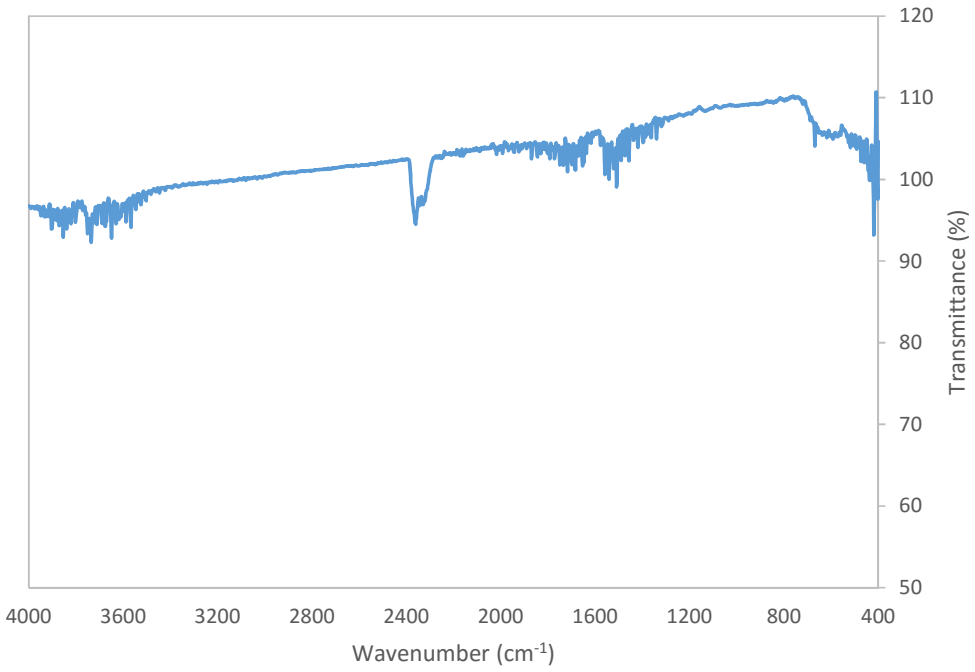

Figure 17. Std 13 run 11

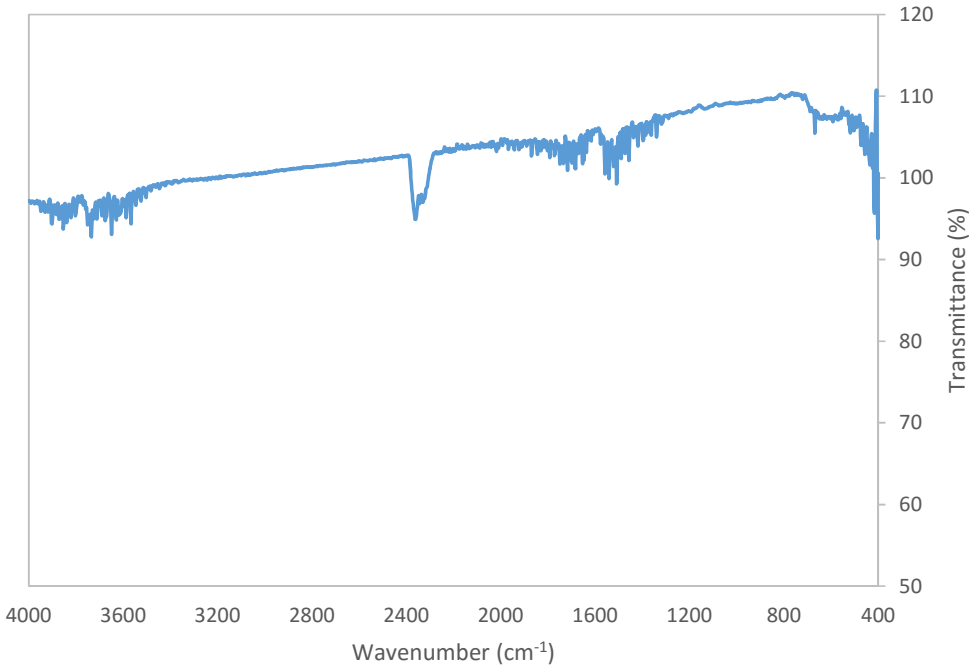

Figure 18 Std 14 run 3

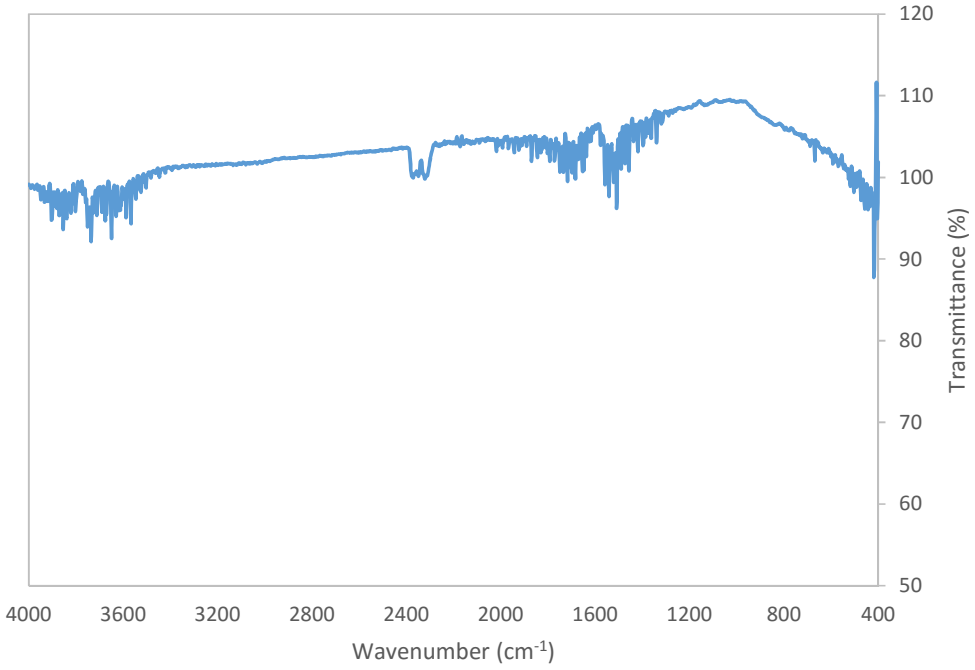

Figure 19. Std 15 run 13

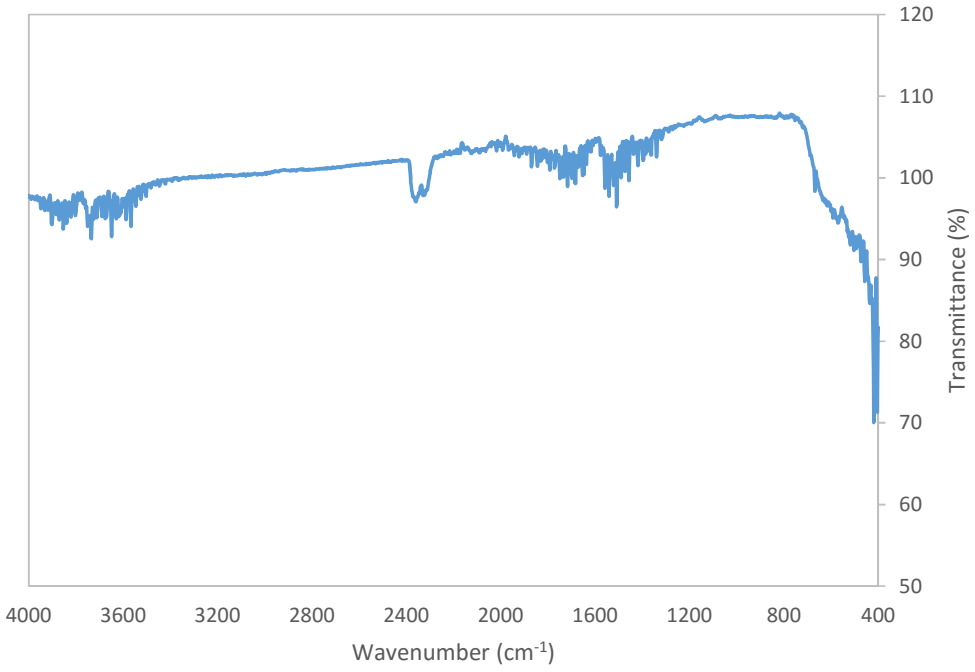

Figure 20. Std 16 Run 12 uncalcined

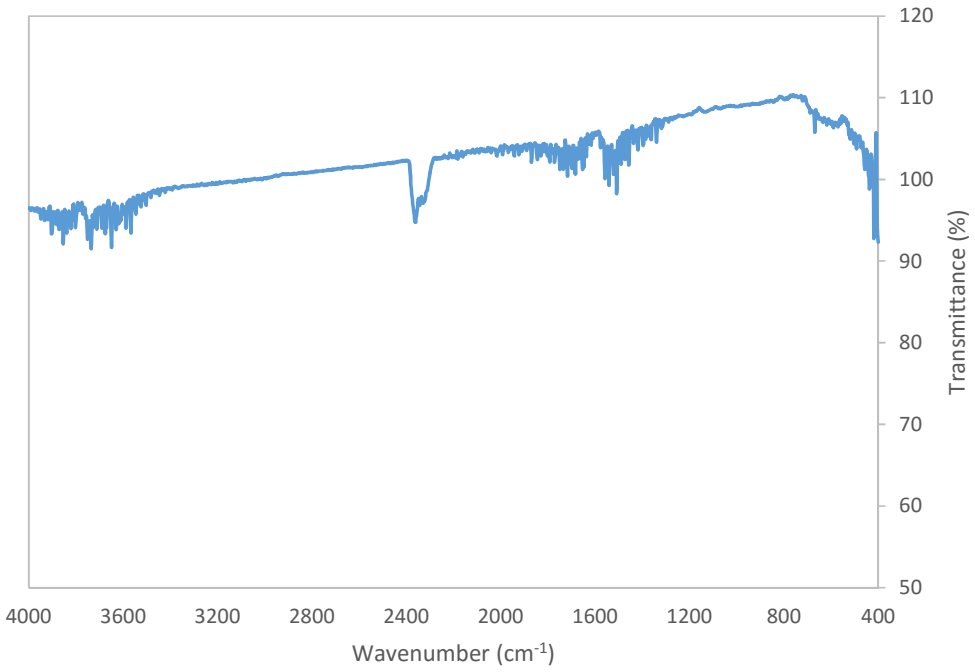

Figure 21. Std 16 run 12 Calcined

Decomposition grind IR spectra.

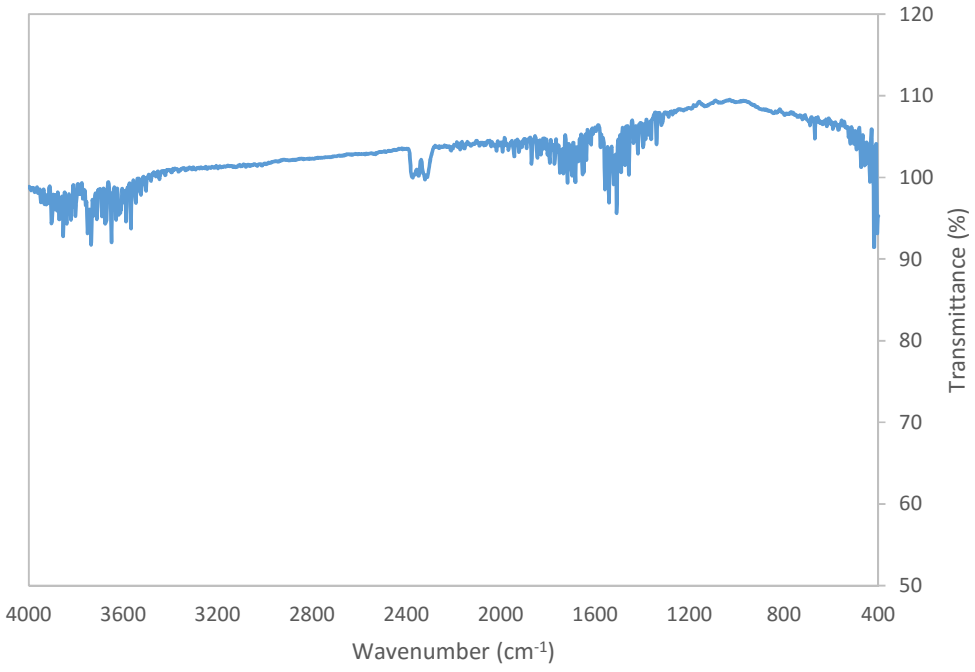

Figure 22. 0.5wt%Pt 1.0wt%Co/Al2O3

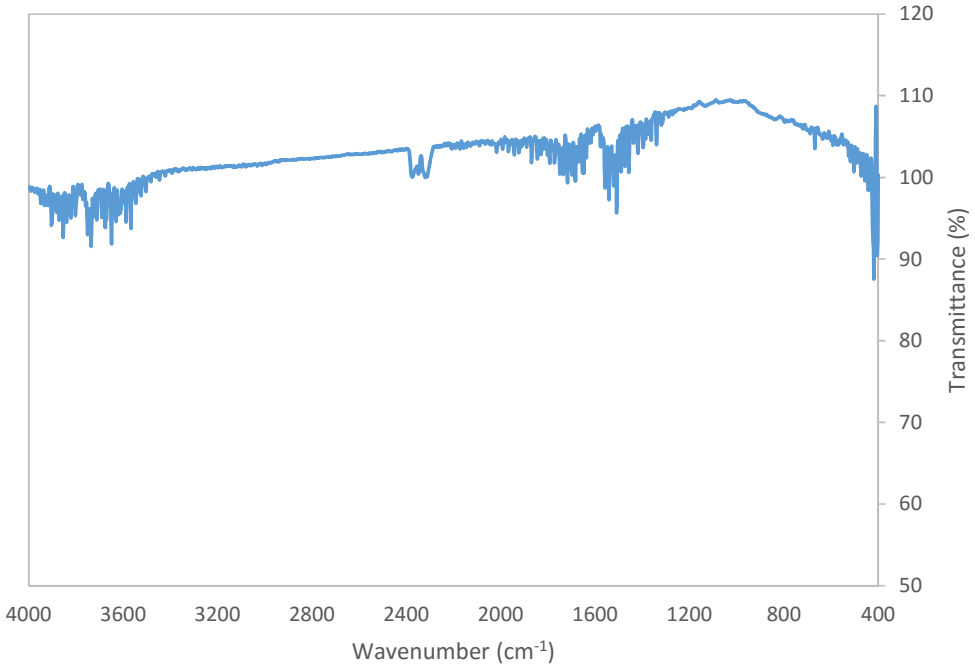

Figure 23. 0.5wt%Pt 0.5wt%Co/Al2O3

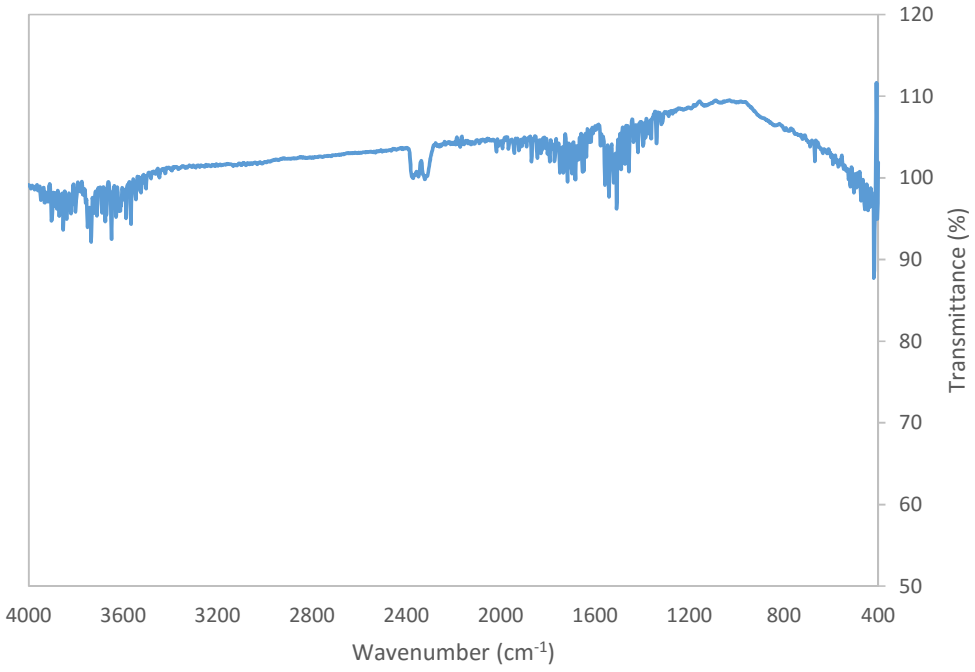

Figure 24. 0.5wt%Pt 0.25wt%Co/Al2O3

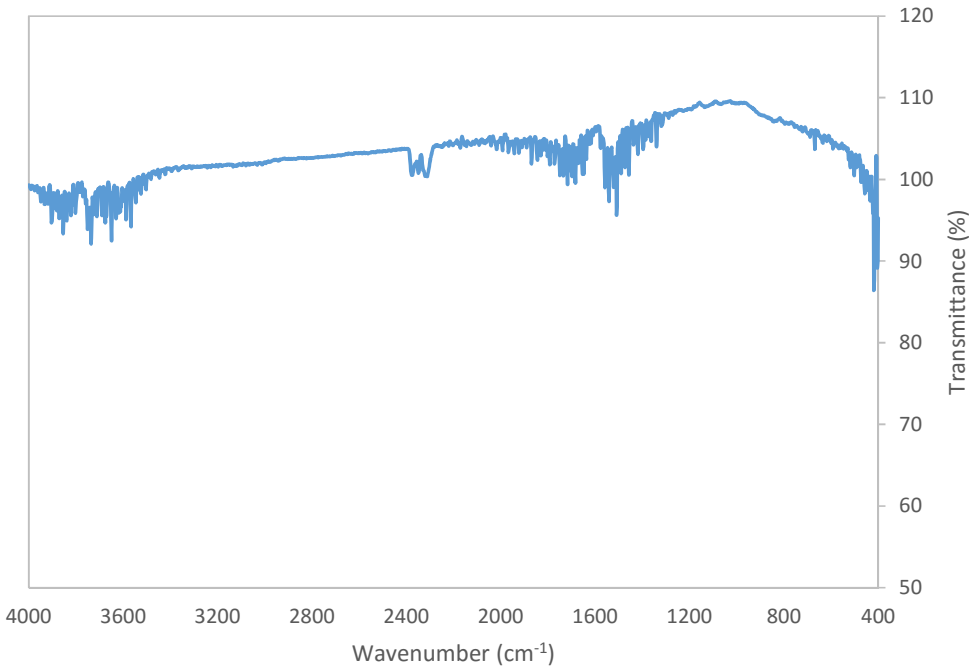

Figure 25. 0.5wt%Pt 0.125wt%Co/Al2O3

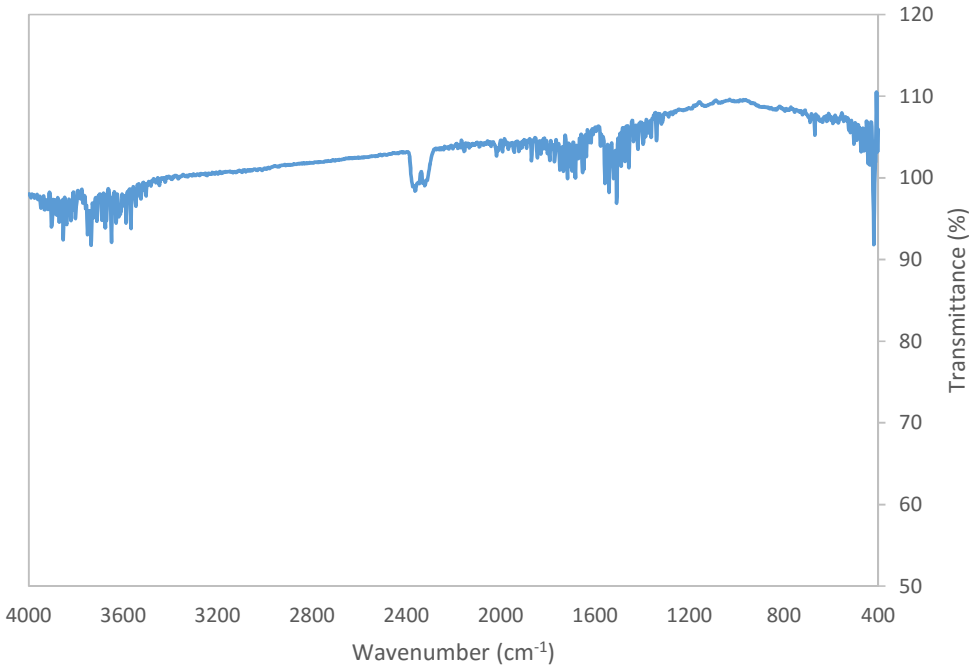

Figure 26. 0.5wt%Pt 1.0wt%Fe/Al2O3, Fe^{2+} precursor

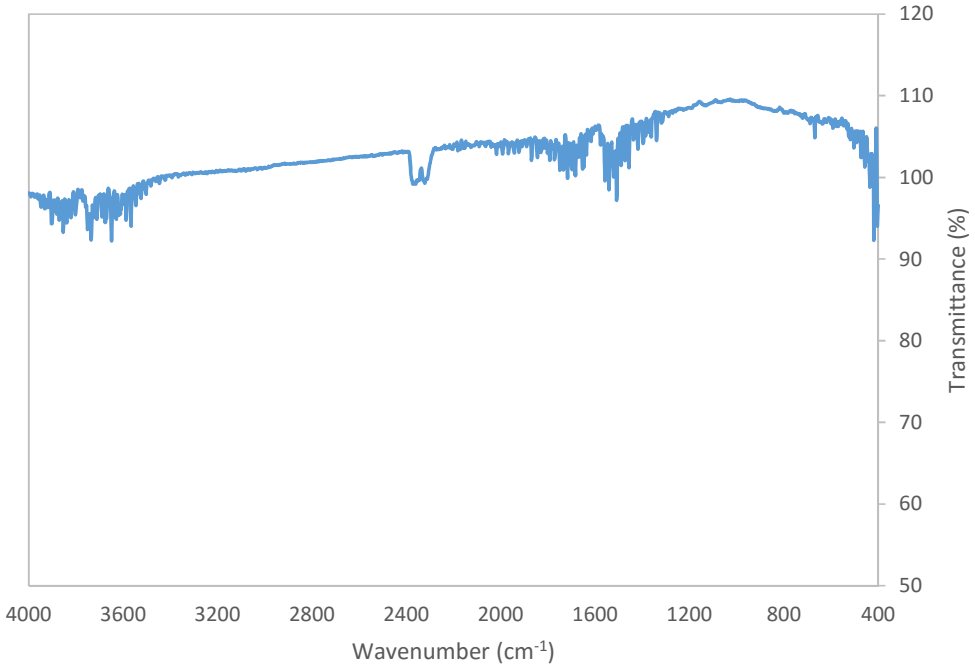

Figure 27. 0.5wt%Pt 0.5wt%Fe/Al2O3, Fe2+ precursor

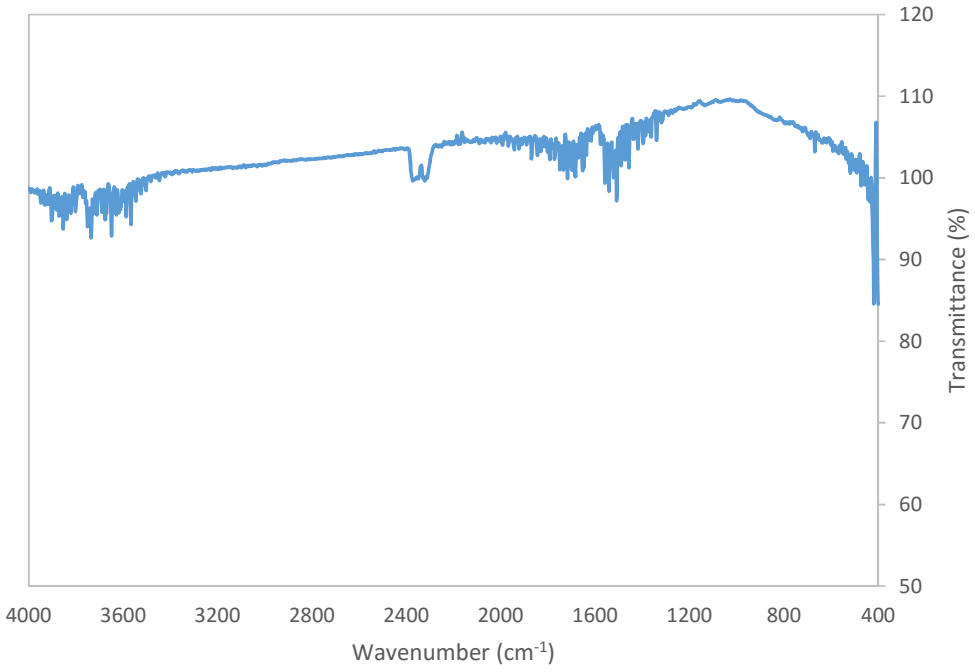

Figure 28 0.5wt%Pt 0.25wt%Fe/Al2O3, Fe2+ precursor

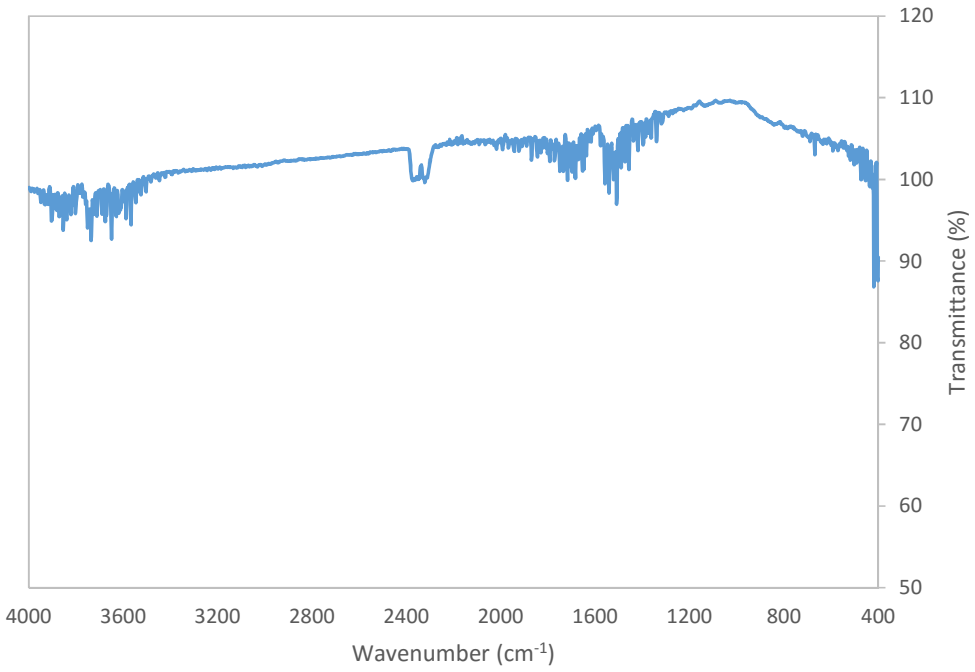

Figure 29. 0.5wt%Pt 0.125wt%Fe/Al2O3, Fe2+ precursor

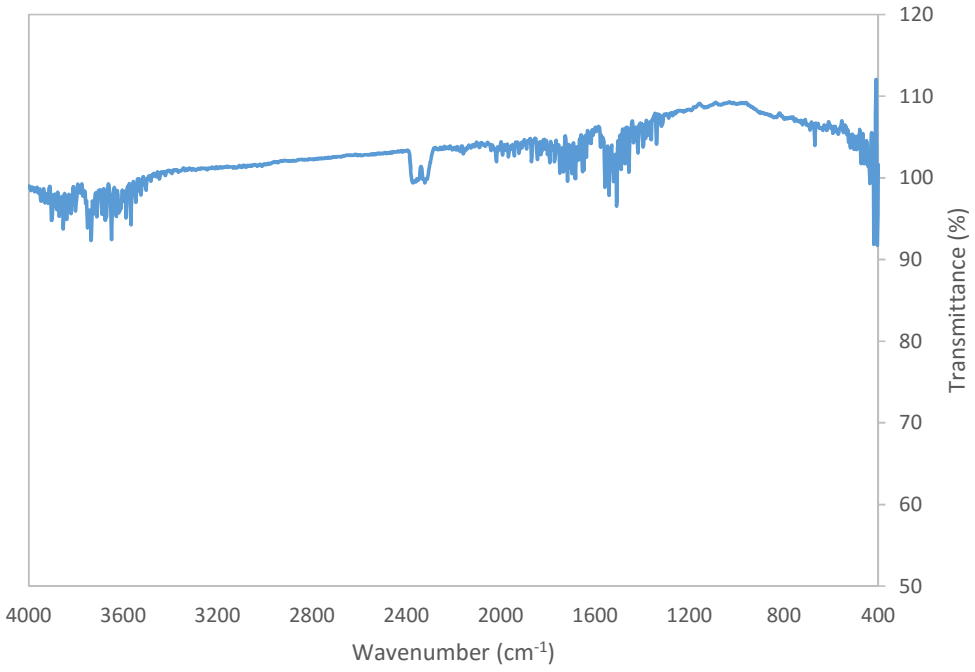

Figure 30. 0.5wt%Pt 1.0wt%Fe/Al2O3, Fe3+ precursor

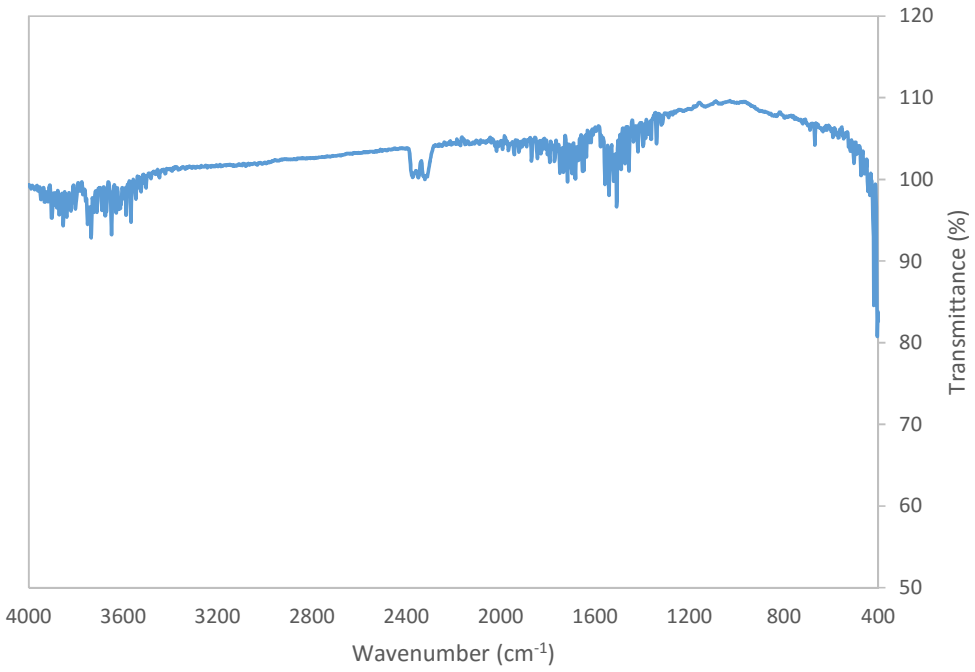

Figure 31. 0.5wt%Pt 0.5wt%Fe/Al2O3, Fe3+ precursor

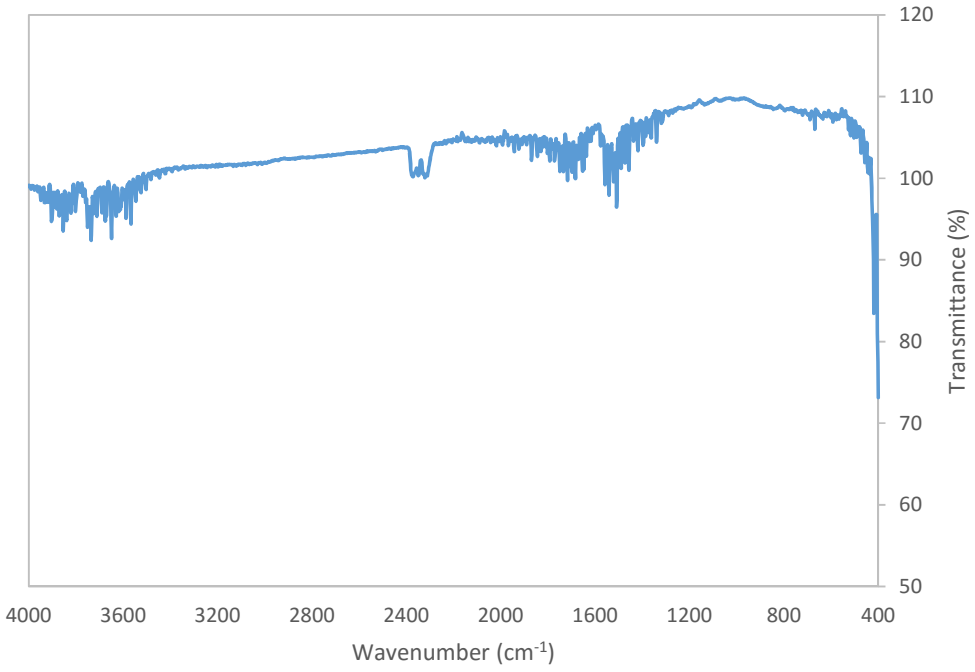

Figure 32. 0.5wt%Pt 0.25wt%Fe/Al2O3, Fe3+ precursor

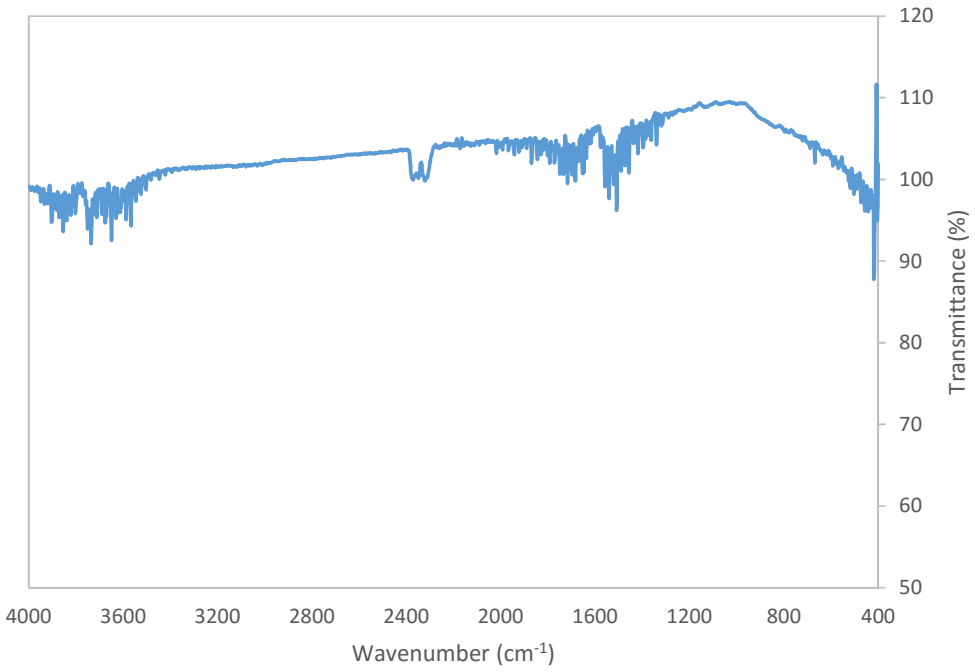

Figure 33. 0.5wt%Pt 0.125wt%Fe/Al2O3, Fe3+ precursor

DOE Response Table

Std	Factor 1 A:Speed RPM	Factor 2 B:Duration h	Factor 3 C:Hydration %wt	Factor 4 D:Halfway Pause m	Factor 5 E:Ion substituted	Factor 6 F:Silver loading equivs	Factor 7 G:Calcination	Response 1 CO T10 Celcius	Response 2 CO T50 Celcius	Response 3 CO T90 Celcius	Response 4 Propane T10 Celcius
11	600	12	3	30	Mn	0.15	Yes	209	271	N/A	362
13	600	9	6	30	Mn	0.15	No	163	218	N/A	355
4	650	12	3	0	La	0.3	Yes	153	191	N/A	302
6	650	9	6	0	La	0.3	No	163	286	N/A	369
5	600	9	6	0	Mn	0.3	Yes	255	327	N/A	395
10	650	9	3	30	Mn	0.3	No	125	216	N/A	366
16	650	12	6	30	Mn	0.3	Yes	300	321	N/A	404
1	600	9	3	0	La	0.15	No	175	263	N/A	356
7	600	12	6	0	La	0.15	Yes	190	306	N/A	340
8	650	12	6	0	Mn	0.15	No	163	229	N/A	342
14	650	9	6	30	La	0.15	Yes	173	243	N/A	306
15	600	12	6	30	La	0.3	No	170	241	N/A	365
2	650	9	3	0	Mn	0.15	Yes	208	255	N/A	352
12	650	12	3	30	La	0.15	No	155	262	N/A	346
3	600	12	3	0	Mn	0.3	No	155	235	N/A	330
9	600	9	3	30	La	0.3	Yes	160	229	N/A	310

Response 5 Propane T50 Celcius	Response 6 Propane T90 Celcius	Response 7 NO conv 200c %	Response 8 NO conv 250c %	Response 9 NO conv 300c %	Response 10 NO conv 350c %	Response 11 NO conv 400c %	Response 12 NO conv 450c %	Response 13 NO conv 500c %	Response 14 NO2 conv 200c %	Response 15 NO2 conv 250c %	Response 16 NO2 conv 300c %
N/A	N/A	8.20395	2.14683	1.83055	15.6795	5.39582	3.11482	3.21066	0	0	0
N/A	N/A	0.429062	0	24.4375	41.6762	31.312	19.3268	0	0	0	27.4932
N/A	N/A	0	13.1502	27.3166	36.2914	28.8057	17.4565	9.04518	0.0950169	10.6313	34.3539
N/A	N/A	4.24869	8.40699	2.8626	4.38931	0	0	0	0	0	0
N/A	N/A	0.305509	0.38435	1.69508	0.236523	0	0	4.95713	0	0	0
N/A	N/A	0	0	0	8.1615	29.2798	42.2173	47.8373	0	0	0
N/A	N/A	0	0	0	0	17.9497	14.3559	0	0	0	0
N/A	N/A	0	0.834907	0	11.4203	24.4608	9.47222	0	0	0	0
N/A	N/A	1.06432	3.50764	0	0	0	0	0	0	0	0
N/A	N/A	1.65971	0	0	21.4909	34.4841	21.6711	0	0	0	0
N/A	N/A	6.10246	4.19544	0	0	0	0.46387	0	0	0	0
N/A	N/A	0	0	0.987965	27.187	38.4767	30.1419	13.0322	0	0	0
N/A	N/A	0	0	0	8.91329	14.7655	13.0071	0	0	0	0
N/A	N/A	0	0	0	19.5109	28.7631	20.1377	2.21594	0	0	0
N/A	N/A	3.12043	0.565578	0	0	15.2999	0	0	0.705001	0.60586	3.22758
N/A	N/A	4.7354	0	0	1.81115	2.49033	0	0	0	0	2.69596

Response 17 NO2 conv 350c %	Response 18 NO2 conv 400c %	Response 19 NO2 conv 450c %	Response 20 NO2 conv 500c %	Response 21 N2O conv 200c %	Response 22 N2O conv 250c %	Response 23 N2O conv 300c %	Response 24 N2O conv 350c %	Response 25 N2O conv 400c %	Response 26 N2O conv 450c %	Response 27 N2O conv 500c %	Response 28 CO conv 200c %
7.48514	7.7535	8.27104	8.27104	1.92639	1.52386	1.38969	3.75695	1.52386	1.65804	0.910485	4.29887
48.8965	35.8214	24.3285	24.3285	1.78014	0.968145	0.499688	0.510098	0.437227	0.395586	0.614199	30.2127
43.8239	44.3623	28.5684	28.5684	1.55194	2.49155	0.601774	0.548986	0.432855	0.380068	0.538429	59.1199
0	0	0	0	2.12389	1.89485	1.71786	2.54034	2.405	1.29099	1.30141	24.4525
3.43401	14.6043	9.43182	9.43182	1.79845	2.08613	2.36349	3.68225	5.29126	2.96591	2.72987	1.40293
7.17239	28.0074	39.3861	39.3861	2.29434	1.56056	0.909467	1.79826	0.392724	0.372055	0.372055	38.8996
2.30468	24.1146	16.9891	16.9891	1.9981	1.98753	1.94524	1.92409	0.740036	0.972619	0.782324	0.984619
16.4107	31.2973	19.0121	19.0121	1.53564	1.6617	1.15746	0.73344	0.38964	0.66468	0.64176	16.9455
0	1.01559	1.40542	1.40542	2.24661	2.14403	2.00041	2.17481	1.48748	2.36972	1.49774	12.1504
16.9411	33.3435	18.9939	18.9939	1.35163	1.15854	0.50813	0.579268	0.406504	0.335366	0.386179	27.7299
0.631446	3.02042	15.2178	15.2178	1.98905	1.68386	1.32604	0.957693	1.32604	0.736687	0.557777	18.7204
19.9654	31.1595	23.381	23.381	1.90363	1.83077	1.12943	0.701339	0.382549	0.346115	0.291466	19.6227
13.6537	21.1133	26.8032	26.8032	2.46939	1.97551	1.65655	1.76973	0.524745	0.555613	0.617347	3.82521
14.1697	29.646	25.2141	25.2141	1.3331	1.70389	1.17419	0.909332	0.317825	0.273682	0.238369	25.4633
2.02688	21.4695	5.89337	5.89337	2.15907	2.07094	0.980392	0.68297	0.716017	0.638907	0.727032	30.5345
3.01257	7.41629	2.15869	2.15869	1.55426	1.35278	2.07234	1.82289	3.82807	1.93802	1.77492	28.7156

Response 29 CO conv 250c %	Response 30 CO conv 300c %	Response 31 C3H8 conv 300c %	Response 32 C3H8 conv 350c %	Response 33 C3H8 conv 400c %	Response 34 C3H8 conv 450c %	Response 35 C3H8 conv 500c %	Response 36 Yeild g
35.0291	70.4076	0.745785	5.80739	23.8651	44.8573	61.7931	3.8304
83.7481	99.0517	2.71992	8.5627	22.042	39.1545	51.2235	8.0135
93.5376	97.8898	8.76572	41.7387	74.2106	90.5726	96.5016	5.8406
40.1282	53.8482	2.34028	6.57301	15.4285	28.5601	36.668	6.8151
7.54317	31.987	0	2.26878	10.7687	30.0726	50.7263	4.9615
72.9529	93.616	1.58427	6.84572	15.8654	27.5287	40.2255	14.1441
5.62532	25.6608	0.188324	1.1754	8.68563	27.255	54.6269	4.8374
40.646	77.6985	1.56854	6.4783	17.1895	27.2955	41.0471	2.8251
31.7852	48.4744	2.12786	12.0878	26.3836	36.6608	46.4381	7.6521
65.5059	98.9613	2.75036	11.156	27.4825	43.7599	55.9978	7.196
54.8514	82.4518	8.67935	21.8791	44.3866	65.0225	80.0838	7.4477
56.2615	86.214	1.59813	6.46941	17.1214	43.875	54.0354	4.0711
45.6134	87.8826	0.574473	9.00542	36.2752	61.7863	73.3464	5.4406
43.5447	71.2182	2.97338	10.6412	24.3503	36.8699	58.272	4.4228
57.9788	98.1456	3.78448	14.2852	25.7644	36.6932	43.4638	6.5909
64.182	81.0563	6.33431	25.3504	46.3553	58.1936	64.0586	4.0722